G-protein modulation of ionic currents in cardiac myocytes

Thesis submitted for degree of D.Phil.
to the Faculty Board of Physiological Sciences

Leo Goodstadt

St. Hugh's College
University of Oxford

Michaelmas Term 2000

G-protein Modulation of Ionic Currents in Cardiac Myocytes.

Leo Goodstadt, St. Hugh's College, D. Phil. Michaelmas 2000

The modulation of L-type calcium current (I_{Ca}) and the catecholamine-induced chloride current ($I_{Cl,cAMP}$) by G-protein coupled regulatory pathways were studied in isolated guinea pig cardiac ventricular myocytes using the whole cell patch clamp and flash photolysis techniques. A number of novel findings are reported in this thesis.

The rapid release of GTP, the natural ligand of G-proteins, from its inert caged precursor produced a large enhancement of I_{Ca} which could be detected within 20 ms of the photolysing light pulse. A fast component of this response persisted under conditions of current rundown and inhibition of cAMP-dependent phosphorylation. This suggests the involvement of a membrane-delimited pathway not dependent on soluble second messengers. The photorelease of the non-hydrolysable GTPγS caused a biphasic increase in I_{Ca} in the majority of myocytes and a sustained response in the others.

Pipette dialysis with GTPγS had a three-fold effect: pertussis toxin-sensitive inhibition of the I_{Ca} responses to isoprenaline, forskolin and photoreleased GTP; competitive inhibition of the enhancement of I_{Ca} by further photoreleased GTPγS; and modulation of the kinetics of cAMP-dependent activation of $I_{Cl,cAMP}$ and I_{Ca} without any significant changes in their magnitudes.

The flash photolysis of caged cAMP produced large increases in both $I_{Cl,cAMP}$ and I_{Ca} but the latter was more than twice as sensitive to cAMP (EC_{50} = ~1.10 µM and ~0.47 µM).

Urotensin II has recently been identified as the ligand for a previously orphaned G-protein coupled receptor, and has been shown to be a potent chronic vasoconstrictor. This thesis reports an additional modulatory effect on $I_{Cl,cAMP}$. 150 µM urotensin II had no effect on its own but potentiated responses to sub-maximal sympathetic stimulation.

Estrogen reduces forskolin- and isoprenaline-stimulated cAMP accumulation in the rat heart and inhibits cardiac I_{Ca} via a G-protein. However, the application of 30 µM 17β-estradiol to guinea pig myocytes in the presence of low doses of either forskolin (0.25-0.5 µM) or isoprenaline (20 nM) produced large increases in $I_{Cl,cAMP}$. This effect was mediated by a cell-surface receptor. The involvement of nitric oxide synthase (NOS) was not required, unlike in acute estrogenic responses in vascular endothelia. Raloxifene, a selective estrogen receptor modulator (SERM), was similarly able to potentiate the results of sympathetic stimulation but with a much slower time course.

Contents

List of Tables

List of Figures

Chapter Five Effects of chronic application of GTPγS

Chapter Six Urotensin II

Chapter Seven Estrogenic Agonists

Chapter One

Introduction

The co-ordination of a multi-cellular organism is a highly complex process in which G-proteins play a vital part. These heterotrimeric guanine-nucleotide (G-) binding proteins are self-terminating molecular switches activated by neurohormonal receptors. They play a central role in mediating the responses to many hormones and neurotransmitters (so-called "first messengers") passed from one cell to another. These ligands are recognised by their cognate cell surface receptor proteins embedded in the cytoplasmic membrane. The specificity of the binding between agonist and receptor allows a multiplicity of agents each to elicit a different response. The stimulus can then be forwarded by the receptors without penetration of the agonist, often through the further release of small molecules or ions (i.e. "second messengers"). Signalling cascades allow incoming stimuli to be propagated rapidly throughout the cell interior as well as allowing them to be either amplified or further modulated in a complex manner.

The discovery and characterization of G-proteins have confirmed Rodbell's hypothesis (Rodbell *et al.*, 1971) that a guanylyl-sensitive coupling element is interposed between hormone receptor and effector. G-proteins are heterotrimers consisting of $\alpha\beta\gamma$ subunits. Following the activation by an associated receptor, the guanine nucleotide-binding site is opened, resulting in the release of GDP and the binding of GTP. The

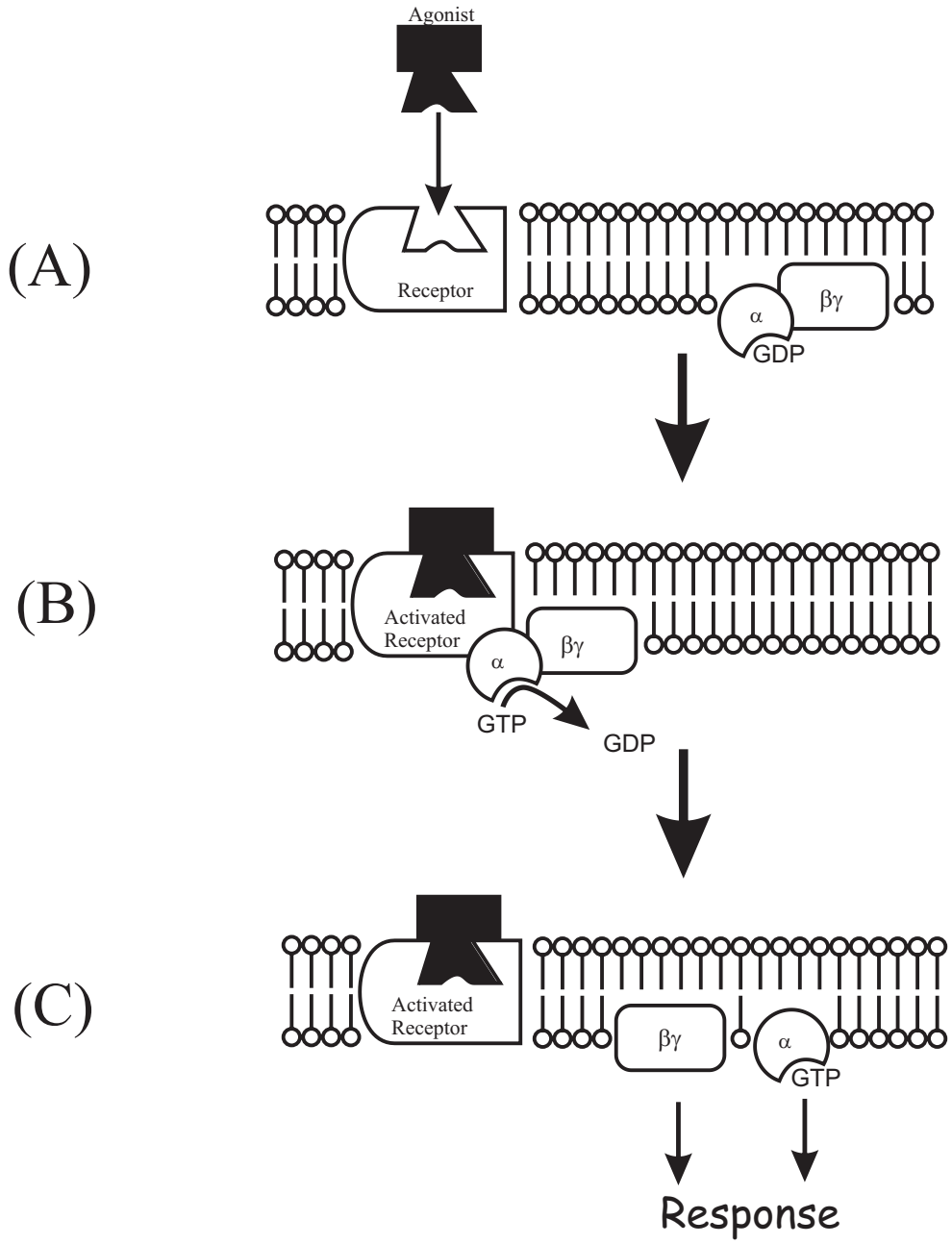

Figure 1.1

Schematic diagram of the cellular response mediated by G-proteins.

The binding of the ligand activates the receptor protein (A). The ligand-bound receptor complex promotes the exchange of GTP for GDP on the α-subunit of the G-protein trimer (B), causing the dissociation of the G_{α} and $G_{\beta\gamma}$ subunits. The $G_{\beta\gamma}$ subunits and the activated GTP-bound G_{α} subunits have separate and specific effects on different effector systems to evoke different cellular responses (C).

resulting cleavage of the G-protein may lead to the activation or regulation of a wide range of different targets, including enzymes such as adenylyl cyclase or phospholipase C, and ionic channels specific for K^+, Ca^{2+}, and Na^+ (figure 1.1). G-proteins are intrinsic GTPases. They are returned to an inactive state with hydrolysis of the bound GTP.

This thesis describes a wide-ranging investigation of G-protein coupled systems. The modulation of calcium (I_{Ca}) and chloride (I_{Cl}) currents in guinea-pig cardiac ventricular myocytes was used as a test system for characterising regulatory pathways. A number of novel findings are reported. These include the ability of rapidly photo-released GTP to produce sustained increases in I_{Ca} (Chapter 4); the multiple effects produced by the intracellular introduction of the non-hydrolysable guanine nucleotide analogue GTPγS (Chapter 5); and the differential modulation of I_{Ca} and I_{Cl} during sympathetic stimulation (Chapter 5). Chapter 6 contains a preliminary study of the responses due to the newly discovered G-protein coupled receptor for the neuropeptide Urotensin II, and Chapter 7 reports the stimulation of I_{Cl} by estrogenic agonists previously suggested to have a G-protein mediated inhibitory effect on I_{Ca} in the same tissue. The final chapter (Chapter 8) consists of a brief review of the entire study. Current research relevant to this thesis is summarised in the rest of chapter 1.

1.1 G-protein-coupled membrane receptor proteins

The demands of multi-cellular communication have meant a huge proliferation in G-protein coupled receptors (GPCRs), by far the largest family of cytoplasmic membrane protein receptors. Thus, while single cell yeast has only two GPCR genes, they make up some 5% of the 19100 sequenced genes from the nematode *Caenorhabditis*

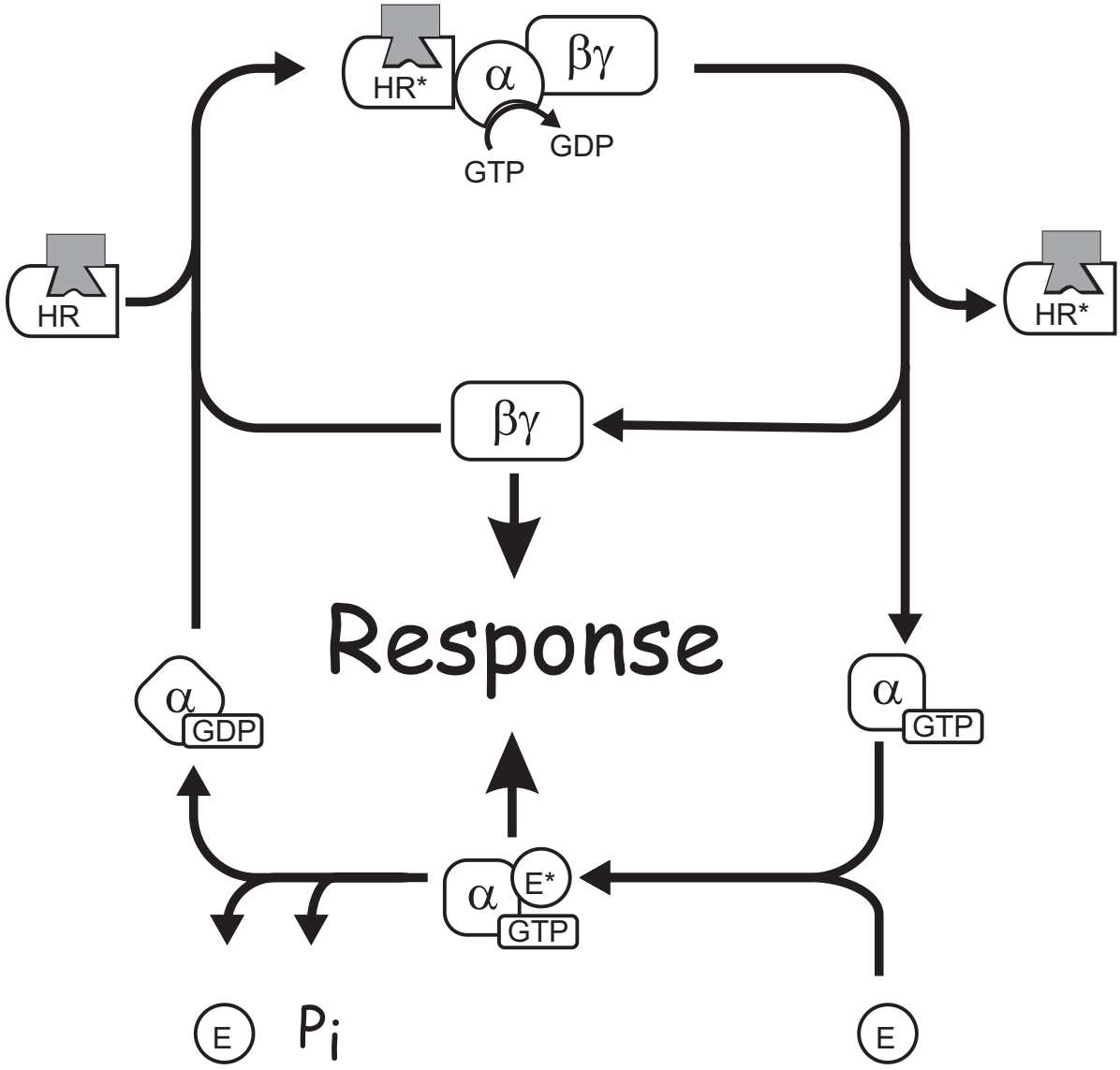

Figure 1.2

Schematic representation of the G-protein cycle. The ligand bound activated receptor (HR*) causes the exchange of GTP for GDP on the a-subunit of the G-protein trimer. This causes the dissociation of the G_a-subunit and the bg subunits from the receptor. The $G_{\beta\gamma}$ subunits and the activated GTP-bound G_α-subunit have separate and specific effects on different effectors (E*) until the intinsic hydrolase activity on the G_α-subunit catalyses the hydrolysis of the bound GTP to GDP. This allows the reassociation and inactivation of the G-protein.

elegans (Bargman, 1998). By analogy, the human GPCR metafamily could total 6,000 or more, most of which will be chemoattractant (odorant) receptors. Already, 300 non-odorant mammalian genes have been recognised, comprising three families.

1.1.1 Structure and function of G-protein coupled receptors

The low-abundance β-adrenoreceptor (βAR) was first purified using affinity chromatographic techniques (Shorr *et al.*, 1981), and the primary sequence of hamster-βAR was reported in 1986 (Dixon *et al.*, 1986). The cloning of other G-protein-coupled receptors has revealed a high degree of conservation in protein sequences.

1.1.1.1 Heptahelical structure of GPCRs

The characteristic presence of seven membrane-spanning α-helices in GPCRs has been determined by high-resolution electron diffraction studies of bacteriorhodopsin and confirmed by hydropathicity analysis (Roper *et al.*, 1994, Henderson & Schertter, 1990). Site-directed anti-peptide antibodies established that the NH_2-terminal domain and three of the segment domains are exofacial. The other three additional segments and the COOH-terminal were localized to the cytoplasmic face (Wang *et al.*, 1989, 1990). Though the schematic diagram in figure 1.2 is in a convenient serpentine form, photo-affinity labelling with high affinity antagonists shows that the receptor is organised, in reality, more like a basket of membrane spanning regions (Hockerman *et al.*, 1996, Strader *et al.*, 1995).

1.1.1.2 Ligand binding site

The ligand-binding site in receptors has been characterised mainly in studies of the β-adrenergic receptor. All of the evidence points to a locus within the plane of the seven trans-membrane domains, as much of the hydrophilic loops can be excised without affecting ligand binding. The introduction of specific mutations has isolated individual amino acids which interact with the agonist. Biophysical studies locate the β-adrenergic-binding site within a pocket in the receptor deep inside the membrane spanning domains (Fong & Strader, 1994). The surprising degree of identity between various G-protein coupled receptors at this putative ligand-binding site may explain the relative difficulty often encountered in finding totally specific ligands.

1.1.1.3 Isomerisation between active and basal conformations

Directed-mutations, site-selective fluorescent labelling and X-ray crystallography have all helped to formulate a surprisingly simple biochemical model for the operation of GPCRs. Structural constraints normally favour an inactive conformation preventing effective interaction between the G-protein and crucial peptide recognition sequences in the intracellular loops. Salt bridges between transmembrane helical domains 3 and 7 have been proposed to constrain the conformation of the rhodopsin (Robinson *et al.*, 1992). Agonist binding would relieve these constraints and allow GPCRs to adopt an active conformation. Purified β_2-receptors labelled with the cysteine-reactive fluorophone IANBD show a linear relationship between biological efficacy and fluorescence changes, and site-selective fluorescence spectroscopy reveals that the movement of transmembrane domains 3 and 6 underlies the isomerisation of GPCR into the active conformation (Gether *et al.*, 1995, 1997).

1.1.2 *Constitutive receptor activity*

The ability of some ligands ("inverse agonists") to depress receptor-mediated functions even in the absence of agonists (Ehlert, 1986) has revealed that a fraction of GPCRs exist in a spontaneously active conformation state (Lefkowitz *et al.,* 1993, Milligan *et al.,* 1995). Constitutive activity is seen most often when the receptor is over-expressed (Bond *et al.,* 1995) but can be observed even physiologically: Mewes *et al.* (1993) report that the β_1-selective antagonist, atenolol, reduced L-type I_{Ca} in isolated cardiac guinea-pig and human ventricular myocytes even in the absence of sympathetic stimulation. Constitutive activity is characterised by elevated basal G-protein activity and increased efficacy of both partial and inverse agonists. The level of basal signal transducing capacity varies among members of the GPCR family and even splice variants, as well as in different species and tissues depending on expression levels and G-protein/receptor stoichiometry.

The extended ternary complex model (Monod *et al.,* 1965, Leff, 1995) provides the simplest conceptual explanation for inverse agonism. The basal state in the absence of agonists is represented by a preponderance of the inactive conformation. Agonists increase the stability of the active conformation and shift the equilibrium towards activated receptors able to couple to G-proteins, while inverse agonists stabilise and thus reduce the proportion of receptors in the inactive state. Although basic thermodynamic considerations suggest a multitude of biochemical states (Tucek, 1997), the conceptual simplification of this all-or-none model of both spontaneous and agonist-induced receptor isomerisation has proved a useful abstraction.

1.1.3 *Receptor interactions with G-proteins*

Various experiments involving directed mutations point to the i_3 domain of the receptor as determining interactions with G protein activities but interactions between all the seven loops, especially with the i_2 domain, also play a part. Activation of the G_s protein by β-adrenergic receptors seems to involve a crucial cysteine residue (Cys341) also found in the amino-terminal tail of a number of other small ligand receptors. Post-transduction palmitoylation may introduce a crucial fourth intracellular loop which interacts with the G-protein. The intracellular i_2 and i_3 domains of some receptors (e.g. muscarinic and α_2-adrenergic) which are known to stimulate G_o and G_i contain copies of a 14-residue peptide sequence which is a strong candidate for the locus of G-protein interaction. The introduction of this short peptide fragment has been shown to directly stimulate G_o and G_i proteins (Strader *et al.*, 1995, Wong & Ross, 1994).

1.2 Guanine nucleotide binding-proteins

The existence of guanosine nucleotide binding proteins was first suggested by the requirement of GTP for hormonal activation of adenylyl cyclase (Rodbell & Birnbaumer, 1971). Catecholamine-stimulated GTPase activity was first assayed in turkey erythrocytes (Cassel & Selinger, 1977). Heterotrimeric G-proteins are part of a superfamily of regulatory GTP hydrolases which includes RAS and its homologs, and translation elongation factors. X-ray crystallography reveals a common shared core, and there is significant sequence identity suggesting a common evolutionary origin. G-proteins comprise three polypeptides termed $\alpha\beta\gamma$, in order of increasing mass: an α-subunit which contains the binding site for guanosine nucleotides as well as intrinsic

GTPase activity, and a $\beta\gamma$ dimer. The $\beta\gamma$ subunit serves effectively as a functional monomer.

1.2.1 G-protein α subunits

The G_α subunits are a family of 39-52 kDa proteins which are highly conserved at the amino acid level (~45-80%). The 20 genes so far identified fall into four classes on the basis of their homology: $G_\alpha s$ and $G_\alpha i$ activate and inhibit adenylyl cyclase (AC); $G_\alpha q$ activates phospholipase C; and $G_{\alpha 12}/G_{\alpha 13}$ probably regulate cytoskeleton and Na^+/H^+ exchange regulators.

1.2.1.1 Biochemical structure of G_α

G_α subunits are extrinsic membrane proteins, and tethering to the plasma membrane is helped by association with $G_{\beta\gamma}$ and post-translational lipid modification. The latter includes S-palymitoylation at a cysteine near the amino terminus (α_s, $\alpha_{i/o}$) and N-myristoylation at Gly-2 ($\alpha_{i/o}$). The GTP-bound α-subunit activates its specific effector protein still anchored to the cytoplasmic membrane. The construction of site-directed mutations and chimeras has identified consensus sequences responsible for providing a "binding pocket" for nucleotide binding and GTPase activity as well as association with receptors, down stream effector molecules and the $G_{\beta\gamma}$ subunit. In addition, the crystalline structure of the GTPγS bound $G_\alpha t$ has allowed the three dimensional structure to be elucidated (reviewed in Sprang, 1997).

The five-polypeptide loop forming the guanosine nucleotide recognition site is the most highly conserved element in the protein and defines the entire GTP-binding superfamily. The extreme carboxyl terminus of G_α plays a crucial part in determining

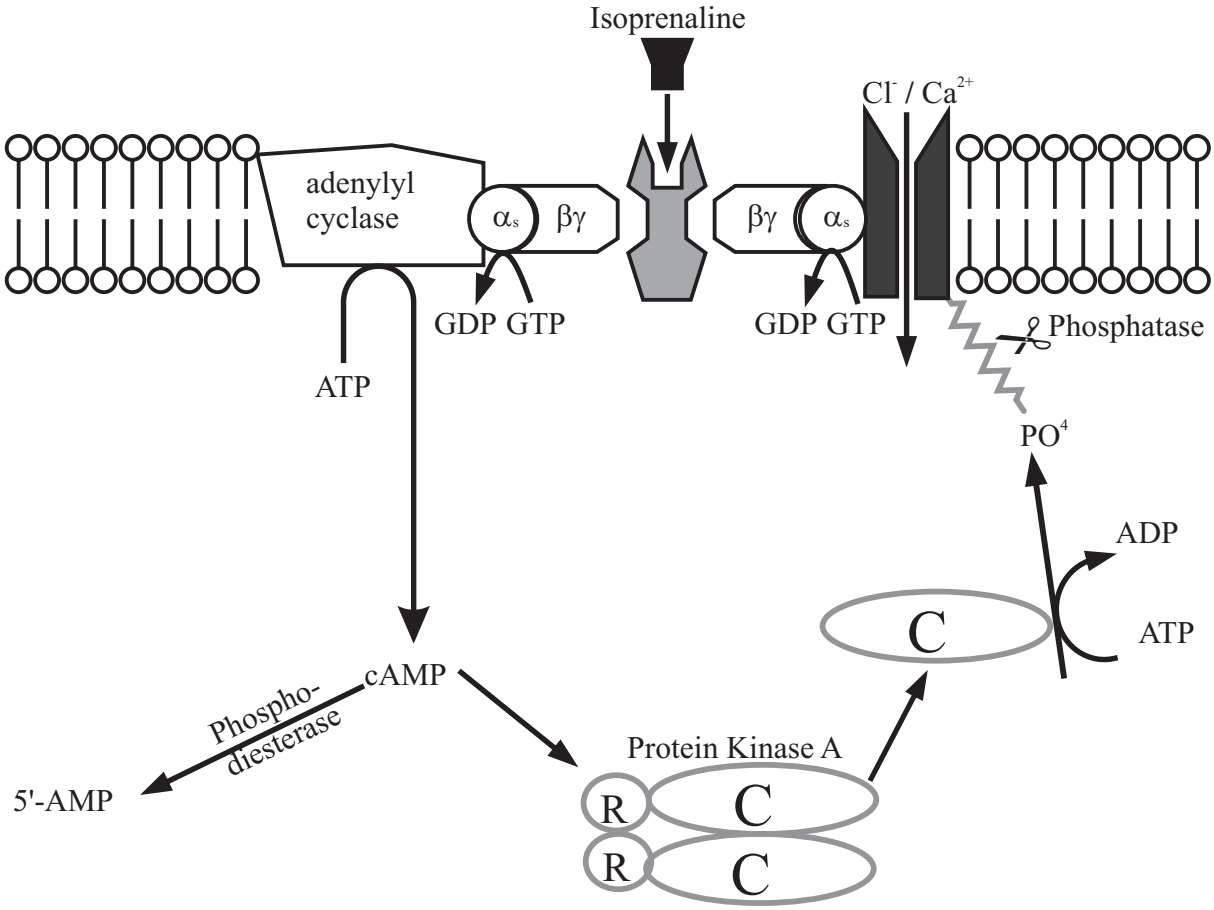

Figure 1.3

Schematic representation of the cAMP-dependent pathway. Binding of the ß-adrenoreceptor agonist promotes dissociation of G_s-protein. Activated $G_{\alpha s}$ subunits cause adenylyl cyclase to catalyse the formation of cAMP from ATP. cAMP binds to the regulatory (R) subunit of cAMP-dependent Protein Kinase A. The separation of the catalytic (C) subunit of cAMP-PKA allows it to phosphorylate ionic channel proteins to increase Cl^- or L-type Ca^{2+} current. When ß-adrenergic stimulation ceases, the G-protein eventually deactivates and reassociates. Production of cAMP stops and cytosolic cAMP is broken down by phosphodiesterase. The regulatory and catalytic subunits of cAMP-PKA recombine. Phosphorylated channels are dephosphorylated by specific phosphatases and

the specificity of G-protein-receptor interactions and can be disrupted by pertussis toxin (PTX), the main exotoxin of *Bordetella pertussis*. PTX catalysis of the ADP-ribosylation of a cysteine residue four residues away from the C-terminus inhibits interaction with the receptor and causes irreversible inactivation of G_i- and G_o- proteins (Gilman, 1987). This effect requires the presence of the $G_{\beta\gamma}$ dimer. The ADP-ribosylation by cholera toxin of G_s proteins of a conserved arginine residue (arg-201), in contrast, permits GTP-binding but abolishes GTPase activity to produce sustained activation (Freissmuth & Gilman, 1989).

1.2.1.2 G-protein activation cycle

The $\beta\gamma$ dimer normally binds to the GDP-bound α subunit of the G-protein to form an inactive heterotrimer. Release of GDP occurs only after a ligand or spontaneously activated heptahelical GPCR stabilises the nucleotide-free form of G_α, which can be considered the transition state for nucleotide exchange (figure 1.3). Though the nucleotide binding sites are virtually identical, the GDP exchange rate varies widely. However, these observed differences in binding affinity represent free energies that differ by only 1-3 kcal/mol (Sprang, 1997).

If GTP subsequently binds to G_α, this results in a change in conformation of three flexible regions, usually designated switch I-III, to an active conformation with a lowered affinity for both the receptor and $G_{\beta\gamma}$ (Wall *et al.*, 1995). GTP binding, therefore, leads to subunit dissociation and cleavage from the activated receptor. The exchange of GTP for GDP is kinetically irreversible: $G_{\beta\gamma}$ is required to stabilise the receptor-G_α interface (Phillips & Cerione, 1992) and G_α cannot reengage the receptor until the heterotrimer is reformed. Specific contacts between the γ-phosphate of GTP

and the switch II region also seem to stabilise potential effector binding sites, but all three switch regions form significant contacts with both $G_{\beta\gamma}$ and effectors (Sprang, 1997).

Energy derived from G-protein effector interactions contributes to the stability of the GTP complex and promotes the approach to the transition state for GTP hydrolysis. Intrinsic GTPase activity of the G-protein eventually auto-hydrolyses GTP to GDP. This causes the switch II region to collapse, dissipating the GTP binding energy and allowing G_α and $G_{\beta\gamma}$ subunits to reform the inactive trimeric G-protein again. Both G_αs and G_αi are sluggish hydrolases (3 min^{-1} for G_αi; Gilman, 1997, Bourne & Stryer, 1992) which seems inconsistent with known kinetics of signal transduction. The binding of other G-proteins to their cognate effector enzymes has been found to promote GTPase activity (e.g. $PLC_{\beta1}$ and G_αq; Biddlecome *et al.*, 1996), much like the effects of GTPase-accelerating proteins (GAPs) on RAS. The adenylyl cyclases and other effectors of G_αs and G_αi may serve a similar function.

If one assumes that the GTP:GDP ratio in the proximity of the G-protein is very high and that GTP binds rapidly to the empty site on a G_α subunit that has just released GDP, then the fraction of α subunits that are GTP-bound and activated in the above scheme can be derived. Cells contain ~100 μM GTP and 10 μM GDP with the k_d for GTP association with G_α in the nanomolar range (Bourne *et al.*, 1991). With the assumption that the GTP and GDP concentrations in the immediate vicinity of the G-protein are the same as in the bulk of the cytosol, the proportion of activated G_α should depend on both the relative rate of dissociation of GDP from the G-protein-GDP complex and the hydrolysis of GTP. If the two processes are governed by the rate

constants $k_{\text{GDP diss.}}$ and $k_{\text{GTP hydro.}}$, then the ratio between the GTP-bound active and the GDP-bound inactive forms can be given by:

$$[G_\alpha \bullet GTP^*] / [G_\alpha \bullet GDP] = k_{\text{GDP diss.}} / k_{\text{GTP hydro.}}$$

The role of the ligand-bound receptor and guanine nucleotide exchange factors (GEFs) would be to increase $k_{\text{GDP diss.}}$, thereby increasing $[G_\alpha \cdot GTP^*]$, while guanine nucleotide dissociation inhibitors (GDIs) have the opposite effect. A number of regulators of G protein signalling (RGS) which can increase (GAPs) or decrease $k_{\text{GTP hydro}}$ has been found for various heterotrimeric G-proteins (Bergman *et al.*, 1996) but not yet for G_αs. Given the *in vitro* measurements of basal $k_{\text{GDP diss.}}$ (<=0.1 min^{-1}) and $k_{\text{GTP hydro.}}$ (>= 3min^{-1}), the above scheme also suggests that the G-protein coupled system is normally clamped in the "off" state.

1.2.1.3 G-protein βγ dimers

The $G_{\beta\gamma}$ dimer is a tightly non-covalently bound complex which can only be separated under denaturing conditions (Schmidt *et al.*, 1992). Mammalian $\beta\gamma$ are attached to the plasma membrane by modification at the C-terminus of G_γ by a 20-carbon geranylgeranyl moiety. Prenylation is required for high affinity interaction with $G_{\beta\gamma}$ and adenylyl cyclase (Iniguez-Lluhi *et al.*, 1992), membrane tethering (Muntz *et al.*, 1992) and receptor coupling (Kisselev *et al.*, 1994).

Six cDNA have been identified so far for G_β ($\beta_{1\text{-}6}$), each of ~35 kDa and consisting of 340 residues sharing 55-90% identity. In other words, G_β is far more highly conserved than G_γ or G_α. In contrast, the 12 G_γ subunits, which contain 68-74 residues

(~8 kDa), are more diverse and can be divided into three subclasses based on their ~25-75% identity (Ray *et al.*, 1995). This has lead to the suggestion that the G_{γ} subunits are responsible for the functional specificity of the different $G_{\beta\gamma}$ dimers. There is evidence for expression of β_{1-3} and $\gamma_{5,}\gamma_{7,}\gamma_{10}$ and γ_{11} in the heart (Ray, 1996).

The $\beta\gamma$-subunits compete at the G_{α} effector binding sites and also increase the affinity of α-subunits for GDP by trapping the nucleotide in its binding pocket, both through increasing the rate of association and decreasing the rate of dissociation (Brandt & Ross, 1985). $G_{\beta\gamma}$ can also interact directly with different effector molecules, including muscarinic-gated atrial K^{+} channels (Logothetis *et al.*, 1987), phospholipase C-β_3 (Smrcka & Sternweis, 1993) and phospholipase A_2 (Kim *et al.*, 1989). Thus, one can also view G_{α} subunits as $G_{\beta\gamma}$ inhibitors.

There is no evidence for the separate activation of $G_{\beta\gamma}$ other than following the GTP binding and dissociation of G_{α} subunits. G_{α} auto-catalysed hydrolysis of GTP has a dual function in turning off the bifurcating $G_{\beta\gamma}$ and G_{α} mediated signalling pathways. The addition of GTP-bound α subunit can reverse the interaction of $G_{\beta\gamma}$ with its target. The most likely explanation is that the critical residues on the $G_{\beta\gamma}$ are only exposed after dissociation from G_{α}. Virtually no differences in the crystalline structure of $G_{\beta\gamma}$ even in the G_{α} binding regions can be detected between the bound forms and free $G_{\beta\gamma}$ (Wall *et al.*, 1995).

So far, the different forms of $G_{\beta\gamma}$ subunits seem functionally equivalent to and interchangeable between G-protein heterotrimers. The known $G_{\beta\gamma}$ subunits are less diverse than the G_{α}, with G_{β} and G_{γ} associating selectively both *in vitro* and *in vivo*.

Different $G_{\beta\gamma}$ subunits can interact with G_α and have similar activities (Graf *et al.*, 1992). The possible lack of target specificity has given rise to a number of questions. If all activation of any G-protein produces free $G_{\beta\gamma}$, then activities attributed to $G_{\beta\gamma}$ should always be visible regardless of the cause of the stimulus. Clearly, the very specific effects of the wide spectrum of hormones and neurotransmitters indicate that this is not so. The paradoxical ability of $G_{\beta\gamma}$ to act antagonistically to their G_α subunits in some systems has added to the puzzle. For example, the activation of the G_S-protein produces $G_{\alpha s}$ which stimulates adenylyl cyclase (AC). Yet, the $G_{\beta\gamma}$ liberated at the same time may have the opposite effect on some AC isoforms.

One possible explanation might be the differing levels of expression of different G-proteins in the cell and, thus, the varying relative concentrations of $G_{\beta\gamma}$ subunits which may be liberated on activation of G proteins. The reported effects of $G_{\beta\gamma}$ often require concentrations of one to two orders of magnitude greater than for G_α. Effective modulation by $G_{\beta\gamma}$ may only occur with G-proteins that are present at high levels. Thus, in the guinea pig ventricular myocyte, the $G_{\beta\gamma}$ liberated from G_S may be insufficient to have a significant effect on adenylyl cyclase, whereas activation of the much more abundant G_i protein might produce efficacious levels of $G_{\beta\gamma}$. Clearly, different tissue distribution of different G-protein subunit types, as well as the various GPCR and effectors, is of great importance.

An alternative explanation is that different G-protein systems are selectively concentrated in membrane microdomains. Signalling polypeptides, including receptors, G-proteins and effectors, might be found in close proximity (Neubig, 1994, Wedegaertner *et al.*, 1993, Iniguez-lluhi *et al.*, 1993) possibly in association with the

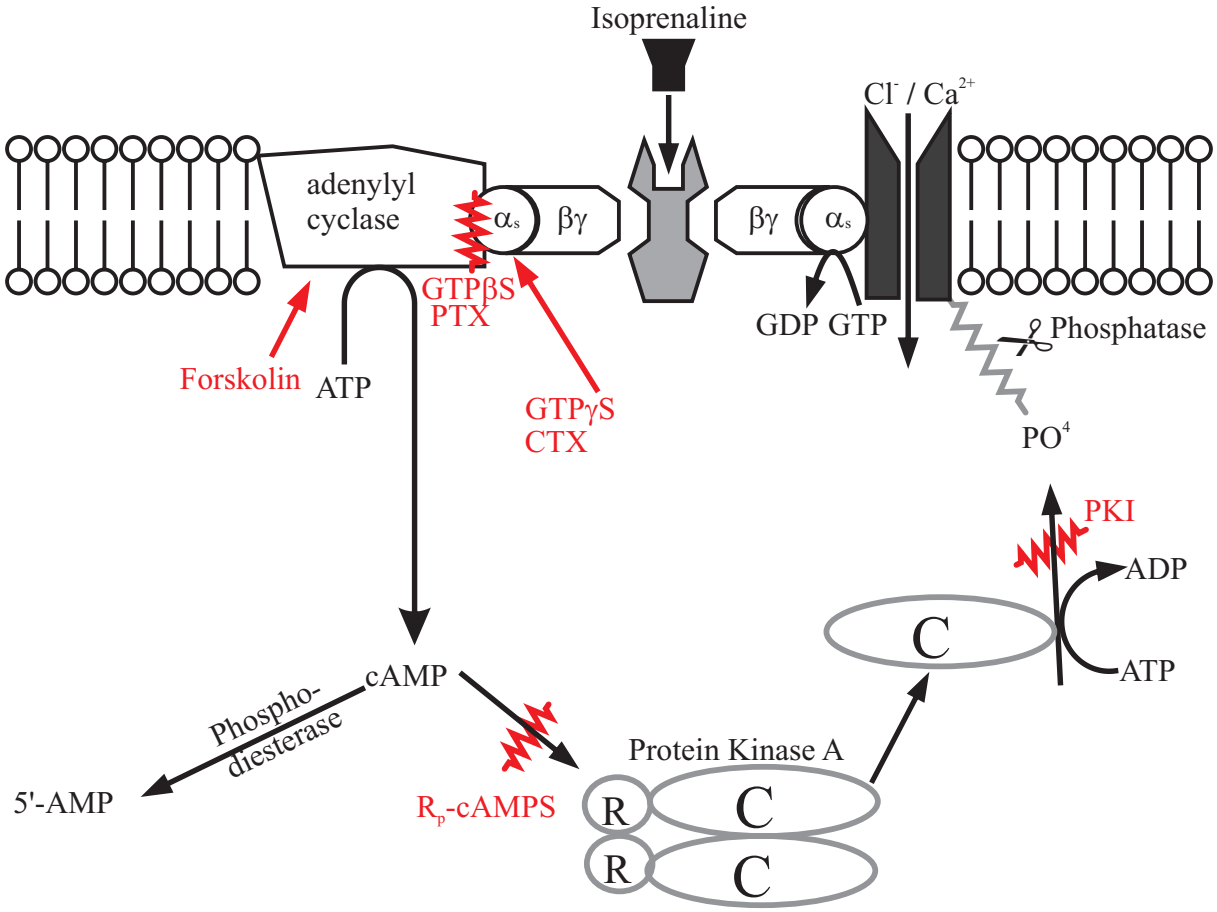

Figure 1.4

Schematic representation of the various points where the cAMP dependent response to ß-adrenergic agonist can be stimulated or blocked. Incubation of cholera toxin (CTX) induces constitutive activity in G_s-proteins while pertussis toxin incubation inactivates G_i-proteins. GTPγS and GDPßS are non-hydrolysed GTP analogues which produce persistent activation and deactivation of G-proteins. Forskolin binds to and activates adenylyl cyclase. R_pcAMPS is a cAMP antagonist and the phosphorylatory activity of cAMP-PKA can be blocked by Protein Kinase Inhibitor (PKI).

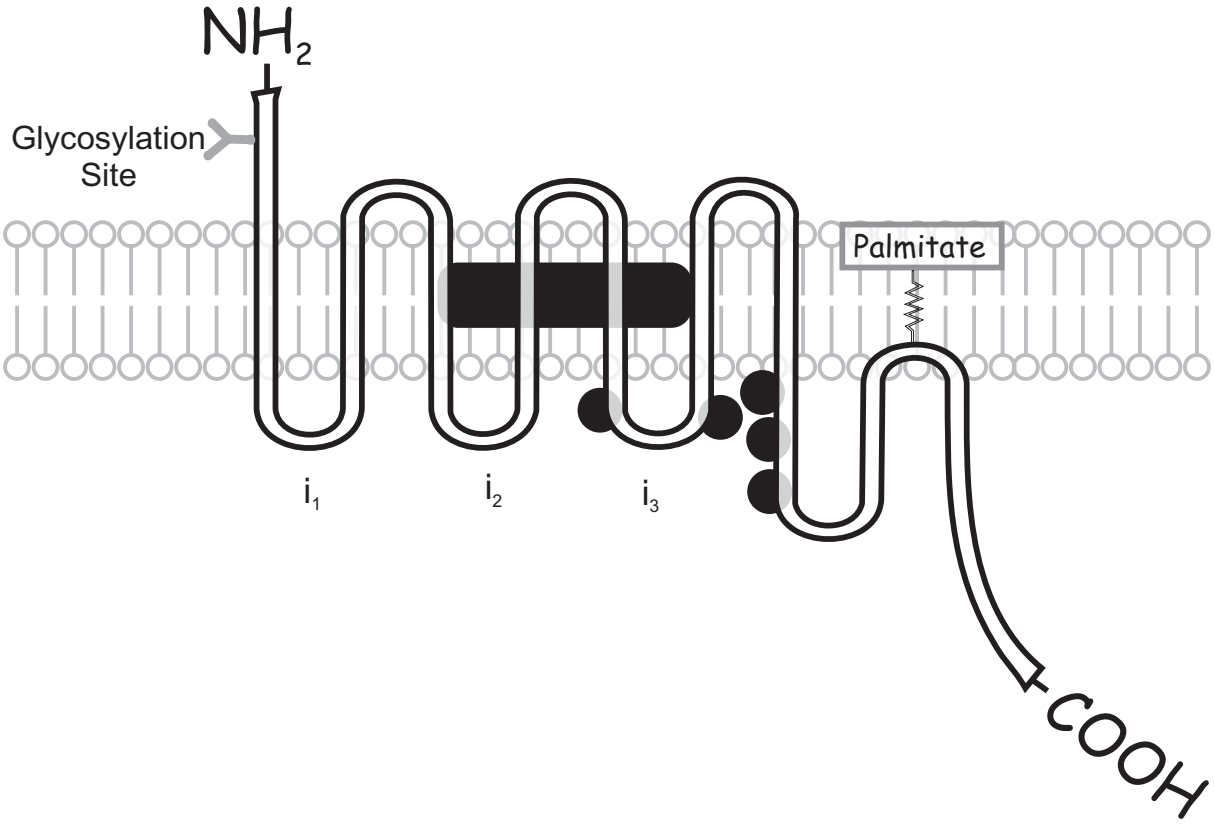

Figure 1.5

Schematic representation of a heptahelical G-protein coupled receptor embedded in cell membrane phospholipids. The extracellular amino side contains multiple glycosylation sites. Ligand binding takes place in the plane of the seven transmembrane domains (marked with a solid bar) in a deep pocket over 11Å within the membrane. Post-transduction palmitoylation introduces a fourth intracellular loop in the adrenergic receptor family. Site mutation sites on the second and third intracellular loops lead to constitutive activation of the receptor indicating possible G-protein coupling regions.

cytoskeleton (Song *et al.*, 1996). Stimulation of the receptor would provide very fast modulation of the target. The activated and dissociated G-proteins subunits would remain in the locality, forming a closed system. This would contribute to specificity of hormone stimulation and increase the fidelity of signal transmission.

1.3 The cAMP dependent cascade

The classical example of an effector molecule for G-proteins has been the enzyme adenylyl cyclase which catalyses the production of the soluble second messenger adenosine 3′,5′-monophosphate (cyclic AMP or cAMP) from Mg^{2+}-ATP. The role of cAMP was first recognised in the hyperglycaemic response to adrenaline and glucagon in the liver by Earl Sutherland in the late 1950s (Rall *et al.*, 1957, Rall & Sutherland, 1958). The stimulation of adenylyl cyclase, typically by $G_{\alpha s}$, leads to an increase in cAMP levels which, in turn, activates ubiquitous cAMP-dependent kinases (Protein Kinase A or cAMP-PKA). Protein phosphorylation using ATP as the phosphate donor produces the final physiological effect, for example, an increase in the opening probability of ionic channels (figure 1.4).

Adenylyl cyclases are large (~120 kDa) membrane bound single polypeptides which were first purified using affinity chromatography (Pfeuffer & Metzger, 1985). Nine mammalian isoforms have so far been cloned from complementary DNA. They consist of two large (~40 kDa) cytoplasmic domains (C_1 and C_2) which each follow a transmembrane stretch with six alpha helices (M_1 and M_2) (figure 1.5). The C_1 and C_2 domains have ~230 residues (C_{1a} and C_{2a}) that share more than 50% identity and together form the catalytic core (Tang *et al.*, 1995). The diterpene forskolin derived from the root of the Indian plant *Coleus forskolhii* binds to a highly conserved hydrophobic

crevice at the C_{1a}, C_{2a} interface. The binding affinity (Kd) corresponds to the EC_{50} for forskolin activation of adenylyl cyclase (Dessauer *et al.*, 1997).

The $G_{\alpha s}$ binds to residues ~30 Å away from the catalytic site (Yan *et al.*, 1997) to stimulate catalysis allosterically, probably by a rotational alignment of C_1 and C_2 allowing both Mg^{2+} and ATP binding, and transition state stabilisation. $G_{\alpha i}$ inhibits adenylyl cyclase activation by attachment to a site pseudosymmetrically related to the $G_{\alpha s}$ binding groove and may rotate C_1 in the opposite direction to that induced by $G_{\alpha s}$ (Hurley, 1999). The type V and VI adenylyl cyclases expressed mainly in the heart (Sunhara *et al.*, 1996, Gao *et al.*, 1997) are only inhibited by $G_{\alpha i}$ and do not interact with $G_{\beta\gamma}$ (Taussig *et al.*, 1993, 1994).

PKA normally exists in an inactive holoenzyme complex consisting of two regulatory and two catalytic subunits. The cAMP mediated dissociation frees the phosphorylatory activity of the catalytic subunits (Corbin *et al.*, 1977):

$$R_2C_2 + 4\,cAMP \rightarrow R_2\,cAMP_4 + 2C$$

The initial presentation of a ligand at the receptor molecule is amplified at each turn in the cAMP-dependent cascade. Each ligand-bound receptor can activate multiple G-proteins molecules. Each adenylyl cyclase molecule produces many cAMP molecules. Finally, a single protein kinase molecule can phosphorylate many serine and threonine residues. Eventually, stimulation ends with the hydrolysis of GTP and the inactivation and re-association of the G-protein. The activity of adenylyl cyclase persists for only as long as activated G_{α} is present. The elevated levels of cAMP are restored by the action of

cAMP phosphodiesterases, and the phosphorylation of the final target proteins is reversed by protein phosphatases (figure 4).

The use of the gigaohm patch pipette seal as a lateral diffusion barrier has provided conclusive proof of the physiological role of soluble second messengers such as cAMP. Application of the neurotransmitter serotonin to sensory nerurons from the abdominal ganglion of *Aplysia* would be expected to activate only receptors outside the patch. The closure of potassium channel inside the patch electrode can only be explained by the diffusion of such a soluble second messenger inside the cell (Camardo *et al.*, 1983).

1.3.1 Stimulation of cardiac calcium current

The β-adrenergic stimulation of the L-type Ca^{2+} channel is one of the best studied hormonal systems. Unequivocal evidence has accumulated to demonstrate that this stimulatory pathway is mediated by the G_s-protein, production of cAMP and protein kinase A phosphorylation of the channel protein. Cardiac myocytes were among the first excitable cells whose membrane properties were shown to be regulated by cAMP (Tsien, 1973; Reuter, 1974). The application of isoprenaline increases cardiac calcium current (I_{Ca}) with a threshold and half-maximal dosage of ~1 and ~50 nM respectively.

1.3.1.1 Evidence from the stimulation of the cAMP cascade

The involvement of the cAMP in the β-adrenergic stimulation of cardiac calcium current has been demonstrated in electophysiological experiments observing I_{Ca} directly or indirectly during a number of biochemical or pharmacological interventions known to stimulate the cascade. These have included the application of cAMP, membrane-

permeable derivatives of cAMP or derivatives which are resistant to hydrolysis by phosphodiesterase, activators of adenylyl cyclase and inhibitors of phosphodiesterase.

Direct stimulation of adenylyl cyclase by forskolin increases I_{Ca} by the same degree as β-adrenoreceptor stimulation (Seamon & Wetzel, 1984). The direct application of membrane permeable analogues of cAMP such as dibromo-cAMP has the same effect (Reuter, 1974). Xanthine derivatives such as 3-isobutyl-1-methylxanthine (IBMX) inhibit phosphodiesterase activity, preventing cAMP hydrolysis and thus increasing both I_{Ca} and the upstroke velocity of Ca^{2+} dependent slow action potentials. The rapid release of intracellular cAMP from its caged derivative, o-nitrobenzyl cAMP, by flash photolysis also causes rapid elevation of I_{Ca} (Nargeot *et al.*, 1983). Similarly, addition of the catalytic (C) subunit of Protein Kinase A leads to an increase in I_{ca} (Osterrieder, 1982). The increases of I_{Ca}, whether by application of isoprenaline, cAMP or PKA C-subunit, were of similar magnitude. At maximal concentrations, however, the effects are not additive, suggesting that all three act on a common pathway. Finally, evidence that phosphorylation causes the β-adrenergic stimulation of I_{Ca} is provided by the use of the ATP analogue adenosine-5′-O-(3-thiosulphate) (ATPγS) which causes irreversible thiophosphorylation of proteins immune to the action of naturally occurring phosphatases. Intracellular application of ATPγS causes a slow but steady rise in I_{Ca} (no doubt due to basal phosphorylatory activity), which turns into a dramatic and sustained increase in I_{Ca} when the myocyte is additionally superfused with threshold concentrations of isoprenaline (Kameyama, M. *et al.*, 1986).

The dose-response curve for activation of I_{Ca} by β-agonists (isoprenolol), cAMP and PKA can all be predicted from the levels of second messengers produced by

β-adrenoreceptor activation. The estimated cAMP concentrations for half-maximal activation of Protein Kinase A was 5 μM which is within reasonable range of *in vitro* measurements (Kameyama, M. *et al.*, 1985, Corbin & Keely, 1977).

1.3.1.2 Evidence from the blockade of the cAMP cascade

The use of a variety of agents which block the cAMP cascade at different points has demonstrated that this pathway is responsible for the effects of pharmacological manipulation of cAMP levels (figure 1.6). As expected, these agents also prevent *β*-adrenergic stimulation from increasing cardiac I_{Ca}. Adenosine 3′,5′-(R_p)-monophosphorothioate (R_pcAMPS) is a cAMP analogue which binds to the regulatory R-subunit of cAMP-dependent protein kinase A and prevents cAMP-caused dissociation and activation of the holoenzyme (DeWit *et al.*, 1984, Van Hastert *et al.*, 1984). The application of R_pcAMPS inhibits the effects of isoprenaline (Hesheler *et al.*, 1987) and forskolin. Protein kinase inhibitor (PKI), a heat stable synthetic peptide, inhibits the response to sympathetic stimulation of I_{Ca} (Ashby & Walsh, 1972). The application of the purified R-subunit of the cAMP-PKA (Ostreider *et al.*, 1986; Kameyama *et al.*, 1985) has a similar effect, presumably by binding to and inactivating free catalytic C-subunits. This inhibitory action of the cAMP-PKA R-subunits can be reversed in turn by isoprenaline, apparently by producing cAMP to bind to the injected R subunits and preventing them from mopping up the C subunits. The effects of *β*-adrenergic stimulation of I_{ca} are largely suppressed by the infusion of 5′-adenylyl-imidodiphosphate (AMP-PNP), a non-hydrolyzable ATP analogue whose γ-phosphate is not available as a donor for protein kinases (REF).

1.3.2 *Physiological inhibition of the cAMP cascade*

Cholinergic muscarinic receptors are also linked to the cAMP cascade. However, the response to ligand binding is mediated through the G_i-protein rather than G_S, and the effect is to reduce rather than increase adenylyl cyclase activity. G_{α_i} has a direct inhibitory effect on cardiac type V & VI adenylyl cyclase. $G_{\beta\gamma}$ subunits released by dissociation of the G_i-protein may also have an inhibitory role in reversing G_s stimulation through mass action by encouraging the reformation and inactivation of the G-protein. The convergence of the different pathways allows complex modulatory patterns to provide sensitive fine-tuning of any response.

1.4 G-protein mediated cardiac Ca^{2+} channel modulation

The G_s-protein which stimulates adenylyl cyclase mediates important effects of *β*-adrenergic catecholamines such as the increase in rate and force of contraction in the heart. A key feature in both these positive chronotropic and ionotropic effects is the enhancement of L-type Ca current ($I_{Ca,L}$) in cardiac atrial and ventricular myocytes and pacemaker tissue. This is one of the best-studied examples of G-protein mediated intracellular signalling pathways.

The levels of calcium concentration have long been recognised as vitally important for the control and modulation of essential cellular responses in the heart. Voltage-gated L-type Ca^{2+} channels in the cytoplasmic membrane are a primary regulatory site of Ca^{2+} homeostasis. Calcium current through this 1,4-dihydropyridine sensitive channel underlies the plateau of the cardiac action potential and is the most important route of entry for Ca^{2+} into cardiac myocytes. First described in the heart, $I_{Ca,L}$

is characterized by high Ca^{2+} sensitivity and selective modulation by neurotransmitters, G-proteins and second messengers (Hess *et al.*, 1986).

The amount of Ca^{2+} that enters the cell via $I_{Ca,L}$ seems insufficient to activate the myofilaments directly in either human or guinea pig ventricular cells, making a contribution of around 10% to the total amount of systolic Ca^{2+} (Wier, 1990). However, Ca^{2+} entry into the restricted space between plasma membrane and the sarcoplasmic reticulum (Sham *et al.*, 1995) results in an elevation of local internal Ca^{2+} from baseline values of ~0.05 μM to peaks of ~7 μM (Lòpez-Lòpez *et al.*, 1995). This is sufficient to trigger Ca^{2+} release from internal stores in the sarcoplasmic reticulum (Fabiato, 1985; Nabauer *et al.*, 1989) via the ryanodine receptor Ca^{2+} release protein (RyR-2) (Smith *et al.*, 1986; Rousseau *et al.*, 1986; Holmberg & Williams, 1989), which initiates the contraction of the myocyte. The entry of calcium ions is balanced by active extrusion of Ca^{2+} across the sarcolemma and re-sequestration by internal Ca^{2+} stores. A change in I_{Ca} may result both in an immediate increase in internal Ca^{2+} concentration and, indirectly, in more sequestration and discharge of Ca^{2+} from internal stores and, hence, an increased availability of systolic free Ca^{2+} for activation of the contractile mechanism. The consequences would include an increase in peak tension, a reduction in time-to-peak tension and an increase in the rate of relaxation, i.e., a positive ionotropic effect.

Current through these channels ($I_{Ca,L}$) activates rapidly during action potentials, reaching a peak within 10 ms and inactivating over the next hundred ms.

1.4.1 *Structure of L-type Ca^{2+} channels*

Initial purification and molecular cloning of the skeletal L-type channel and subsequent homology screening studies have revealed that the cardiac channel ($Ca_v1.2$) is

a heterooligomeric complex consisting of multiple subunits: $\alpha_{1}1.2$ ($\alpha 1C_{1}$ in older nomenclature), the intracellular β_{2a}, and $\alpha_{2}\delta$ (posttranslationally cleaved into the extracellular α_{2} covalently linked by disulphide bonds to the transmembrane δ) (Biel *et al.*, 1991, Hofmann *et al.*, 1999). The co-expression of the rabbit $\alpha_{1}1.2$, $\alpha_{2}\delta$ and β_{2} subunits is sufficient to induce L-type currents in human embryonic kidney (HEK 293) and Chinese hamster ovary cells which were comparable in size to cardiac myocytes (Zong *et al.*, 1995). The pore-forming $\alpha_{1}1.2$ contains the high affinity 1,4-dihydropyridine (DHP) binding site, voltage sensor, selectivity filter and the ion-conduction pathway. It is also responsible for both voltage and Ca^{2+}-dependent inactivation (Zong & Hofmann, 1996) and is, thus, the principal component of the voltage-sensitive channel.

1.4.1.1 L-type Ca^{2+} channel α subunit

Hydropathic analysis of $\alpha_{1}1.2$ subunit indicates four repetitive domains of similarity (I-IV) each containing five hydrophobic α helices and one amphiphatic segment spanning the membrane (S1-S6) and surrounding a central ion permeation pore. The permeation pathway is formed partly by linker regions between each S_5 and S6 transmembrane segment. By analogy with the deduced potassium channel structure, the pore is envisaged to be in the shape of an inverted tepee converging to a narrow intracellular zone. Mutational analysis suggests just four glutamic acid residues form a single high affinity binding site responsible for Ca^{2+} selectivity, which may be accessed by two Ca^{2+} ions at a time to allow rapid permeation (Ellinor *et al.*, 1995). Both the short amino-terminal and the long carboxyl-terminal tails of $\alpha 1$ are located in the cytoplasm.

Deletion mutations suggest that the latter serves as a critical component of the gating structure that influences inactivation properties of the channel.

1.4.1.2 Other L-type Ca^{2+} channel subunits and accessory polypeptides

Both the α_2/δ and β subunits are constituents of the cardiac channel complex and can induce changes in channel activity (Mori *et al.*, 1991; Varadi *et al.*, 1991). Co-expression of both $\alpha_2\delta$ and β_{1a} with the cardiac α_1 subunit in *Xenopus* oocytes results in an increase in current amplitude, activation at more negative membrane potentials, a steeper voltage dependence of activation and inactivation and a more rapid current time course (Singer *et al.*, 1991). The β subunit also helps in the translocation of α subunits to the sarcolemmal surface (Gao *et al.*, 1999) and may be essential for modulation by protein kinase C (Bouron *et al.*, 1995).

Other accessory polypeptides in close association with the channel may be necessary for its physiological behaviour. The *in vivo* interaction between α_1 subunit and the cardiac ryanodine receptor (RyR-2) may depend on a co-immunoprecipitating 22kDa protein, sorcin (Meyers *et al.*, 1998), suggesting that modulation of small peptides could provide a further source of regulation of L-type Ca^{2+} channel activity.

1.4.2 Pharmacology of L-type Ca^{2+} channels

L-type channels are selective targets for three groups of classical calcium channel blockers: the 1,4-dihydropyridines (DHPs), phenylalkylamines and benzothiazepines. Chimeric constructs demonstrate that all three bind to the transmembrane region of repeat IV of the α_1 subunit (Hofmann *et al.*, 2000), with additional sites on repeat II and repeat I for DHP. The specificity of agonists is higher than antagonists in different cell

types. In the cardiac myocyte, however, $I_{Ca,L}$ is completely blocked by sub-micromolar concentrations of DHP antagonists.

1.4.3 Biophysical characteristics of L-type Ca^{2+} channels

Upon depolarisation, permeability to calcium in the cardiac myocyte increases dramatically over a period of several ms before decreasing to the baseline level over a period of hundreds of milliseconds. This biphasic behaviour results from two separable gating processes, voltage-dependent activation and inactivation.

1.4.3.1 Activation kinetics

L-type Ca^{2+} channels do not open until the membrane potential becomes more positive than about -40 mV. Large depolarisations produce corresponding rapid activation of $I_{Ca,L}$, and peak currents are maximal for depolarising pulses to +10 mV. Single channel recordings reveal that opening probabilities are steeply voltage-dependent reaching a plateau after -10 mV. Further depolarisations decrease the dispersals in the distributions of openings, so that the individual openings sum together more effectively to give a greater peak current (Zagotta & Aldrich, 1990).

A typical 200 ms depolarisation will reveal bursts of multiple channel openings of less than 1 ms duration on average, i.e., brief openings are separated by shorter or longer times in the closed state. Descriptions of these gating kinetics are usually based on variants of the following three-state diagram (Fenwick *et al.*, 1982) :

$$C_1 \underset{k_{-1}}{\overset{k_1}{\rightleftharpoons}} C_2 \underset{k_{-2}}{\overset{k_2}{\rightleftharpoons}} O$$

The sequence describes a Markov chain in which k_1 and k_2 are voltage dependent steps leading from the two closed states "C_1" and "C_2" to the conducting open state "O". The occupancy of each state is probabilistic and memory-less. The two closed states would explain the binary closed times distribution where brief closures within each burst would be described by occupancy of the "C_2" state while the channel would be in the "C_1" state between each burst. The rate constants in the model can be computed from time histograms.

1.4.3.2 Mode switching in L-type Ca^{2+} channels

Single channel traces also show periodic sudden changes in gating kinetics. Some test depolarisation traces contain no channel openings at all, i.e. so-called "null" sweeps, while other produce brief openings with single channel conductances of ~7 pS in 10 mM Ca^{2+} and ~15-20 pS with 100 mM Ba^{2+} (Hess *et al.*, 1986; Rosenberg & Chen, 1991). In addition, there are occasional clusters of openings with far longer mean durations. This behaviour is normally observed only during the application of 1,4-dihydropyridine agonists such as BAY K 8644 and CGP 28392 (Brown, A.M. *et al.*, 1984). These different patterns of activity tend to persist for several seconds across test step depolarisations suggesting that they are genuine manifestations of two distinct biological processes, rather than the result of arbitrary kinetic analysis. Hess *et al.*, (1984) have postulated the existence of three different modes of channel behaviour based on reversible allosterical changes in the physical structure with slower kinetics, each with the above two closed states and one open state. Mode 0 describes traces with sparse openings, while Mode 1 describes the common bursts of channel activity with short openings. Finally, traces with

long openings are described by Mode 2. These changes in gating kinetics are never accompanied by variations in single channel conductances.

Mode switching seems to occur spontaneously but can also be induced by depolarisation (Peitrobon & Hess, 1990). Dihydropyridine agonists seem to promote long channel openings (mode 2 behaviour) and while dihydropyridine antagonists induce periods with sparse openings or "null" sweeps (mode 0 behaviour). This can be explained in terms of state-dependent binding (Nowycky *et al.*, 1985, Hess *et al.*, 1984). The antagonists bind preferentially to and stabilise channels in mode 0 conformation, while agonists such as BAY K 8644 bind preferentially to channels in mode 2.

β-adrenoreceptor activation also seems to decrease the number of "null" sweeps observed (Brum *et al.*, 1984, Tsien *et al.*, 1986; Yue *et al.*, 1990; Ochi *et al.*, 1990), as well as increasing the mean channel open time (by 1.5-2 times; Brum *et al.*, 1984) and incidence of channel openings (Bean *et al.*, 1984). As with the application of dihydropyridine agonists, the amplitude of the unitary current was not affected. In terms of the above modal schema, stimulation of the *β*-adrenoreceptor pathway, much like the application of dihydropyridine agonists, causes the L-type Ca^{2+} channels to spend more time in the mode 2 configuration and exhibit less mode 0 behaviour.

1.4.3.3 Modeless Model of Ca^{2+} channel gating

The sudden shifts in channel behaviour have also been described in terms of a non-modal model where a fourth state describes channels unavailable for opening seen during "null sweeps", for example in Cavalie *et al.*, (1986). A second open state "O_2" might account for openings for long durations (Brown *et al.*, 1986).

1.4.3.4 Inactivation of L-type Ca^{2+} channels

Macroscopic L-type Ca^{2+} channels exhibit both voltage-dependent and a slower Ca^{2+} entry-dependent inactivation (Kass & Sanguinetti, 1984). Inclusion of a calcium chelator EGTA slows the rate of inactivation of I_{Ca}. Such current-dependent inactivation is not seen when Ba^{2+} is used in place of Ca^{2+} as the charge carrier, and the current decays over several hundred milliseconds (Eckert & Chad, 1984).

The S6 segment of repeat I and its flanking regions and the intracellular carboxy-terminal sequences are critical for the inactivation properties. Ca^{2+}-dependent inactivation serves as a local negative feedback mechanism and seems to require a single binding site with an IC_{50} of 4 μM Ca^{2+}(Haack & Rosenberg, 1994, Höfer *et al.*, 1996). Mutation studies indicate this Ca^{2+} binding site is between residues 1513 and approximately 1700. Its exact locus is, nevertheless, still not entirely clear and may involve an EF-hand binding motif (Babitch, 1990, but see Bernatchez *et al.*, 1998).

I_{Ba} through L-type channels commonly decays with bi-exponential kinetics suggesting that Ca^{2+} independent inactivation also involves both fast and slower voltage-dependent processes. Directed mutagenesis and studies of splice variants, chimeras and pathological wild-type mutations indicate that the molecular determinants of inactivation are widely spread over the α1 subunit and may involve interactions with other proteins. The precise molecular mechanisms involved are, however, still obscure (Hering *et al.*, 2000).

1.4.4 Physiological phosphorylation of the cardiac L-type channel

cAMP-dependent phosphorylation of the α_1 subunit or a closely associated protein increases the current 3 to 7- fold (Kameyama *et al.*, 1985; Haase *et al.*, 1993,

Sculptoreanu *et al.*, 1993). The increase in Ca^{2+} current following *β*-adrenergic stimulation is accompanied by a significant negative shift of the voltage-dependent parameters of L-type channels, including both activation and inactivation kinetics (Tiaho, Nargeot & Richard, 1991). A negative shift in the voltage dependence of the gating charge movement has been recorded in embryonic chick cardiac cells, suggesting that the core channel subunits are modulated by phosphorylation (Josephson & Sperelakis, 1991).

The mechanism causing channel modulation *in vivo* is controversial and may be dependent on the expression of different splice variants and posttranslational truncations at the COOH-terminal. At least two different phophorylation sites seem to be involved since the modulatory changes can be differentially affected by phosphatase inhibitors (Hartzell *et al.*, 1995, Ono & Fozzard, 1993).

1.4.4.1 Reconstitution of protein kinase mediated current facilitation

Where *Xenopus* oocytes have been injected with cardiac mRNA, cardiac L-type channels have been expressed with the requisite electro-physiological and pharmacological characteristics, including response to both *β*-adrenergic agonists and injected cAMP. The potentiation mimics perfectly native ventricular cells and can be blocked by cAMP-PKA inhibitors (Lory *et al.*, 1990). However, even though high levels of expression L-type Ca^{2+} channels have been achieved with the injection of Ca^{2+} channel subunit cloned mRNA, the calcium currents have not been potentiated by PKA even under conditions optimised to promote phosphorylation (Zong *et al.*, 1995). This failure is due most probably to the additional requirement of the cAMP kinase anchoring protein AKAP 79 or its kin (Gao *et al.*, 1997).

Another possibility is the partial proteolysis of a potential cAMP-PKA phophorylation site on the carboxy-terminal of the $\alpha_1$1.2 in transfected cells (Yoshida, A. *et al.*, 1992). The primary sequence for $\alpha_1$1.2 contains several consensus sequences for the PKA-mediated phosphorylation which are not present in the short form purified from cardiac muscle (Chang & Hosey, 1988; Schneider & Hofmann, 1988). Whether this post-translational truncation is also seen *in vivo* in the intact myocyte is still a matter of some controversy.

1.4.5 *Phosphorylation and maintenance of basal activity of* $I_{Ca,L}$

Phosphorylation of L-type Ca^{2+} channels in response to β-adrenoreceptor stimulation leads to enhancement of activity including an increase in the number of active channels susceptible to activation by depolarisation. It has been suggested that basal phosphorylation is also necessary for the channels to open. Ca^{2+} channels activity is characterised by a gradual run-down which is particularly pronounced in excised patches. This can be slowed or even temporarily reduced by adding ATP and Mg^{2+}, cAMP or the catalytic subunit of cAMP-PKA to the intracellular medium (Chad, *et al.*, 1987). Channel survival in excised patches and inactivation is prolonged by phosphorylation and accelerated by de-phosphorylation. However, Kameyama *et al.*, (1988) have presented evidence that an elutable intracellular component rather than dephosphorylation is responsible for run-down. However, this is not to say that constituent basal cAMP-dependent phosphorylation of the channel does not maintain the level of calcium current found physiologically.

1.4.6 Direct modulation of L-type Ca^{2+} channels by the G_s-protein

1.4.6.1 "Membrane-delimited" modulation of ionic channels

Most examples of G-proteins as modulators of ion channel function involve the production and diffusion of soluble second messengers as an intermediate step. Ion channels were previously considered to be downstream targets of cytoplasmic regulatory pathways rather than G-protein effectors in the same way as adenylyl cyclase or cGMP phosphodiesterase. This view has changed with the discovery of a growing number of ion channel proteins which interact directly with various G-proteins. In some systems, the evidence suggests that the regulatory pathway does not involve the diffusion of soluble second messengers but does not rule out mediation by other membrane regulatory proteins. The term "membrane-delimited" serves to cover all these different cases.

Strong evidence for direct modulation of ion channels was first obtained for muscarinic (M_2) activated inward-rectifying atrial K^+ channels (K^+[Ach]). The involvement of soluble second messengers was ruled out because K^+[Ach] channels in a membrane patch were only opened by pipette ACh and in the bath: the walls of the pipette forming a diffusion barrier. A G-protein link was nevertheless pointed to by the long channel activation response time, the absolute requirement of GTP, the blocking effects of pertussis toxin incubation, and the ability both of non-hydrolysable GTP analogues to sustain K^+ current after ACh withdrawal and GTPγS to evoke single channel currents directly. When activated PTX-sensitive $G_{\alpha,i}$ subunit was applied to K^+[Ach] channels in excised, inside-out patches, single channel current could be observed. Antibodies specific to $G_{\alpha i3}$ blocked the muscarinic response (Codina *et al.*, 1987, Yatani *et al.*, 1987). Full activation of $I_{K,ACh}$ requires $G_{\beta\gamma}$. The application of purified bovine $G_{\beta\gamma}$

recruited cardiac muscarinic-gated K+ channels more effectively though at a higher concentration (Logothetis *et al.*, 1987, also Nanavati *et al.,* 1990).

These results have been followed rapidly by numerous other examples of membrane-delimited G-protein channel modulation, including $G_{\alpha,o}$ activation of an inwardly rectifying K^+ channel in the hippocampus, $G_{\alpha,s}$ modulation of cardiac pacemaker hyper-polarisation activated non-specific channel (I_f) in sinoatrial node cells (Yatani & Brown, 1990) and of cardiac Na^+ channels (Schubert *et al.*, 1989).

1.4.6.2 Indirect Evidence for direct modulation of Ca^{2+} channels

It has also been proposed that the G_s-protein can modulate L-type Ca^{2+} channel function. Cardiac L-type channels do not contain the characteristic central QXXER motif (Herlitze *et al.*, 1997) associated with direct inhibition by G protein $\beta\gamma$ subunits in N- and P-type Ca^{2+} channels. Little biochemical research been performed on the possibility of an equivalent structure in L-type channels.

Indirect evidence has accrued from functional studies for "membrane delimited" G-protein mediated modulation of $I_{Ca,L}$. The adenylyl cyclase activator forskolin is unable to completely mimic the effects of isoprenaline application (Breitwieser & Szabo, 1985). A small component of isoprenaline-stimulated I_{Ca} also has sub-second latencies, i.e., orders of magnitude faster than either the remainder of the increase or the forskolin response (Yatani & Brown, 1989). The suggestion is that the required diffusion of second messengers would be too slow for these responses.

When guinea-pig cardiac myocytes were dialyzed with a ATP-free solution containing low Ca_i, and a cocktail of phosphorylation-pathway inhibitory agents including the non-hydrolyzable ATP analogue AMP-PNP and the adenylyl cyclase

inhibitor adenosine 5′-O-(2-thiodiphosphate), isoprenaline but not forskolin was still able to evoke an increase in I_{Ca} (Pelzer *et al.*, 1990, Shuba *et al.*, 1990). The dialysis of the cells with GTPγS or activated G_s-protein, along with the phosphorylatory inhibition cocktail, was also each able to produce an approximately 50% enhancement (Pelzer *et al.*, 1990).

GTPγS and GTP prolonged the survival of excised Ca^{2+} channels in excised membrane patches independent of the presence of cAMP, ATP and cAMP-PKA. This required the presence of isoprenaline or the dihydropyridine agonist BAYK 8644 in the patch pipette. Activated G_s-protein and activated $G_{\alpha,s}$ subunits were both able to mimic the effects of the combination of isoprenaline and GTPγS.

1.4.6.3 Direct Evidence for direct modulation of Ca^{2+} channels

Direct evidence for a membrane-delimited modulation of I_{Ca} by adrenoreceptor activation without intervention of a soluble second messenger comes from reconstitution experiments in planar lipid bilayers of skeletal muscle and cardiac channel (Yatani *et al.*, 1988, Imoto *et al.*, 1988). Gαs in the presence of BAYK8644 potentiated the probability of channel opening 13-25-fold for partially purified cardiac sarcolemmal vesicles incorporated in artificial lipid bilayers (Imoto *et al.*, 1988). The complete absence of a high-energy phosphate donor ruled out the involvement of protein phosphorylation, e.g. via cAMP-PKA as the channel modulator. In addition, biochemical investigations show the association of $G\alpha_s$ with purified skeletal L-type calcium channels (Hamilton *et al.*, 1991). GMP-PNP increases the ability of a dihydropyridine agonist to displace an antagonist (Bergamaschi *et al.*, 1988) suggesting a direct influence of

G-proteins on the L-type channel. Taken together with evidence from functional studies, the case for a membrane-delimited pathway for G-protein stimulation of cardiac L-type Ca^{2+} channels is very strong.

1.4.6.4 Querying the existence of a membrane-delimited pathway

The experiments on rat, guinea pig and frog cardiac myocytes of Hartzell *et al.*, (1991) have challenged the above conclusion. They did not observe any residue response to isoprenaline following dialysis with the cAMP antagonist R_pcAMPS and the protein kinase inhibitor PKI. Furthermore, they did not record any rapid response in the order of hundreds of millisecond to the application of isoprenaline to guinea pig myocytes using a fast perfusion system. Instead an increase in I_{Ca} was seen only after 10-20 s after the stimulus.

The most likely explanation for the discrepancy in the guinea pig responses is that Hartzell *et al.* (1991) performed their experiments at room temperature (18.5-21°C, Fischmeister & Hartzell, 1986). This would account for the extraordinary latency observed for the isoprenaline response in guinea pigs. Although this temperature is adequate for experiments with frogs, it is less suitable for the rat or guinea-pig since enzymatic processes would be approximately three times slower than those found physiologically. The effects of G_s are often small so that they might be unresolved at room temperature.

In frog myocytes, Hartzell *et al.* (1991) do not see a rapid cAMP-independent component to isoprenaline application. It seems likely that the membrane-delimited pathway is absent or of little consequence in this tissue. Rapid exposure to isoprenaline or GTPγS by extracellular and intracellular flash photolysis respectively does not reveal a

rapid cAMP-independent increase in I_{Ca} (Frace *et al.*, 1993). In contrast to guinea-pig myocytes, frog myocytes seem to exhibit a lag period following exposure to isoprenaline.

1.4.6.5 Relative contributions of the direct and cAMP-dependent pathways

There has been considerable variation in the proposed contributions of the putative membrane-delimited pathway for the *β*-adrenergic response. Yatani and Brown (1989) suggest that at low concentrations of isoprenaline, the membrane-delimited pathway is predominant, whilst at high concentrations, the slow response due to cAMP-dependent phosphorylation predominates. In their experiments, the former is only able to contribute around 5% to the maximal response of isoprenaline. In contrast, cell dialysis with GTPγS, activated $G_{\alpha,s}$ subunit and *β*-adrenergic stimulation under conditions inhibiting phosphorylation were able to evoke increases in I_{Ca} which were 35-50% of control isoprenaline responses (Shuba *et al.*, 1990; Pelzer *et al.*, 1991). In the studies of Cavalie *et al.* (1991), 1 μM isoprenaline produced an increase in I_{Ca} density from 12 to 40 $\mu A/cm^2$ or ~230%. This was reduced in the presence of R_pcAMPS to a change in I_{Ca} density from 9 to 17 $\mu A/cm^2$ or ~190%. The diversity of experimental approaches used to study the relative contributions of the two pathways and the varying disruption of the physiological state of the myocytes offer the most probable explanation for this variability. It may also be that it is more difficult to abolish cAMP-dependent phosphorylation than was generally thought.

1.4.6.6 The physiological role of a membrane-delimited pathway

Unlike the activation of muscarinic atrial K^+[Ach] channels where the role of the PTX-sensitive G_i-protein is constitutive, there is already parallel cAMP-dependent phosphorylation linking β-adrenergic stimulation to I_{Ca}. All the evidence indicates that this second messenger mediated pathway plays a predominant role in modulation of L-type Ca^{2+} channel activity which is, no doubt, why a cAMP-independent response might have been overlooked.

A membrane-delimited pathway is not only important as an alternative means of channel modulation, albeit one which may have a faster response. The differential coupling of receptors or G-proteins to different regulatory systems can provide extra flexibility in a modulating physiological response, in this case, an increase in I_{Ca}. Agonists of low intrinsic efficiency might activate only the most efficiently coupled of these processes and produce a response profile different from that of a more potent agonist. It may also be that the membrane delimited pathway really comes into its own only under conditions inhibiting phosphorylation, e.g., with low intracellular ATP under ischaemia.

It has been suggested by Yatani and Brown (1989) that a membrane-delimited and faster pathway may account for the ability of cardiac sympathetic nerves to change heart rate within a single beat. In support of this notion, it appears that rapid application of isoprenaline and its subsequent interaction with β-adrenoreceptor produce a biphasic increase in current through L-type channels using Ba^{2+} as the charge carrier. At 20-22°C, there is an initial increase in I_{Ba} with a time constant around 150 ms followed by a more gradual increase with a time constant of 56 s. It is suggested that these two increases are

due to the two different pathways. However, it is likely that parasympathetic modulation with its know fast responses plays the determining role in setting the cardiac rhythm.

Even in frog hearts, parasympathetic nervous stimulation can induce a negative inotropic effect within 1 s, whilst the positive inotropic effect in response to sympathetic nervous stimulation can take in excess of 5 s to develop (Hartzell *et al.*, 1991). In mammalian canine sino atrial node cells, such a negative inotropic effect occurs within ~210 ms, whereas the converse response following sympathetic nervous stimulation requires ~950 (Spear *et al.*, 1979).

Cavalie *et al.*, 1991 have suggested an alternative view: that the cAMP-dependent and membrane delimited pathways might interact with one other. They provide evidence that concurrent cAMP-independent stimulation at intermediate levels can enhance the cAMP-dependent response. In contrast to other reports (Yatani *et al.*, 1989), they find that at maximal stimulation, the two pathways are not additive. They postulate that this might be because the cAMP-dependent mechanisms might interfere with further modulation via the G_s pathway. They also report that the direct pathway reduces the number of null traces seen in single channel recording, pointing to increases channel availability which may underlie the priming effect they see.

1.5 G-protein mediated Cl^- channel modulation in the heart

The catecholamine activated chloride conductance was first discovered as an isoprenaline-induced Na^+-dependent inward current in isolated guinea-pig ventricular myocytes (Egan *et al.*, 1987) which was insensitive to blockers of Ca^{2+}, K^+ and Na^+ channels. The sensitivity to sodium was later shown to be mostly due to muscarinic agonist activity of the Na^+ ion substitutes used (Tareen *et al.*, 1992, Zakharov *et al.*,

1993). The first evidence that the charge carrier was Cl^- came from two separate groups (Bahinski *et al.*, 1989; Harvey & Hume, 1989) using guinea pig and rabbit ventricular myocytes.

1.5.1 Chloride channel biophysics

cAMP-dependent chloride current ($I_{Cl,cAMP}$) exhibits time and voltage independence, outward rectification in asymmetrical Cl^- and is regulated by cAMP-dependent PKA phosphorylation subsequent to G-protein-mediated stimulation of the adenylyl cyclase (Bahinski *et al.*, 1989; Harvey & Hume, 1989).

1.5.1.1 Single channel recordings

Cell recording in attached and excised patches membranes of guinea-pig ventricular myocytes (Ehara & Ishihara, 1990; Ehara & Matsuura, 1991) revealed a small conductance (~13 pS) channel. Outward rectification could be seen in asymmetric Cl^-, but the current voltage relationship was ohmic when the concentrations were symmetrical (~150 mM Cl^-) with no voltage dependence of gating. Rates of opening and closing were slow, but mean open times were relatively long (200-700 ms) with inward currents showing faster bursting activity. The outward rectification may be due in part to voltage-dependent occlusion by large anions of the cytoplasmic channel opening (Lindsell & Hanrahan, 1996). With a maximum membrane conductance of around 20-100 pS/pF, this gives a channel density of ~7.7 pF^{-1} or ~1000 per cell.

1.5.1.2 Cl^- channel blockers

$I_{Cl,cAMP}$ is relatively insensitive to stilbene disulphonic acid derivatives like SITS but blocked by carboxylic acid derivatives like anthracene-9-carboxylic acid (9-AC) and

diphenylamine-2-carboxylic acid (DPC); sulfonylureas like glibenclamide; arylaminobenzoates like clofibric acid and its analogues. All but the latter compounds appear to have additional non-specific effects, for example inhibition of protein phosphatases (Zhou *et al.*, 1997).

1.5.1.3 $I_{Cl,cAMP}$ is carried by the cystic fibrosis transmembrane regulator protein

The similarities in channel biophysics between $I_{Cl,cAMP}$ and currents through the expressed cystic fibrosis transmembrane regulator (CFTR) suggest that these two currents could be identical and carried by the same channel protein. They have similar rectification, anion selectivity, regulation by cAMP-dependent PKA, sensitivity to Cl^- channel blockers, and a dependence on hydrolysable nucleotides for activation. The ability of CFTR antisense oligonucleotides to reduce $I_{Cl,cAMP}$ density in acutely cultured guinea pig ventricular myocytes (Hart *et al.*, 1996) has conclusively demonstrated that CFTR is responsible for $I_{Cl,cAMP}$. James *et al.* (1996) have quantified CFTR mRNA levels in the guinea-pig heart, showing a strong correlation with $I_{Cl,cAMP}$ densities which were lower in the atria and highest in ventricular epicardial cells.

1.5.2 Cystic Fibrosis Transmembrane Regulator

Mutational defects in the cystic fibrosis transmembrane regulator (CFTR) cause the disease of the same name (CF). With the cloning of the gene (Riordan *et al.*, 1989), it became clear that the gene product functions as an ion-selective small conductance channel in epithelia.

1.5.2.1 CFTR structure

The CFTR is composed of 1480 residues. Sequence homology places it within the ATP-binding cassette (ABC) transporter superfamily. All members of the family have

two repeating transmembrane domains (TMD), each of which has six membrane spanning helices in CFTR (M1-6, M7-12) and two nucleotide-binding domains (NBD_A and NBD_B) (figure 1.7). In addition, CFTR has a large regulatory domain (R) that has numerous consensus sites for PKA and PKC.

1.5.2.2 CFTR is an ion channel

The introduction of expressible CFTR cDNA into cells either with the CF mutation or which do not normally express CFTR results in the appearance of a Cl^- conductance regulated by cAMP and similar to that found in epithelial cells. However, the best evidence that CFTR forms a Cl^- pore comes from recombinant CFTR from Sf9 purified to homogeneity, re-constituted into synthetic phospholipid vesicles cells and thence into planar lipid bilayers. This produces a typical small (~10 pS in symmetric physiological Cl^-) ohmic-conductance Cl^- channel after activation by PKA catalytic subunit and ATP (Bear *et al.*, 1992). Site directed mutagenesis experiments which modify the pore permeation characteristics suggest that residues in M1, M5, M6 and M12 form part of the ion conduction pathway of the pore region and provide the final evidence that CFTR is pore forming (Anderson *et al.*, 1999, Dawson *et al.*, 1999).

1.5.2.3 Cardiac CFTR is an alternatively spliced variant of epithelial CFTR

Although cardiac and epithelial chloride conductances share the same general biophysical characteristics, they have different single channel conductances. Cardiac CFTR channels also have a higher probability of opening (P_o=0.7-0.8 as opposed to 0.4-0.5). cDNA cloning from an amplified transcript in the rabbit ventricle (Horowitz *et al.*, 1993) indicates that the cardiac variant has a deletion of 30 residues at the COOH

terminal end of the first cytoplasmic loop between M1 and M2, corresponding to an intron-exon junction. This suggesting that alternative splicing (exon 5-) accounts for the CFTR isoform in the heart. Otherwise the cardiac transcript shares > 95 identity with human epithelial CFTR.

1.5.3 CFTR channel phosphorylation

Activation of CFTR is a two-step process requiring both PKA and PKC phosphorylation of the R domain and binding of ATP to the Nucleotide Binding Domain (NBD). The requirement for hydrolysable nucleotides has been established for $I_{Cl,cAMP}$ in the heart (Nagel *et al.*, 1994).

1.5.3.1 Protein kinase A phosphorylation

CFTR contains at least 10 putative consensus serine/threonine phosphorylation sites, the majority (8) of which are in the R domain. PKA readily phosphorylates the R domain to a stoichiometry of at least 5 mol/mol (Picciotto *et al.*, 1992) corresponding to at least three functionally distinct electrophysiological states. The different phosphorylation sites have different sensitivities to PKA and make different contributions to channel regulation (Gadsby & Nagel, 1995).

1.5.3.2 Protein kinase C phosphorylation

Protein kinase C (PKC) phosphorylates CFTR to a stoichiometry of ~2 mol/mol (Picciotto *et al.*, 1992), most probably by Ca^{2+} independent PKC-ε (Liedtke & Cole, 1998). PKC potentiates subsequent CFTR channel activation by PKA in intact cardiac myocytes (Middleton & Harvey, 1998). Constitutive phosphorylation by cellular PKC is a prerequisite for subsequent PKA activation (Fischer *et al.*, 1998) and

PKC does not alter the number of active channels in excised patches but reduces mean closed time after PKA activation (Jia *et al.*, 1997). Whether either PKA or PKC is stimulatory or permissive probably depends on the relative basal activities of the two kinases in different species and experimental conditions. Permeabilized patch recordings suggest that phorbol esters activate CFTR currents only after they are pre-exposed to low concentrations of isoprenaline. These PKC activators also increased the magnitude of the response to supramaximal isoprenaline treatment (Middleton & Harvey, 1998).

1.5.3.3 Other protein kinases

The membrane-associated cGMP-dependent protein kinase G (PKG_{II}) phosphorylates the R domain of CFTR efficiently *in vitro* (> 5 mol/mol; Picciotto *et al.*, 1992). *In vivo* in NIH-3T3 and rat intestinal IEC-CF7 cells, it is about as effective as PKA (French *et al.*, 1995). The effects of cGMP are likely to be complex and tissue specific. cGMP is also expected to potentiate the results of PKA phosphorylation via type II cGMP-inhibited phosphodiesterase (Harrison *et al.*, 1986, Ono *et al.*, 1992). The effects of tyrosine kinases have been less well characterised, but tyrosine Kinase $p60^{c\text{-}Src}$ is known to phosphorylate CFTR and increases chloride channel activity even in the presence of PKA inhibitor (Jia *et al.*, 1997).

1.5.3.4 De-phosphorylation of the chloride channel

Deactivation of the chloride conductance following the removal of *β*-adrenergic stimulation is rapid, indicating that the channel is a good substrate for endogenous protein phosphatases (Hwang *et al.*, 1993). There seem to be at least two groups of phosphorylation sites with different phosphatase specificities. The fully phosphorylated

channel is dephosporylated by an okadaic acid insensitive phosphatase, most probably the Ca^{2+} insensitive PP2C (Gadsby & Nairn, 1999). The okadaic acid-sensitive phosphatase (PP2A) dephosphorylates partially phosphorylated channels. Inhibitor-1 peptide, a specific inhibitor of phosphatase 1, failed to affect forskolin evoked I_{Cl} (Hwang *et al.*, 1993).

1.5.4 Regulation of $I_{Cl,cAMP}$ through CFTR channel

1.5.4.1 Both CFTR channel opening and closing depends on ATP hydrolysis

Li *et al.* (1996) have shown that purified reconstituted epithelial CFTR hydrolyses ATP at approximately the same rate at which channels open and close. PKA-dependent stimulation of ATPase activity was attributed to an increased affinity of ATP with no alteration of the maximal hydrolysis rate. This was accompanied by a shift of the Hill co-efficient from 1 to 2 for the fully phosphorylated protein, indicating the recruitment of a second ATP binding site. Hydrolysable ATP analogues and Mg^{2+} are required for channel opening. The open state can be stabilized by the using P_i analogues orthovanadate and beryllium fluoride to trap ADP, the product of ATP hydrolysis (Baukrowitz *et al.*, 1994) implying that ATP hydrolysis precedes or accompanies channel opening.

The addition of a non-hydrolysable analogue such as AMP-PNP or ATPγS prolongs the open state in the simultaneous presence of ATP, suggesting that ATP hydrolysis at a second site permits channel closing (Hwang *et al.*, 1994). Once in the open state, washout of all Mg^{2+} and ATP can result in prolonged opening (Dousmanis *et al.*, 1996). These findings suggest that the there are two separate ATP binding sites controlling opening and closing.

1.5.4.2 NBD_1 opens and NBD_2 closes

Functional analysis of site direction mutations suggests that the ATP hydrolysis binding site for opening is on NBD1 and the closing site on NBD2. The rate of CFTR opening is slowed without affecting closing kinetics by a site directed mutation in NBD1 while the corresponding mutation at NBD2 only accelerated channel closing (Carson & Welsh, 1995). In this four state model (Senior & Gasdsby, 1997), the second nucleotide-binding site at NBD2 is only available when the channel is open and after hydrolysis of ATP bound to NBD1. Subsequent tight binding of ATP to NBD2 stabilizes the open state until it is terminated by (NBD2) ATP hydrolysis (figure 1.8).

1.5.4.3 Role of channel phosphorylation

Sequential phosphorylation events are suggested to explain the regulatory effects of PKA. Channels exhibit modal gating behaviour, and open probability (P_o) may correlate with the phosphorylation state of the channel (low P_o for P_1 state, high P_o for P_1 P_2 state) (Fischer & Machen, 1994). For partially phosphorylated channels, ATP hydrolysis at NBD_A causes brief channel openings (low P_o). Further phosphorylation makes the NBD_B ATP site available for binding which stabilizes channel openings (high P_o). Hydrolysis of the ATP bound to NBD_A causes channel closures. In other words, ATP hydrolysis at NBD_A initiates channel bursts while ATP hydrolysis at NBD_B terminates channel bursts (Carson *et al.*, 1995).

1.5.5 No membrane-delimited pathway regulates $I_{Cl,cAMP}$

There has been no suggestion of membrane-delimited regulation of $I_{Cl,cAMP}$. Unlike the case of I_{Ca}, blockers of the cAMP-dependent phosphorylatory pathway are able to completely abolish the ability of sympathetic stimulation to induce $I_{Cl,cAMP}$

(Gadsby & Nairn, 1999). PKI completely abolished the isoprenaline activated I_{Cl} even in the presence of GTPγS, and no further *β*-adrenergic response could be seen subsequent to maximal stimulation by forskolin or intracellular cAMP (Hwang *et al.*, 1993).

It is instead possible that $I_{Cl,cAMP}$ has a higher sensitivity to regulatory phosphorylation by PKA. The response to exogenous isoprenaline can be apparently greater when recorded using the permeabilised patch technique (Zakharov & Harvey, 1995) when less disturbance of the intracellular milieu and regulatory components can be expected.

1.5.6 *Physiological significance of the $I_{Cl,cAMP}$*

In physiologically asymmetrical Cl^- concentrations, activation of $I_{Cl,cAMP}$ should have little effect on the resting membrane potential because the Nernst potential for chloride (E_{Cl}) is closer to the resting membrane potential and because of outward rectification. During the action potential plateau, though, significant outward current will be contributed, tending to repolarise the membrane or causing a shortening of the action potential duration. Thus, β-adrenergic stimulation can augment Ca^{2+} entry without significant changes in the profile of the action potential. Accordingly, a prediction might be that if $I_{Cl,cAMP}$ plays a significant role in the human heart (a matter still of some controversy but see LeBlais *et al.*, 1999), patients suffering from cystic fibrosis might run a higher risk of arrhythmias during sympathetic stress. Epicardial cells have a higher density of I_{Cl} activated by *β*-adrenergic stimulation than in the endocardium. If $I_{Cl,cAMP}$ were activated by basal *β*-adrenergic activity, this would explain why epicardial cells have shorter action potential duration (Takano & Noma, 1992).

Chapter Two

Methods and Materials

2.1 Preparation of ventricular myocytes

The isolation from mature cardiac tissue of myocytes with structural and functional properties resembling those of cells in the intact myocardium has been one of the most important advances in cardiac electro-physiology. The homogenous population of ventricular myocytes separated from other myocardial types by cell enrichment techniques has allowed consistent investigations into ventricular function. More importantly, the removal of extra-cellular complexities reduces ambiguities of experimental interpretation. The elimination of factors associated with the syncytial nature of multi-cellular preparations or the restricted extra-cellular space has allowed the electrical membrane properties of individual cardiac myocytes to be examined directly in isolation.

2.1.1 *Background*

Initial attempts to obtain single myocytes using enzymatic dispersion failed to yield individual cells which functioned normally when bathed in solutions containing physiological concentrations of calcium. The damage to the myocytes was due in part to calcium deprivation and often hypokalaemia during cell isolation. The production of calcium tolerant cells from adult rat hearts by Gould and Powell (1972) was in this sense

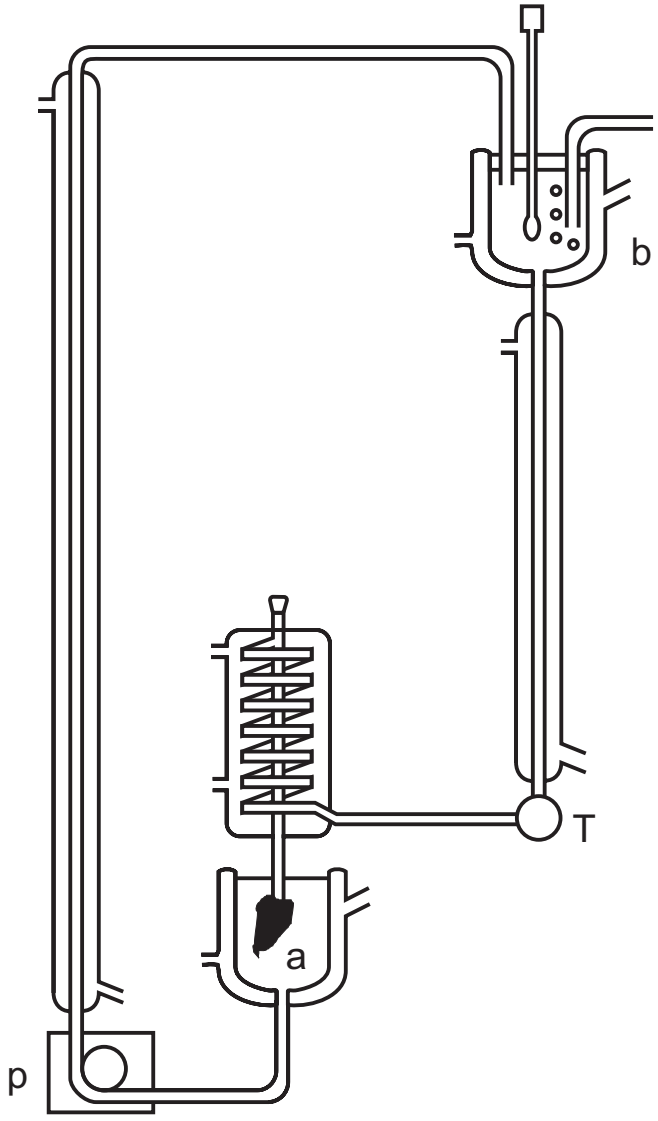

Figure 2.1

Schematic representation of the Langendorff system used to isolate guinea-pig ventricular myocytes ventricular myocytes. The flow rate was controlled by tap T. The perfusate kept at 37°C flows through a perfusion column leading into reservoir b where the guinea-pig heart was cannulated through the aorta. Peristaltic pump P recirculates the perfusing medium which is gassed with a O_2 / CO_2 mixture via a line into reservoir b to maintain the pH at 7.40.

a significant breakthrough. All the experiments in this thesis were performed using guinea-pig cardiac myocytes isolated from guinea-pig ventricles by enzymatic dispersion according to the methods of Powell *et al.* (1980) pioneered in this laboratory. The healthy myocytes which make up a majority of the isolated cells prepared in this manner can be readily identified by their morphology which resembles that of cells in intact tissue. These include the characteristic irregular, elongated and branching "rod" shapes which arise due to the cleavage of individual myocytes from their neighbours at the intercalated disks. The average length of the ventricular myocytes used was in the order of 100 by 20 μm. Myofibrils were visible as prominent cross striations. The minority of damaged myocytes could be identified easily by their different (rounded) morphology.

2.1.2 Procedure

Female guinea pigs of around 350 g in weight were killed by cervical dislocation, and their hearts were removed with the greatest dispatch. Incisions were made through the skin, and via the diaphragm and rib cage to expose the thoracic cavity. The pericardial membrane was removed along with tissue around the aorta. This vessel was clamped just before the bifurcation at the aortic arch and severed above the clamp. The heart was then freed from the surrounding tissue and removed into ice-cold Ringer solution with added heparin and weighed. At this time, the majority of hearts were still in a beating state.

The apparatus in Figure 2.1 was used in a modified Langendorff system to isolate ventricular myocytes. The system was initially pre-perfused with a nominally Ca^{2+}-free oxygenated HEPES Ringer solution containing 100 μM EGTA. The excised heart was mounted via the aorta on the end of the glass cannula ("A" in Figure 2.1) for 5 minutes of reverse aortic perfusion at a pressure of 70 mmHg until clear of blood. This initial

perfusate was retained. The remaining buffer was re-circulated at a flow rate of 10 ml/min. For harvesting of ventricular myocytes, incisions through the atria could be made. The remainder of the major blood vessels attached to the heart were removed at this point and subtracted from the previously obtained fresh weight measured.

After 5 minutes, the heart was switched to a recycling enzymatic perfusate (in reservoir B in figure 2.1) containing protease and bacterial collagenase for a further 10 minutes. Within the first 1½ minutes of this procedure, the coronary effluent from well-perfused hearts would become noticeably more viscous and charged with blood. The heart was removed from the cannula at this point and re-weighed. (Oedema induced by the enzymatic perfusion can bring a weight increase of 80-120%). The atria were trimmed away along the atrioventricular septum for harvesting of ventricular cells and the remaining ventricles sliced with a sharp blade into rough strips (~3-4 mm).

The resulting tissue was gently stirred (1 Hz) in a Teflon container with 5 ml fresh enzymatic Ringer. At 3 successive ten minutes intervals, the dissociated heart cells in the perfusate were removed and added to 15 ml low Ca^{2+} gassed "washing solution" at 37°C (standard Tyrode with 0.5 mM Ca^{2+}, 1% bovine serum albumin (Fraction V); the latter provides initial mechanical stability to isolated cells.) and then centrifuged very gently at around 37 g (300 rpm) for 1½ minutes. The resulting pellets were re-dispersed in another 20 ml washing solution before being centrifuged again. Finally the washed cell pellets of harvested myocytes were re-suspended in Dulbecco's culture medium (DMEM) containing 1.8 mM Ca^{2+} and supplemented with HEPES and 2% (v/v) serum substitute (Ultroser G, Gibco UK), at room temperature. Roughly 20-30% of the cells obtained in suspension were rounded with no organized structure and were contracted

myocytes damaged by the isolation procedure. The majority of the cells were rod-shaped and considered to be functional intact myocytes. These almost never show visible spontaneous contractions even after dialysis with the patch pipette during whole-cell patch clamp experiments. This can also be taken as an indicator of the health of the cells, as well as the Ca^{2+} buffering power of the dialysing solution.

Aliquots of the cell suspension were transferred to a small Perspex bath of ~0.5 ml volume for electro-physiological recording at 37°C. The temperature of the superfusate was maintained using a thermocouple probe attached to the recording chamber.

Experiments were performed within 24 hours of cell isolation. For incubation with pharmacological agents, cells were kept at room temperature or 37°C for the required time, and, if necessary, the agents were washed out by exchanging the incubation solution for HEPES supplemented culture medium. The cells were then kept at room temperature before the experiments. When any of these incubations reduced the number of viable cells, i.e. those which were not in a contracted state and hence Ca^{2+} overloaded, this will be indicated in the accompanying text.

2.2 Patch Clamp

2.2.1 *A summary of the patch clamp technique*

The patch clamp technique (Neher & Sakmann, 1976) initially allowed the recording of single-channel currents in a small patch of biological membrane. Further developments which produced seal resistances almost two orders of magnitude higher (Hamill *et al.*, 1981) have given a sensitivity high enough to measure currents in the order of picoamperes with a time resolution of milliseconds. The high resistance of the

patch clamp seal ensures that most of the current originating from the cells flows into the pipette and from there into the current measurement circuitry. This allows the membranes to be voltage clamped without the use of separate microelectrodes (Sigworth & Neher, 1980).

The use of the patch clamp pipette in the whole cell configuration provides low resistance access to the cell interior. Moieties with small molecule weight can be freely perfused into the interior of the cell to allow rapid manipulation of the intracellular milieu. If one of the priorities is to minimize disturbances to the intracellular environment and avoid washing out regulatory molecules, the perforated or permeabilised patch technique (Horn & Marty, 1988) can be used instead. Monovalent ionophores such as nystatin or amphotericin provide electrical continuity between the pipette electrode and the cytoplasm without allowing the free diffusion of cytoplasmic compounds away from the cell. The access resistance depends on the number of ionophores incorporated into the plasma membrane between pipette tip and cell, and is necessarily higher than when the patch is ruptured entirely. Thus this procedure is ideally suited to the recording of either smaller or time-independent currents.

A current to voltage converter located within the head stage of the patch clamp apparatus is necessary for the recording of ionic currents. This consists of a low noise operational amplifier in parallel with a 10 to 50 GΩ feedback resistor. The operational amplifier amplifies the single channel current to a level equivalent to the voltage drop across the resistor. The resulting signal can then be further amplified to useful levels. The frequency response of the current to voltage converter has also to be compensated for. The converter initially has a rising exponential step with a fairly long time constant

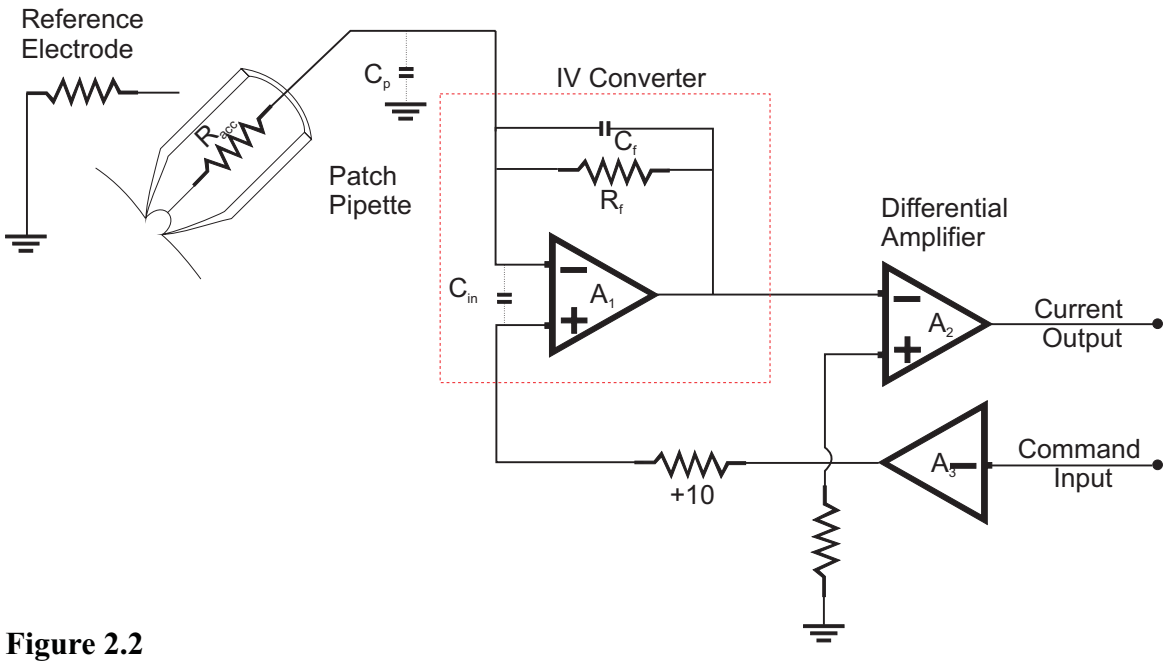

Figure 2.2

Simplified circuit diagram of the patch clamp recording system. An IV converter is mounted on a micro-manipulator plugged directly into the pipette holder. R_{acc} is the pipette access resistance and C_p the total pipette and holder capacitance. A_1, A_2 and A_3 are operational amplifiers with associated resistor networks chosen for low voltage noise. The converter consists of a low noise feedback resistor (represented by the R_fC_f circuit) connected in parallel with the operational amplifier A_1 (with input capacitance C_{in}) enclosed within a shield (broken line) to reduce noise. The high resistance feedback resistor provides for high current sensitivity and the operational amplifier is capable of very high frequency responses (~10 kHz). Pipette current flows to the negative terminal of A_1. The voltage output of A_1 is equivalent to the voltage drop across the feedback resistor R_f. Provided that most of the membrane current flows into the pipette, i.e. if there is a high seal resistance (>1GW), an effective voltage clamp can be maintained by a command voltage applied to the positive terminal of A_1. After passing through the differential amplifier, the output of A_1 is frequency corrected and the command voltage subtracted before the current can be recorded.

(~1 ms) but can be corrected by "inverse filtering" which adds a slow exponential decay response to give the desired square pulse. A schematic diagram is in Figure 2.2.

For voltage clamping, a command voltage can be applied to the other input of the operational amplifier whose output will then vary the current across the feedback resistor in a feedback loop until the potential of the pipette electrode is equivalent to the command voltage. This requires "giga-seal" resistances. The output of the current voltage converter will then be equivalent to whatever differential voltage resulting from current flow through ionic channels is being measured plus the known applied command voltage which can be subtracted out.

The main advantage of the giga-seal patch recording technique is the improvement by over an order of magnitude in the resolution of current recordings. This resolution is limited by background noise from the membrane, pipette and recording devices. The most serious potential source of noise arises from a thin film of solution that creeps up the outer wall of a patch pipette. A Sylgard coating applied to the pipette prevents the formation of this film and the thickness of the coating increases the capacitance across the pipette walls thus reducing the noise considerably. It also helps to use, instead of flint electrode glass, borosilicate with a lower conductivity, especially at high frequencies. Finally the pipette access resistance and the tip capacitance constitute another noise source which can be reduced by using pipettes with steeper tip tapers.

For the effective formation of a patch seal with giga-ohm resistances, tight membrane-glass contact is required. The existence of such a tight seal is suggested by the diffusion barrier even to small molecules across the patch seal and the absence of "rim" leakage currents seen with thick walled suction pipettes. The seal resistances in excess of

10 GΩ are consistent only with glass-membrane separations in the order of 1 Å, i.e. within the distance of chemical bonds. This suggests that the seal involves direct contact between the glass surface and the lipophilic membrane, such as occurs during the transfer of insoluble surface monolayers onto glass substrates (Langmuir, 1938). A clean glass surface on the patch pipette is a primary requirement, therefore, for the formation of giga-ohm seals. This was satisfied by using a fresh pipette for each seal and avoiding negative pressure when moving the tip through the air-water interface. In addition, the bathing solutions were allowed to flow through the perfusion system for some time after the isolated cells were first applied to remove any debris from the enzymatic dispersion treatment. The use of HEPES-buffered pipette solutions prevents Ca^{2+} crystals from forming at the pipette tip.

The patch seal forms when the pipette tip is held against the membrane. Upon suction, the membrane at the pipette tip is distorted and forms an Ω-shaped protrusion (Neher 1981). The increase in area of glass membrane contact explains a gradual 2-4-fold increase of seal resistance to between 50-200 MΩ. Formation of the giga-seal of resistances in the order of 10 MΩ is sudden and an all-or-nothing occurrence.

Single channel currents in the cell-attached configuration can be recorded after formation of the giga-seal. The mechanical stability of the giga-ohm seal allows the membrane patch to be isolated from the cell and different media applied to both sides of the membrane. Two further types of cell-free patches can then be formed by partially disrupting the membrane patch while leaving an intact seal: an inside-out or an outside-out patch with the extra-cellular or cytoplasmic membrane surface respectively exposed to the bath solution. Alternatively, if the membrane spanning the pipette is ruptured or if

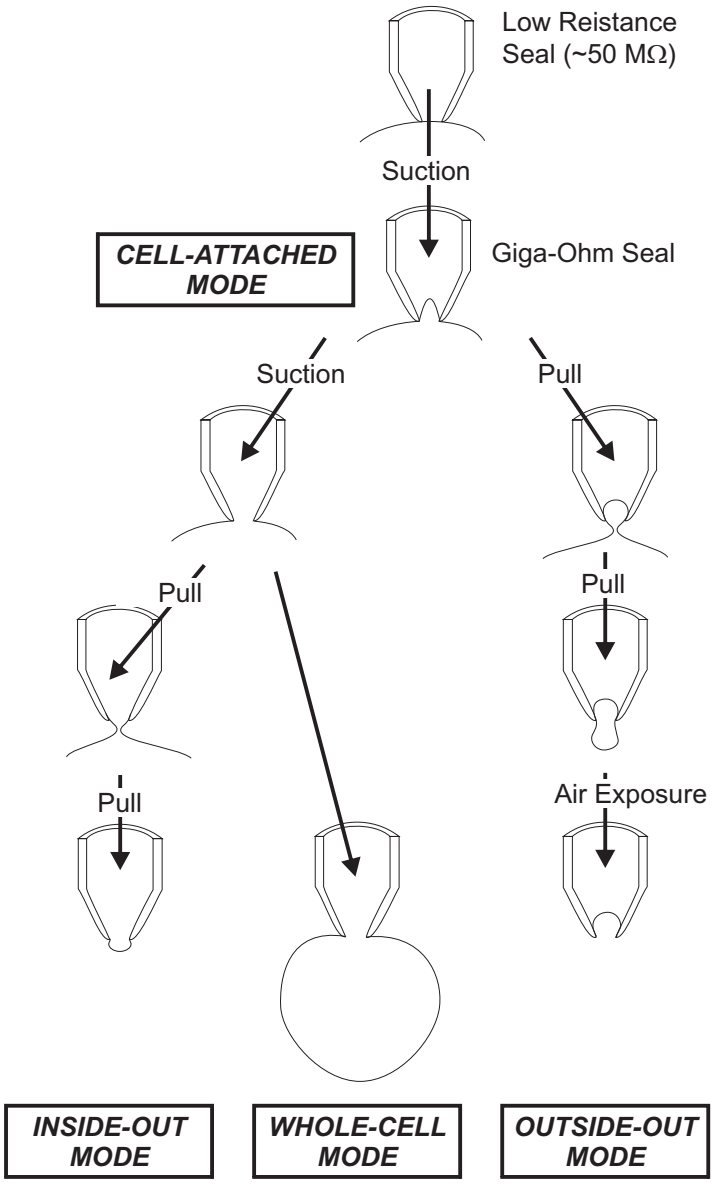

Figure 2.3

Schematic diagram for the formation of the four patch-clamp recording configurations. The low resistance seal that forms when a clean pipette tip contacts the cell can be converted into a giga-ohm seal by the application of a slight negative pressure to the patch pipette. This gives the cell-attached configuration which allows recording of single channel openings under the pipette. Further suction will rupture the membrane across the cell without disrupting the integrity of the seal, giving access to the interior of the cell and allowing the voltage-clamped currents from the whole cell to be recorded.

an ionophore such as amphotericin or nystatin is included in the pipette solution, ionic currents in the whole cell can be recorded. All five configurations are illustrated in Figure 2.3. Only data recorded in the whole-cell mode are presented in this thesis.

2.2.2 *Fabrication of patch electrodes*

Patch electrodes were made in a way similar to the technique of Hamill *et al.* (1981) using a two-stage vertical electrode puller (Narishige Scientific Instrument Lab, Tokyo). Borosilicate glass capillaries with an external diameter of 2.0 mm (Clark Electromedical, Pangbourne, England) and 1.5 mm (Narishige, Tokyo) were used to make electrodes for recording in the whole cell mode. A two-stage pulling process was used to produce two almost identical patch electrodes with tip diameters in the order of 1-2 μm. The resulting patch pipettes had a filled tip resistance in bath of 1.5 – 2.0 MΩ for recording of whole cell calcium currents in chapters 4 and 5 and 2.0 – 3.0 MΩ for the ramp protocols used in chapters 6 and 7.

Occasionally heat polishing and Silgard coating was used in preparing the electrodes. The former was performed by bringing the tip close to a glass bead on a glowing platinum wire 0.1 mm in diameter. The glass bead of approximately 0.5 mm in diameter effectively prevents metal ions from the heating element from coating and contaminating the electrode. Fire polishing smoothes and rounds the pipette apex and removes dust and impurities from the glass, thus in theory, aiding tight seal formation. However, in practice, fire polishing did not make any noticeable difference. Silgard coating was not performed regularly because the size of the whole cell currents (measured in nA rather than pA) was such that pipette noise was seldom a factor.

2.3 Experimental apparatus

Electrodes were back-filled with electrolyte solutions which were first passed through syringe filters (Millex GS) with an effective pore size of 0.22 μm to prevent the accumulation of small particles and dust which would hinder GΩ seal formation. Care was taken to remove air bubbles from the pipette tip.

The patch pipettes were placed in a suction electrode holder (Clark Electromedical). The suction outlet was connected by silicone rubber either to a syringe to which positive or negative pressure could be applied by mouth or, alternatively, via a valve to a vacuum pump whereby varying amounts of negative pressure monitored by an electronic gauge could be produced. The electrode holder was attached to the amplifier head stage mounted on a micromanipulator. A Nikon Diaphot microscope (Telford, UK) enclosed in a Faraday cage with a magnification of 600x was used to view the cells.

Whole cell current was recorded using an Axopatch (Axon Instruments; Foster City, CA, USA) 1-C patch-clamp amplifier or the Axopatch 200A model. Calcium currents recorded in chapters 4 and 5 were filtered at either 10 or 3 kHz. Recordings using ramp protocols in chapters 6 and 7 were filtered at 1 kHz.

Gigaseal formation was monitored on a dual beam storage oscilloscope or within the *pClamp* programme (Axon). Whole cell calcium current was recorded simultaneously on tape using a Sony PCM video system modified for electrophysiological recording and the data was analysed off-line using *VCAN* (Dempster, 1988) and *pClamp* on IBM pc-compatible computers after digitising at 2 kHz using a CED 1401 interface (Cambridge, UK). Chloride current data in chapters 6 and 7 were

acquired using the Digidata 1200 system and *pClamp* (both from Axon) and stored digitally on computers.

2.4 Experimental protocol

2.4.1 *Flash photolysis*

Caged compounds were photolysed between 10 and 15 minutes after formation of a stable whole cell voltage clamp, thereby allowing test compounds enough time to dialyse the cell interior (Pusch *et al.*, 1988). Similar results could be obtained even when flash photolysis occurred only 5-7 minutes of cell dialysis. On each occasions, a single light flash was triggered 20 ms before the onset of the voltage-clamp test pulse. A brief electrical artefact, apparently caused by the 12 kV flash lamp trigger pulse, could be detected and was used as a marker.

2.4.2 *Recording protocol*

The patch electrode for whole cell recording filled with internal solution was placed in the pipette holder. The electrode potentials could then be offset for zero current. The conductance to 2 mV test pulses was monitored continuously either on an oscilloscope or via the ClampEx (Axon) programme. The pipette was lowered until a roughly 2-fold increase in resistance signalled adequate contact between the micropipette and the cell surface. Giga-ohm seals could then be produced by gentle suction to around 25 cm·H_2O holding the electrode at -40 mV. Compensation for pipette capacity transients synchronous with the rising and falling edges of the command test pulses was made at the amplifier. A further pulse of stronger suction caused rupture of the membrane across the pipette tip allowing dialysis of the pipette solution into the

cell and recording of the whole cell current. A holding potential of -80 mV was then applied.

Any junction potentials were calculated within the *ClampEx* programme (Axon, Barry, P.H. (1994)) and compensated for.

2.5 Solutions

The solutions used were designed to isolate calcium and chloride current (chapters 4 and 5), and additionally to pharmacologically block calcium current (chapters 6 and 7). K^+ channels were blocked by the use of Cs^+ and Ba^{2+} and Na^+-Ca^{2+} exchange suppressed with the use of intracellular Ca^{2+} buffer EGTA. Ca^{2+} channels were blocked by nicardipine.

2.5.1 Superfusate

In all experiments measuring whole-cell calcium current (chapters 4 and 5), the bath solution contained (in mM): NaCl 144, CsCl 5.4, $CaCl_2$ 1.8, $MgCl_2$ 1.0, glucose 5.6 and HEPES 5; in chapters 6 and 7, the solution used consisted of (in mM): NaCl 144, CsCl 5.4, $CaCl_2$ 1.8, $MgCl_2$ 1.0, glucose 11.2, $BaCl_2$ 2.0, HEPES 5.0 and nicardipine 1.0 (see solutions 1 & 2 in table 2.1). The pH was adjusted at room temperature (~22°C) to 7.25 with NaOH and cells were superfused at 36 °C.

Patch clamp seals were obtained in solutions identical to those above but with the CsCl replaced by the same concentrations of KCl. The exchange of caesium for potassium was complete within 1.5 minutes after going into whole-cell mode.

PTX, isoprenaline, β-Estradiol-BSA, N-ω-nitro-L-arginine (Sigma), goby and human Urotensin II (Peninsula) and "photolytic by-products" were all added to the superfusate and applied by bath perfusion. Forskolin and β-estradiol (Sigma) stock

solutions were made up in DMSO and ethanol respectively. At the concentrations used (up to 0.3% v/v), these two solvents had little detectable effect on membrane currents but, as a precaution, control solutions contained matching levels of either vehicle.

2.5.2 *Dialysing solutions*

The dialysing solution for calcium current recordings in chapters 4 and 5 contained within the pipette (in mM): CsCl 130, $CaCl_2$ 1, ATP.Mg 1, PCr 5, EGTA 10, HEPES 10 (solution 3 in table 2.2). The free Ca^{++} concentration of the dialysing solution was calculated to be around 6 nM using software developed by Denton, RM and England PJ, University of Bristol. The intracellular solution used in chapters 6 and 7 consisted of (in mM): CsCl 20, CsAsp 110, EGTA 5, ATP.Mg 5, HEPES 5, PCr 10, GTP 0.1 (solution 4 in table 2.2). The pH was adjusted at room temperature to 7.2-7.3. All of the above chemicals were obtained from Sigma (Poole, UK).

Caged GTP, caged cAMP (Novabiochem, Nottingham), Caged GTPγS, R_p-cAMPS (Biolog, Bremen, West Germany), and DTT, GTPγS, cAMP, protein kinase inhibitor (PKI), isoprenaline, forskolin (Sigma) and 1-(2-nitrophenyl) ethanol ("caged water") were added to the internal solution in the patch pipette as indicated in the text. Where caged compounds were used, the pipettes solutions were kept on ice and away from light.

2.5.3 *Solution exchange*

Experiments were performed using a bath with a volume of ~0.5 ml. The flow rate of the superfusing electrolytes was maintained at ~1.1 ml/min by either a gravity feed or using circulating water pumps and an Akers level-sensing system. Either was

sufficient to maintain a steady volume and the bath temperature showed little fluctuation, even from one experimental session to the next.

Superfusing solutions were changed either using miniature electronic fluid valves (Lee) or by switching mechanically between reservoirs supplying the bath. Where pharmacological agents were applied, the time for the response to be seen was calculated from the first arrival of the new solution at the chamber indicated by an air bubble introduced for this purpose. Complete exchange of solutions took around 30-40 seconds using the disappearance of inward rectifier K^+ current at -80 mV after switching to K^+-free, Cs^+-Tyrode solution as a measure.

2.5.4 PTX incubation

Where the application of PTX is referred to in the text (chapter 5), this was always performed by incubation in culture medium containing PTX for 4 hours at 37°C. This high temperature was chosen because of reports that PTX incubation at room temperature may be ineffective even after 12-24 h (Parsons *et al.*, 1991). The internalisation of the holo-toxin may be the temperature-dependent rate-limiting step (Ui, 1990). Subsequent to the incubation, the cells were kept at room temperature (~22°C) in culture medium with PTX for 3-4 hours. At this point, though most of the cells were in a state of irreversible contracture, sufficient rod shaped myocytes remained for electrophysiological recordings.

2.6 Voltage protocols

After formation of the Giga-ohm seal, the superfusing solution was switched to Cs^+-containing K^+-free Tyrode before commencement of recording in the whole-cell mode. The presence of external Ba^{2+}, and Cs in both dialysing and superfusing solutions

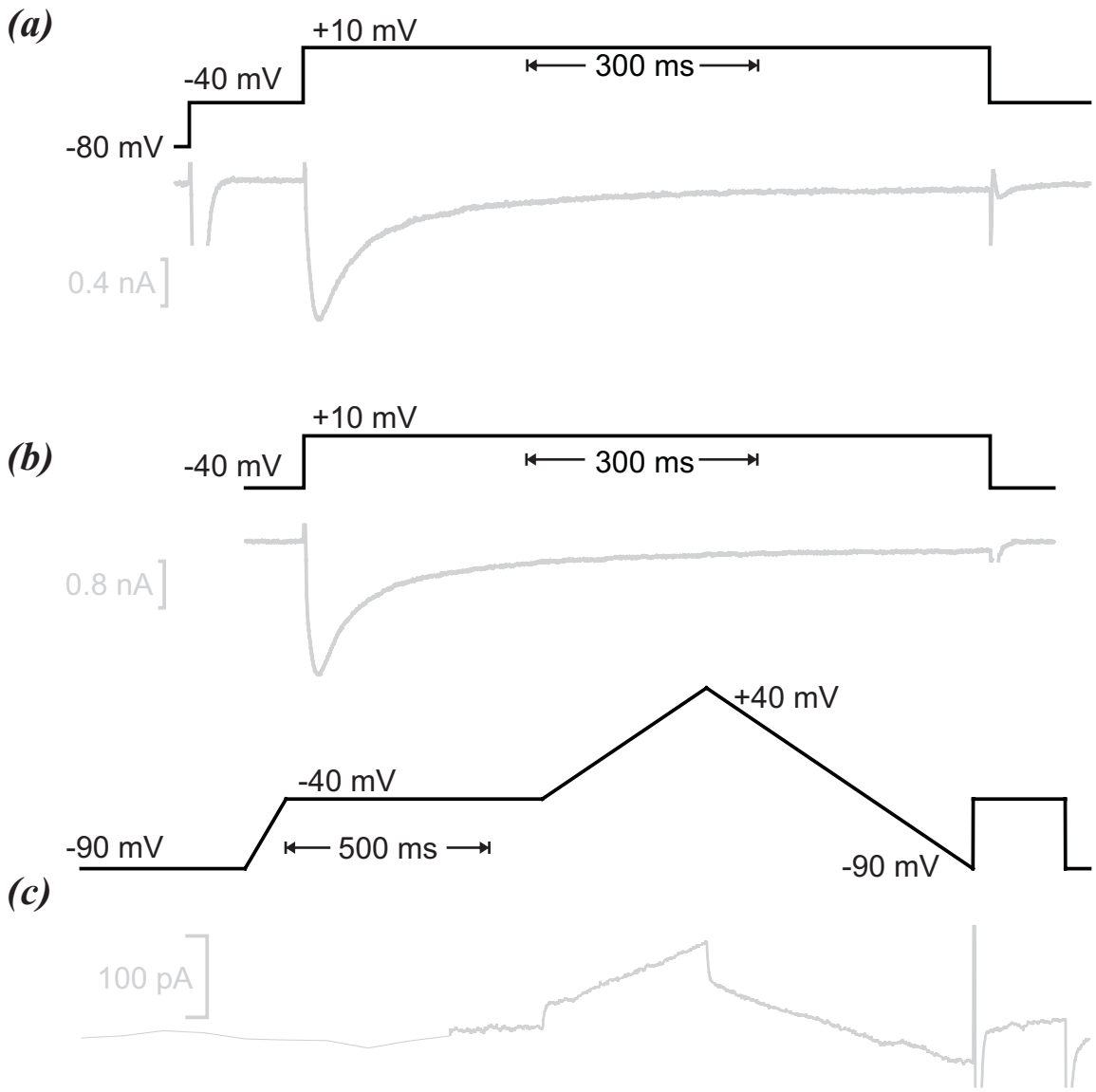

Figure 2.4

Three experimental protocols with "typical" traces shown beneath. Out of range Na^+ and capacitative transients have been digitally truncated for clarity.

(*a*) ,(*b*) Voltage protocols used to record L-type Ca^{2+} currents. Myocytes were held at -80 mV or, less often, at -40 mV . In the former case , an additional preconditioning step to -40 mV was made to inactivate Na^+ and T-type Ca^{2+} currents. A test pulse to +10 mV maximally stimulated I_{Ca}.

(*c*) Voltage ramps used for catecholamine-activated chloride currents. Myocytes were held at -90 mV and stepped to -40 mV to inactivate Na^+ and T-type Ca^{2+} currents. Ramp pulses extended to +40 mV and -90 mV, both at a rate of 0.2 V/S.

and blocks both the inwardly rectifying and the delayed-rectifier channels carrying potassium current.

2.6.1 Ca^{2+} current recordings

In a few initial experiments, the holding potential was kept at -40 mV rather than -80 mV (Figure 2.4a). Though this made little difference to the results seen in most cells, the frequency of seeing more rapid run-down in Ca^{2+} current seemed subjectively higher. At -40 mV, the sodium current should be completely inactivated. T-type Ca^{2+} current is fully inactivated at a holding potential of -50 mV (Hirano, Fozzard and January, 1989; Bean, 1989). Every five seconds, the voltage was stepped to +10 mV for 300 ms, eliciting a well-clamped inward current which under these conditions can be identified as exclusively L-type calcium current (I_{Ca}) and can be blocked by calcium antagonists such as nicardipine.

In the vast majority of the results with calcium current presented in this thesis, a holding potential of -80 mV was used, near the physiological resting potential of guinea-pig ventricular myocytes (Figure 2.4b). Every five seconds the voltage was stepped to -40 mV, to +10 mV for 300 ms, then back to -40 mV. The initial voltage step produces a large transient inward sodium current on top of membrane capacitative transients. After 300 ms at -40 mV, the sodium and T-type Ca^{2+} currents should be completely inactivated.

2.6.2 Changes in holding current during I_{Ca} recording

Under some experimental conditions described in this thesis, an additional inward current could be clearly seen at both -40 mV and -80 mV. Given its pharmacological properties, lack of time dependence, the sensitivity to changes in the

ionic gradients and outward rectification, this current can be identified as the catecholamine-induced chloride current ($I_{Cl,cAMP}$). This current made a negligible contribution to cell conductance at +10 mV with symmetrical Cl^- concentrations. Steady-state current levels at the end of the 300 ms test pulses were not appreciably different at +10 mV and 0 mV under these conditions. Thus this experimental protocol allowed changes in both calcium and chloride current to be tracked at the same time in the same cell in response to the same stimuli.

2.6.3 *Recording chloride current*

The time-independent catecholamine-induced Cl^- currents described in chapters 6 and 7 were recorded using the voltage protocol in figure 2.4c and in the presence of nicardipine to minimize calcium current. Briefly, the cells were held at -90 mV. Every 10 seconds, the membrane potential was stepped to -40 mV to inactivate I_{Na} and I_f and then ramps (dV/dt = ±0.2 V/S) pulses were initiated from -40 to +40 mV and then from +40 to -90 mV before returning to -40 mV and then back to the holding potential of -90 mV. The sampling frequency was 1 kHz, and no filtering was employed to remove the sodium currents superimposed on the capacitative transients seen when stepping from -90 to -40 mV. Minimal residue calcium current contamination was seen only during the depolarising ramp.

2.7 Calcium and holding current analysis

Calcium currents were measured relative to the current level after 280 ms in the control pulse immediately preceding the experimental intervention whether by photolysis of caged compounds or application of pharmacological agents. Analysis of the

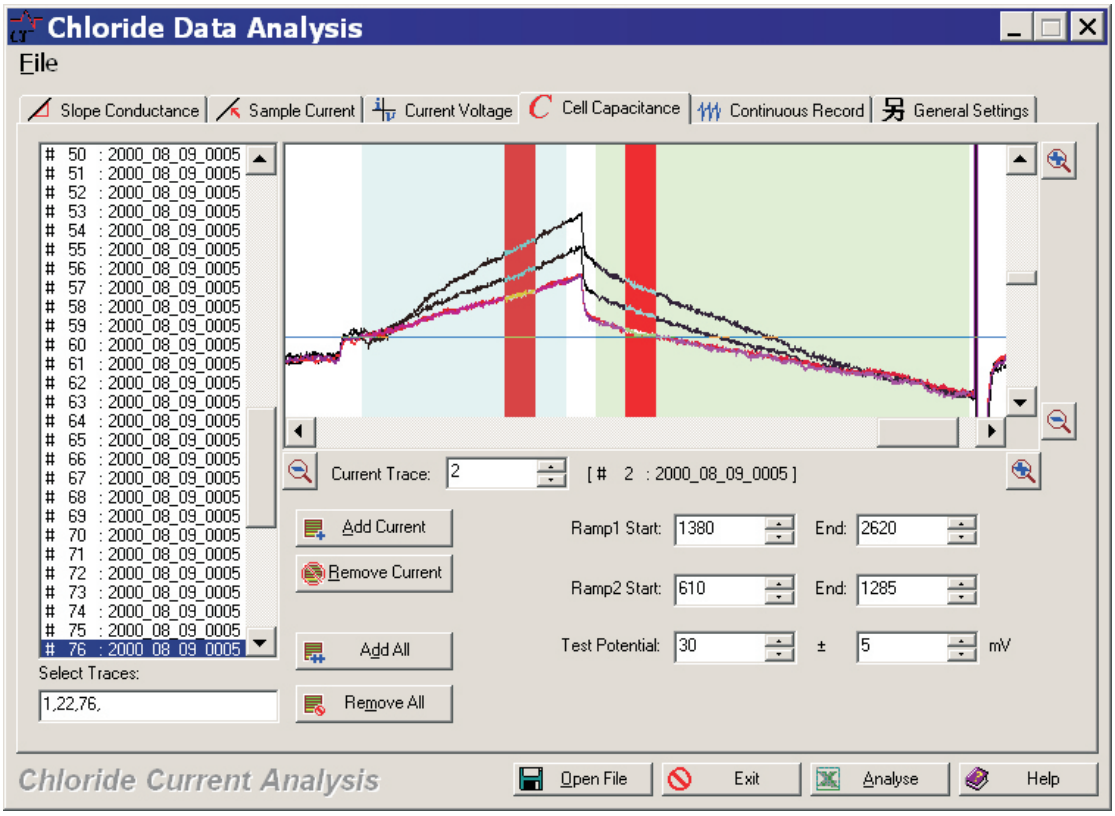

Figure 2.5

A screen snapshot of the *ClAnalyse* programme in cell capacitance analysis mode. The main part of the display shows three records (nos. 1, 22, 76) from the open data file. The hyperpolarising and depolarising ramp regions have been selected (marked in light green and blue respectively) and the values for the current analysis voltage range entered (30 ± 5 mV). The resulting parts of the ramps are selected automatically.

current signals was performed off-line using "*VCAN*" developed by J Dempster (Dempster, 1988). The digitisation rate was at .45 ms.

2.8 Chloride Current Analysis

The chloride current results presented in chapters 6 and 7 were acquired using the *Clampex* (Axon) programme and then analysed with "*Clanalyse*", a research tool developed as part of the work for this thesis (figure 2.5). This programme essentially reads data files produced by Axon Data *ClampEx* or *Clampfit*, performs the necessary analysis and places the results directly into Microsoft *Excel* as numerical data and the corresponding graphs. Comprising roughly 12,000 lines in C++, *Clanalyse* was designed to be protocol-neutral insofar as there are no hard-coded settings or assumptions made *a priori* about sampling rates or the voltage protocol used to evoke and record currents. Instead, sampling regions in the recording protocol in each data file which contain the hyper-polarising and depolarising ramps can be defined interactively. This flexibility extends to the selection of individual records within each data file as well as the settings of various analysis parameters, such as the values or ranges of membrane potentials at which sampling should occur. The intention was not only to remove the need for constant further programming but also to allow the necessary experimentation to discover the optimal analysis parameters.

Clanalyse can automatically produce the time courses for changes in cell capacitance, changes in the average current and slope conductance over specified ranges of a voltage ramp as well as the current-voltage relationships during particular ramps. The continuous current recordings shown in this thesis were also the work of *Clanalyse*.

Only hyperpolarising voltage ramps were used for all measurements except when monitoring cell capacitance changes. Notwithstanding the nicardipine in the superfusate, this procedure minimizes the risks of contamination with residue calcium current.

The average slope conductance and average currents were measured from samples obtained over a voltage range from +10 mV to -10 mV and +5 mV to -5 mV respectively. Changes in any non-specific leak currents would be expected to be minimal around 0 mV. The alternative of measuring slope conductance at the theoretical chloride Nernst reversal potential of ~-55 mV was considered but with the asymmetrical chloride concentrations used, there was significant outward rectification at negative potentials.

The cell capacitance were measured by comparing the currents at equivalent membrane potentials during the corresponding points in depolarising and hyperpolarising voltage ramps:

$$C_m = \frac{\Delta I}{2 \bullet \Delta \delta V / \delta \tau}$$

(*Clanalyse* itself does not assume that the hyperpolarising and depolarising ramps have the same rates of change.). Sample points on the ramps between +25 and +35 mV were used in the calculations. This range was chosen to minimize residue calcium current contamination, to reduce noise due to random fluctuations during the ramp and to allow membrane parameters to settle down immediately after the commencement of the hyperpolarising ramp.

The continuous current records presented in the figures in chapters 6 and 7 were obtained without additional analogue filtering. The compressed time scale means, however, that saturating sodium and capacitative transients would have obscured the evoked chloride current. For that reason, the sodium transients were digitally excised, as an alternative to heavy analogue filtering, by simply not including samples immediately after depolarisations to -40 mV (i.e. when I_{Na} was evoked).

2.9 Presentation of results

Numerical data are given as mean ± standard error of the mean with statistical significance being assessed using paired or unpaired Student's t-test as appropriate. Unless otherwise indicated, significance of data refers to 95% confidence intervals ($p < 0.05$).

Corel *Draw* was used as the page composition programme for all the figures in this thesis which was otherwise written in Microsoft *Word*.

Table 2.1 Superfusing solutions

	Solution 1 (Chapters 4,5)	**Solution 2** (Chapters 6,7)
Nicardipine		1.0 mM
$BaCl_2$		0.2 mM
$CaCl_2$	1.8 mM	1.8 mM
CsCl	5.4 mM	5.4 mM
glucose	5.6 mM	11.2 mM
HEPES	5.0 mM	5.0 mM
$MgCl_2$	1.0 mM	1.0 mM
NaCl	144.0 mM	144.0 mM

Table 2.2 Dialysing solutions

	Solution 3 (Chapters 4,5)	**Solution 4** (Chapters 6,7)
$CaCl_2$	1.0 mM	
Mg-ATP	1.0 mM	5.0 mM
PCr	5.0 mM	10.0 mM
EGTA	10.0 mM	5.0 mM
HEPES	10.0 mM	5.0 mM
CsCl	130.0 mM	20.0 mM
CsAsp		110.0 mM
GTP		0.1 mM

Chapter Three

Efficiency of Flash Photolysis

3.1 Introduction

A high temporal resolution is an essential requirement of techniques used to study the kinetics of biological processes at the cellular level, particularly those which involve complicated modulatory pathways with multiple steps. Diffusion delays and the accompanying spatial and temporal inhomogeneities in any introduced pharmacological agents or substrates are major obstacles. A related complication is the often inadequate and uncertain rates of decline in the concentration of the reagents or the "off-rate" of the stimulus. The release by flash photolysis of regulatory molecules is one of the novel photochemical techniques addressing such difficulties. The flash photolysis technique is particularly well suited to organized systems for *in situ* experiments where systems may be modified additionally by desensitisation or down-regulation of receptor or response systems. This approach comes into its own where the alternative of fast perfusion systems which allow rapid manipulations of the experimental milieu is inappropriate, often because they would represent an unacceptable perturbation in physiological conditions in the study of intact intracellular systems.

"Caged compounds" derive their popular name because of the way the biological activity or the recognition by physiological systems of these pharmacological agents has

been disabled by chemical modification. These biologically inert precursor compounds are either introduced into the cytoplasm of the cell via a perfusion pipette or added to the superfusate. When the concentration of the photosensitive compound has reached steady state levels, it is subjected to an intense pulse of radiation which catalyses the rapid cleavage of the desired free agent. These procedures can initiate processes in less than 1 ms and represent a major breakthrough in the study of cellular function. Typically, this technique is used to examine *in situ* equilibrium responses or the kinetics of any responses following rapid concentration jumps of an applied pharmacological agent (Gurney & Lester, 1987).

Kaplan *et al.* (1978) were the first to use the term "caged" compound in describing P^3-1-(2-nitrophenyl)ethyl ester of ATP (caged ATP). The 2-nitrophenylethyl group of caged ATP is cleaved away by UV light to yield ATP. Caged cyclic nucleotides were first synthesised and physiologically tested by Korth and Engels (1979) and used to study cardiac I_{Ca} (Nargeot *et al.*, 1983). These caged compounds have been designed with the following properties in mind: (A) the caged compound should be biological inert; (B) the photolysis rate should be sufficiently fast and the quantum efficiency high enough to yield effective concentrations on a useful time scale; (C) the side-products of photolysis should have negligible biological activity at the concentrations generated; and (D) the photolysis reaction should be activated at $\lambda \geq 300$ nm to minimize photo-damage to endogenous proteins or nucleotides in the cell.

There has been extensive interest in the photochemistry of the removable *o*-nitrobenzyl group and its derivatives. The quantum efficiency of these caged compounds varies from 0.5-0.6 for caged ATP (Kaplan *et al.*, 1978) to only about 0.35

for caged GTPγS (Walker *et al.*, 1989). The time scale of the photolysis of photolabile compounds is obviously of great importance to such experiments. Photo-cleavage of nitrophenyl esters liberates a proton and a water-insoluble sulfhydryl-reactive side product on hydrolysis. Therefore, the measurement of the "pH jump" can give an accurate picture of the photolysis process. Nerbonne *et al.*, have found that there is a high efficiency of photorelease (0.25-0.5) which varies little with the structure of the protecting or leaving group, with the pH, dielectric constant or ionic strength of the medium. The release of protons appeared to be complete within 5 ms.

The effects of the 2-nitrosocacetophenones photo-by-products can be tested for, and eliminated if necessary, by the use of glutathione or dithiothreitol (DTT). The potential for toxicity can be a limiting factor in the amounts of caged compounds that can be hydrolysed. This is generally only a concern when very high levels of photoreleased nucleotides are required, e.g. photo-releasing millimolar quantities of ATP to activate muscle fibres.

Photolabile precursors of cAMP, GTP and its analogue GTPγS have been used in flash photolysis experiments described in this thesis. These nucleotides can be alkylated on their phosphate groups with 1-(2-nitrophenyl) diazoethane, 1-(3,4-dimethoxy-6-nitrophenyl) diazoethane and 4,5-dimethoxy-2-nitrophenyl diazomethane. The phorbol esters formed as a result are biologically inert and are photosensitive to near UV irradiation at 300-360 nm which causes their photochemical conversion back to the active compound (Dolphin *et al.*, 1988).

The amount of nucleotide which can be released depends on the initial concentration of the precursor substrate and the efficiency of conversion of the

experimental system which would obviously vary from one setup to another, depending on the UV lamp and the optics. For the purposes of the experiments using the flash photolysis described in this thesis, it was important to quantify the UV photorelease of cAMP, GTP and GTPγS not only to ensure that the amounts involved were within a reasonable range of physiological concentrations but also to verify that the release from the photolabile precursors fell within a narrow and consistent range. In other words, it was necessary to ensure that the experimental stimulus in applying these nucleotides was reproducible. To this end, High Performance Liquid Chromatograph (HPLC) was used.

3.2 Methods

3.2.1 *UV Photolysis*

Photolysis of caged compounds was effected by a flash of UV light from a Xenon arc "flash lamp" (Martilla *et al.*, 1977; Hi-Tech, UK) coupled to the rear port of the Nikon Diaphot microscope (Telford, UK). The light pulse of around 1 ms duration was directed at a cell through a 40x objective (Nikon Fluor 40/1.30 oil) using either a 385 nm or a 430 nm long-pass dichroic mirror (DM430, Omega Optical, Brattleboro, VT DM385, Nikon, Tokyo). These mirrors reflect wavelengths of < 385 or < 430 nm (wavelengths of the order of 360 nm are generally required for photolysis of caged compounds). The longer duration of flash-lamp pulses when compared to pulsed laser excitation results in a greater photorelease through multiple excitations.

3.2.2 *Sample preparation*

Caged GTP (50 mM) or caged GTPγS (50 mM) was diluted in 100 mM NaH_2PO_4 along with 1 mM or 0.5 mM GMP as an internal standard. Caged cAMP was dissolved in water to 50 mM. 0.1-0.2 µl of each of these solutions were injected at a time into a drop

of paraffin oil (volume ~20 µl) placed on a cover slip using a positive displacement pipette. The volume of the solution containing the caged sample inside the oil was such that using the standard microscope objective used in all experiments in this thesis, the droplet radius was not more than a quarter of that of the field of vision (at 600x magnification). In other words, when the droplet was brought into focus, it was in the centre of field and would be irradiated in its entirety by the UV flash directed down the objective lens. The sample was subject to either one or five flashes of UV light, with ten seconds between each discharge in the latter case, more than sufficient for the recharging of the current source for the flash lamp. Subsequently, a 20 µl volume containing the irradiated solution in the paraffin oil was collected and frozen at -20°C for not more than 24 hours before analysis.

3.2.3 *HPLC protocol*

Quantification was performed using HPLC (Applied Chromatograph Systems, Macclesfield, Cheshire) linked to a reverse phase C18 column (Techsthere 50 SD). The eluting solutions were NaH_2PO_4 buffer (0.7 M; pH 4.0) for caged GTP and caged GTPγS, and CH_3CN and water (3:7 v/v) for caged cAMP. A spectrophotometer (Applied Chromatograph Systems) set at 254 nM and sensitive to sub-micro-molar concentrations of nucleotides was used to detect released GTP and GTPγS as well as the GMP used as the internal standard for caged guanylyl nucleotides. GMP was included because it was not possible to detect separately and thus measure the peaks for these two caged compounds using these buffers. A separate internal standard was not necessary and was not used for the analysis of the photolysis of caged cAMP.

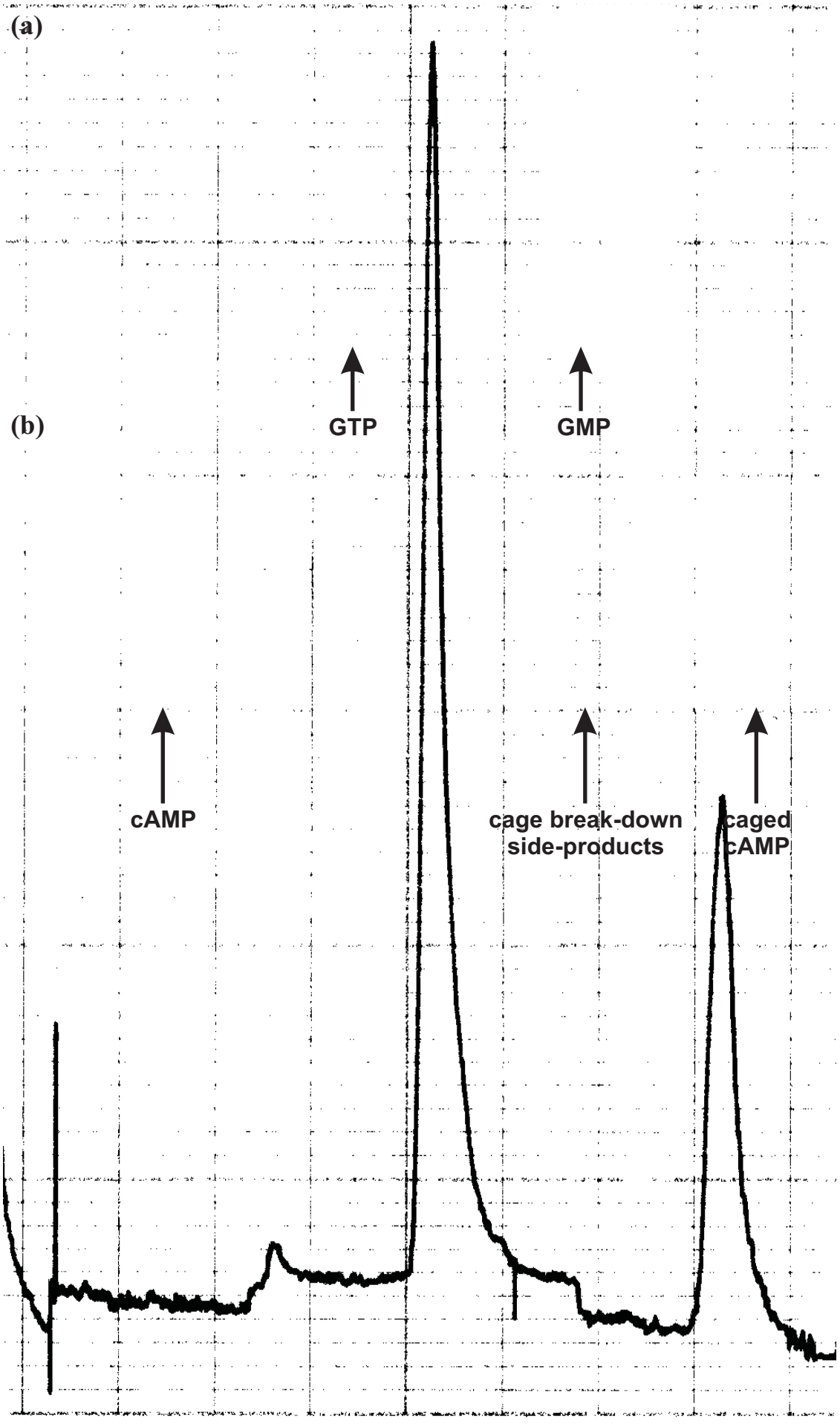
(a)
(b)
GTP
GMP
cAMP
cage break-down
side-products
caged
cAMP

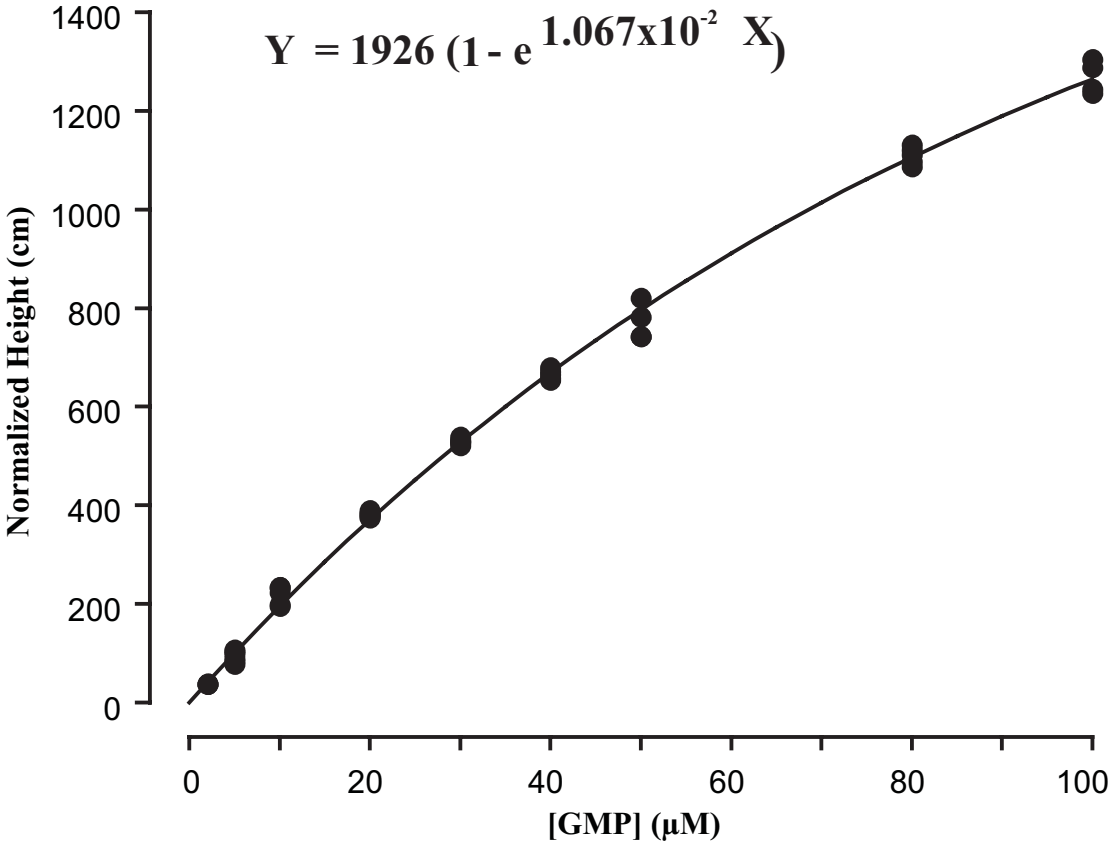

Figure 3.2

HPLC Calibration curve for GMP. This is a plot of GMP concentration against the height of the detected peaks, normalised for the different amplification gains. GMP was used as the internal standard for calculating the concentration of caged GTP and caged GTPγS. The results up to 100 μM GMP were well fitted by the exponential equation shown inset.

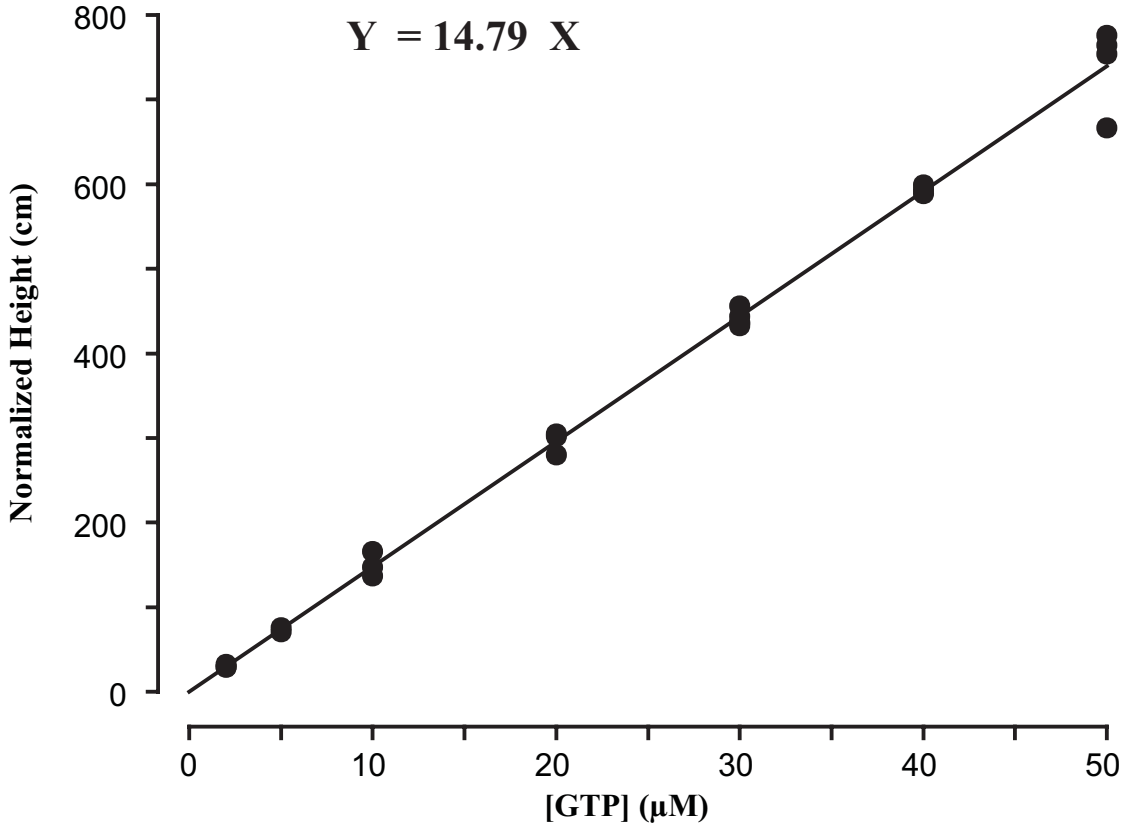

Figure 3.3

The HPLC calibration curve for GTP. The heights of the observed peaks normalised with the amplification gain were plotted against GTP concentration. The equation governing the linear relationship up to a GTP concentration of 50 µM is inset.

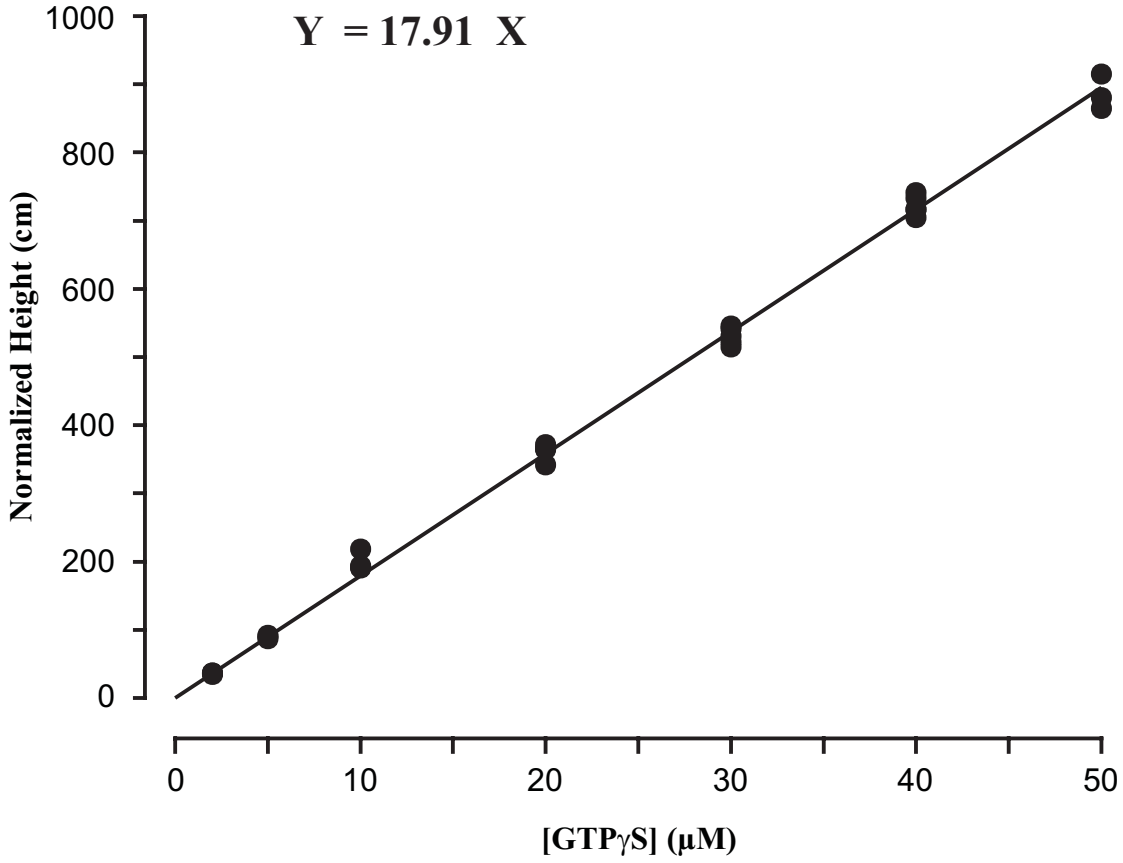

Figure 3.4

The HPLC calibration curve for GTPγS. The heights of the observed peaks normalised for the amplification gain were plotted against GTPγS concentration. These results like those for GTP (in figure 3.2) were well fitted by a linear equation (inset) up to a GTPγS concentration of 50 μM.

Before analysis, the samples were further diluted in 60 µl of the eluting solution. Each sample could usually provide two injections each of 30 µl. Since the injection loop volume was 20 µl, the excess solution ensured that a constant volume was injected each time and that contamination from any possible residue in the loop was avoided.

3.3 Results:

3.3.1 *Efficiency of the photo-release of GTP and GTPγS*

At a flow rate of 1 ml min^{-1}, the retention times for GMP, GTP and GTPγS were ~6.8 min, ~4.0 min ~5 min respectively. Clearly resolved, well defined and reproducible peaks for all three moieties could be distinguished (Figure 3.1). Though a peak representing the caged compounds could not be seen during the normal course of analysis, a sharp peak could be detected when the column was washed out with methanol at the end of each session, corresponding to the very long retention times seen under this protocol. Some minor peaks were also seen in the analysis of GTP, one of which could be accounted for by the presence of GDP. The solvent fronts and injection artefacts could be seen at high gains but as they occurred around 2 minutes after injection, they could be clearly distinguished from the peaks.

Calibrating curves were obtained by analysing known concentrations of the nucleotides. The graph for GMP showed a good fit with a rectangular hyperbola curve (Figure 3.2). In the cases of GTP and GTPγS, there was a linear relationship between nucleotide concentration and the height of the resulting peaks for the sub-mM concentrations detected, with the coefficients of determination (r^2) equal to 0.997 and 0.993 (Figure 3.3 and 3.4).

The concentration of the caged precursors to GTP and GTPγS remaining in the photolysed sample were calculated from the levels of the internal standard (GMP). The levels of liberated GTP and GTPγS could be ascertained directly from their calibration graphs.

A single flash of UV light resulted in the photorelease of 1.8 ±0.2% (n=19) of GTP equivalent to the release of 89.2 ±10.6 μM when 5 mM GTP is included in the pipette solution. Five flashes produced 7.9 ±1.3% (n=6) equivalent to the release of 395.0 ±63.5 μM or 86.7 ±8.5 μM of GTP per flash of UV light. Either value is similar to the concentration found inside the cell physiologically (Breitwieser & Szabo, 1988). Prolonged exposure to UV light, i.e. over 40 minutes, resulted in the almost complete photolysis of the caged GTP in the samples (97.6 ±1.5%; n=4).

In the case of GTPγS, a single flash of UV light photolysed 1.5 ±0.4% (n=11) equivalent to 15 ±0.38 μM with 1 mM caged GTPγS. Five flashes produced 4.2 ±0.6% (n=8), a release equivalent to 41.7 ±5.9 μM GTPγS.

3.3.2 *Efficiency of the release of cAMP*

At a flow rate of 1 ml/min, a well-defined peak was detected after ~1.5 minutes for cAMP. The caged precursor produced a peak after ~9.1 minutes and breakdown of the cage resulted in a third peak at ~6.9 minutes. Because the caged compound could be detected directly, it was not necessary to include another internal standard as with the measurement of the release of the guanylyl nucleotides.

Calibrating curves were obtained by analysing known concentrations of the nucleotides. There was a linear relationship between the concentration of cAMP and the

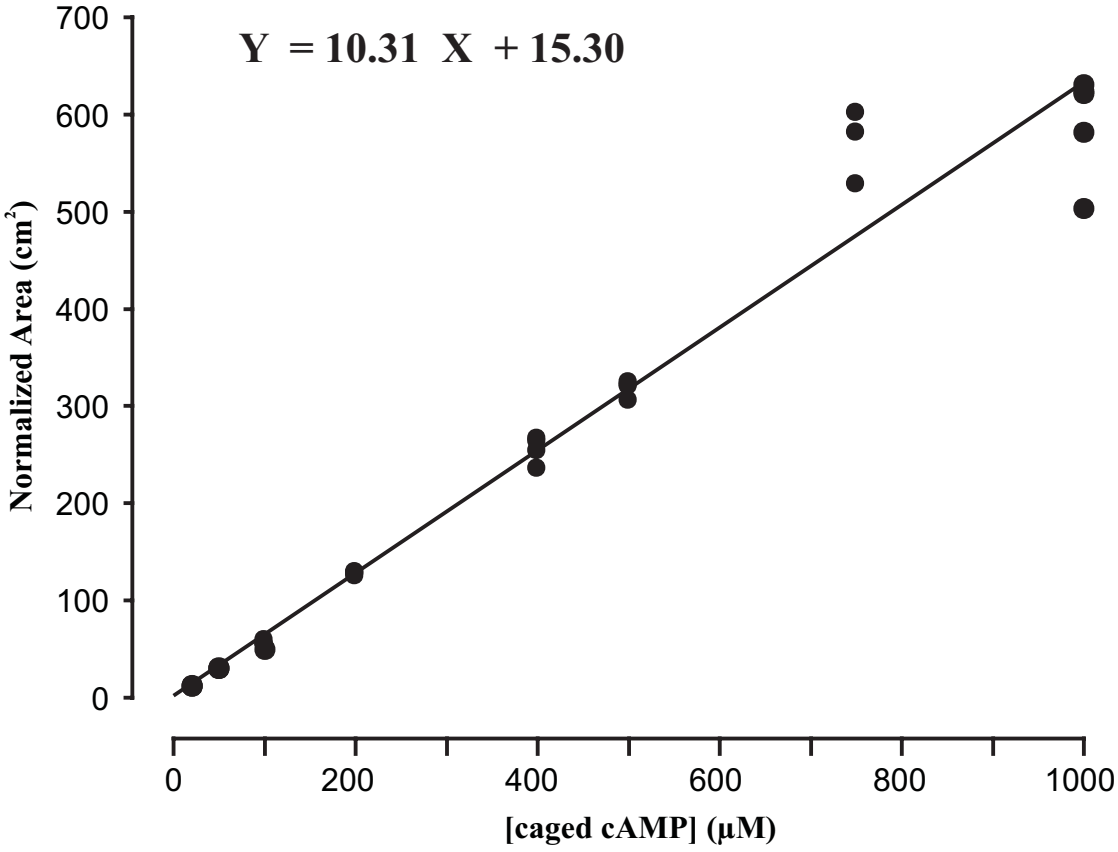

Figure 3.5

The HPLC calibration curve for caged cAMP. Though the heights of the observed peaks showed a degree of variation, the plot, shown above, of the integrated area under each peak against the concentration of the caged molecule is well defined. The areas have been normalised for different amplitude gains. The equation governing the linear relationship up to a caged cAMP concentration of 1 mM is printed inset. The results are well fitted by these parameters particularly at lower concentrations. Unlike the HPLC analysis of the photo-release of GTP or GTPγS, the caged precursor of cAMP could be directly detecte used as a separate peakd with the protocol. No separate internal standard was therefore necessary.

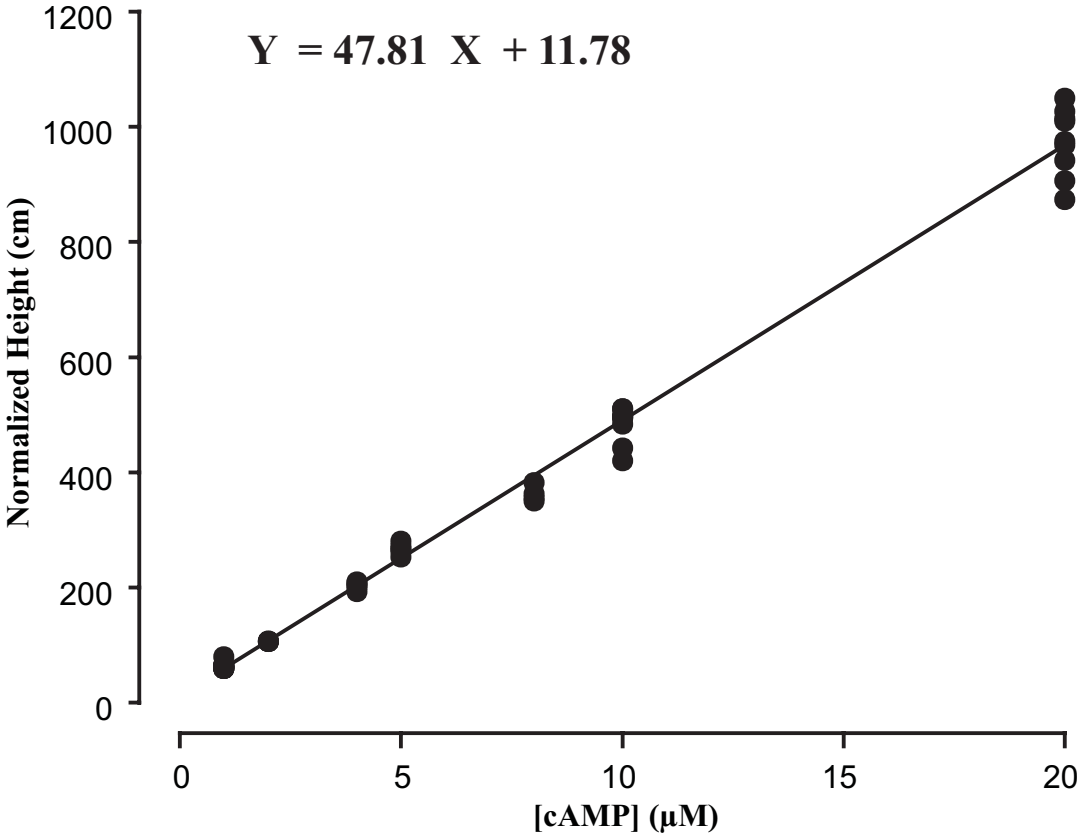

Figure 3.6

The HPLC calibration curve for cAMP. The heights of the observed peaks normalised with the amplification gain were plotted against the cAMP concentration. The results were well fitted by a linear equation (inset) up to a cAMP concentration of 20 µM. The values for the photo-release of cAMP from its caged precursor detected under HPLC all fell within the range of the cAMP values shown in the calibration graph.

heights of the peaks detected with a co-efficient of determination r^2 = 0.990 (figure 3.5). The peaks for caged cAMP were less well defined but the plot of the integration of the area under the peaks against concentration was also linear with r^2 = 0.966 (figure 3.6).

A single flash of UV light resulted in the photorelease of 0.46 ±0.07% (n=18) of cAMP equivalent to the release of 4.64 ±0.7 µM when 1 mM cAMP is included in the pipette solution. Five flashes produced 2.9 ±0.3% (n=12) equivalent to the release of 29.1 ±3.1 µM or 5.82 ±0.6 µM of cAMP per flash of UV light.

3.3.3 *Degradation of caged compounds*

The manufacturers claim 99% purity in the cases of caged GTP and GTPγS and 97% purity in the case of caged cAMP as detected by HPLC. This is confirmed by these results. However, for all the nucleotides used, exposure to room temperature over 24 hours resulted in significant release from the photolabile precursor. In the case of GTPγS this resulted in the release of 4.5 ±1.2% (n=5) and for caged cAMP, 6.4 ±1.6% (n=31). Both of these levels are considerable compared to the normal rates of release in response to single UV flashes. Significant thermal hydrolysis was not detected when normal procedures in handling the caged compounds were followed. This justified the care taken to ensure that solutions containing the caged compound were kept on ice and away from direct sunlight during physiological experiments.

Chapter Four

Effects of Photo-release of GTP

4.1 Introduction

It is known that G-proteins mediate the transduction of the stimulus from the presentation of a β-adrenergic agent, for example, isoprenaline, at the membrane receptor to its final intracellular effects (e.g., the activation of calcium current in cardiac ventricular myocytes). This chapter describes experiments to investigate the involvement of G-protein pathways and their underlying kinetics. The natural endogenous ligand of G-proteins is GTP. However, in the absence of any agonist, this nucleoside would be expected to be rapidly hydrolysed. Thus, much of the previous work has focused on use of GTPγS, the slowly hydrolysed thiophosphate analogue of GTP (Pelzer *et al.*, 1990; Shuba *et al.*, 1990). The slower hydrolysation of GTPγS not only prevents it from being degraded prematurely inside the cell but also causes sustained activation of the G-protein.

There is good evidence that G-proteins not only activate cytoplasmic enzymes such as adenylyl cyclase which leads to cAMP-dependent phosphorylation of the ion channels but may also be directly coupled to a membrane-delimited pathway regulating channel activity. The α-subunits of G_i-proteins can directly stimulate muscarinic (Yatani *et al.*, 1987) K^+ channels and inhibit hyperpolarization activated non-specific (I_f)

channels in cardiac myocytes. The proposal that the G_s-protein in this tissue not only couples membrane β-adrenoreceptors to adenylyl cyclase but also has a fast direct membrane-delimited effect on L-type Ca^{2+}-channels (Yatani *et al.*, 1987) is more controversial. Pelzer *et al.* (1990) have shown that I_{Ca} can be increased by isoprenaline in ventricular myocytes under conditions unable to support a response to forskolin and hence phosphorylation, suggesting that I_{Ca} modulation may involve an additional non-cAMP-dependent pathway. Hartzell *et al.* (1992), however, suggest that such a fast pathway is not present, since they only found an increase in I_{Ca} seconds after applying isoprenaline via a fast switching perfusion system.

The technique of flash photolysis allows a rapid jump in GTP concentration inside the cell. This permits direct activation of the G-protein to further investigate this controversial question. Each UV flash releases a quantity of GTP (89.2 $\pm$10.6 µM, see section 3.3.1) from its photolabile precursor sufficient to double the estimated physiological levels (100 µM, Bourne *et al.*,1991). In the absence of any agonist, GTP might be expected to be rapidly hydrolysed to GDP without causing any response. However, photoreleased GTP still produces a rapid and sustained increase in calcium conductance. The results presented below show that the calcium current (I_{Ca}) is carried through L-type Ca^{2+} channels and may be separated into two components, one of which is mediated by cAMP-dependent phosphorylation. The other part of the response is transient, very rapid and seen within 20 ms of the photolysis of caged GTP, and is resistant to blockade of the cAMP dependent pathway.

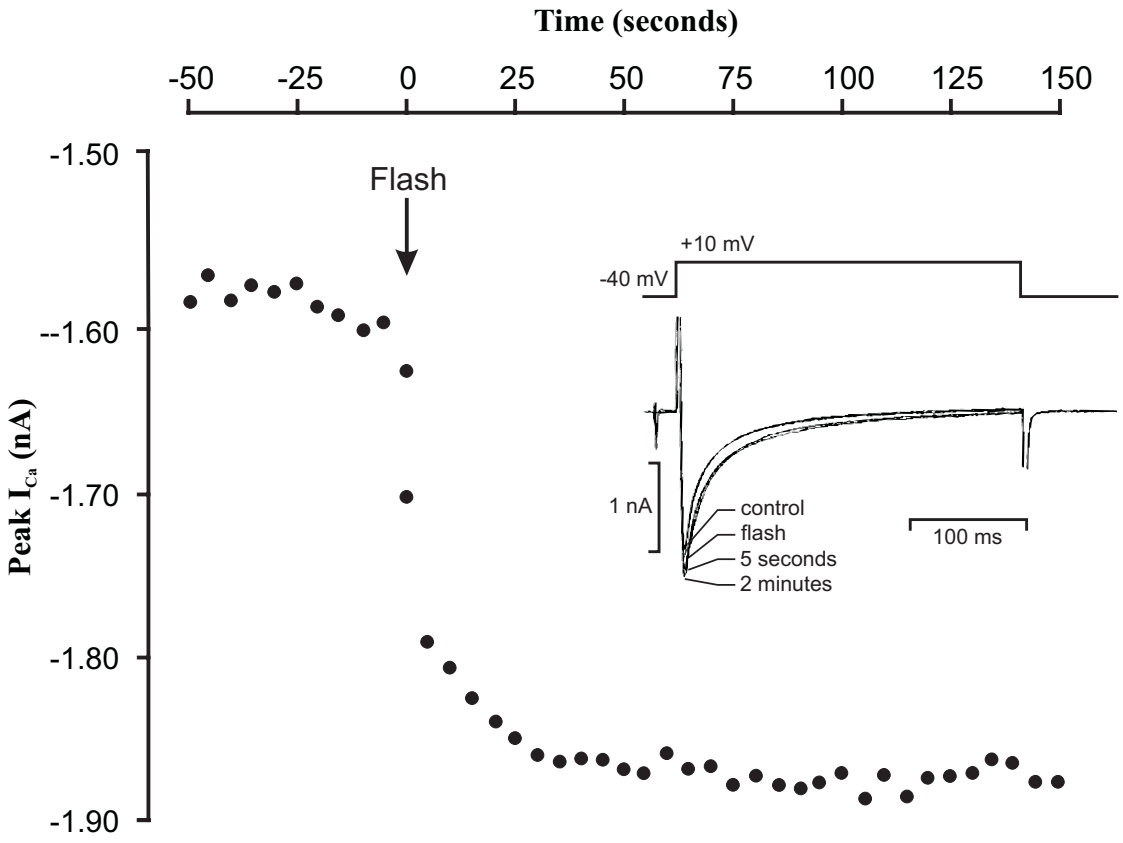

Figure 4.1a

A plot of peak I_{Ca} against time in a single ventricular cardiac myocyte. In this cell, the flash photolysis of 5 mM caged GTP produced a sustained increase in calcium current. A single uv light flash 20ms before a voltage clamp pulse (at time 0 on the graph) induced a marked increase in peak I_{Ca} which reached a plateau 150-200 seconds after the stimulus. Inset are non-leak subtracted raw current traces from the same cell. The calcium currents shown were recorded at test potentials of +10 mV. Pre-conditioning depolarizations to -40mV were designed to inactivate sodium and T-type calcium channels. The traces shown were obtained immediately before and after the light pulse, and after 5 and 120 seconds. These clearly illustrate the maintained rise in calcium current.

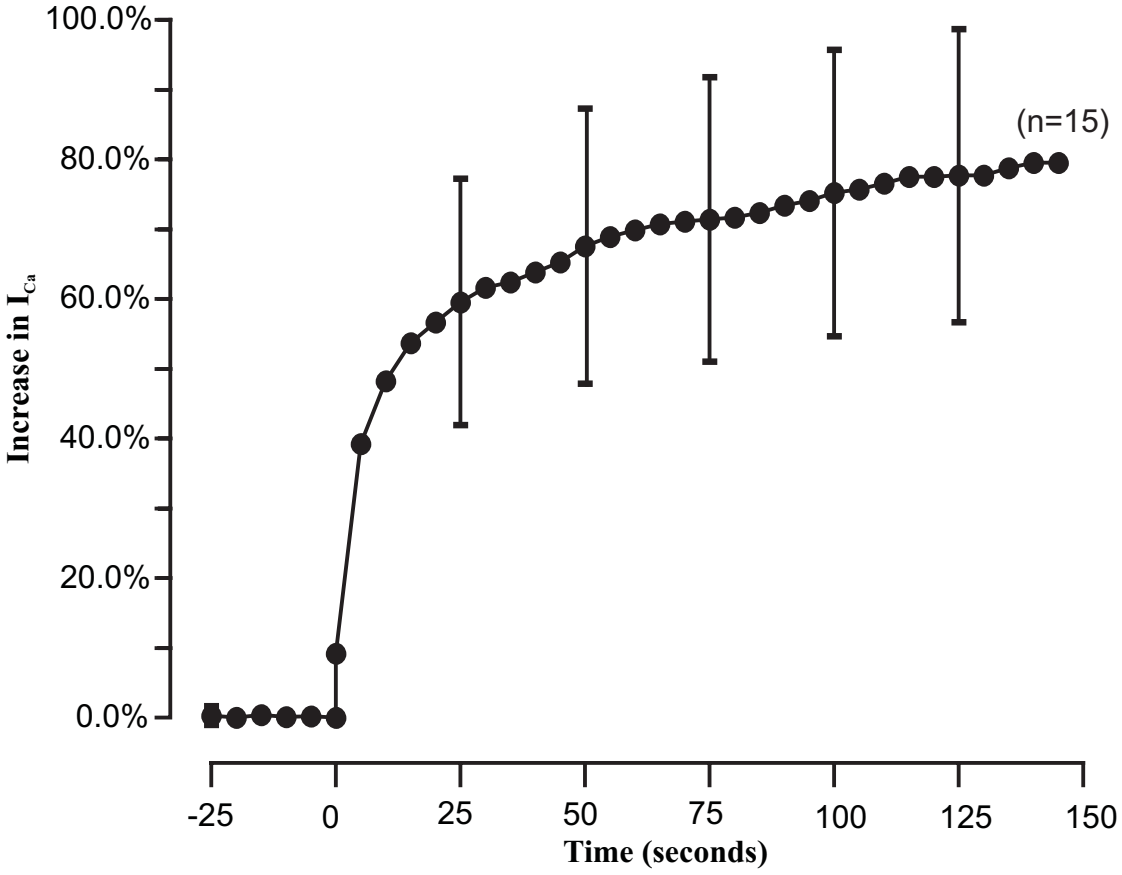

Figure 4.1b

Results showing the average time course for sustained responses in peak I_{Ca} to photoreleased GTP. The increase relative to control in non-leak-subtracted peak Ca^{2+} currents recorded during a test potential of +10mV from a holding potential of -80mV were plot against time. The cell was dialysed with 5 mM GTP. A single light flash 20ms before the onset of a voltage-clamp pulse induced a sustained response in I_{Ca} which only reached a plateau 180-200 seconds after the stimulus. The vertical error bars show the standard errors of the mean at those intervals and the number of experiments is printed to the right of the graph.

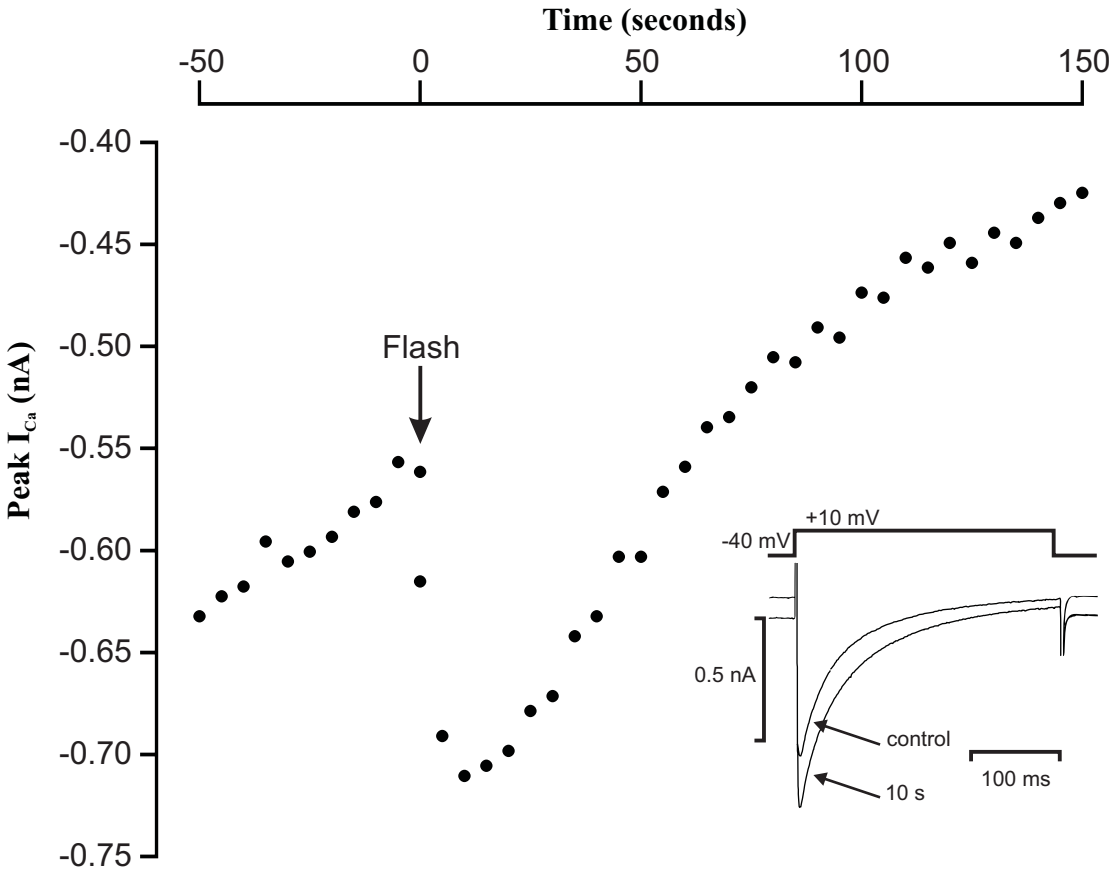

Figure 4.2

A plot of peak I_{Ca} against time in a single ventricular cardiac myocyte. In this cell, the flash photolysis of 5 mM caged GTP only produced a transient increase in calcium current. A single light flash 20ms (at time = 0 on the graph) before a voltage clamp pulse induced an increase in peak I_{Ca} which reached a peak a mere 10 seconds after the stimulus before declining rapidly. What was evident in this cell was rapid rundown of calcium current before the photorelease of GTP. The currents resumed the same course of decline after 100 - 150 seconds.

Inset are non-leak subtracted raw current traces from the same cell. The calcium currents shown were recorded with a test potential of +10 mV from a pre-conditioning voltage of -40 mV. The traces shown were obtained immediately before the flash photolysis, and after 10 and 150 seconds.

4.2 Results:

For the experiments described in this chapter, any flash photolysis of caged GTP was effected around 10 minutes after the formation of a whole-cell patch clamp seal by UV flash (as described in chapter 2). Where isoprenaline, forskolin and "photolytic by-products" were added to the superfusing solution, this was achieved by replacing the standard external solution (solution 1 in table 2.1) with one containing the additional compounds via bath perfusion. The time-to-peak responses were calculated from the moment the new solutions arrived in the bath (detected by visual observation) and thus have an approximate error in the range of ±0.5 s.

4.2.1 *Effects of photoreleased GTP*

A single flash of UV light directed at a cell dialysed with the standard internal solution (solution 3 in table 2.2) containing 5 mM caged-GTP induced a rapid increase in calcium current (I_{Ca}), which could be detected with a voltage-clamp depolarisation step within 20 ms of the flash. This was generally followed by a more gradual sustained increase in peak I_{Ca} (figure 4.1a). The mean increase in 13 cells was 67.5 ±16.8% and the time course for this increase had a time to peak of 157 ±26 s (see figure 4.1b). The initial jump in I_{Ca} seen after 20 ms had a mean of 9.4% ± 1.2%.

In six other cells, a transient increase in peak calcium current was observed. Figure 4.2 shows a typical response of this kind. This seemed to be associated with a run-down in I_{Ca} seen before photolysis, and hence also smaller initial I_{Ca}. Mean I_{Ca} before the UV flash was -1.1 ±0.12 nA (n=13) in cells where sustained increases were seen but only -0.78 ±0.17 nA (n=6) with current run-down and transient responses. In these cells, the photoreleased GTP produced a mean increase of 76.1 ±28.8% which reached

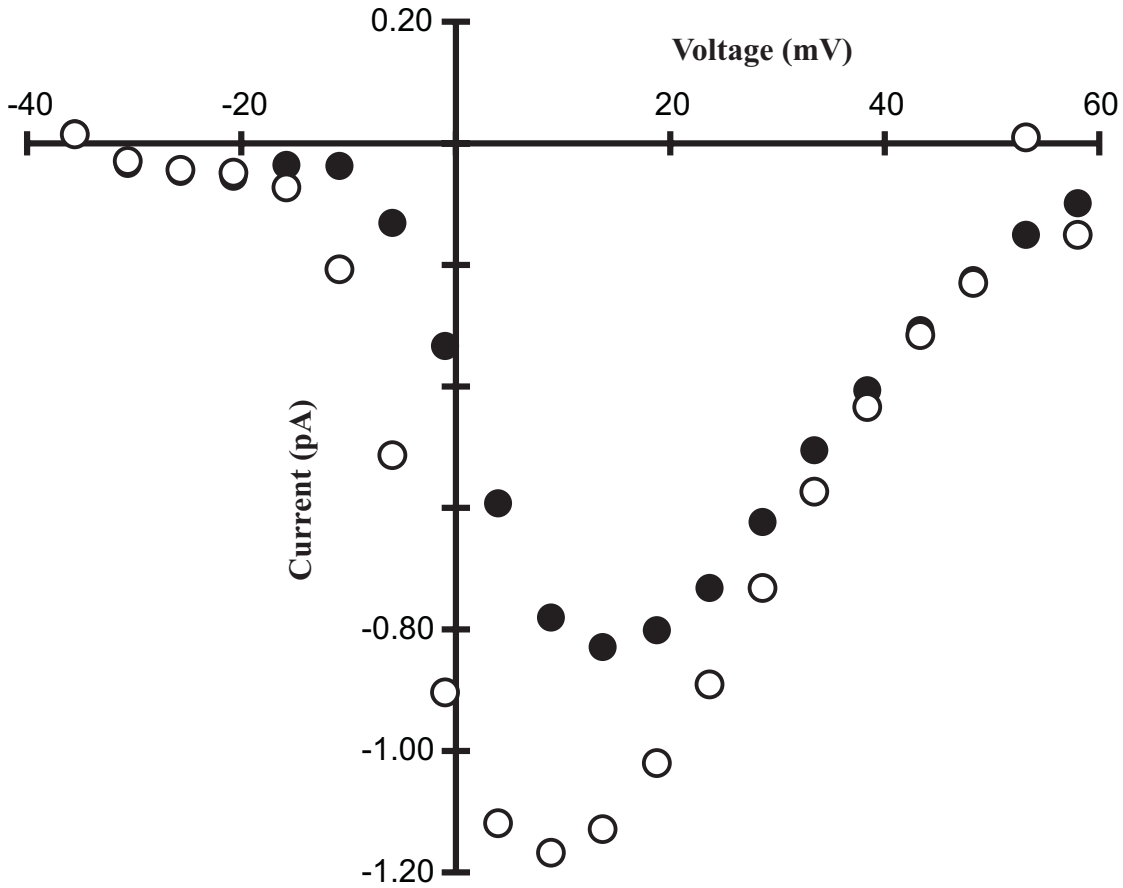

Figure 4.3

A plot of the current voltage relationship of the peak I_{Ca} seen before (●) and after (○) the flash photolysis of 5mM caged GTP. Depolarisations to around +10 mV before the release of GTP produced the maximum I_{Ca}. The photolysis of caged GTP caused an increase in calcium current with a shift to the left in the peak of the IV-curve. Test voltage steps were made from pre-conditioning depolarizations to -40 mV to inactivate sodium and T-type calcium currents.

a peak after a mere 16.7 ±2.5 s. The rates of run-down before GTP was released and after the response had run its course (~60 s after the UV flash) were broadly similar.

4.2.2 Current change is due to I_{Ca}

This activating effect of photoreleased GTP was evident over a range of test potentials. Cells were voltage clamped at -40 mV and then a voltage step to different test potentials was applied for 300 ms. Current amplitudes were measured relative to the current level 280 ms after initiation of the voltage clamp test pulse. Current-voltage (I-V) plots obtained from five cells show a bell-shaped relationship typical for $I_{Ca,L}$ in different preparations (McDonald *et al.*, 1994). A comparison of the currents recorded just before the photorelease of GTP and approximately 3 minutes later shows an increase in peak I_{Ca} from -0.82 ±0.19 nA to -1.36 ±0.22 nA, with a shift in the maximum current density from +15.3 ±1.9 mV to +11.3 ±1.3 mV (figure 4.3). These results are consistent with the reported effects on I_{Ca} of stimulation of β-adrenergic pathways in cardiac myocytes (Bean *et al.*, 1984) or the actions of the dihydropyridine BayK8644 (Brown *et al.*, 1986).

The dialysing solution and the experimental protocol used were designed to isolate I_{Ca}. However, to remove the possibility that the change in current following the flash was due to contamination by any other ionic current, "Ca^{2+} antagonists" nicardipine (2 μM) or Ni^{2+} (5 mM) were applied after the rapid release of photolabile GTP. Both completely abolished the time dependent current observed, confirming that the results were due entirely to the stimulation of L-type Ca^{2+} current without any additional contribution from other ionic currents.

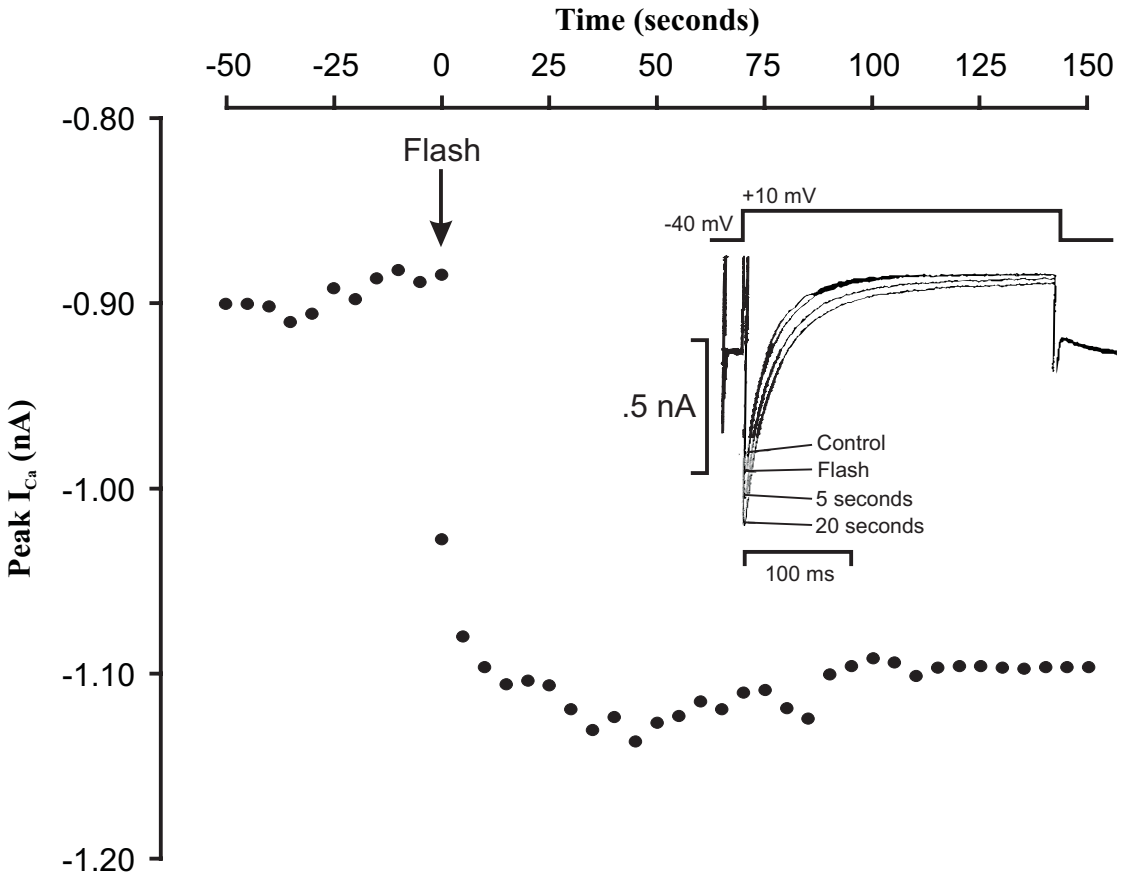

Figure 4.4a

A plot of peak I_{Ca} against time for the calcium current recorded from a single cardiac ventricular myocyte. The cells were co-dialysed with 5 mM caged GTP and 10 mM dithiothrietol (DTT). A single flash 20ms before the test pulse at time = 0 produced an large immediate increase in I_{Ca} and the response was sustained even after 2.5 minutes.

Inset are non-leak subtracted raw current traces from the same cell. The calcium currents shown were recorded at test potentials of +10 mV after pre-conditioning steps to -40 mV. Traces immediately before and after the flash, after 5 seconds, and at the peak of the response are shown.

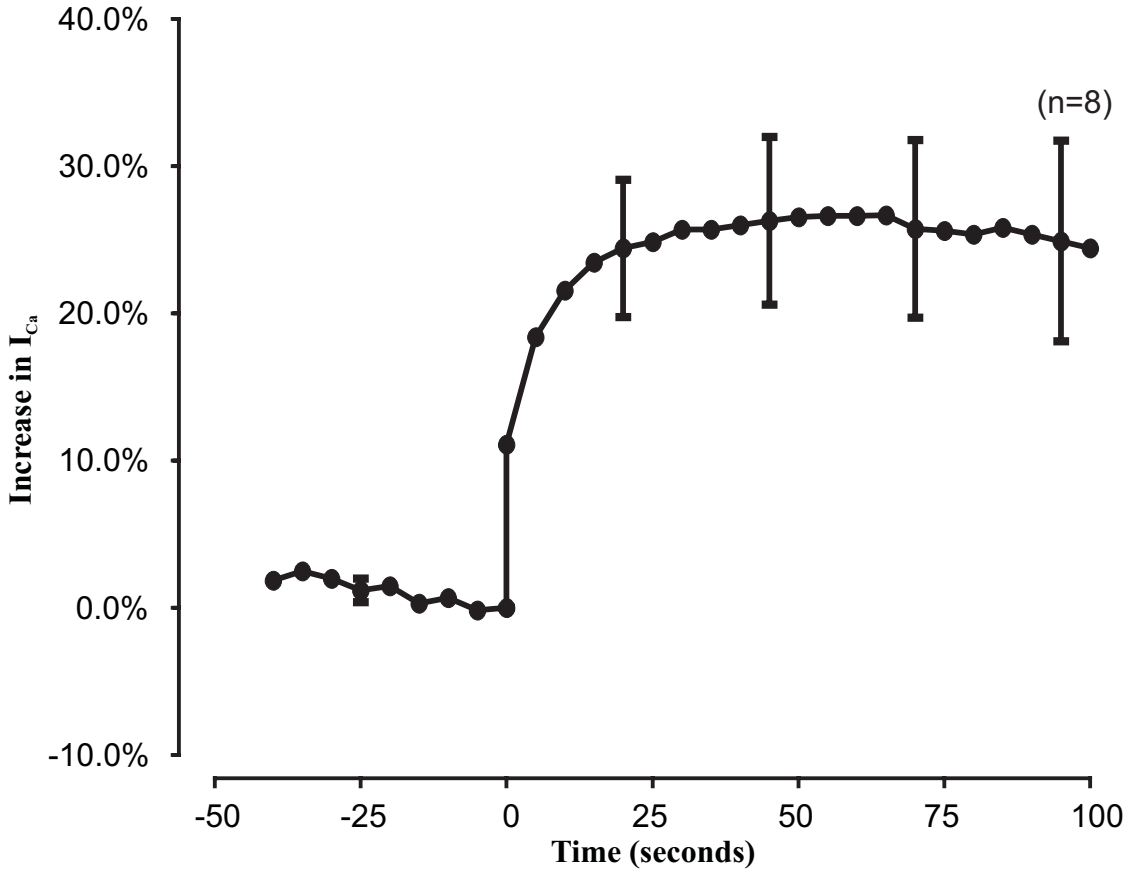

Figure 4.4b

A graph showing the average time course of the results of photolysis of 5 mM caged GTP in the presence of DTT. The values were calculated as percentage increases from the control peak I_{Ca} seen just before the flash photolysis. As in the single cell in figure 4.4a, the averaged response shows that I_{Ca} increases significantly within 20ms before rising to a plateau. The increase in I_{Ca} is reduced however when compared with the responses to photoreleased GTP in the absence of DTT (figure 4.1). This may be a non-specific effect of the sulphydryl. The vertical error bars show the standard errors of the mean at those intervals and the number of experiments is printed to the right of the graph.

4.2.3 *Validation of the flash photolysis technique*

4.2.3.1 Effects of UV light pulses alone

Before examining further the effects of photolysis of caged GTP, it was important to show that the current increases were due to the release of GTP and not the result of either the UV light pulse *per se* or photolytic by-products. Control experiments performed in the absence of any caged compounds indicate that the UV flash alone had little effect on $I_{Ca.}$ A blip with a mean size of 1.1 ±0.1% was seen at the first test pulse 20 ms after the UV flash (n=4) but there were no significant changes in I_{Ca} afterwards.

4.2.3.2 Effects of GSH and DTT on photoreleased GTP

The effects of the photolysis of 5 mM caged GTP were also examined in the separate presence in the dialysing solution of two sulphydryl compounds which rapidly sequester photolytic by-products. Inclusion of 10 mM glutathione (GSH) did not significantly alter the response to the photorelease of GTP, which increased I_{Ca} by 44.1 ±4.6% with a response time to peak of 118 ±26 s (n=4).

Figure 4.4a sets out the results of the photolysis of 5 mM caged GTP from a myocytes co-dialysed with 10 mM dithiothrietol (DTT). The profile of the response was much the same as those from cells showing a sustained response to photoreleased GTP alone. The accompanying figure 4.4b sets out the average time course. Again, the responses were qualitatively similar to control, though both magnitude of response (28.8 ±5.8%; n=5) and time to peak (58 ±13 s; n=5) were significantly reduced.

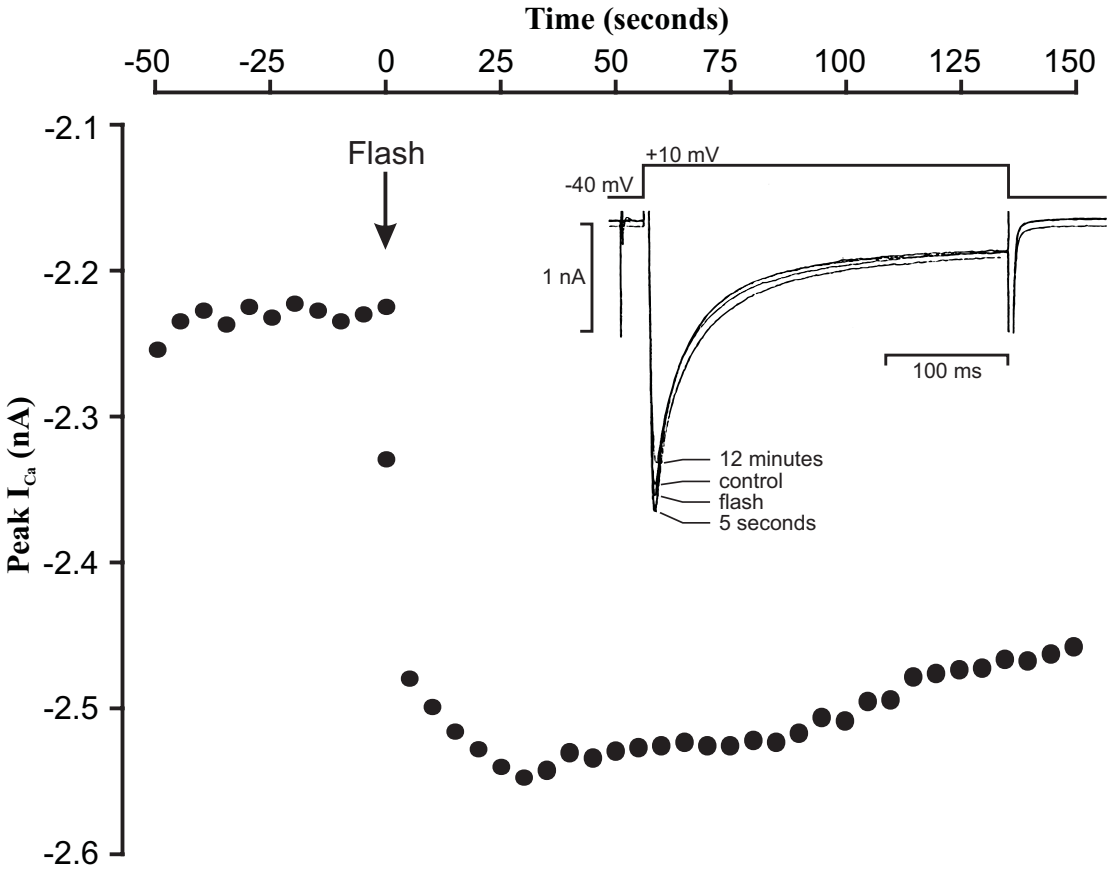

Figure 4.5a

A graph showing the response in a single cardiac ventricular myocyte to photoreleased GTP in the presence of a further 10 mM GTP. The cells were co-dialysed with 5 mM caged GTP and 10 mM uncaged GTP. A single flash 20ms before the test pulse at time = 0 produced an large immediate increase in I_{Ca} which reached a reduced but sustained plateau.

Inset are non-leak subtracted raw current traces from the same cell. The calcium currents shown were recorded at test potentials of +10 mV after pre-conditioning steps to -40 mV. Traces immediately before and after the flash and at the peak of the response are shown.

4.2.3.3 "Caged Water"

The photolysis of "caged water" (see chapter 2) produces water and, via di-radical intermediates, a nitrosoketone photolytic by-product (2-nitrosoacetophenone) identical to that found in photolysis of caged GTP. The application of a UV flash to cells dialysed with 5 mM (n=5) or 10 mM (n=2) "caged water" produced either no change in I_{Ca} or induced a slight decrease. The extra-cellular application of photolytic by-products obtained from the bulk photolysis of "caged water" at an approximate concentration of 1.25 mM (assuming a molecular mass of 165 for nitrosoketone) also produced no change in I_{Ca}. In the light of these results, it seems extremely unlikely that the effects of photolysis of caged GTP were due to anything else other than the photorelease of GTP.

4.2.4 Photorelease of GTP in the presence of 10 mM ambient GTP

Figure 4.5a sets out the results of the photorelease of GTP when 10 mM GTP was already present in the dialysing solution. Although there was a rapid increase in calcium current rising to a plateau, similar to the sustained responses to photoreleased GTP alone, the magnitude of the changes was much reduced. This was reflected in the mean results. The presence of 10 mM GTP in the dialysing solution reduced the peak response to 21.3% ±11.2 (n=5). The immediate increase within 20 ms of the UV flash was also much diminished at 3.8 ±1.4% (n=5) and the response reached a plateau within 20-25 s. The average peak I_{Ca} after photorelease of GTP was -1.68 ±0.28 nA (n=5), which was not significantly different from the control response (-1.50 ±0.15 nA; n=19). This suggests that both dialysing and photoreleased GTP act at the same site competitively. It seems likely that 10 mM GTP in the pipette-dialysing solution provides a nearly saturating concentration of GTP for the effect on I_{Ca} and that only a small further

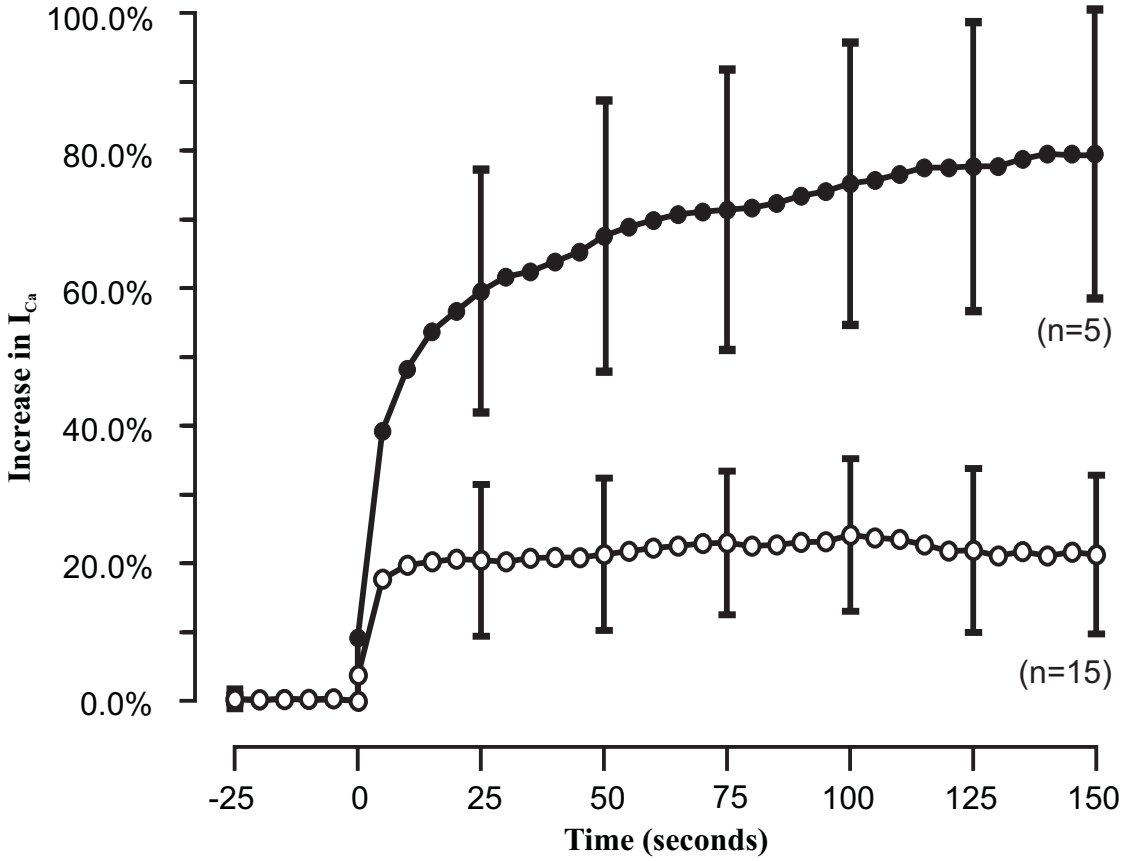

Figure 4.5b

A graph showing the average time course of the results of photolysis of 5 mM caged GTP in the presence (○) and absence (●) of a high concentration of GTP. The response were calculated as a percentage increase from the control peak I_{Ca} seen just before the flash photolysis. The inclusion of high levels of GTP greatly reduced the response to further photoreleased GTP. The plateau response was more inhibited by the pre-dialysis with GTP than the initial jump in I_{Ca} seen during the test pulse 20ms after the light flash. The vertical error bars show the standard errors of the mean at those intervals and the number of experiments is printed to the right of each curve.

increase is possible. This reduced effect (figure 4.5b) may be contrasted with the control sustained response where I_{Ca} was still increasing steadily after 150 s (figure 4.1b).

4.2.5 Photorelease of GTP with GTPγS or GDPβS

To investigate whether the increase in I_{Ca} was due to the effects of photoreleased GTP on G-proteins, experiments were carried out with the additional presence in the dialysing solution of either of two non-hydrolysable guanine-nucleotide analogues nucleotides, GTPγS and GDPβS, which are known to stimulate or block respectively G-protein dependent pathways.

4.2.5.1 Effectiveness of GDPβS

The effectiveness of intracellular GDPβS in inhibiting G-protein activation was first demonstrated by its ability to block increases in I_{Ca} evoked by extra-cellular application of isoprenaline. The standard superfusing solution (solution 1, table 2.1) was replaced with one containing 1 μM isoprenaline until at least two minutes after the maximum effect was observed. The average increase in I_{Ca} was 158.6 ±31.2% (n=12), which occurred 196 ±22 s (n=12) after the isoprenaline-containing solution arrived at the perfusing chamber. When this experiment was repeated with 1 mM GDPβS and 5 mM caged GTP in the pipette solution, no significant change was observed in either the increase in I_{Ca} (145.5 ±10.7%; n=8) or the time to peak response (205 ±30 s) after the application of 1 μM isoprenaline. Omission of caged-GTP from the dialysing solution did not significantly change the response to isoprenaline (95.7 ±27.3%; 178 ±19 s; n=4).

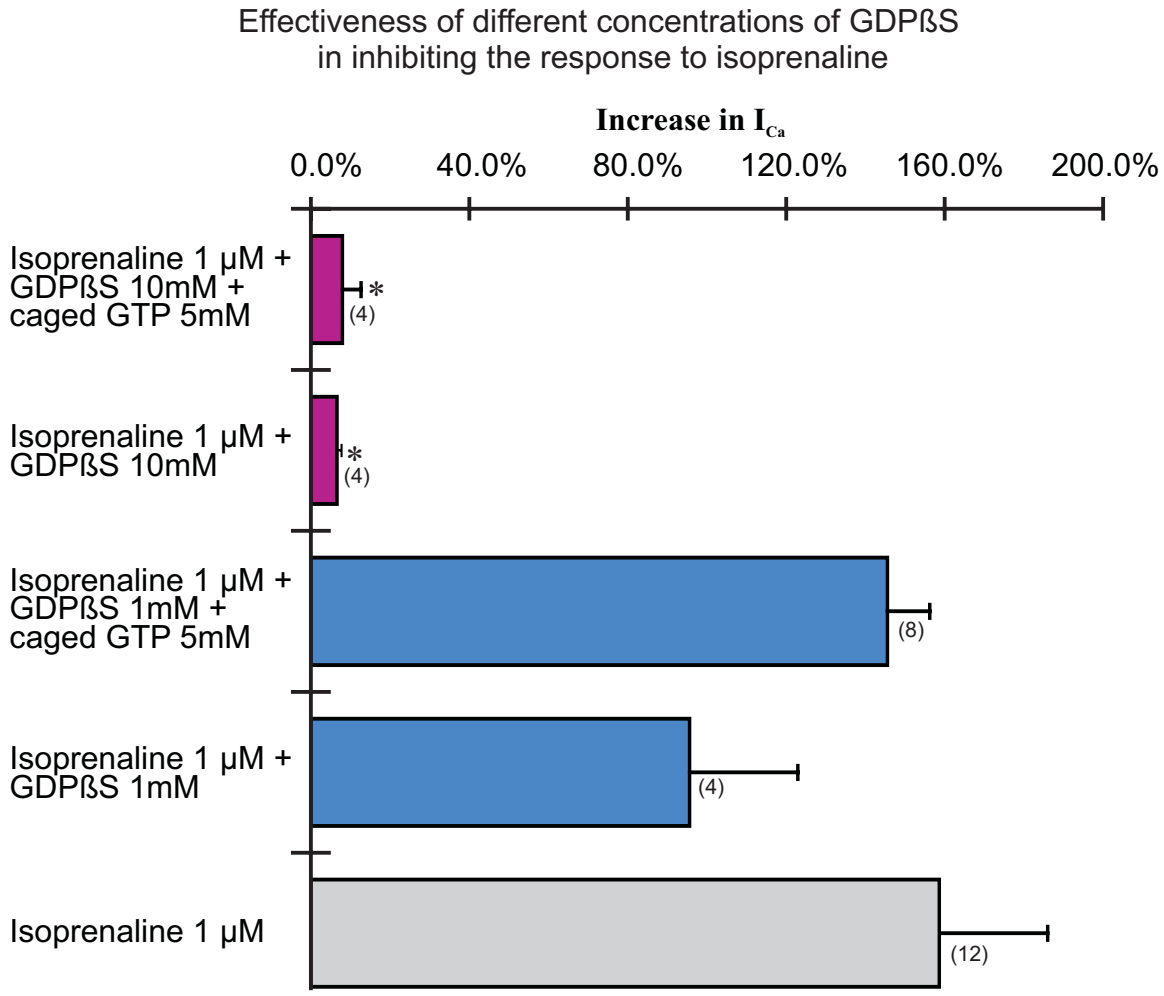

Figure 4.6

A bar graph showing that 1 µM GDPßS is not sufficient to significantly inhibit the average response to 1 µM isoprenaline. This was true whether caged GTP (5 mM) was present or not. However, at 10 mM, GDPßS almost complete abolishes the response to isoprenaline, again whether or not caged GTP was present or not. The number of cells for each experiment are indicated beside the error bars and asterisks (*) indicate significant differences ($p < 0.05$) from the isoprenaline response.

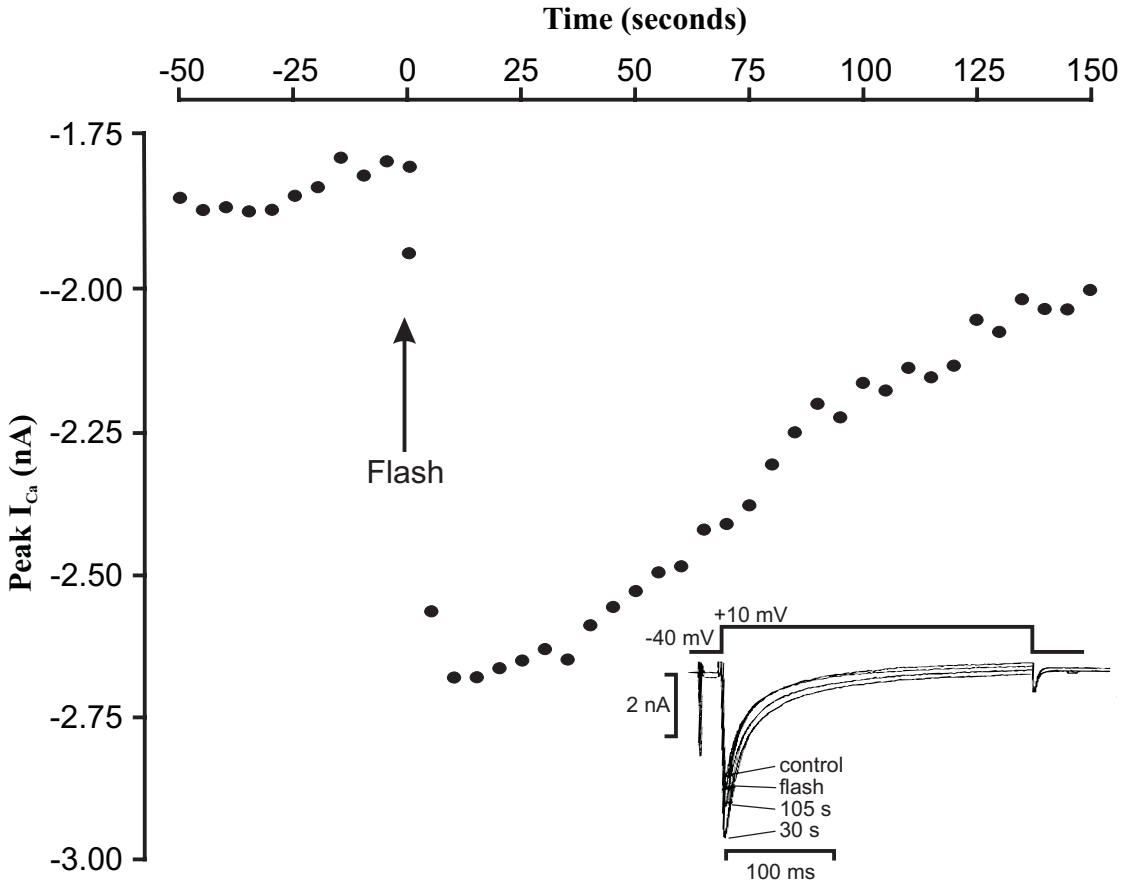

Figure 4.7a

A plot of peak I_{Ca} against time for the calcium current recorded from a single ventricular myocyte dialysed with a solution containing 5 mM caged GTP and 1 mM GDPßS. A single light flash elicited a rapid increase in I_{Ca} which declined gradually with time.

Inset are non-leak subtracted raw current traces from the same cell. The calcium currents shown were recorded at test potentials of +10 mV after pre-conditioning steps to -40 mV. The traces shown were obtained immediately before and after the flash, at the peak of the response, and after 105s.

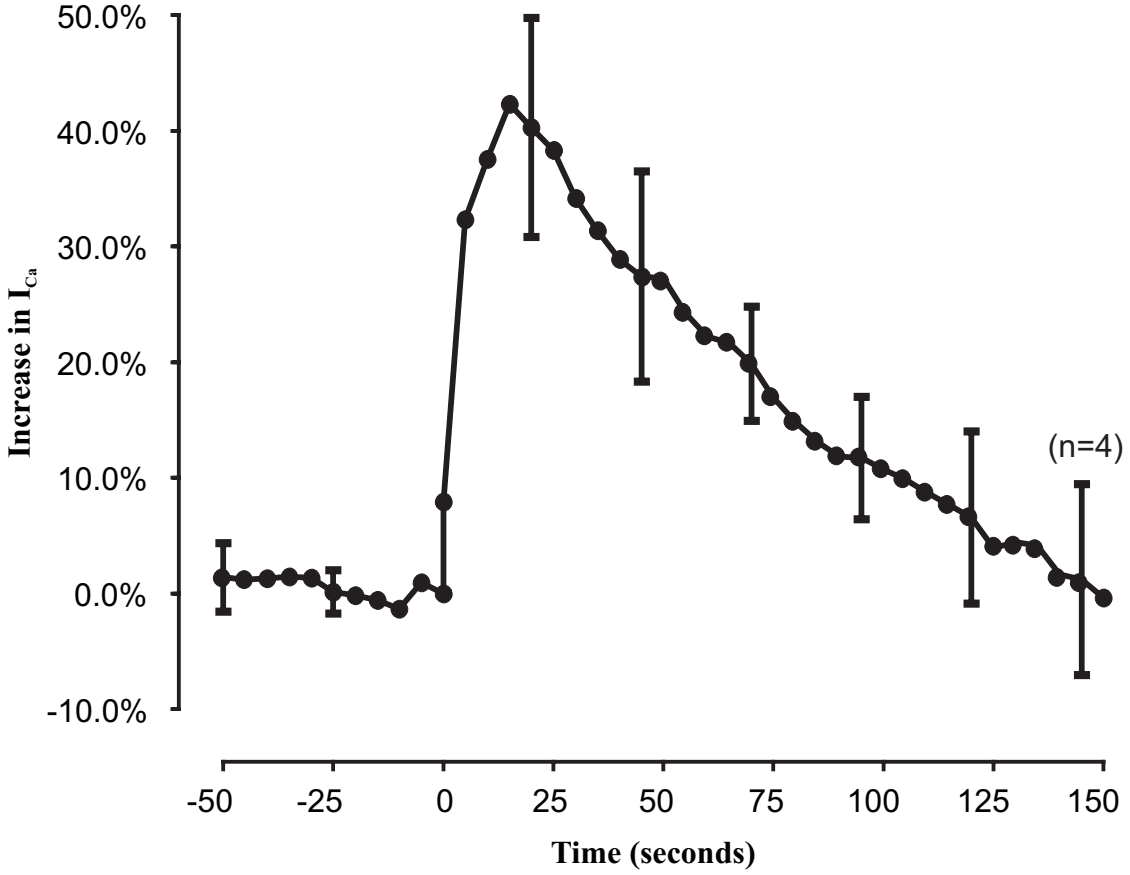

Figure 4.7b

A graph showing the average time course of the results of photolysis of 5 mM caged GTP in the presence of 1mM GDPßS in 4 cells (out of 7) which showed an inhibitory effect for GDPßS. The response were calculated as percentage increases from the control peak I_{Ca} seen just before the flash photolysis. The inclusion of this concentration of GDPßS was able to inhibit but not abolish the response of peak I_{Ca} to photoreleased GTP in these cells. What is most obvious is the absence of a sustained component. In control cells, a transient response is only seen when the I_{Ca} exhibits rapid rundown before flash photolysis. The initial rapid increase in I_{Ca} seen by the time of the test pulse 20ms after the light flash remained. The vertical error bars show the standard errors of the mean at those intervals and the number of experiments is printed to the right of the graph.

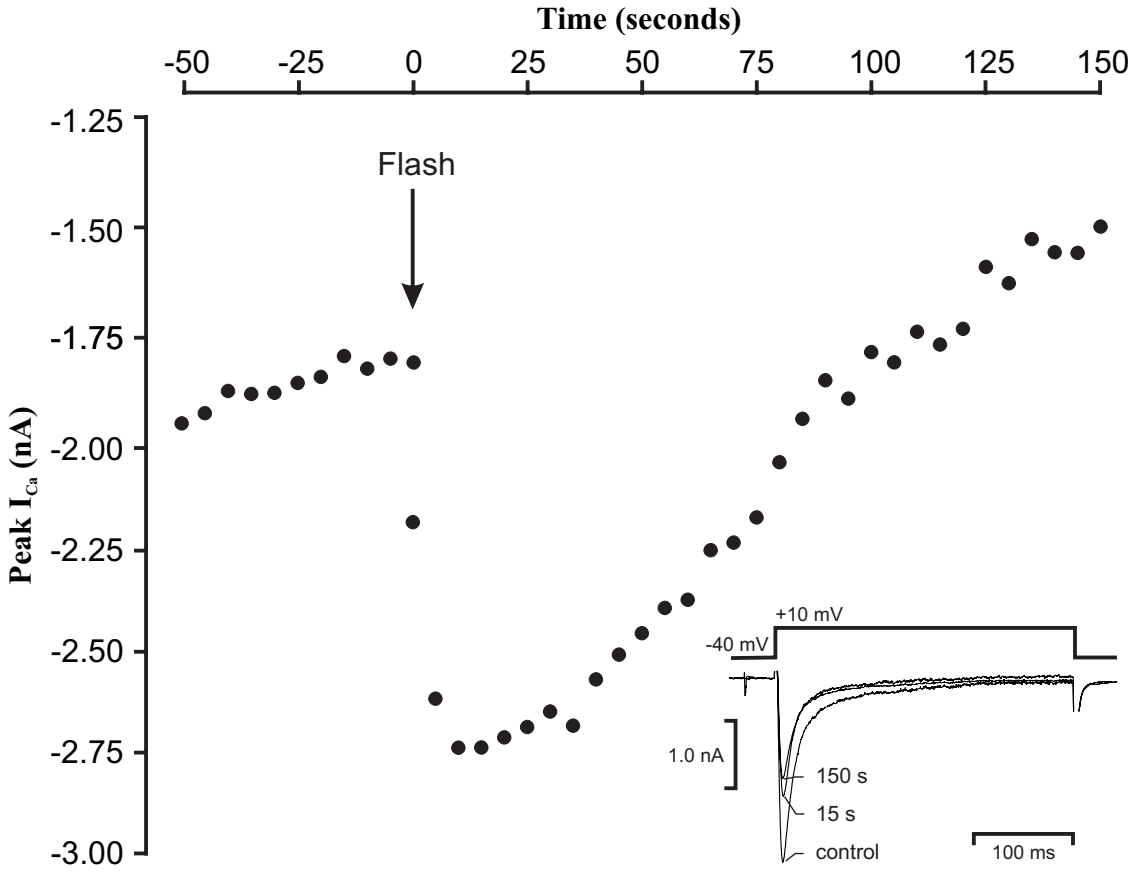

Figure 4.8a

A plot of peak I_{Ca} against time for the calcium current recorded from a single ventricular myocyte after flash photolysis of 5 mM caged GTP in the presence of 1 mM GTPγS. A single light flash elicited a rapid increase in I_{Ca} which declined gradually with time. Both the control current and the response to photoreleased GTP were reduced in this cell and peak I_{Ca} can be seen to be declining even before the application of the light flash.

Inset are non-leak subtracted raw current traces from the same cell. The calcium currents shown were recorded at test potentials of +10 mV after pre-conditioning steps to -40 mV. The traces shown were obtained immediately before photolysis, at the peak of the response (15 s) and after 150s when the current has declined substantially.

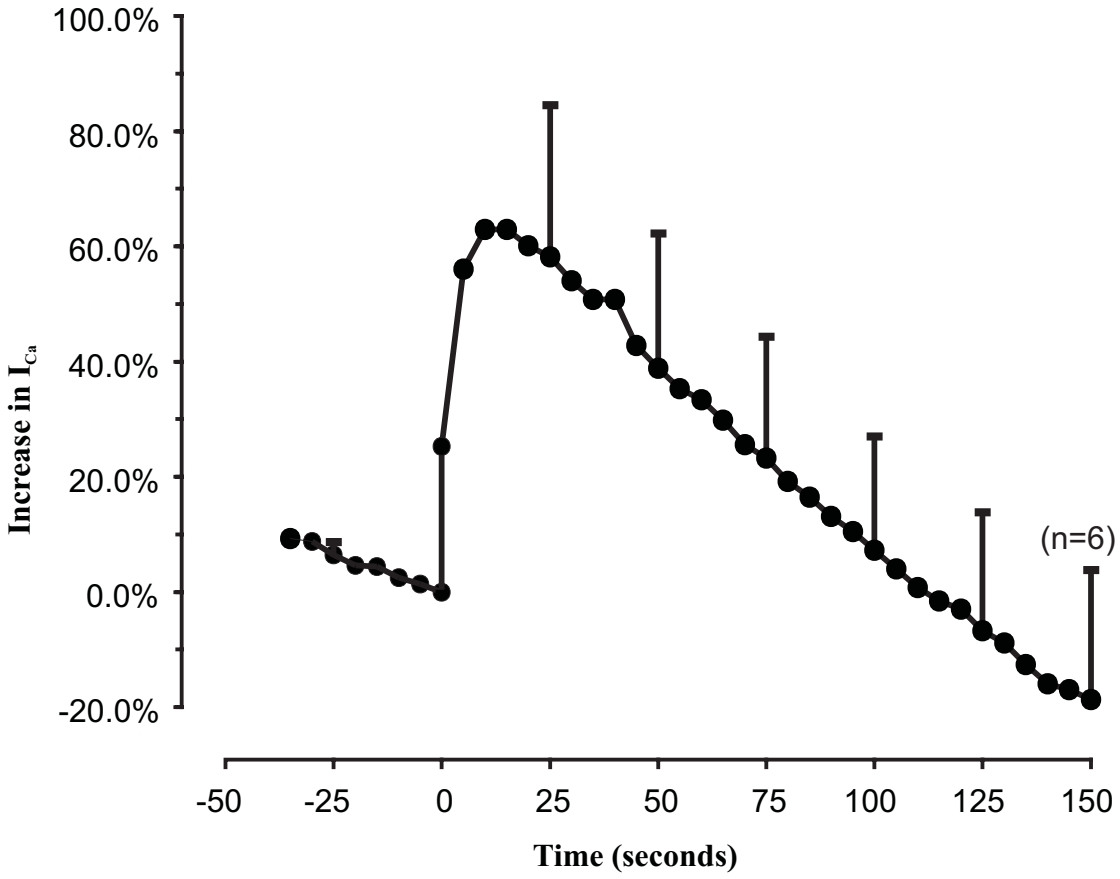

Figure 4.8b

A graph showing the average time course of the results of photolysis of 5 mM caged GTP in the presence of 1mM GTPγS. The responses were calculated as percentage increases from the control peak I_{Ca} before the UV flash. The inclusion of GTPγS inhibited the response of peak I_{Ca} to photoreleased GTP as compared with the control response (figure 4.1b). Only a reduced transient response to photoreleased GTP was seen. The average currents were declining before the light flash at time = 0. The initial rapid increase in I_{Ca} seen during the test pulse 20ms after the light flash was not abolished by the GTPγS inhibition. The vertical error bars show the standard errors of the mean at those intervals and the number of experiments is printed to the right of the graph.

A significant reduction in the isoprenaline response was only recorded when an increased concentration of GDPβS of 10 mM was used, which drastically reduced the increase of I_{Ca} to 6.6±1.2% (n=4). The addition of caged GTP to the intracellular solution did not prevent this reduction of the isoprenaline response by GDPβS (8.0 ±4.6%; n=4). In summary (see figure 4.6), only 10 mM GDPβS was sufficient to abolish the response to isoprenaline using this experimental protocol; 1 mM GDPβS was inadequate.

4.2.5.2 GDPβS and photoreleased GTP

Photolysis of 5 mM caged GTP in three cells co-dialysed with 1 mM GDPβS produced an increase in I_{Ca} similar to that seen in control conditions without GDPβS. However, in a further four cells, only a transient increase of 42.7 ±10.5% with a mean time to peak of 14 ±1 s was observed (figure 4.7). When the concentration of GDPβS in the intracellular solution was increased to 10 mM, this transient response was seen in six out of eight cells. Photorelease of GTP resulted in a short-lived increase in peak I_{Ca} of 80.6 ±17.2% with a time to peak of 15 ±2 s (n=6). The control response was seen in the other two cells.

4.2.5.3 GTPγS and photoreleased GTP

Figure 4.8a sets out a typical response to the photorelease of GTP in the presence of 1 mM GTPγS. There was a short-lived increase in I_{Ca} which reached a sharp peak before declining below control levels. This transient response was seen in all six cells tested (figure 4.8b): a rise in peak I_{Ca} to 71.6 ±26.1% (n=6) after 13 ±2 s (n=6) before decreasing markedly below control levels. Run-down was seen in all the cells, and

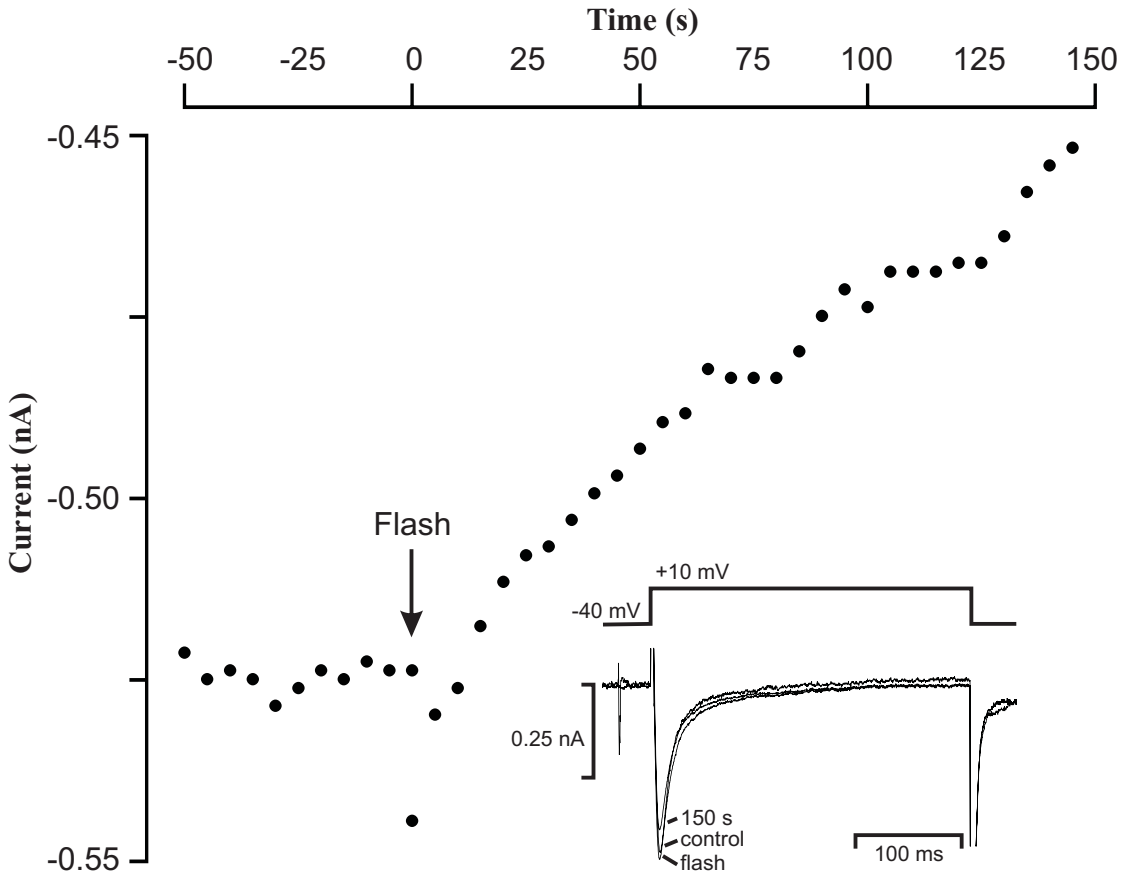

Figure 4.9a

A typical response to photo-releasing GTP in the presence of a saturating (10 mM) concentration of cAMP. Peak I_{Ca} from a single ventricular myocyte dialysed with a solution containing 5 mM caged GTP and 10 mM cAMP was plot against time. A single light flash elicited a small but rapid increase in I_{Ca} which declined almost immediately to control levels.

Inset are non-leak subtracted raw current traces from the same cell. The calcium currents shown were recorded at test potentials of +10 mV after pre-conditioning steps to -40 mV. The traces shown were obtained immediately before and after the flash and also after 150s when a substantial decline in peak calcium current has occurred.

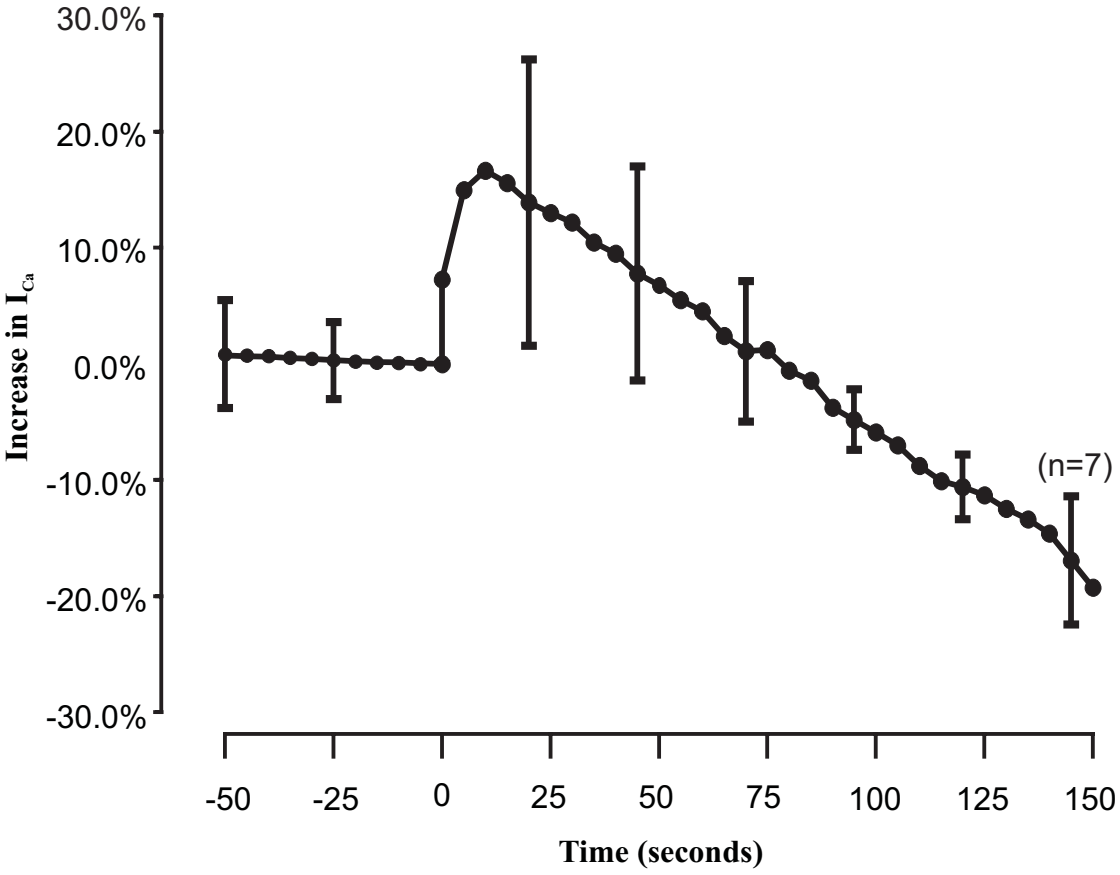

Figure 4.9b

A graph showing the average time course of the results of photolysis of 5 mM caged GTP in the presence of 10 mM cAMP. The response were calculated as percentage increases from the control peak I_{Ca} just before the UV flash. The inclusion of 10 mM cAMP inhibited the response of peak I_{Ca} to photorelease GTP compared with the control response. Instead, only a reduced transient rise could be seen. The average currents were declining before the light flash at time = 0 and after the initial increase, this decline resumed at a steeper rate. The initial rapid increase in I_{Ca} seen during the test pulse 20ms after the light flash was however preserved. The vertical error bars show the standard errors of the mean at those intervals and the number of experiments is printed to the right of the graph.

the peak I_{Ca} before the UV photolysis was initiated was marked reduced (-0.55 ±0.1 nA; n=6 compared with -1.1 ±0.12 nA; n=19).

4.2.6 cAMP-dependent phosphorylation

To examine whether the increases in I_{Ca} invoked by photorelease of GTP were entirely mediated via cAMP-dependent phosphorylation, experiments were performed in the presence of cAMP, R_p-cAMPS (a cyclic AMP antagonist; Van Hastert *et al.*, 1984) and Protein Kinase Inhibitor.

4.2.6.1 Excess cAMP and photoreleased GTP

Cells were dialysed with 10 mM cAMP and 5 mM caged GTP. This high concentration of cAMP was designed to ensure maximal stimulation of cAMP-dependent phosphorylation despite the known high level of phosphodiesterase activity in cardiac ventricular myocytes (Cavalie *et al.*, 1991). This was confirmed by the high peak I_{Ca} seen even before the UV light pulse (-4.14 ±0.46; n=6), i.e. cAMP caused a run-up of calcium current. Photorelease of GTP resulted in a further increase in I_{Ca} of only 4.4 ±0.5% (n=6), with a time to peak within 20 ms of the photorelease of GTP (figure 4.9a). In one other cell, the magnitude of the GTP-induced increase in I_{Ca} was 41.6% peaking after 10 s. In all cases, the current declined gradually after the initial peak. Figure 4.9b shows the average time course. Even after including the contributions from the one anomalous cell, the profile of the change was markedly different from what was seen when cAMP was absent.

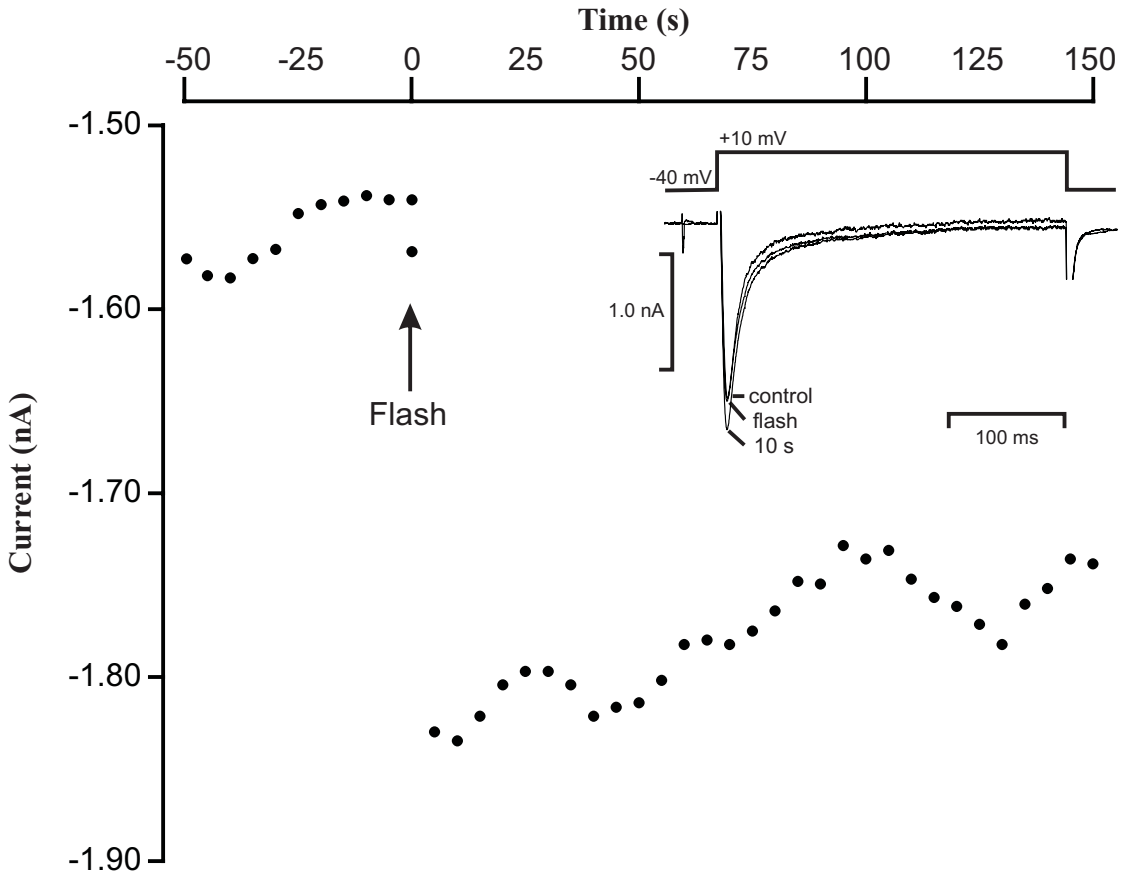

Figure 4.10a

A plot of peak I_{Ca} against time for the calcium current recorded from a single ventricular myocyte after flash photolysis of 5 mM caged GTP in the presence of 1 mM R_p-cAMPS. The maximal response to photo-released GTP was substantially reduced in this cell and the current peaked after less than 15 seconds. The response declined slowly from the peak after the flash..

Inset are non-leak subtracted raw current traces from the same cell. The calcium currents shown were recorded at test potentials of +10 mV after pre-conditioning steps to -40 mV. Traces immediately before and after the flash and at the peak of the response are shown.

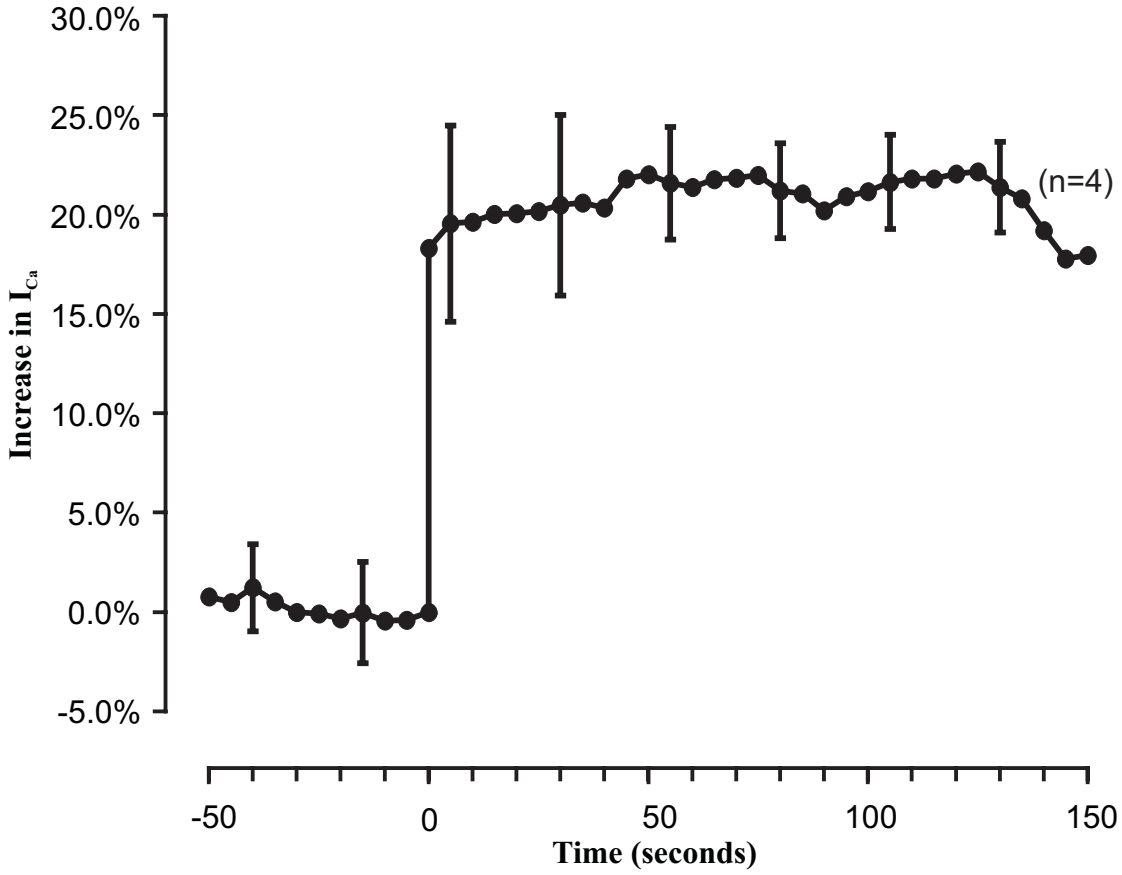

Figure 4.10b

A graph showing the average time course of the result of the photolysis of 5 mM caged GTP in the presence of R_p-cAMPS. The responses were calculated as a percentage increase from the control peak I_{Ca} seen just before the flash photolysis. As in the result from the single cell in 4.10a, the average responses show that R_p-cAMPS substantially reduces the increase in peak I_{Ca} seen. The profile of the response is very different from control, with a plateau in the increase in peak I_{Ca} seen very rapidly which was sustained over a long time. Little further increases in the current were seen after the first 15 s. The vertical error bars show the standard errors of the mean at those intervals and the number of experiments is printed to the right of the graph.

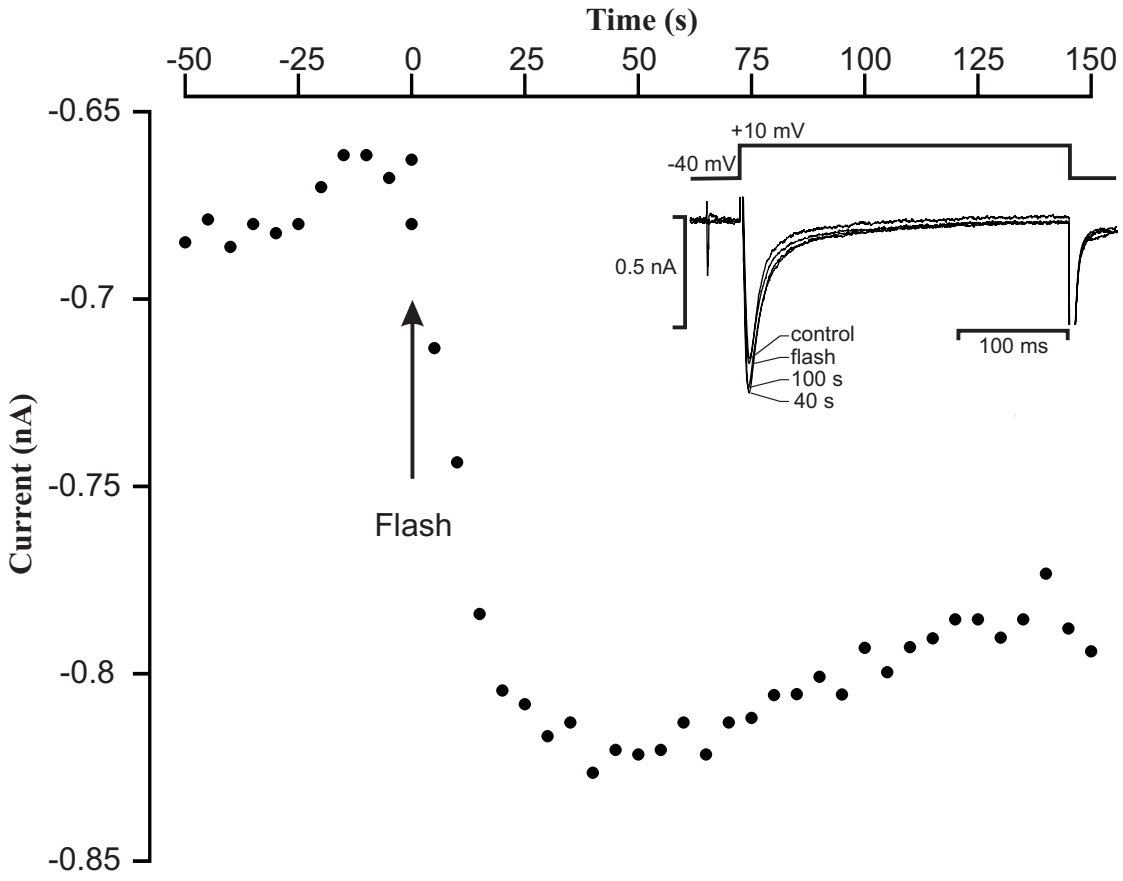

Figure 4.11a

A plot of peak I_{Ca} against time in a single ventricular cardiac myocyte. The flash photolysis of 5 mM GTP in the presence of protein kinase inhibitor (PKI) produced a much smaller response compared to the average seen in figure 4.1 without PKI. A single light flash 20 ms (at time 0 on the graph) before a voltage clamp pulse induced an increase in peak I_{Ca} which reached a peak around 40 seconds after the stimulus and declined slowly afterwards.

Inset are non-leak subtracted raw current traces from the same cell. The calcium currents shown were recorded at test potentials of +10 mV after pre-conditioning steps to -40 mV. Traces immediately before and after the flash and at the peak of the response are shown.

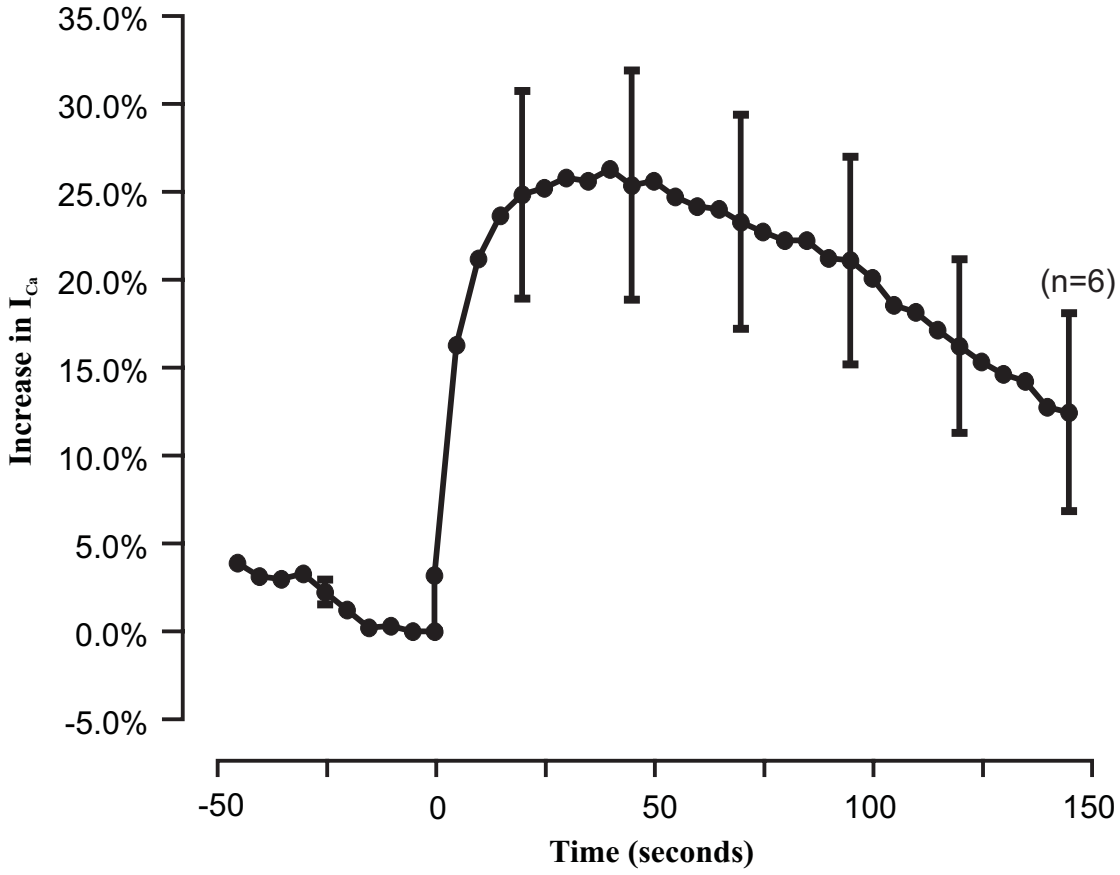

Figure 4.11b

A graph showing the average time course of changes in calcium current after photolysis of 5 mM caged GTP in the presence of protein kinase inhibitor. The responses were calculated as percentage increases from the control peak I_{Ca} seen just before the UV pulse. As in the results from the single cell in 4.11a, the average responses show that protein kinase inhibitor substantially reduces the GTP-evoked increase in peak I_{Ca}. The profile of the response is very different from control, with a peak after around 40-50 seconds followed by a gradual decline. The vertical error bars show the standard errors of the mean at those intervals and the number of experiments is printed to the right of the graph.

4.2.6.2 R_p-cAMPS and photoreleased GTP

To further determine whether response to photoreleased GTP was due to the cAMP-dependent pathway, cells were co-dialysed with 1 mM R_p-cAMPS, which is a cAMP antagonist at protein kinase A (Shuba *et al.*, 1990, Trautwein & Hescheler, 1990). This concentration of R_p-cAMPS was sufficient to abolish the increase in I_{Ca} evoked by the application of 10μM forskolin (n=4), which otherwise produced an increase of 140.5 ±27.5% (n=4). Inclusion of R_p-cAMPS resulted in a smaller response after photorelease of GTP compared to control (figure 4.10a). A significant reduction was found for both the increase in I_{Ca} (18.3 ±4.8%; n=5) and the time to peak response (18 ±5 s; n=5). Examining the average time course (figure 4.10b), the impact of R_p-cAMPS was even more obvious. After the first 10 s, little further increase in I_{Ca} could be detected. This was in marked contrast to control sustained responses which were still increasing after 150 s (figure 4.1b).

4.2.6.3 PKI and photoreleased GTP

Similar results were obtained for photorelease of GTP in the presence of 22.5 μM Protein Kinase Inhibitor (figure 4.11a). The magnitude of the transient response (27.2 ±6.0%; n=6) and the time to peak (36 ±7 s; n=6) were significantly reduced compared with control. Also evident was current run-down before the photorelease of GTP, which was mirrored in the rate of gradual decline in I_{Ca} after the response maximum was reached (figure 4.11b).

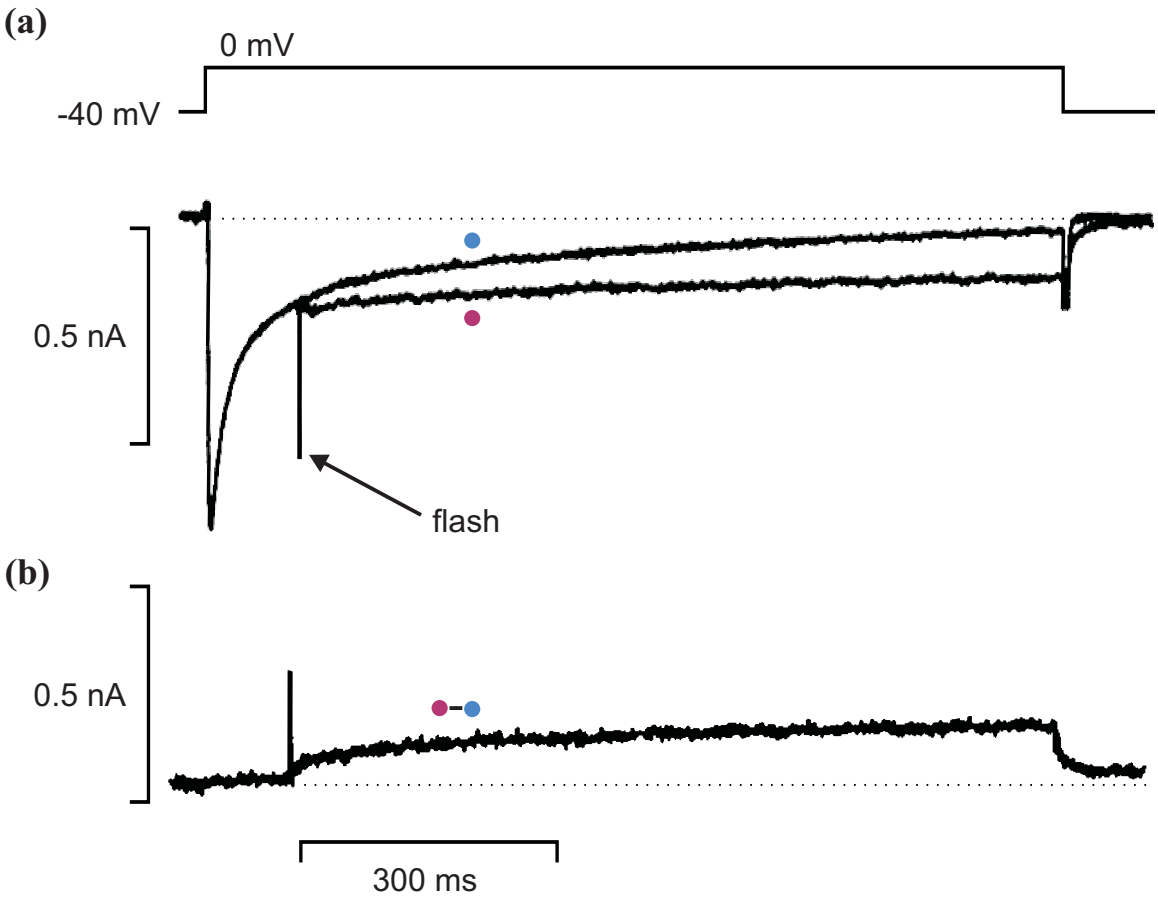

Figure 4.12

A graph showing the results of the flash photolysis of 5 mM caged GTP in the presence of 10 mM DTT. External Ca^{2+} was replaced by Ba^{2+} in the superfusing solution.(a) Two superimposed Ba^{2+} currents recorded using a 1 s long voltage step to 0 mV from a holding potential of -40 mV. A UV light pulse evoked 150 ms after the onset of the test pulse caused an increase in I_{Ba} (●) over that of control (●) after ~ 5 ms.

(b) The difference current (●—●) shows the time course for the increase in $I_{Ba.}$ In this cell, the current could be fit by a single exponential with a time constant of 389 ms.

4.2.7 Kinetics of increased current

Evident in the above experiments was a residual and rapid response in I_{Ca} to photoreleased GTP which was not abolished by high levels of intracellular cAMP, or the presence of either R_p-cAMPS or PKI. The increase in I_{Ca} was apparent during the first voltage depolarisation test pulse 20 ms after the UV light pulse. The increase of I_{Ca} pooled from all the above experiments with cAMP, R_p-cAMPS or PKI immediately after the UV flash (20 ms) was 24.4 ±5.5% (n=15). This is similar to what was observed with the photorelease of GTP under control conditions (23.7 ± 4.0%; n=15) and when GTP was photoreleased in the presence of either GSH (26.7 ±4.4%; n=4) or DTT (24.4 ±4.7%). This is in contrast to the pooled data from experiments using "caged water". This produced a much smaller increase in I_{Ca} 20 ms after photolysis of 0.7 ±0.5% (n=7), which is not significantly different from the 1.1 ±0.1% increase (n=4) produced by the UV pulse in the absence of any caged compounds.

The kinetics of this initial rapid response were examined by evoking Ba^{2+} currents (using 1.8 mM Ba^{2+} as the charge carrier in place of Ca in the external solution). The larger currents and slower time constants of current inactivation allowed the increase in I_{Ba} evoked by photorelease of GTP during the course of a 1 s long voltage-clamp depolarisation step to be analysed (figure 4.12). The time course of the increase in I_{Ba} could be fitted with a single exponential function with a mean time constant of 413 ±48 ms (n=4) after a delay of 20 ±5 ms (n=4). When Ca^{2+} was used as the charge carrier, a similar profile was seen though the increase was too small to fit reliably with an exponential function. The inactivation kinetics of the increased I_{Ba} were compared to that of the control. Before the photorelease of GTP, the kinetic profile for the decay of I_{Ba}

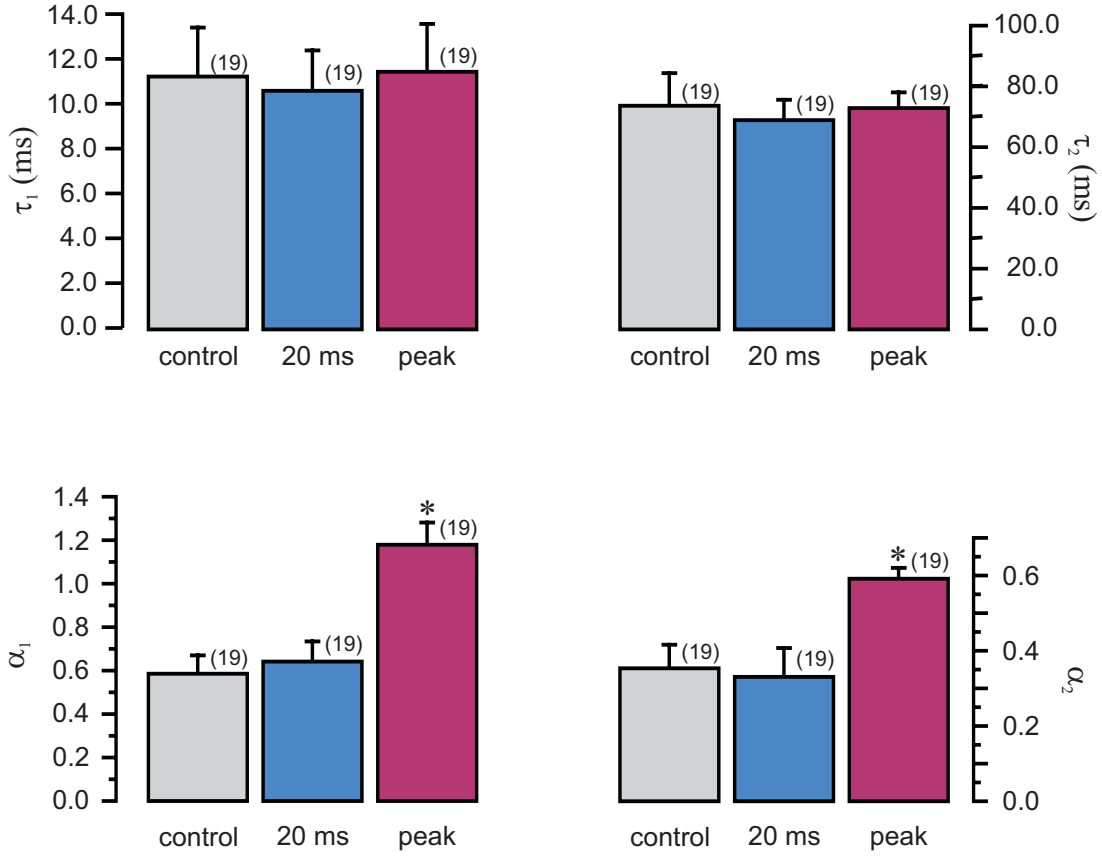

Figure 4.13

The decay of I_{Ca} in the 19 cells which showed a sustained response to photoreleased GTP could be well fitted by two exponentials. The time constants (τ_1 and τ_2) before the UV flash were 11.3 ±2.2 ms and 73.6 ±10.7 ms, not significantly different from their values at the peak of the response (11.5 ±2.1 ms; 72.9 ±5.2 ms). Significant changes from control values ($p < 0.05$) are indicated by asterisks.

could be fitted with two exponential with time constants of 27 ±4 ms and 310 ±5 ms respectively (n=4). The inactivation kinetics of the increased I_{Ba} immediately following the UV flash were not statistically different at 25 ±4 ms and 323 ±11 ms (figure 4.13).

4.3 Discussion

The results presented in this chapter describe a novel phenomenon: the evocation of a large increase in calcium current in cardiac ventricular myocytes by the rapid release of GTP inside the cell even in the absence of an agonist. This increased current occurred over a range of voltage potentials and was abolished by "calcium antagonists" known to block L-type calcium channels. The leftward shift in the current-voltage curve after the photorelease of GTP is consistent with the effects of the G-protein mediated β-adrenergic stimulation of I_{Ca} by isoprenaline (Bean *et al.*, 1984).

4.3.1 *Current run-down and phosphorylation state*

In most cells, the photorelease of GTP produced a large sustained increase in I_{Ca}. In some cells, however, only a transient response was seen. In all of these cells, rapid run-down of I_{Ca} was seen before the UV flash. The frequency of observing cells with run-down in calcium current seemed to be lower when the cells were held at -80 mV, the physiological resting membrane potential for ventricular myocytes. It has been suggested that L-type Ca^{2+} channels are kept in an activatable state by PKA phosphorylation (Yatani *et al.*, 1987) and that run-down of I_{Ca} is due in part to dephosphorylation of the channels. This would be supported by the similar though much more marked run-down and the short-lived responses also seen with PKI which inhibits channel phosphorylation. Though there is no obvious reason for the run-down or the transient response to photoreleased GTP observed in these cells, one possibility might be an alteration in the balance

between basal activity of kinases connected to the β-adrenergic pathway (e.g. PKA) and protein phosphatases. If there are changes in the level of constitutive activity of β-adrenoreceptors, this will be apparent both in the capacity for G-proteins to be activated by increased GTP (transient reduced responses) and in differences in basal adenylyl cyclase activity and hence ultimately channel phosphorylation (current run-down).

4.3.2 Locus of action of photoreleased GTP

GDP binds almost irreversibly *in vitro* to $G_{\alpha\beta\gamma}$ heterotrimers (Gilman, 1987). Nucleotide exchange is postulated to occur only after activated heptahelical G-protein coupled receptors stabilize the transition state, i.e. the nucleotide-free form of G_α. If the GTP:GDP ratio is sufficiently high, the GTP-bound form would predominate after such an exchange leading to dissociation and activation of the G-protein. In such a scheme, changing the intracellular GTP concentrations would not provide any stimulus in the absence of agonist-bound receptors. In that light, the results presented here are somewhat surprising.

The most obvious explanation is that local GTP concentrations in the vicinity of the G-protein are not saturating, at least in this experimental system, and that there is a degree of constitutive β-adrenoreceptor activity in the guinea-pig ventricular myocytes (Mewes *et al.*, 1993). There is abundant evidence from "inverse agonism" that a fraction of G-protein coupled receptors exist in spontaneously active conformation states and can interact with G-proteins even in the absence of agonists (Ehlert, 1986; see chapter 1 for a full discussion). The sudden flood of GTP released by the photolysis of caged GTP would greatly potentiate the action of constitutively active receptors. This hypothesis is supported by the ability of excess ambient GTP to diminish the response to

photoreleased GTP. The extra guanine nucleotide would increase the pre-existing GTP:GDP ratio and reduce the impact of any further changes in GTP subsequent to the photolysis.

Agonist-activation of receptor molecules may be the only main physiological regulator of G-protein coupled effects. However, it is clear from the results presented here that the rapid photorelease of the hydrolysable nucleotide GTP serves as well as its non-hydrolysable analogue as a useful experimental technique to rapidly stimulate G-protein pathways. In addition, these results show that the rate-limiting steps under these conditions for activation of I_{Ca} are located elsewhere in the chain of events coupling agonist occupancy of β-adrenoreceptors to activation of calcium channels.

4.3.3 *Validity of the flash photolysis technique*

The technique of UV flash photolysis allows rapid photolysis and hence increases over a very short time-scale in intracellular concentrations of a caged compound which would otherwise be difficult or impossible to achieve. This has allowed the kinetics of resulting changes to be examined without consideration of diffusion times, for example, which would be necessary with other techniques. However, it first has to be shown that the experimentation protocol does not by itself effect changes which obscure subsequent results. In the absence of any caged compounds inside the cell, the UV flash produced insignificant changes in I_{Ca}. It has been suggested that the photolytic by-products might be sources of artefacts. This seems to have been ruled out in these experiments as the increase in I_{Ca} induced by photorelease of GTP occurs even in the presence of the free radical scavengers DTT and GSH. In any case, it would be expected that nitrosoketones or highly reactive diradical photolytic by-products would reduce rather than cause the

observed increases in I_{Ca} (Goldhaber *et al.*, 1988). The inability of either the photolysis of "caged water" or the direct addition of photolytic by-products to cause any increases in I_{Ca} further confirms that any current changes observed after the photolysis of caged GTP are due the photorelease of GTP. The reduced magnitude and time-to-peak of the responses to photoreleased GTP in the presence of GSH, but especially DTT, may have been due to the interaction of these two thiol reagents with sulphydryl groups present either on the calcium channel complex or any of the proteins involved in regulating channel activity (Carman-Krzan, 1984).

4.3.4 *Photoreleased GTP in the presence of excess intracellular GTP*

The most obvious explanation for the diminution of the response to photoreleased GTP when the dialysing solution already contains a very high concentration of GTP is that the system is already near maximally stimulated. This is borne out by the high initial peak I_{Ca} before the UV flash. These results are an indirect testimony to the efficiency of the hydrolysis of GTP. Each UV flash liberates 59.3 ±18.4 μM GTP (chapter 3). Yet an inclusion of GTP at a concentration over two orders of magnitude higher still does not completely saturate the system and occlude further response. The steady state concentration of GTP near its site of action must be much lower than that in the dialysing pipette solution. This suggests that local ratios of GTP:GDP in the vicinity of the G-protein might be lower than in the rest of the intracellular environment. This would be easily reconciled with evidence that signalling peptides such as G-proteins, L-type Ca^{2+} channels adenylyl cyclase (V and VI) and β-adrenoreceptors may be concentrated or compartmentalized in selected parts of the

sarcolemma (Neubig, 1994), especially caveolae in smooth muscle (Song *et al.*, 1996) and cardiac myocyte t-tubules (Gao *et al.*, 1997).

It may also be that intracellular GTP concentrations are lower in our experimental systems than they are physiologically. No extra GTP was included as a rule in the pipette solution in other experiments described in this chapter. Undoubtedly, whole cell perfusion produces changes in the intracellular milieu and may cause some disruption to signalling through the adenylyl cyclase system. This is both an advantage and disadvantage compared to recording with permeabilised patches where there is only equilibration of monovalent ions between the pipette and cell interior. However, the degree of interference with cellular signalling pathways is likely to vary considerably from one experimental system to another, depending critically on cell size and pipette tip diameter. Thus significant temperature-dependent run-down in $I_{Cl,cAMP}$ response to isoprenaline (Zakharov & Harvey, 1995) or the absolute necessity of internal GTP for a consistent isoprenaline response in dialysed myocytes (Horie *et al.*, 1992) has not been observed under the experimental conditions described in this thesis. This may be explained at least in part by the use of pipettes with less wide tips (~1.5 to 2.0 MΩ instead of ~1.0 MΩ). In any case, the persistence of the response to photoreleased GTP pre-perfused with chronic excess GTP suggests that GTP washout was not a critical factor in any of the experiments described in this chapter.

4.3.5 *cAMP, R_p-cAMPS and Protein Kinase Inhibitor*

The less than 5% increase in I_{Ca} with the photorelease of GTP under maximal cAMP-stimulation matches the results of Cavalie *et al.* (1991) who report that isoprenaline was only able to produce similar sized response under these conditions. The

results of photolysis of caged GTP in the presence of R_p-cAMPS or Protein Kinase Inhibitor clearly demonstrate that the control response to photoreleased GTP is mediated mainly via cAMP-dependent phosphorylation as both greatly reduce the increase in I_{Ca}. However, a reduced response was seen even under conditions where the effects of 10 mM forskolin were abolished and hence, it seems, the cAMP-dependent pathway was completely blocked. The possibility that photoreleased GTP produces such an elevated level of cAMP that responses persist despite the levels R_p-cAMPS or Protein Kinase Inhibitor must be extremely unlikely. Hence, the persistence of this rapid increase in I_{Ca} suggests that another as yet uncharacterised pathway exists for the rapid activation of Ca^{2+} channels alongside the well-known and more predominant cAMP mediated phosphorylatory pathway.

These results also confirm that L-type Ca^{2+} channels require PKA-mediated phosphorylation for activation (Yatani *et al.*, 1988). The association of run-down with the transient responses seen in a minority of cells after photoreleased GTP is corroborated by the responses in the additional presence of PKI. This would be explained if increased run-down of I_{Ca} is at least in part the result of channel dephosphorylation (Belles *et al.*, 1988). Under these conditions, GTP only produced a short-lived response of reduced magnitude.

4.3.6 *GDPβS*

The results with GDP*β*S are somewhat puzzling. At concentrations (10 mM) which almost completely abolish the response to isoprenaline, an increase in I_{Ca} could still be evoked by the photorelease of GTP. However, the addition of intracellular GDP*β*S did cause the resulting increase in I_{Ca} to become transient in six out of the eight cells with

10 mM GDPβS and in over half the cells examined with 1 mM GDPβS. The obvious suggestion might be that only the sustained component of the increase in I_{Ca} evoked by photorelease of GTP is mediated by a G-protein which would be blocked by GDPβS. The transient component would involve, then, some as yet unknown pathway. However, reports have appeared in the literature about the variability of the action of GDPβS on I_{Ca}. GDPβS reduces but does not abolish increases in I_{Ca} mediated through cAMP-dependent phosphorylation in atrial myocytes (Yatani & Brown, 1989) and does not prevent inhibition of L-type Ca^{2+} channels by photoreleased GTPγS in mouse pancreatic β-cells (Ammala *et al.*, 1992). Even in the presence of 10 mM GDPβS, an albeit very small part of the isoprenaline-induced increase in I_{Ca} remains (7.3 $\pm$2.2%; n=8 from control 158.6 $\pm$31.2%; n=12). It seems that even at these high concentrations of GDPβS, G-protein mediated responses are incompletely blocked, especially for direct stimulation by photoreleased GTP with which GDPβS would have to compete for binding sites.

It is, nevertheless, also possible that the increase in I_{Ca} evoked by the photoreleased GTP are made up of two components responses, one transient and the other sustained, involving separate G-protein mediated pathways. The sustained response would be due to the activation of adenylyl cyclase and cAMP-dependent phosphorylation. $\beta\gamma$ subunits of the G_s-protein might be responsible for the transient response (Federman *et al.*, 1992), or the α-subunit may modulate directly the L-type Ca^{2+} channel in a manner similar to their effects on the activity of enzymes such as adenylyl cyclase and cGMP-specific phosphodiesterase (Hamilton *et al.*, 1991).

Hartzell *et al.* (1988) found that although the omission of GTP does not affect the response of I_{Ca} to isoprenaline, it was required for the inhibitory effect of R_p-cAMPS to be complete in their experiments. A possibility they discuss is that two different G-proteins may be involved with the direct G-protein effect requiring higher GTP concentrations (Hartzell *et al.*, 1992). However, it is as likely that the same G_s-protein α-subunit may be involved in both pathways with different affinities for the different effector proteins. This would be exhibited in a differing dependence on GTP concentration. The greater GTP sensitivity of a non-cAMP dependent pathway which is suggested by Hartzell *et al.* (1988), would tally with the facility of inhibition by GDPβS of the sustained component of the response to photoreleased GTP, which involves PKA phosphorylation, as compared with the transient component which does not.

4.3.7 GTPγS

The inhibitory effects of 1 mM GTPγS, which would be expected to produce the sustained stimulation of G-proteins, on isoprenaline and photoreleased nucleotide is probably less surprising. GTPγS would be expected to indiscriminatingly activate a variety of different G-proteins, some of which are known to have an inhibitory effect on Ca^{2+} channel activity (Brown & Birnbaumer, 1990). The other alternative, that GTPγS has already near-maximally activated I_{Ca} before the photolysis of caged GTP is unlikely given the small average amplitude of peak I_{Ca} before the UV flash relative to control. It seems most likely that an initial activation of the calcium current by photoreleased GTP is subsequently overcome by the inhibitory action of other G-proteins activated by GTPγS to produce the transient and reduced increase in I_{Ca} seen. Given that the sustained component of the response to photoreleased GTP has been shown above to depend on

cAMP-dependent phosphorylation, this hypothetical G-protein probably acts at some point along the β-adrenoreceptor/G-protein/adenylyl cyclase/protein kinase A pathway. Alternatively, the inhibitory effect involves a separate pathway which competes with cAMP-dependent phosphorylation to reduce I_{Ca}. These alternative possibilities were pursued in experiments described in the followed chapter.

Table 4.1 I_{Ca} before and after GTP photorelease in different conditions

Amplitude of peak I_{Ca} recorded just before photolysis of caged GTP in the separate presences of free radical scavengers or modulatory nucleotides and the corresponding responses to the photorelease of GTP. Values are given as mean ±s.e.m., with the number of observations in parenthesis.

Pipette dialysing solution	Control I_{Ca} amplitude (nA)	Increase in I_{Ca} after photorelease of GTP
Caged-GTP (5 mM) alone	-1.10 ±0.12 (n=13) (Stable current)	67.5 ±16.8 % (n=13) (Sustained response)
	-0.78 ±0.17 (n=6) (Pronounced run-down)	76.1 ±28.8 % (n=6) (Transient response)
Caged-GTP (5 mM) + DTT (10 mM)	-0.81 ±0.07 (n=5)	28.8 ±5.8 % (n=5)
Caged-GTP (5 mM) + GSH (10 mM)	-1.12 ±0.28 (n=4)	44.1 ±4.6 % (n=4)
Caged-GTP (5 mM) + GTP (10 mM)	-1.42 ±0.26 (n=5)	21.3 ±11.2 % (n=5)
Caged-GTP (5 mM) + GDPβS (1 mM)	-1.02 ±0.12 (n=7)	42.7 ±10.5 % (n=4)
Caged-GTP (5 mM) + GDPβS (10 mM)	-0.81 ±0.22 (n=7)	80.6 ±17.2 % (n=6)
Caged-GTP (5 mM) + GTPγS (1 mM)	-0.55 ±0.11 (n=6)	71.6 ±26.1 % (n=6)
Caged-GTP (5 mM) + cAMP (10 mM)	-4.14 ±0.46 (n=6)	4.4 ±0.5 % (n=6)
Caged-GTP (5 mM) + PKI (22.5 μM)	-0.94 ±0.10 (n=5)	25.0 ±6.7 % (n=5)
Caged-GTP (5 mM) + R_p-cAMPS (1 mM)	-0.93 ±0.22 (n=5)	20.4 ±4.1 % (n=5)

Chapter Five

Effects of chronic application of GTPγS

5.1 Introduction:

The rapid intracellular application of the slowly hydrolysed GTP analogue, GTPγS, by pressure-assisted dialysis (Shuba *et al.*, 1990; Pelzer *et al.*, 1991) is known to increase I_{Ca}. This effect is thought to be mediated by the activation of a G_s-type protein, which, in turn, would increase L-type Ca^{2+} channel activity. GTPγS is resistant to intrinsic G-protein GTPase activity and can thus be expected to produce a sustained activation of the G-protein. In cell-free patches, the inclusion of GTPγS enhances and sustains L-type Ca^{2+} channel activity evoked by isoprenaline (Yatani *et al.*, 1987). One might expect GTPγS to have the same effect under whole-cell conditions. Indeed, low concentrations of GTPγS (<10 μM) potentiate the stimulation of I_{Ca} in response to the activation of H_2 type histamine receptors (Hescheler *et al.*, 1987). The previous chapter has shown that even in the absence of any *β*-adrenergic receptor agonist, the rapid intracellular release of GTP, the native ligand of the G-protein, can also produce a stimulatory effect on I_{Ca}. However, in the course of the experiments, an anomalous inhibitory effect was seen when a high concentration of GTPγS (1 mM) was included in the pipette dialysing solution. This would be consistent with other reports that chronic

administration of 100 μM to 1 mM GTPγS prevents activation of purinergic (Scamps *et al.*, 1992) and histaminergic (H_2) receptor agonists. Scamps *et al.*, suggest that the GTPγS inhibition seen is the result of an uncoupling of H_2 receptors from the catalytic subunit of adenylyl cyclase under maximal stimulation from the GTPγS bound G-protein linking the H_2 receptor. Another possibility would be that an additional inhibitory pathway might be responsible, involving perhaps some other G-protein stimulated by GTPγS.

The results presented here are an investigation into the precise origin of the inhibitory effects of GTPγS and whether this is seen with other sympatho-mimetic stimuli. We examine the effects of the continued GTPγS presence by dialysis on the I_{Ca} response to isoprenaline and forskolin, flash photolysis of caged GTPγS or caged cAMP. In this way, the point of inhibition in the signal transduction pathway can be identified. In addition, the use of the technique of flash photolysis has provided the means to examine the kinetics of the response to changes in GTPγS and cAMP levels.

The stimulation of I_{Ca} by GTPγS through activation of the G_s-type protein is known to involve an increase in activity of adenylyl cyclase which produces the second messenger cAMP to stimulate Protein Kinase A mediated phosphorylation of L-type Ca^{2+} channels. The involvement of a second faster membrane-delimited G_s-type protein not mediated by soluble cytoplasmic second messengers can be demonstrated in cell free preparations and is also supported by the experimental results of the previous chapter. It has been suggested by Pelzer *et al.* (1990) that the two pathways do not only operate independently but that the latter enhances the efficacy of cAMP-dependent

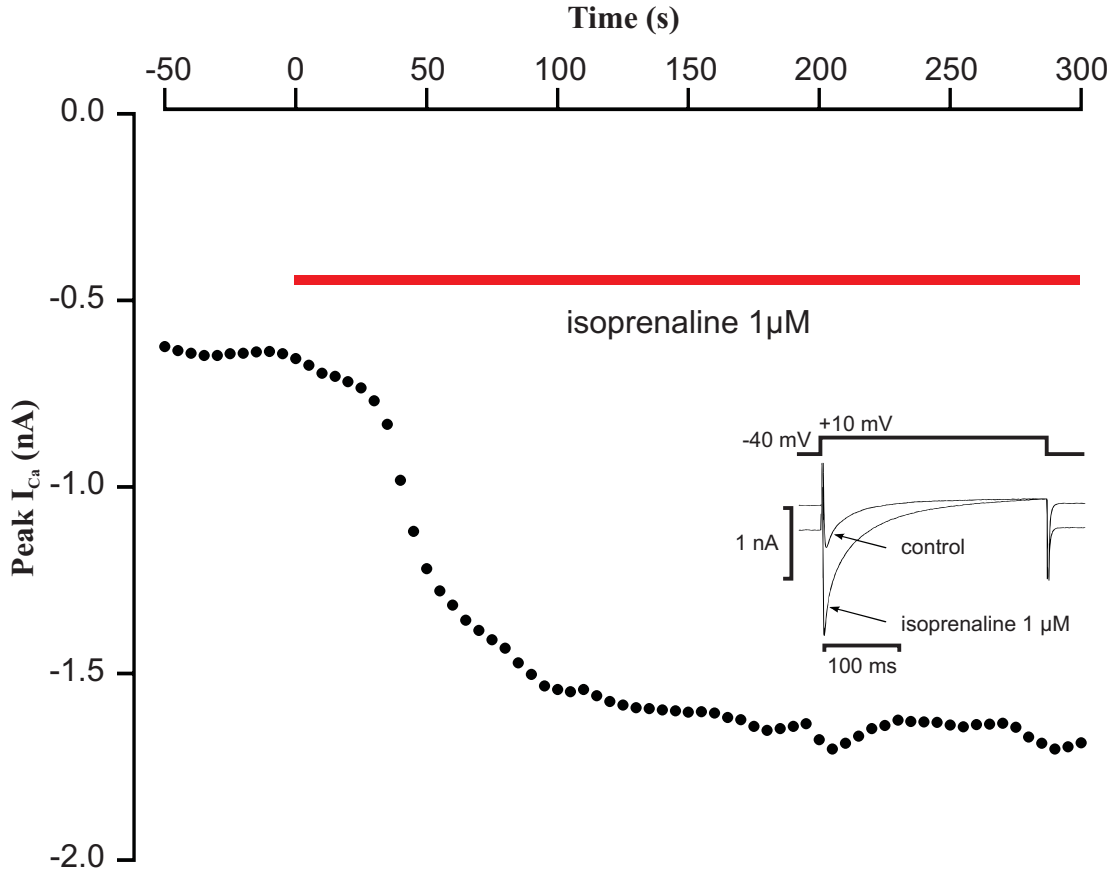

Figure 5.1

A plot of peak I_{Ca} against time in a single ventricular cardiac myocyte. In this cell, the application of 1 μM isoprenaline produced a large sustained increase in calcium current which reached a peak after around 200 seconds. Note the much slower onset compared with responses to photolysis of caged compounds.

Inset are non-leak-subtracted raw current traces from the same cell. The calcium currents shown were recorded at test potentials of +10 mV. Pre-conditioning depolarizations to -40mV were designed to inactivate sodium and T-type calcium channels. The traces shown were obtained immediately before the application and after the response had reached a peak.

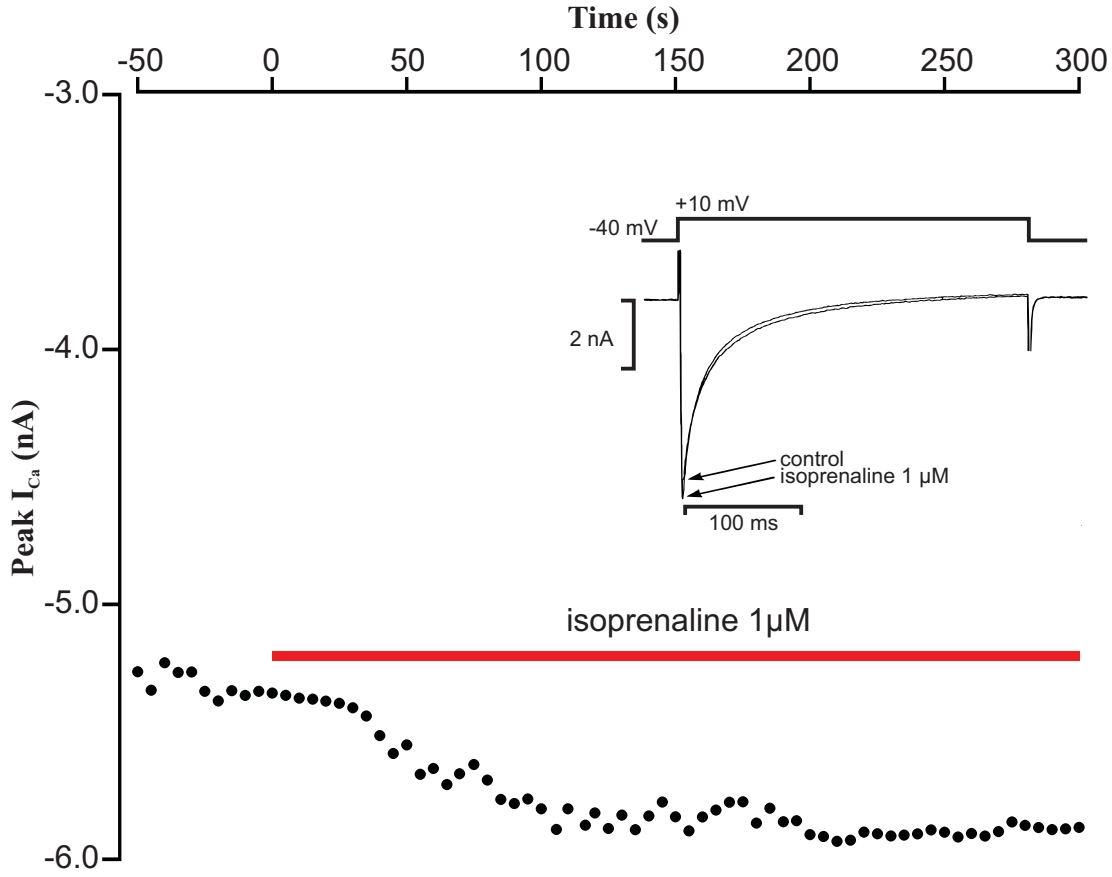

Figure 5.2

A plot of peak I_{Ca} against time in a single ventricular cardiac myocyte. The application of 1 μM isoprenaline in the presence of 10 μM GTPγS produced a much smaller increase compared with the cell in figure 5.1.

Inset are non-leak-subtracted raw current traces from the same cell. The calcium currents shown were recorded at test potentials of +10 mV. Pre-conditioning depolarizations to -40mV were designed to inactivate sodium and T-type calcium channels. The traces shown were obtained immediately before the application and after the response had reached a peak. These clearly show that inclusion of GTPγS drastically reduces the response to isoprenaline.

phosphorylation. In the course of the investigation into the inhibition of sympathetic responses produced by chronically applied GTPγS, an additional novel acceleratory effect of GTPγS on the cAMP-dependent pathway was discovered. Such an increase in the sensitivity of the L-type channels to phosphorylation would be complementary to the findings of Pelzer *et al*. (1990).

The photorelease of cAMP allows rapid and reproducible direct stimulation of the cAMP-dependent pathway, without the need for activation of *β*-adrenoreceptor, G-protein or adenylyl cyclase. On one hand, this removes the variations due to these earlier parts of the pathway and, on the other, allows the behaviour and kinetics of these downstream reactions to be examined in isolation. The released cAMP increases not only I_{Ca} but also $I_{Cl,cAMP}$ reflected in the holding current at -80 mV. This allows the differential modulation of these two responses by the same stimuli in the same cell to be examined.

5.2 Results:

5.2.1 *Responses to isoprenaline attenuated in the presence of GTPγS*

Figure 5.1 shows the effects in a typical cell of the application of 1 μM isoprenaline. As expected, large increases in the amplitude of peak I_{Ca} could be seen (142 ±36%; n=8). Compared with the responses to the photorelease of GTP shown previously and that of cAMP and GTPγS in this chapter, the agonist-elicited increase had a much slower onset. This roughly corresponded to the ~40 s it takes for bath perfusion solution exchange to be completed. The inclusion of 10 μM GTPγS in the dialysis solution caused a marked reduction of the isoprenaline response (figure 5.2). This inhibitory effect was dependent on the concentration of ambient intracellular GTPγS (1 to 1000 μM), with an IC_{50} of around 10 μM (n = 33). Concentrations of GTPγS above

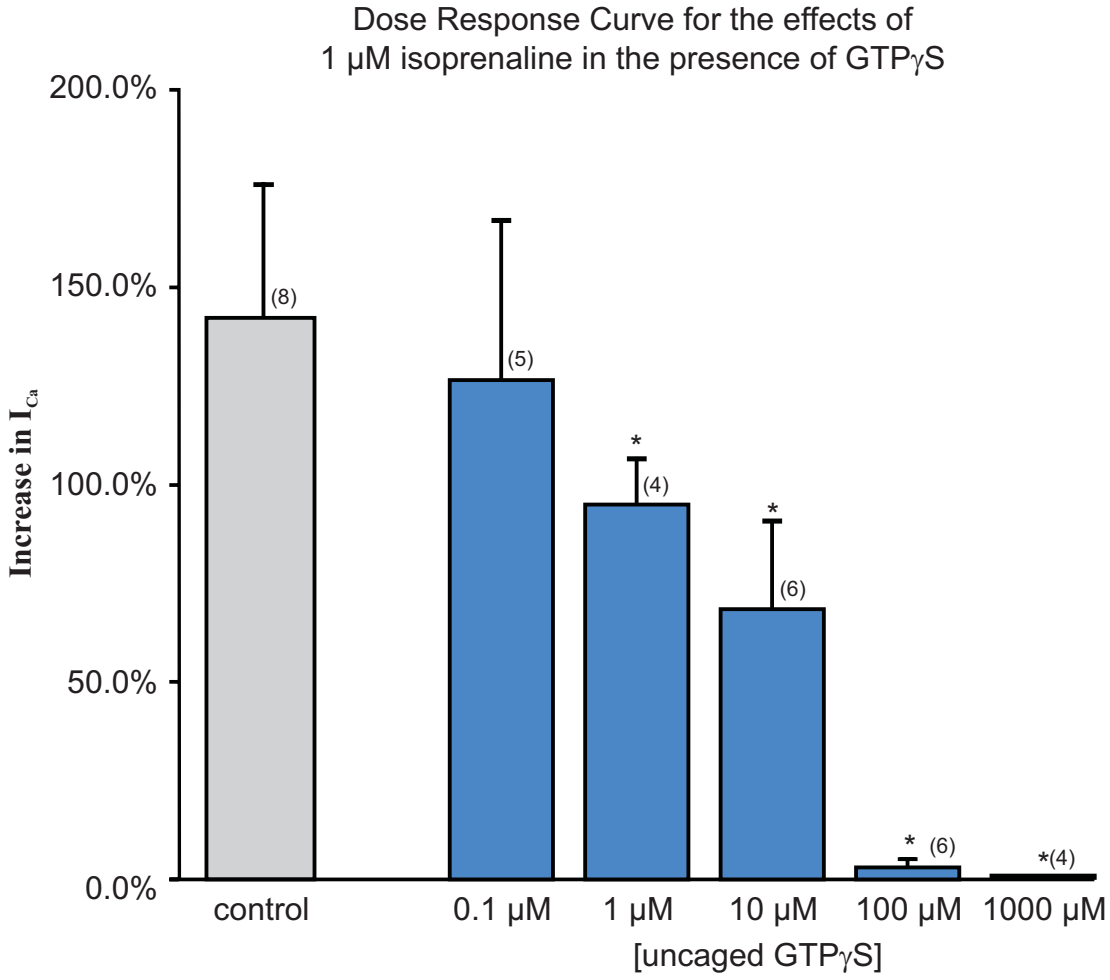

Figure 5.3

Dose response curve for concentration-dependent GTPγS inhibition of the response to 1 μM isoprenaline. This graph shows the ability of different levels of GTPγS to reduce the ability of isoprenaline to enhance I_{Ca}. The IC_{50} for this effect was around 10 μM.

All calcium currents shown were recorded at test potentials of +10 mV after pre-conditioning depolarizations to 40mV. The error bars indicate standard errors of the mean. The number of cells for each experiment are indicated beside the error bars and asterisks indicate significant differences ($p < 0.05$) from the control isoprenaline response.

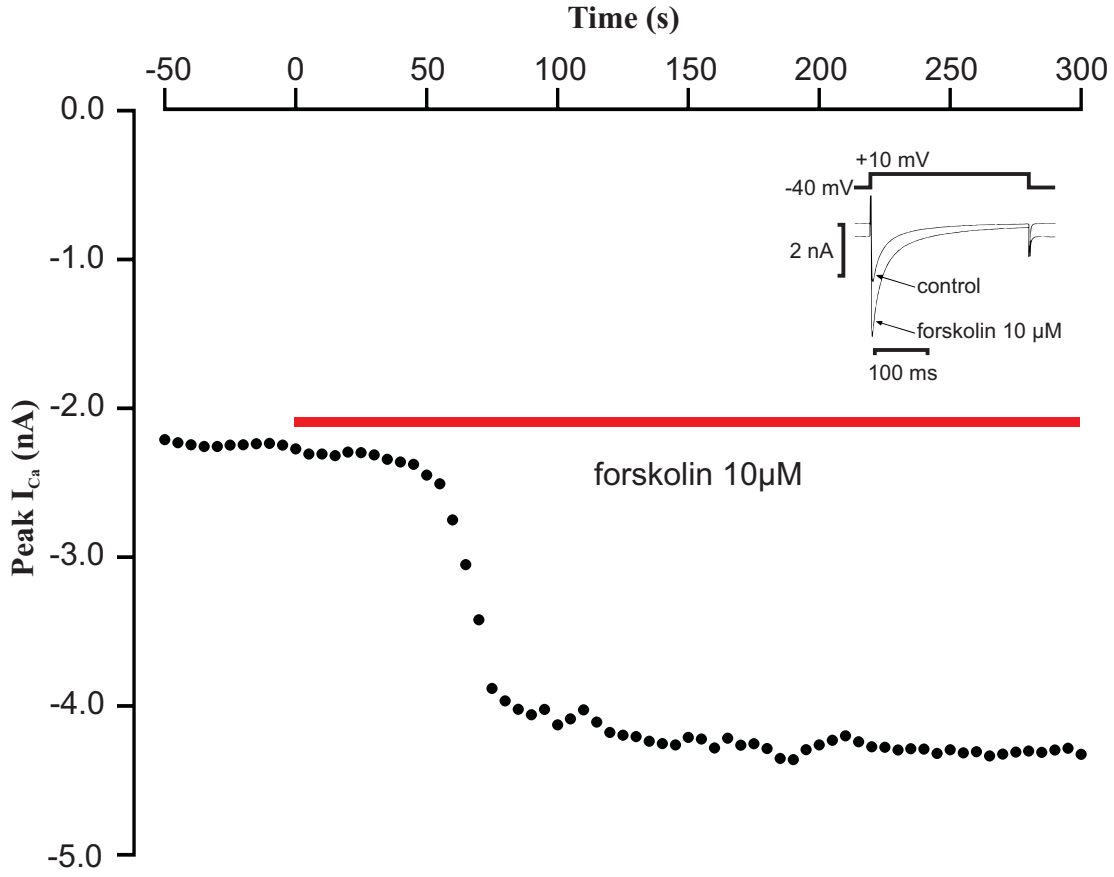

Figure 5.4

A plot of peak I_{Ca} against time in a single ventricular cardiac myocyte showing the response to the application of 10 µM forskolin in the presence of GTPγS. This produced a large sustained increase in calcium current rising to a peak after about 170 seconds. Peak I_{Ca} with forskolin was almost double that of control.

Inset are non-leak-subtracted raw current traces from the same cell. The calcium currents shown were recorded at test potentials of +10 mV. Pre-conditioning depolarizations to -40mV were designed to inactivate sodium and T-type calcium channels. The traces shown were obtained immediately before the application and after the response had reached a peak.

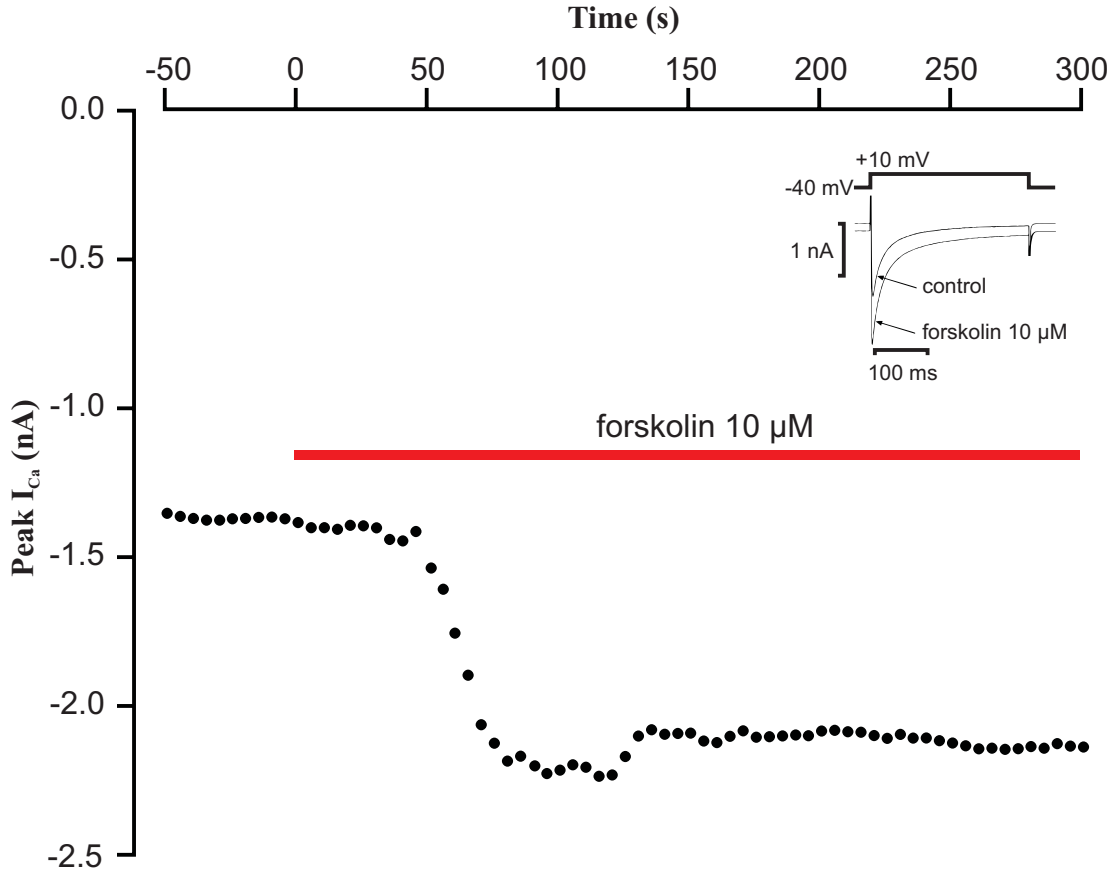

Figure 5.5

A plot of peak I_{Ca} against time in a single ventricular cardiac myocyte showing the response to the application of 10 μM forskolin in the presence of 1mM GTPγS. This produced a large sustained increase in calcium current rising to a peak after about 120 seconds. Inclusion of GTPγS did not seem to have a significant inhibitory effect on the size of the response to forskolin.

Inset are non-leak-subtracted raw current traces from the same cell. The calcium currents shown were recorded at test potentials of +10 mV. Pre-conditioning depolarizations to -40mV were designed to inactivate sodium and T-type calcium channels. The traces shown were obtained immediately before the application of forskolin and after the response had reached a peak.

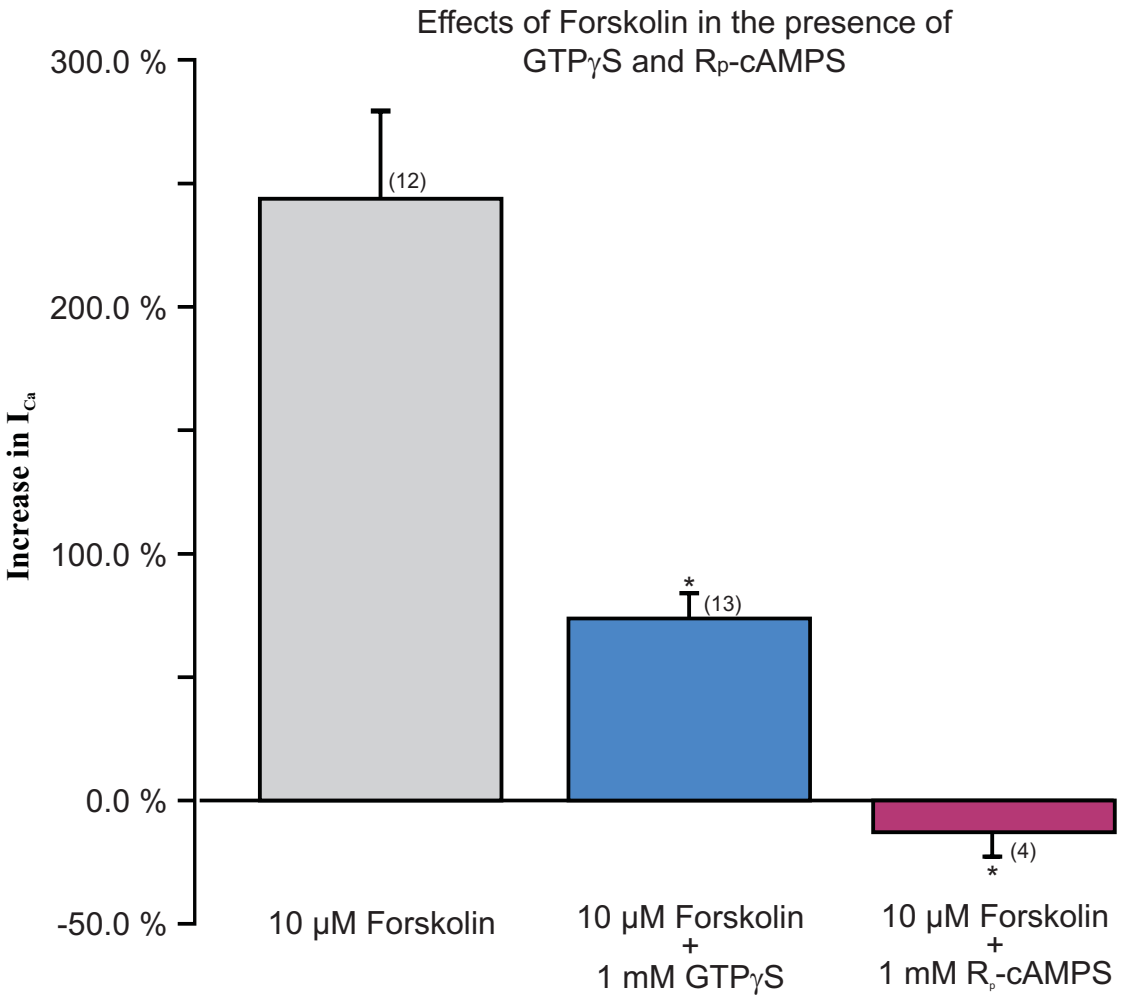

Figure 5.6

This bar graph summarizes the results of experiments with 10 μM forskolin. The application of forskolin alone produces a large increase in peak I_{Ca}, more than double that of control. This ability to enhance calcium current was significantly reduced by the inclusion of 1 mM GTPγS while adding 1mM R_p-cAMPS to the pipette-dialysing solution completely abolished the response.

The number of experiments for each cell are given beside vertical error bars denoting the standard errors of the mean. Both the additions of R_p-cAMPS and GTPγS significantly inhibited (*, $p < 0.05$) the response to forskolin.

100 μM were sufficient, on average, to almost abolish any further effects of 1 μM isoprenaline (figure 5.3).

To determine the loci of the GTPγS inhibition, its effects on other pharmacological agents known to interact with the cAMP-dependent pathway stimulated by isoprenaline were investigated.

5.2.2 Effects of forskolin with and without chronic GTPγS

Forskolin directly activates adenylyl cyclase. Under control conditions, superfusing ventricular myocytes by 10 μM forskolin (figure 5.4) produces a similarly large increase in I_{Ca} (243.8 ±35.8%; n=12) again after an initial lag. This delay was typically longer than that for responses to isoprenaline and that which can be attributed only to solution exchange delays. However, increases in peak I_{Ca} tended to reach their plateaux more rapidly after their onset. Responses to forskolin were completely abolished when the cells were first dialysed with R_p-cAMPS, a cAMP antagonist, confirming that that the effects of forskolin are mediated entirely by a cAMP-dependent pathway.

When 1 mM GTPγS, a concentration which completely abolishes the isoprenaline response, was included in the dialysing solution, the responses to forskolin (figure 5.5) were significantly reduced (73.7 ±10.3%; n=13) compared to control though the time-to peak response was significantly reduced from 187 ±21 s (n=12) to 121 ±14 s (n=13). The various results with forskolin are summarized in figure 5.6.

It seems that the intracellular presence of uncaged GTPγS inhibits the effects of β-adrenoreceptor activation by isoprenaline but not the direct stimulation of adenylyl cyclase by forskolin. On the other hand, the kinetics of cAMP-dependent pathway were

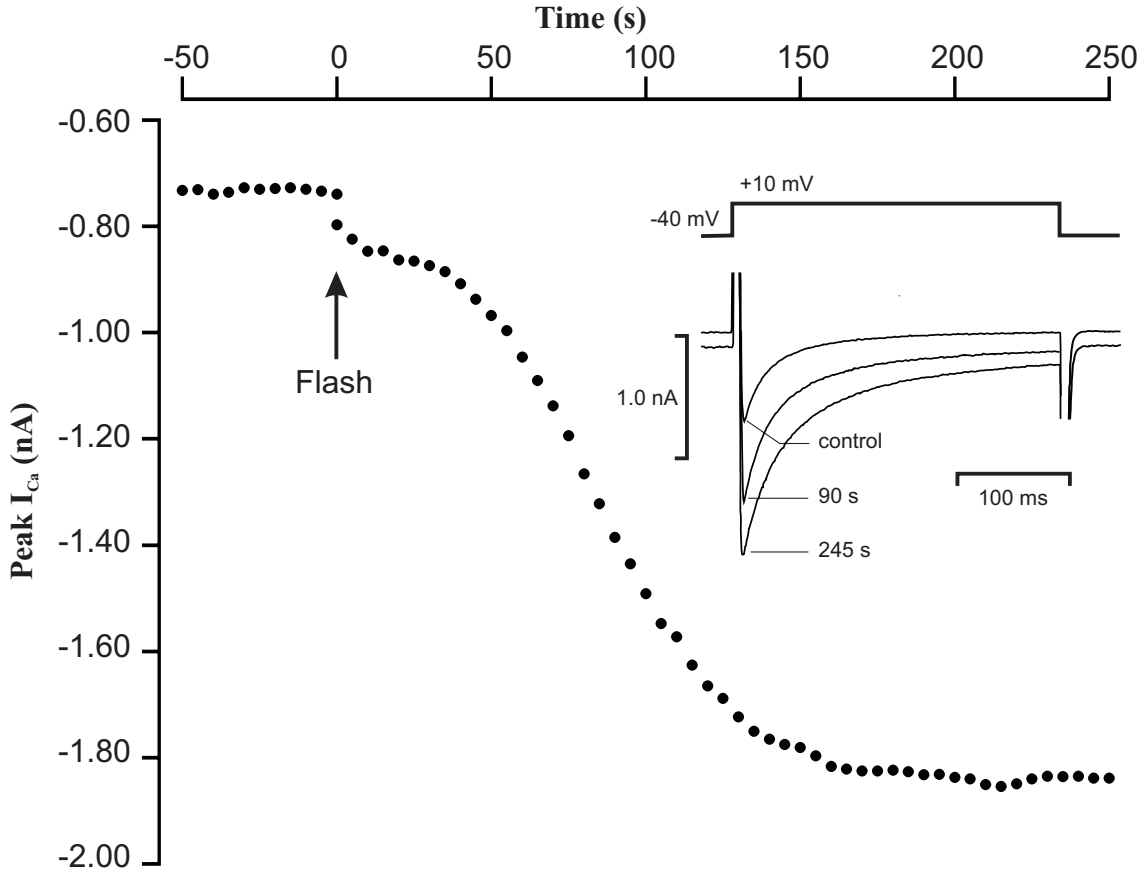

Figure 5.7a

A plot of peak I_{Ca} against time in a single ventricular cardiac myocyte. In this cell, the flash photolysis of 1 mM caged GTPγS produced a biphasic increase in calcium current which reached an initial shoulder after 20-30 seconds before continuing to rise to a plateau. The response peak occurred around 150-200 seconds after the stimulus.

Inset are non-leak-subtracted raw current traces from the same cell. The calcium currents shown were recorded at test potentials of +10 mV. Pre-conditioning depolarizations to -40mV were designed to inactivate sodium and T-type calcium channels. The traces shown were obtained immediately before the light pulse, and after 90 and 245 seconds. They clearly show the large increase in I_{Ca} produced by photo-releasing GTPγS.

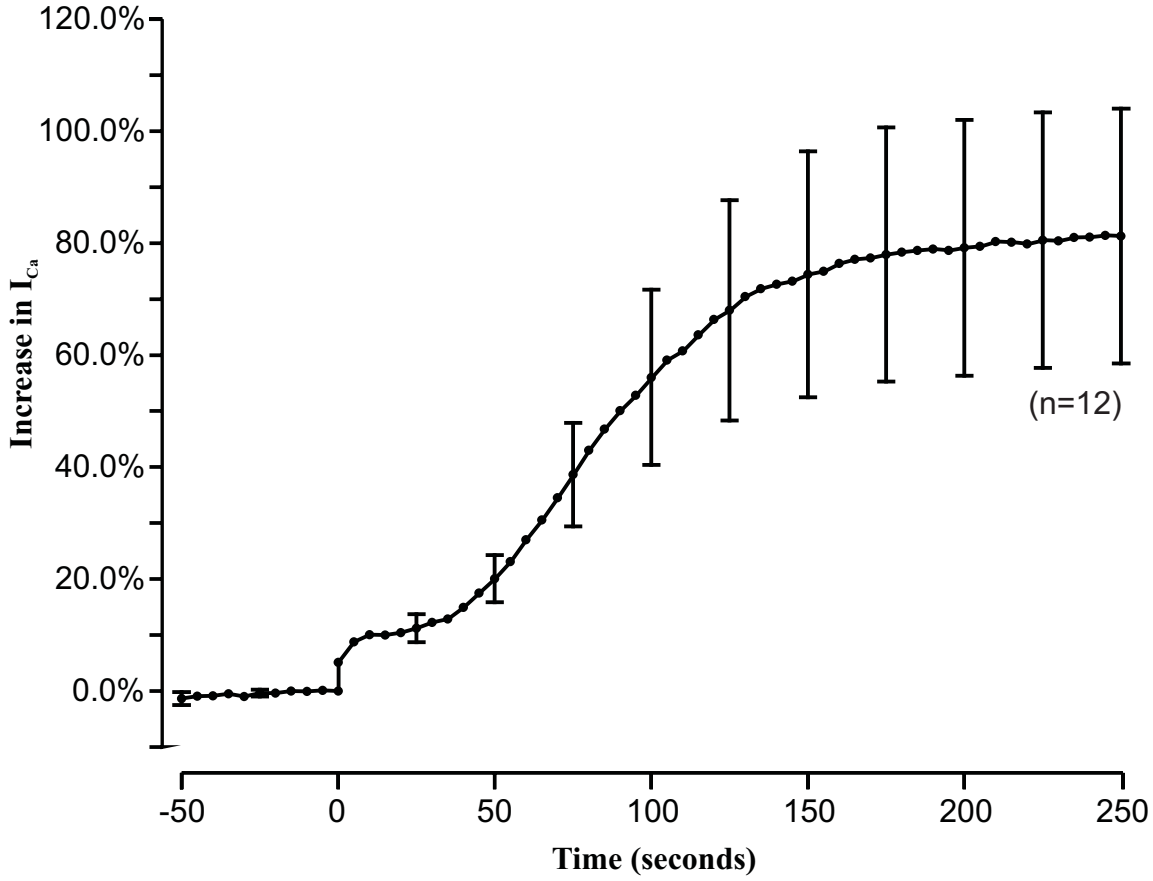

Figure 5.7b

Results showing the average time course for cells which showed a biphasic increase in peak I_{Ca} after the photorelease of GTPγS. The increase relative to control in non-leak-subtracted peak Ca^{2+} currents recorded during a test potential of +10mV. The cell was dialysed with 1 mM GTPγS. A single light flash elicited 20ms before the onset of a voltage-clamp pulse induced an initial increase in I_{Ca} which reached a maximum after around 20 seconds before resuming its rise to a sustained plateau around 200 seconds after the stimulus. Vertical error bars show the standard errors of the mean at those intervals and the number of experiments is printed to the right of the graph.

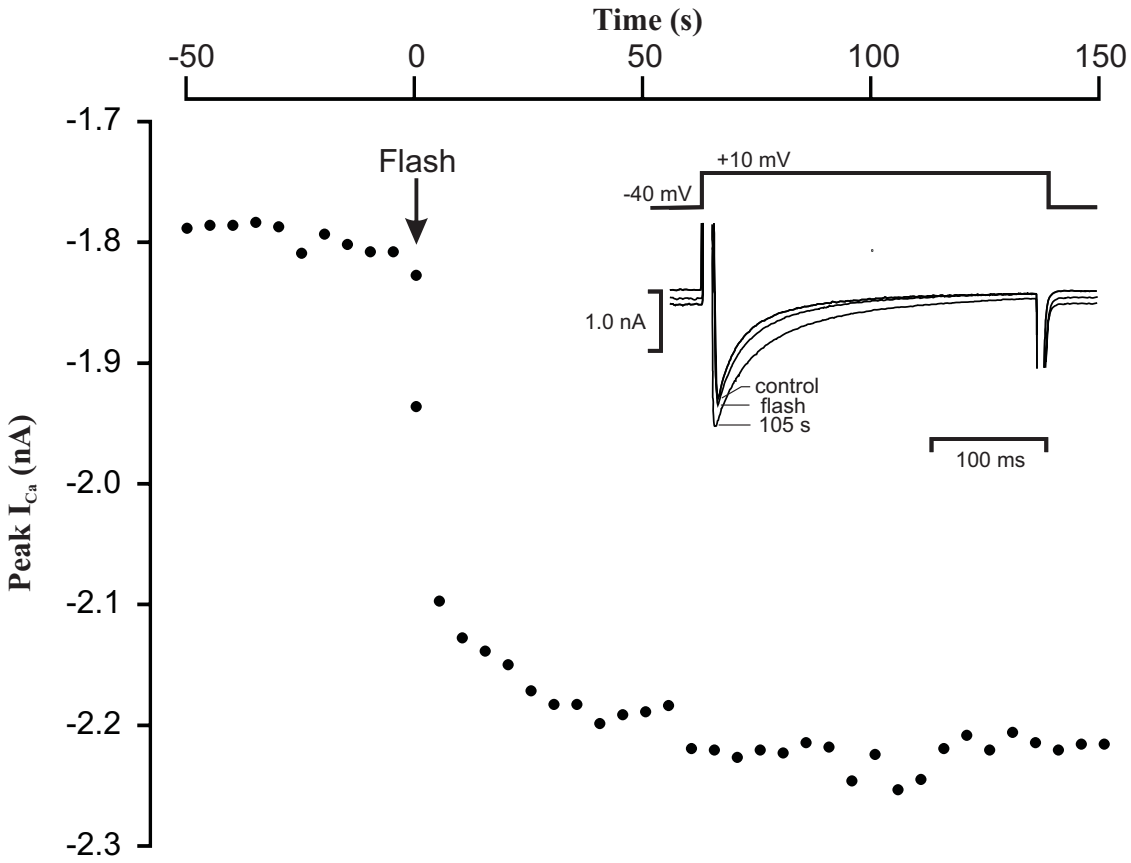

Figure 5.8a

A plot of peak I_{Ca} against time in a single ventricular cardiac myocyte. In this cell, the flash photolysis of 1 mM caged GTPγS produced a large initial jump in calcium current followed by a sustained rise, and reaching a peak 105 seconds after the stimulus.

Inset are non-leak-subtracted raw current traces from the same cell. The calcium currents shown were recorded at test potentials of +10 mV. Pre-conditioning depolarizations to -40mV were designed to inactivate sodium and T-type calcium channels. The traces shown were obtained immediately before and after the light pulse, and when the response had reached a peak.

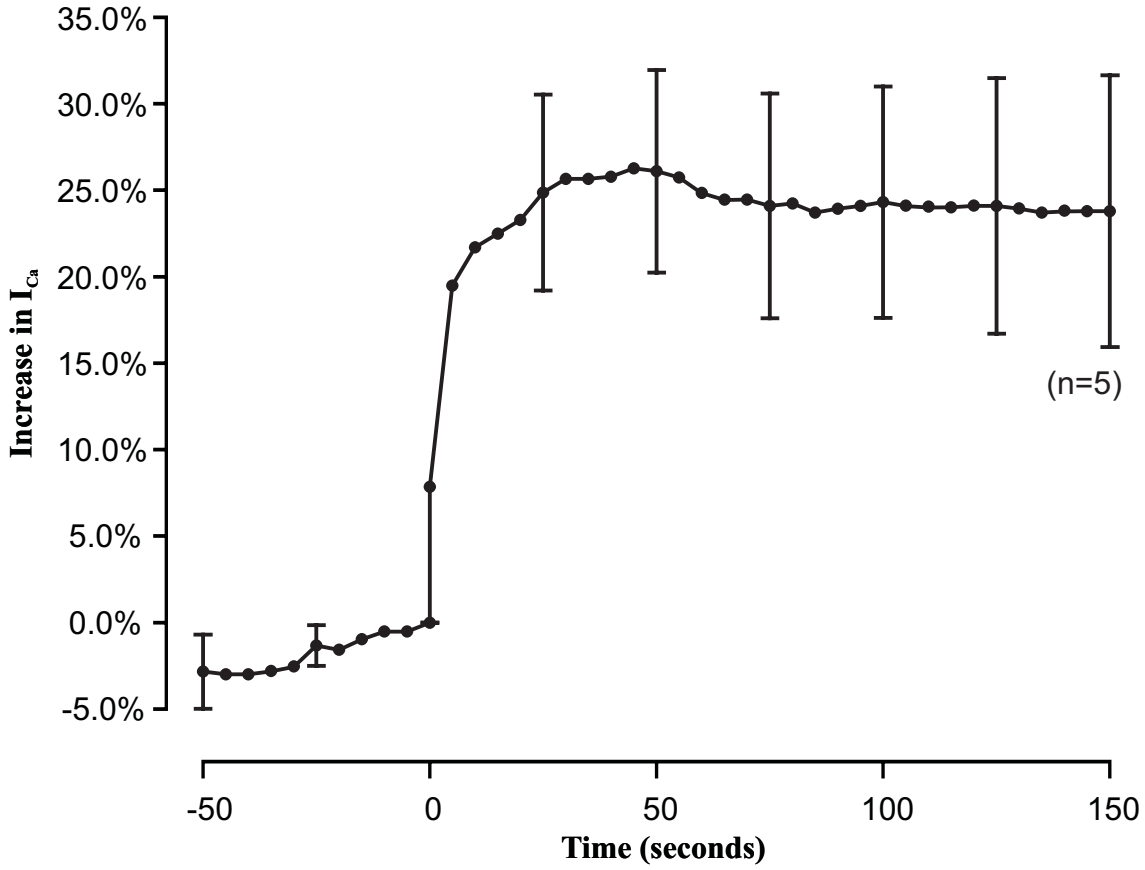

Figure 5.8b

Results showing the average time course for cells which showed a monophasic (sustained) increase in peak I_{Ca} after the photorelease of GTPγS. The average increase in non-leak-subtracted peak Ca^{2+} currents relative to control were plot against time. The myocytes were dialysed with 1 mM GTPγS. A single light flash 20ms before the onset of a voltage-clamp pulse induced an immediate increase in I_{Ca} which rose to a maximum after around 50 seconds after the stimulus. The vertical error bars show the standard errors of the mean at those intervals and the number of experiments is printed to the right of the graph.

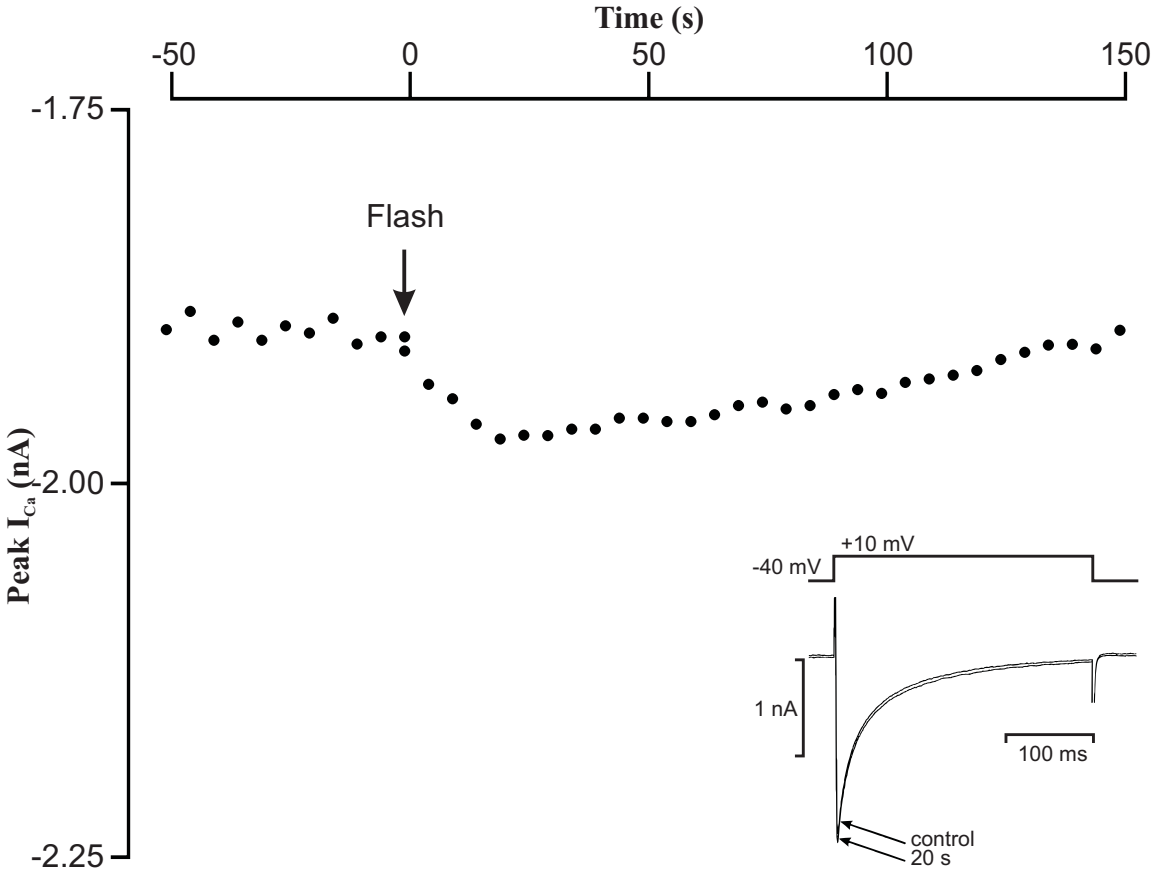

Figure 5.9a

A plot of peak I_{Ca} against time in a single cardiac ventricular myocyte. In this cell, the further photo-release of GTPγS in the presence of 100 μM uncaged GTPγS in the dialysing solution only produces a reduced response compared with cells without ambient GTPγS (see figure 5.1a, 5.2a). Instead of a sustained increase, only a small rise to a peak after 20 seconds is seen. The response then slowly decays back to control levels.

Inset are non-leak-subtracted raw current traces from the same cell. The calcium currents shown were recorded at test potentials of +10 mV. Pre-conditioning depolarizations to -40mV were designed to inactivate sodium and T-type calcium channels. The traces shown were obtained immediately before the light pulse, and when the response had reached a peak.

significantly modulated, with a marked reduction in the times-to-peak response despite the limitations of using gradual bath perfusion to apply forskolin.

5.2.3 Photorelease of GTPγS and cAMP

Perfusion delays are not, of course, a feature of the flash photolysis method, and further investigations into the effects of GTPγS and changes in kinetics proceeded with the photorelease of GTPγS and cAMP.

5.2.3.1 The response to photoreleased GTPγS

Figure 5.7a shows a typical response to photoreleased GTPγS. This biphasic increase after the photolysis of 1 mM GTPγS was seen in a majority of cells tested (figure 5.7b). There was a sharp jump in peak I_{Ca} detectable within 20 ms of the UV flash, much like responses to photoreleased GTP, which rose to an initial plateau after around 20 s before resuming its upward course to a sustained maximum of 72.0 ±11.0% (n=12) with a mean time to peak of 225 ±19 s (n=12). In a further five cells examined, a smaller monophasic increase was seen (figure 5.8a). This was accompanied by a reduced maximum of 26.9 ±7.1% (n=5) with a time-to-peak of 46 ±15 s (n=5; figure 5.8b). The initial rapid initial increase in I_{Ca} of 4.2 ±0.7% (n=17) seen within 20 ms of the UV light flash and photolysis of GTPγS was smaller than that seen with photoreleased GTP (9.4% ± 1.2%) but still statistically significant ($p < 0.05$).

5.2.3.2 Photoreleased GTPγS inhibited by chronic GTPγS

When the photorelease of GTPγS was repeated in cells which had first been co-dialysed with 0.1 to 100 μM uncaged GTPγS, the effects of the further photorelease of GTPγS were reduced relative to control. Figure 5.9a shows a typical response in the

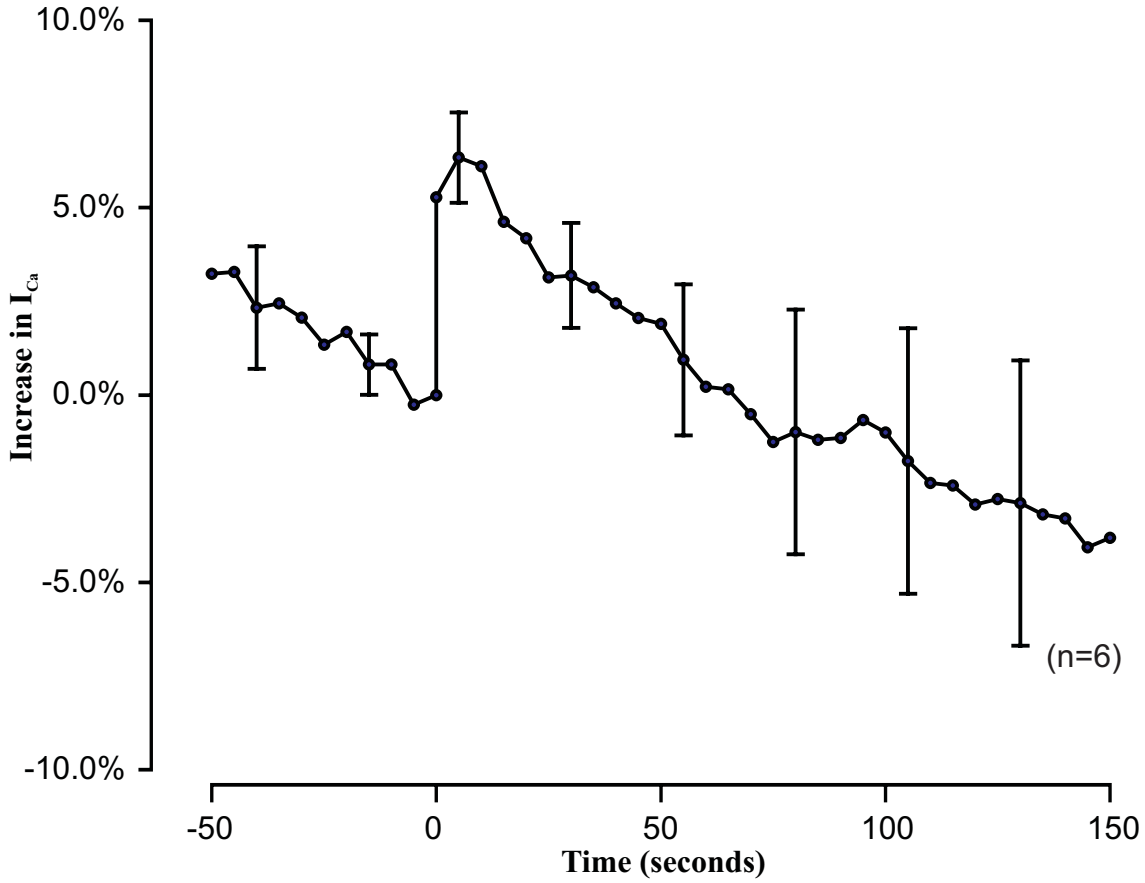

Figure 5.9b

Results showing the average time course for the response to photoreleased GTPγS in the presence of ambient GTPγS. 1 mM caged GTPγS and 100 μM uncaged (free) GTPγS was added to the dialysing solution. The UV photolysis at time = 0 produced a small increase which reached a peak after only 10 seconds before decaying rapidly below control current levels. These responses can be compared to those in figures 5.1b and 5.2b where the photorelease of GTPγS alone produces much larger increases with quite different profiles.

The vertical error bars show the standard errors of the mean at those intervals and the number of experiments is printed to the right of the graph.

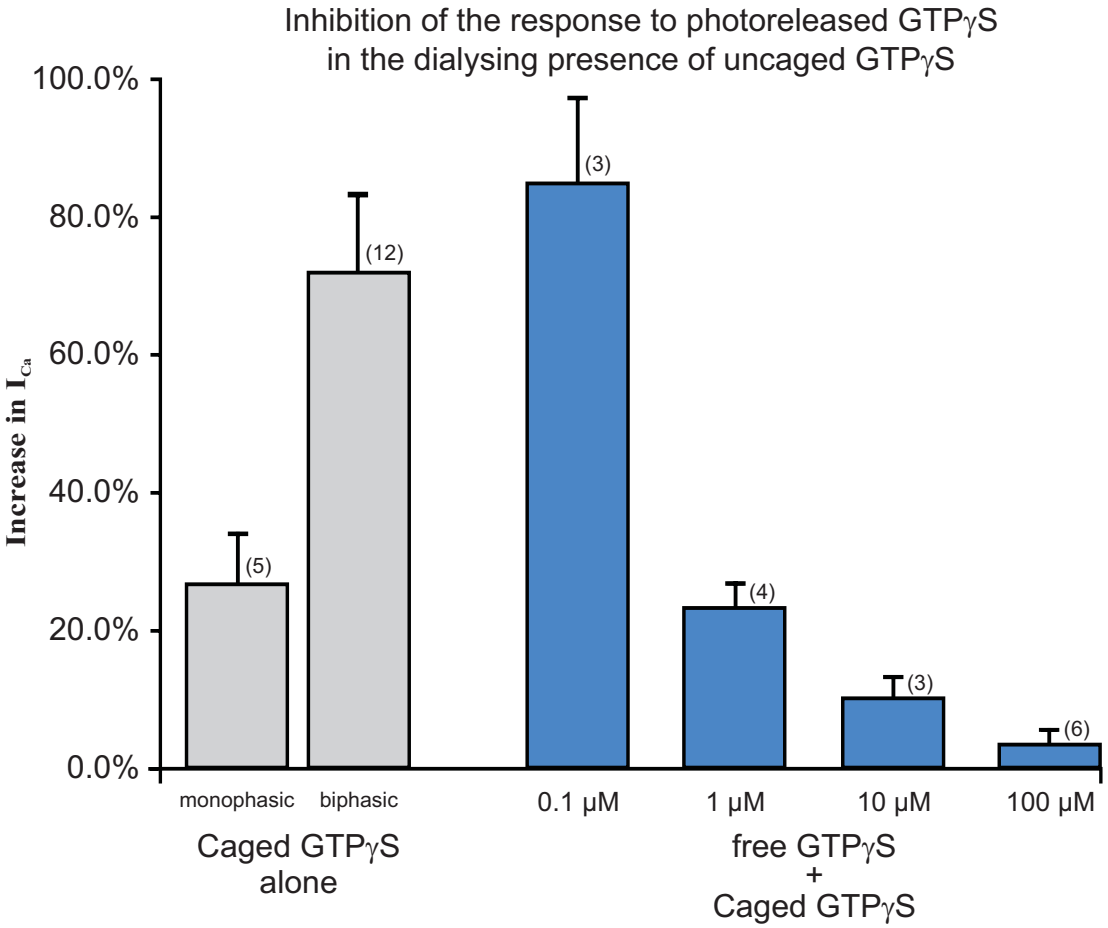

Figure 5.10

This bar graph illustrates the inhibitory effects of ambient uncaged GTPγS in the intracellular dialysing solution on further photorelease of GTPγS. Uncaged GTPγS depresses the response to photolysis of 1 μM caged GTPγS with an IC_{50} of ~1.0 μM. For comparison, the graph includes responses without the presence of uncaged GTPγS whether monophasic or biphasic in profile.

The number of experiments for each cell are given beside vertical error bars denoting standard errors of the mean. Significant differences from the biphasic control responses are indicated by asterisks (*, $p < 0.05$).

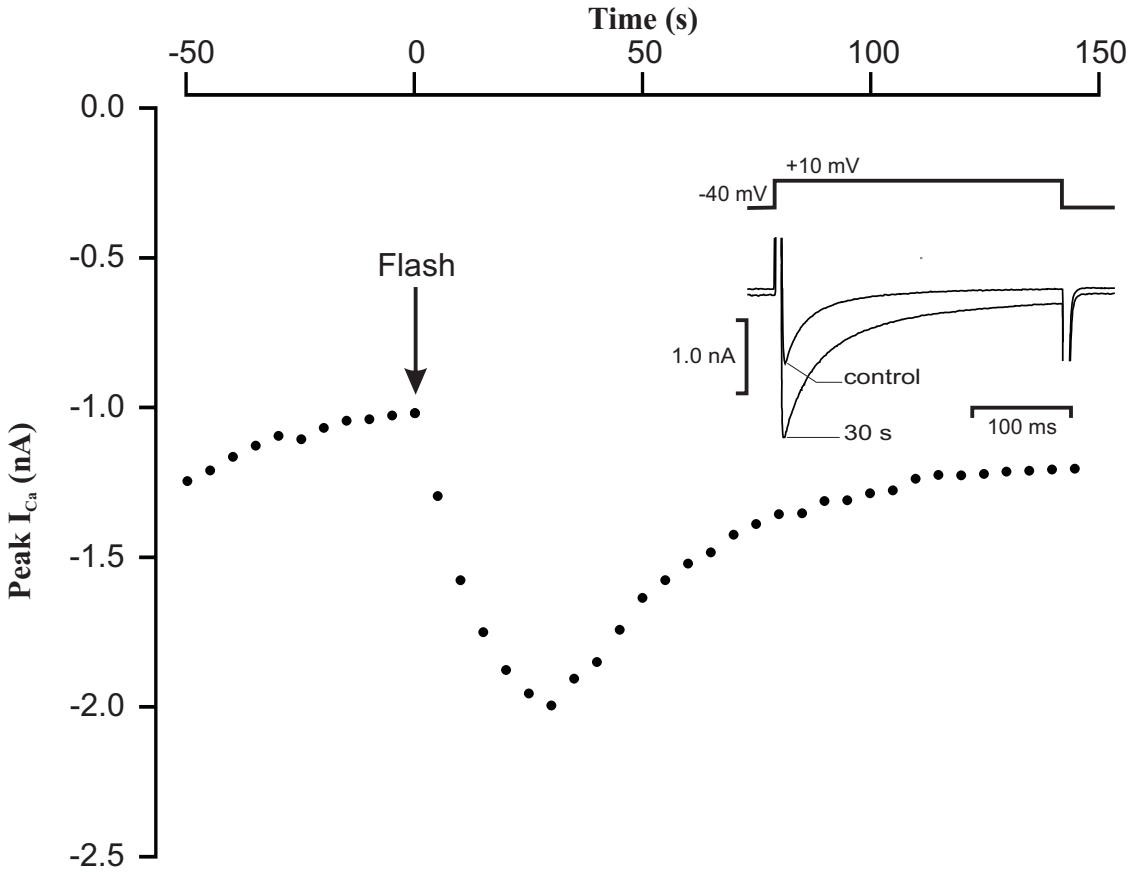

Figure 5.11a

A plot of peak I_{Ca} against time in a single ventricular cardiac myocyte. In this cell, the flash photolysis of 1 mM caged cAMP produced a large increase in calcium current. Unlike in the photolysis of caged GTPγS (figure 5.7a, 5.8a) and caged GTP (figure 4.1a), no immediate enhancement of calcium current in the test pulse 20 ms after the uv light flash. After 5 seconds, however, a large increase could be clearly seen. The response reached a peak after 30 seconds before relaxing slowly, i.e. no sustained rise was seen.

Inset are non-leak-subtracted raw current traces from the same cell. The calcium currents shown were recorded at test potentials of +10 mV. Pre-conditioning depolarizations to -40mV were designed to inactivate sodium and T-type calcium channels. The traces shown were obtained immediately before the light pulse at the peak of the response. They clearly show the large increase in I_{Ca} produced by photo-releasing cAMP.

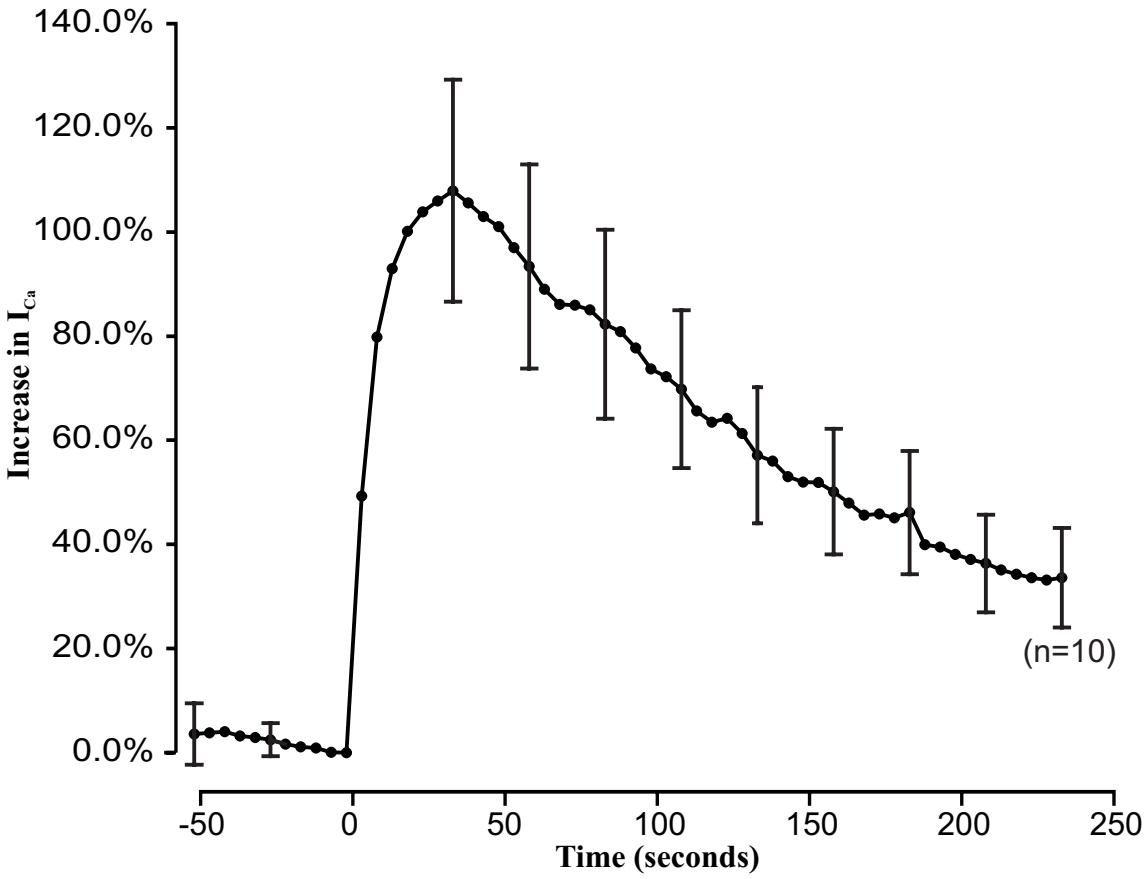

Figure 5.11b

Results showing the average time course for the response to photoreleased cAMP. 1 mM caged cAMP was added to the dialysing solution. The UV photolysis at time = 0 produced an increase in calcium current which could be detected at the test depolarisation 5 seconds later. The average response reached a peak after 35s before relaxing slowly and monotonically.

The vertical error bars show the standard errors of the mean at those intervals and the number of experiments is printed to the right of the graph.

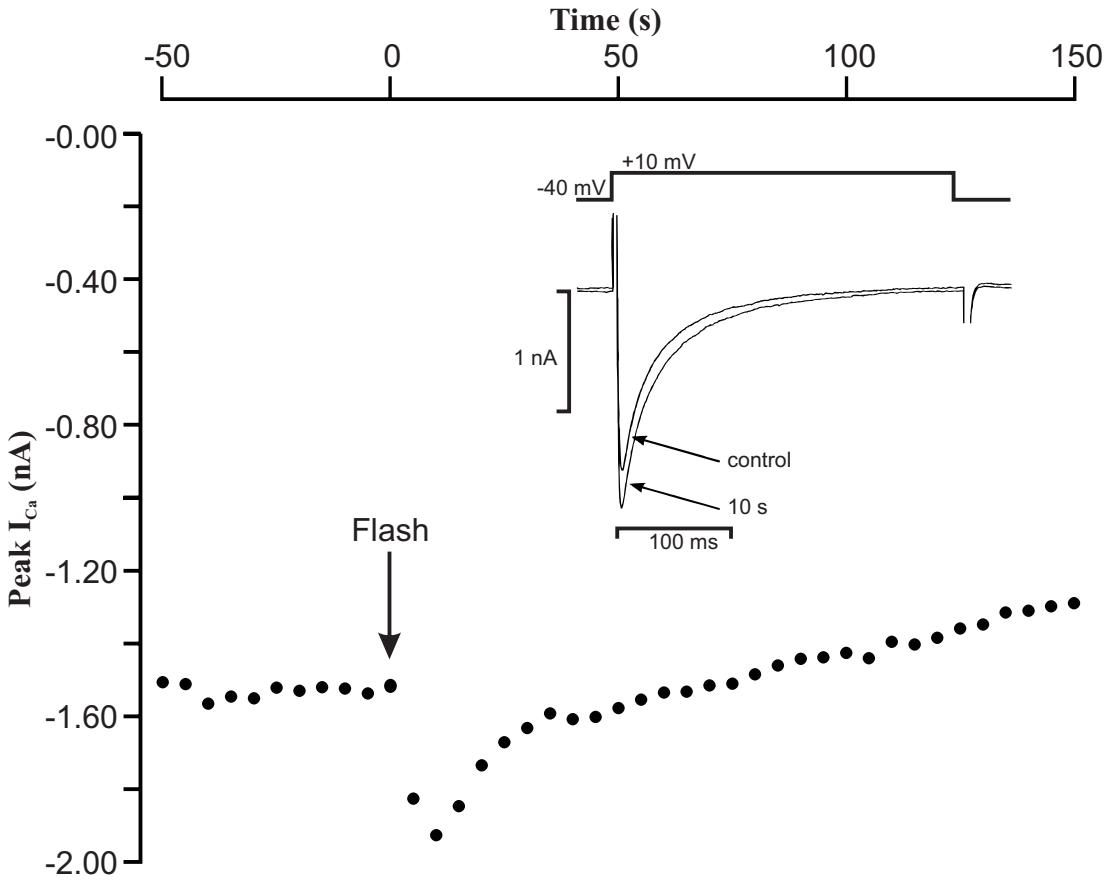

Figure 5.12

A plot of peak I_{Ca} against time in a single ventricular cardiac myocyte. In the presence of R_p-cAMPS, the flash photolysis of 1 mM caged cAMP produced a reduced increase in calcium current compared with the cell in figure 5.11a. An initial increase was seen after 5 seconds, which reached a peak after 10s before decaying rapidly below control levels. Inset are non-leak-subtracted raw current traces from the same cell. The calcium currents shown were recorded at test potentials of +10 mV. Pre-conditioning depolarizations to -40mV were designed to inactivate sodium and T-type calcium channels. The traces shown were obtained immediately before the light pulse, and after 10 seconds at the peak of the response.

presence of 100 μM ambient GTPγS and figure 5.9b the averages from six cells under such experimental conditions. Not only was the response much attenuated but the sustained increase became a merely transient rise. This inhibitory effect of GTPγS was again dose-dependent (figure 5.10) with an IC_{50} of around ~1.0 μM. This is around ten times lower than the equivalent value for the GTPγS inhibition of isoprenaline induced enhancement of I_{Ca}. This inhibition was not due to GDP contamination because when 1 mM GDP was added to the dialysing pipette, responses to further photorelease of GTPγS were similar to those described above.

5.2.3.3 The response to Photoreleased cAMP

The photorelease of cAMP also produced an increase in peak I_{Ca} (figure 5.11a). In contrast to the results with the photorelease of either GTP or GTPγS, no significant increase in I_{Ca} (-3.1 ±1.9%; n=16) was seen within 20 ms of the UV light flash. The profiles of the responses were also significantly different (figure 5.11b). An increase of 117.5 ±22.0% (n=16) with a time-to-peak of 35.5 ±5.3 s (n=16) in I_{Ca} was seen. This began to wane soon after the maximum response was seen and declined by 50% within 101.5 ±18.1 s (n=16).

In the absence of separate sympathetic stimulation, the photorelease of cGMP from its caged precursor did not affect the amplitude of I_{Ca} (n=5) though this would have released identical by-products to the photolysis of caged cAMP.

The ability of cAMP to increase peak I_{Ca} was markedly inhibited by the inclusion of the cAMP antagonist R_p-cAMP in the internal dialysing solution (figure 5.12) with only a change of 27 ±5% (n=4) after 11 ±7 s.

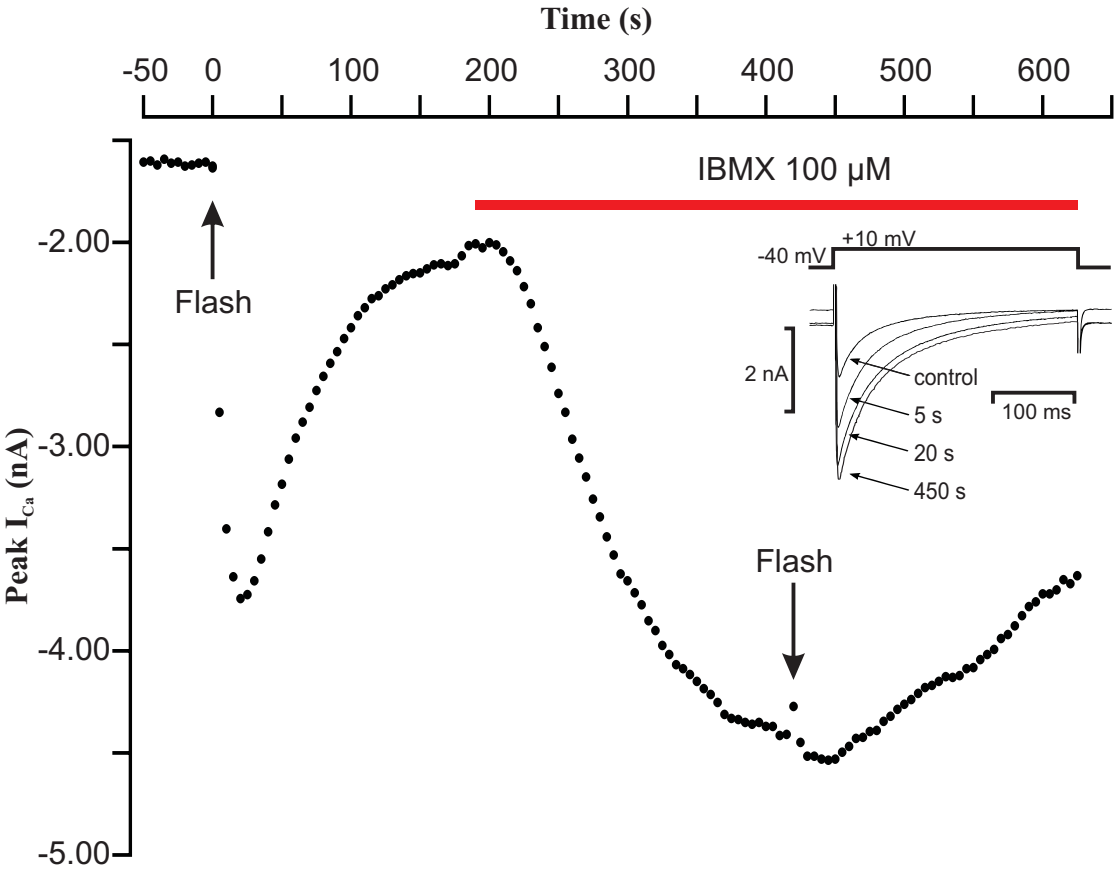

Figure 5.13

A plot of peak I_{Ca} against time in a single ventricular cardiac myocyte. In this cell, the responses to the photorelease of cAMP was examined before and after the application of 100 µM IBMX, a potent non-specific phosphodiesterase inhibitor. The initial uv light pulse produced a rapid increase in calcium current which relaxed slowly. At the 200 second mark, IBMX was applied. This caused a slow run up in calcium current. A subsequent second uv light pulse produced only a marginal further increase.

Inset are non-leak-subtracted raw current traces from the same cell. The calcium currents shown were recorded at test potentials of +10 mV. Pre-conditioning depolarizations to -40mV were designed to inactivate sodium and T-type calcium channels. The traces shown were obtained immediately before the first uv flash, after 5 seconds and then at the peak of the response (20s). The last trace was recorded after 450 seconds at the peak of the response to the second UV flash.

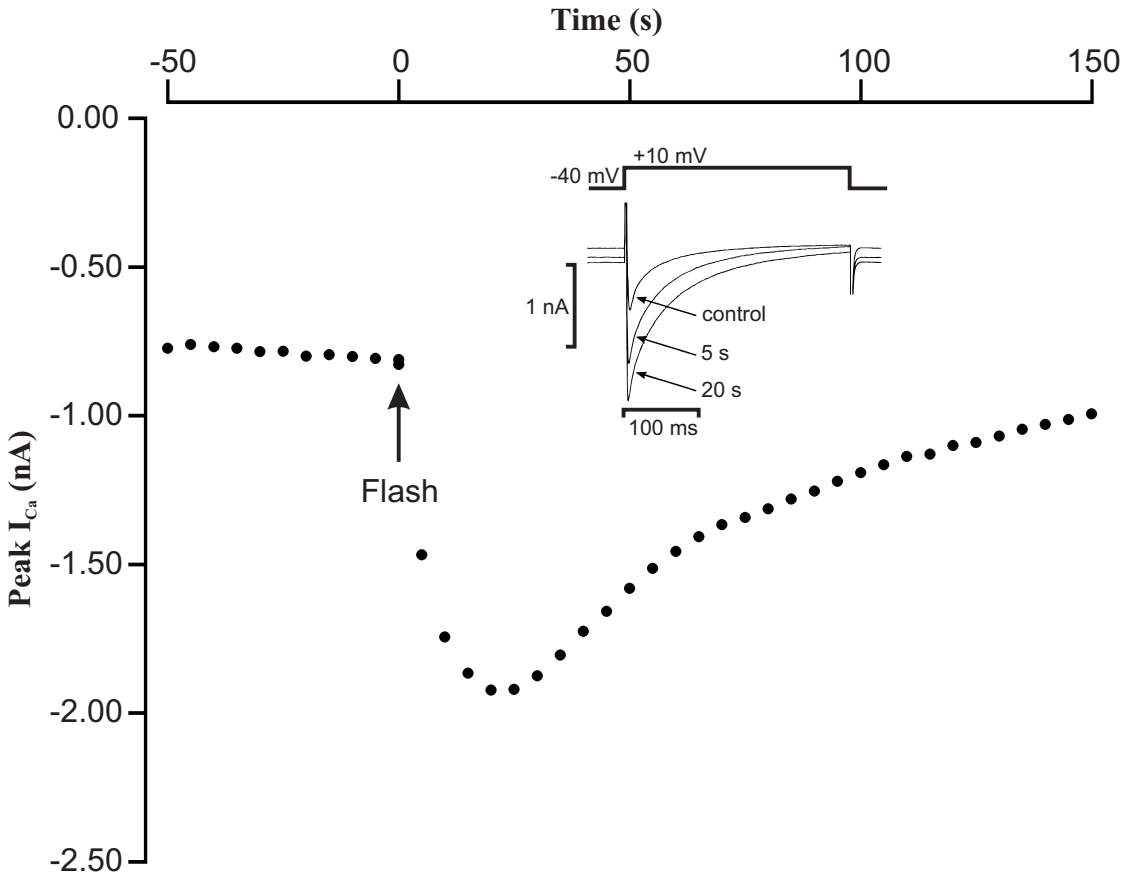

Figure 5.14a

A plot of peak I_{Ca} against time in a single ventricular cardiac myocyte. In this cell, the flash photolysis of 1 mM caged cAMP in the presence of 100μM GTPγS in the dialysing solution produced a response which was not dissimilar from responses in cells where GTPγS was not present (see 5.11a). An rapid increase in calcium current could be detected 5 seconds after the uv light pulse which rose to a peak after 20 seconds before relaxing slowly.

Inset are non-leak-subtracted raw current traces from the same cell. The calcium currents shown were recorded at test potentials of +10 mV. Pre-conditioning depolarizations to -40mV were designed to inactivate sodium and T-type calcium channels. The traces shown were obtained immediately before the light pulse, after 5 seconds and at the peak of the response.

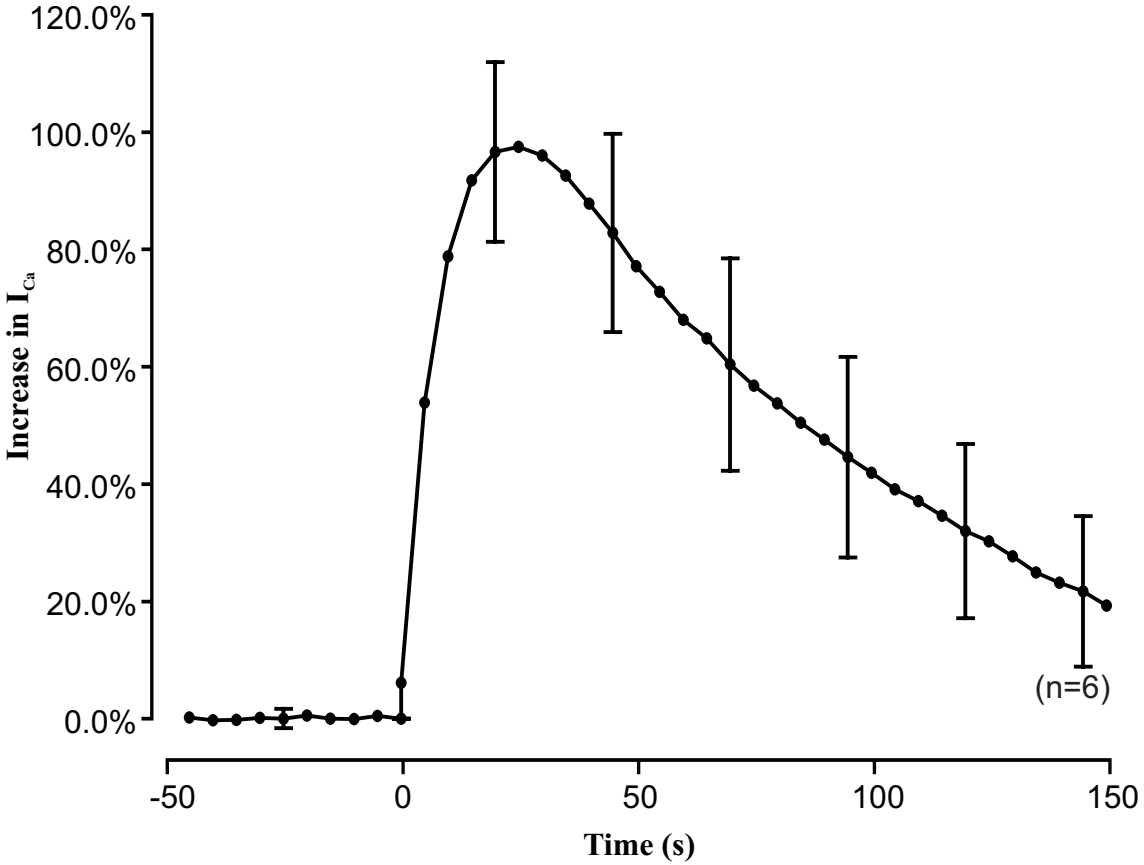

Figure 5.14b

Results showing the average time course for the response to photoreleased cAMP in the presence of uncaged GTPγS. 1 mM caged cAMP and 100 μM GTPγS was added to the dialysing solution. The UV photolysis at time = 0 produced an increase in calcium current which could be detected at the test depolarisation 5 seconds later. The average response reached a peak after 30s before relaxing slowly and mono-tonically. This profile is not appreciably different from that seen when GTPγS is absent (figure 11b).

The vertical error bars show the standard errors of the mean at those intervals and the number of experiments is printed to the right of the graph.

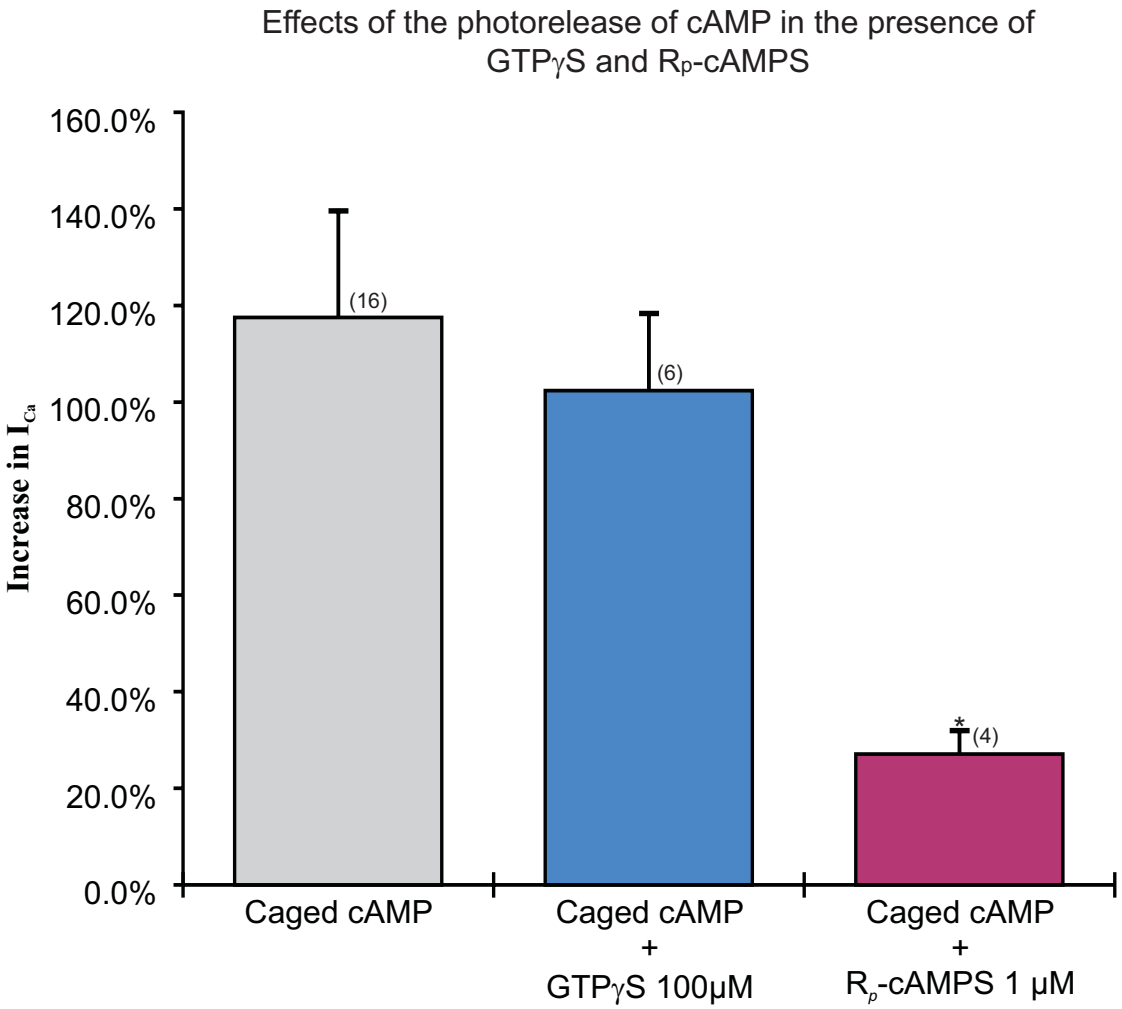

Figure 5.15

This bar graph illustrates the lack of an inhibitory effect of ambient uncaged GTPγS in the intracellular dialysing solution on photoreleased cAMP. The peak responses for photolysis of 1 mM caged cAMP in the presence and absence of GTPγS are not significantly different. In contrast, the inclusion of R_p-cAMPS drastically depresses the cAMP response.

The number of experiments for each cell are given beside the vertical error bars denoting the standard errors of the mean. Significant differences from the control responses to photoreleased cAMP are indicated by asterisks (*, $p < 0.05$).

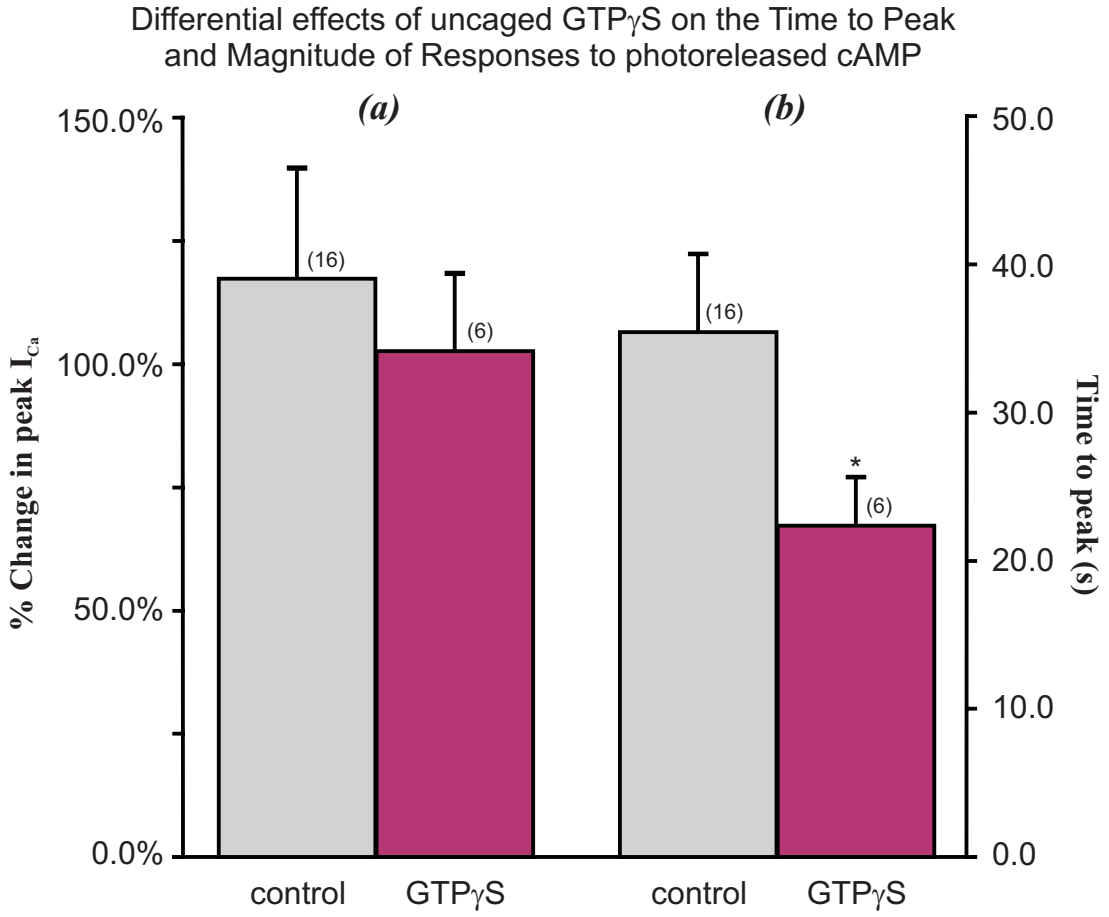

Figure 5.16

This bar graph illustrates the effects of ambient uncaged GTPγS in the pipette dialysing (intracellular) solution on the response to photoreleased cAMP.

(a) The photolysis of 1 mM caged cAMP produced changes in calcium current which were not significantly different in magnitude whether GTPγS was present (the bar marked "GTPγS") or not ("control").

(b) However, when the time courses for the responses was examined, it was clear that the inclusion of GTPγS produced much faster responses in calcium current to photoreleased cAMP. The times-to-peak with GTPγS are significantly different (*, $p < 0.05$) from control.

The error bars indicate standard errors of the mean with the number of cells for each experiment to their right.

100 μM 3-isobutyl-1-methylxanthine (IBMX) caused a large increase in peak I_{Ca} 76.2 ±27.0%. Figure 5.13 shows the results of IBMX in a single myocyte. The photorelease of cAMP initially produces the typical large but transient increase in I_{Ca}. The application of IBMX causes a slow run-up in calcium current. When a second UV light flash was applied after 200 s, no further significant increase in cAMP could be seen. In contrast, when IBMX was not present, two consecutive UV flashes produced similar changes in I_{Ca} provided they were at least 5 minutes apart: the second responses in the same cell were within 92.6 ±4.5% (n=4) of the first.

5.2.3.4 Effects of Photoreleased cAMP unaffected by chronic GTPγS

Dialysing 100 μM GTPγS did not inhibit the increase in peak I_{Ca} produced by the photolysis of caged cAMP. This was in contrast to the inhibitory effect of GTPγS on the activation of I_{Ca} by photoreleased GTPγS, isoprenaline or forskolin. The response in figure 5.14a is not dissimilar to those where GTPγS was absent (figure 5.11a). On average, a maximum increase in peak I_{Ca} occurred of 102.3 ±16.0% (n=6; figure 5.14b). The lack of GTPγS inhibition of responses to photoreleased cAMP is summarized in figure 5.15.

Though GTPγS did not have an inhibitory effect, the time-to-peak response was significantly shorter (22.5 ±3.2 s; n=6), as was the time for the response to decline by 50% from its peak (58.0 ±11.2 s; n=6). A significant increase in I_{Ca} of 6.1 ±3.4% (n=6) occurred within 20 ms of the light flash, compared to -3.1 ±1.9% (n=16) in the absence of chronic application of GTPγS (figure 5.16). This suggests that the dialysing GTPγS may sensitise the system to further cAMP-dependent activation.

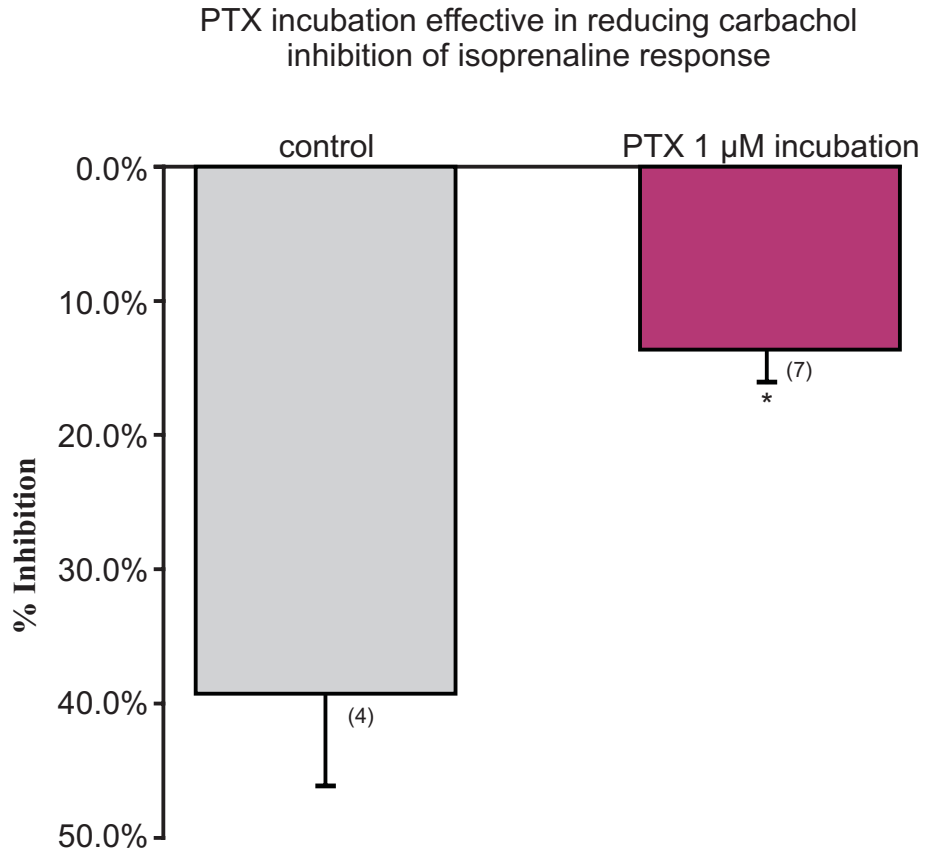

Figure 5.17

This bar graph illustrates the effectiveness of PTX incubation. In control cells, 10 µM carbachol produced a significant diminution of the response to 50 nM isoprenaline (39.3 ±6.9 %). This inhbitory effect of carbachol was significantly reduced after pre-incubation with PTX (13.8 ±2.4 %).

The error bars indicate standard errors of the mean with the number of cells for each experiment to their right.

5.2.4 PTX incubation

If the non-hydrolysable guanosine nucleotide, GTPγS, causes persistent activation of G-proteins, one source of inhibition might be the action of $G_{i\alpha}$, known to be linked to adenylyl cyclase in guinea pig cardiac myocytes. This would account for the inhibition of the responses to both isoprenaline and forskolin but not photoreleased cAMP. In order to test this hypothesis, the effects were examined of incubation with pertussis toxin (see section 2.5.4) which catalyses ADP-ribosylation and inactivation of $G_{i\alpha}$.

5.2.4.1 The effectiveness of PTX incubation

To verify the efficacy of PTX incubation in inactivating the G_i-protein, its effects on the response to muscarinic agonists were tested. It has been shown previously that only after β-adrenoreceptor stimulation do muscarinic agonists have an effect, by acting via cardiac $G_{i\alpha}$ in inhibiting adenylyl cyclase activity (Hescheler *et al.*, 1986). This muscarinic effect should thus be sensitive to PTX.

In control cells, when 10 μM carbachol was applied 1 minute after the response to 1 μM isoprenaline had reached its peak, a substantial inhibition of the isoprenaline response was seen (39.3 ±6.9%; n=4). When cells were dialysed with GTPγS (100 μM), both the enhancement of I_{Ca} due to isoprenaline and the subsequent inhibitory effect of carbachol were removed (n=3), which would be expected if GTPγS and carbachol were both acting through the same G_i-protein pathway. PTX incubation significantly reduces the muscarinic inhibition of the isoprenaline response to 13.6 ±2.5% (n=7; figure 5.17).

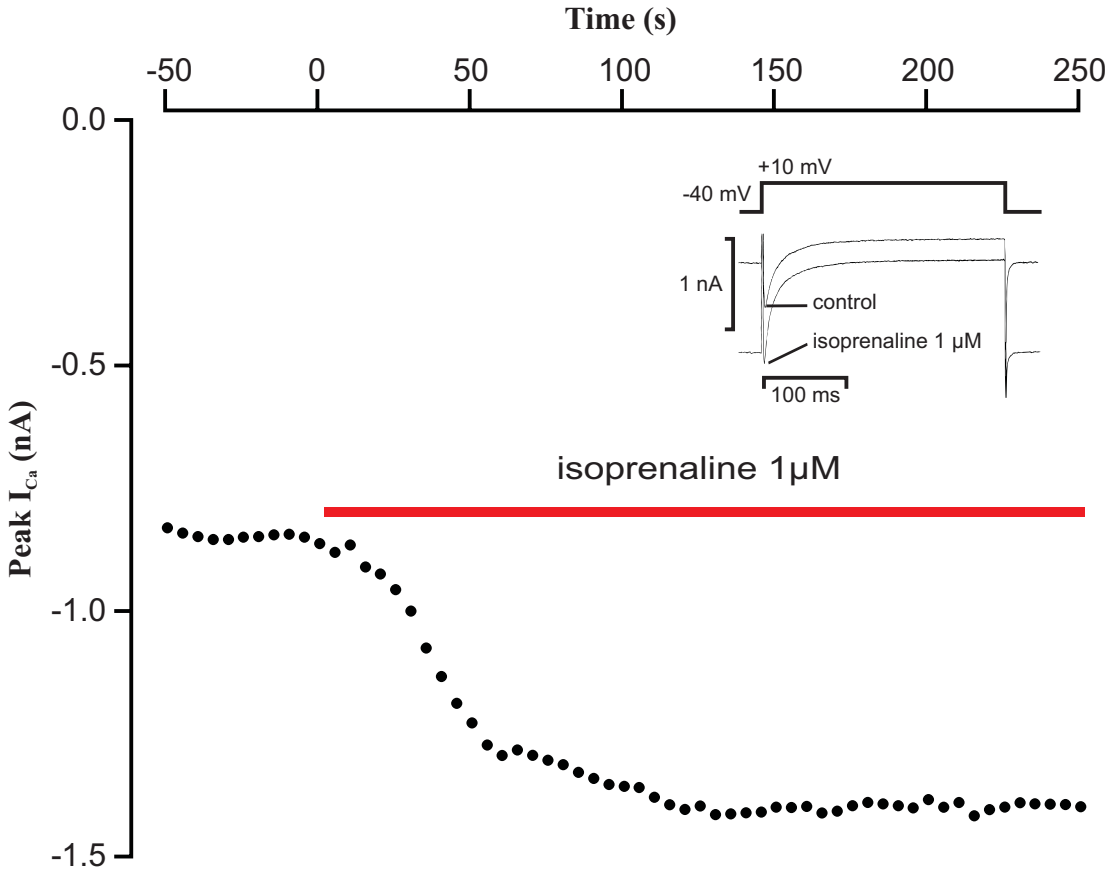

Figure 5.18

A plot of peak I_{Ca} against time in a single ventricular cardiac myocyte. This cell was pre-incubated in PTX and 100 µM GTPγS was included in the pipette dialysing solution. After PTX treatment, the inhibitory effect of GTPγS on the isoprenaline response was largely removed. Application of 1 µM isoprenaline produced a large increase in peak I_{Ca} which reached its peak approximately 130 seconds later.

Inset are non-leak-subtracted raw current traces from the same cell. The calcium currents shown were recorded at test potentials of +10 mV. Pre-conditioning depolarizations to -40mV were designed to inactivate sodium and T-type calcium channels. The traces shown were obtained immediately before the application and after the response had reached its apex.

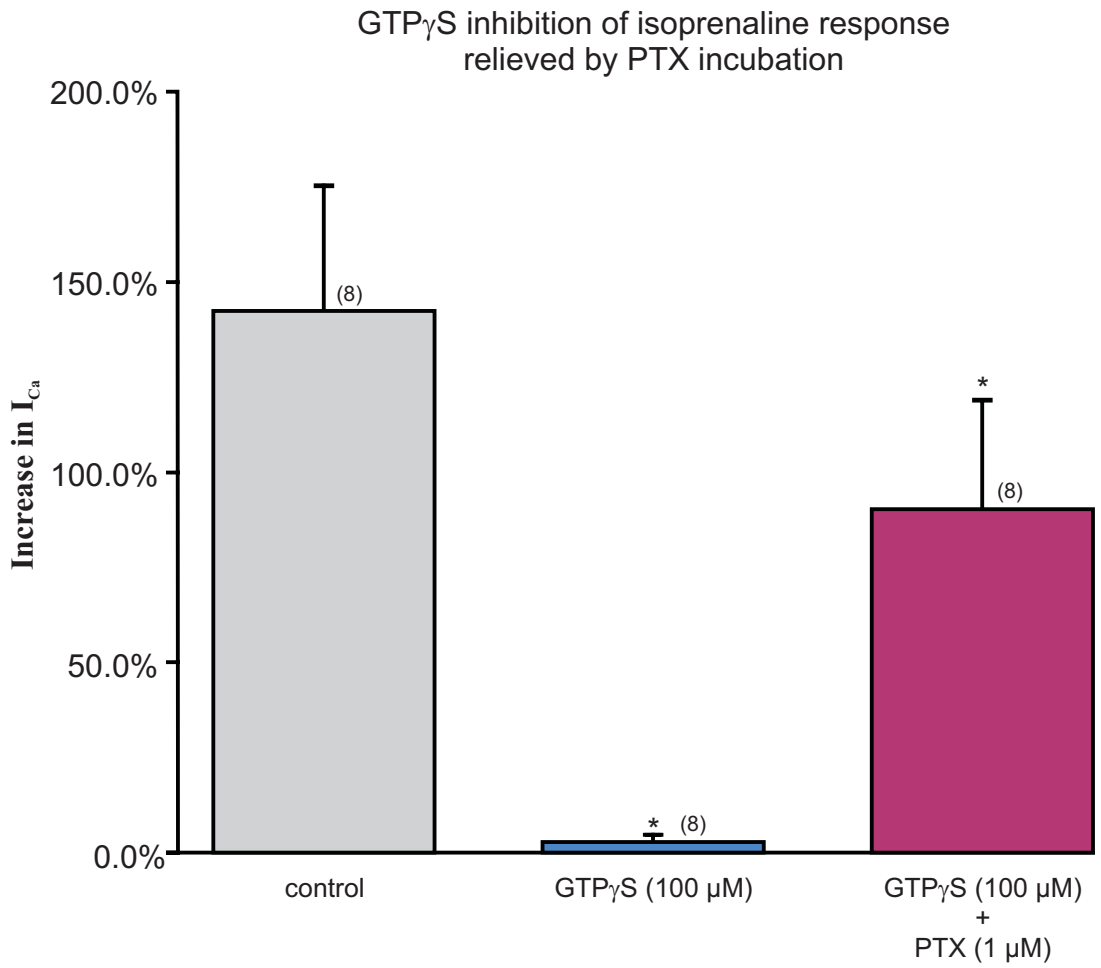

Figure 5.19

This bar graph summarizes the effects of intracelluar GTPγS on the response to isoprenaline, with and without pre-treatment of PTX.

Inclusion of 100 μM GTPγS in the pipette dialysing solution almost completely abolishes the ability of 1μM isoprenaline to enhance calcium current. However, in cells which had been incubated with PTX, this inhibitory action of GTPγS is greatly reduced and the response to isoprenaline recovered.

The error bars indicate standard errors of the mean with the number of cells for each experiment to their right.

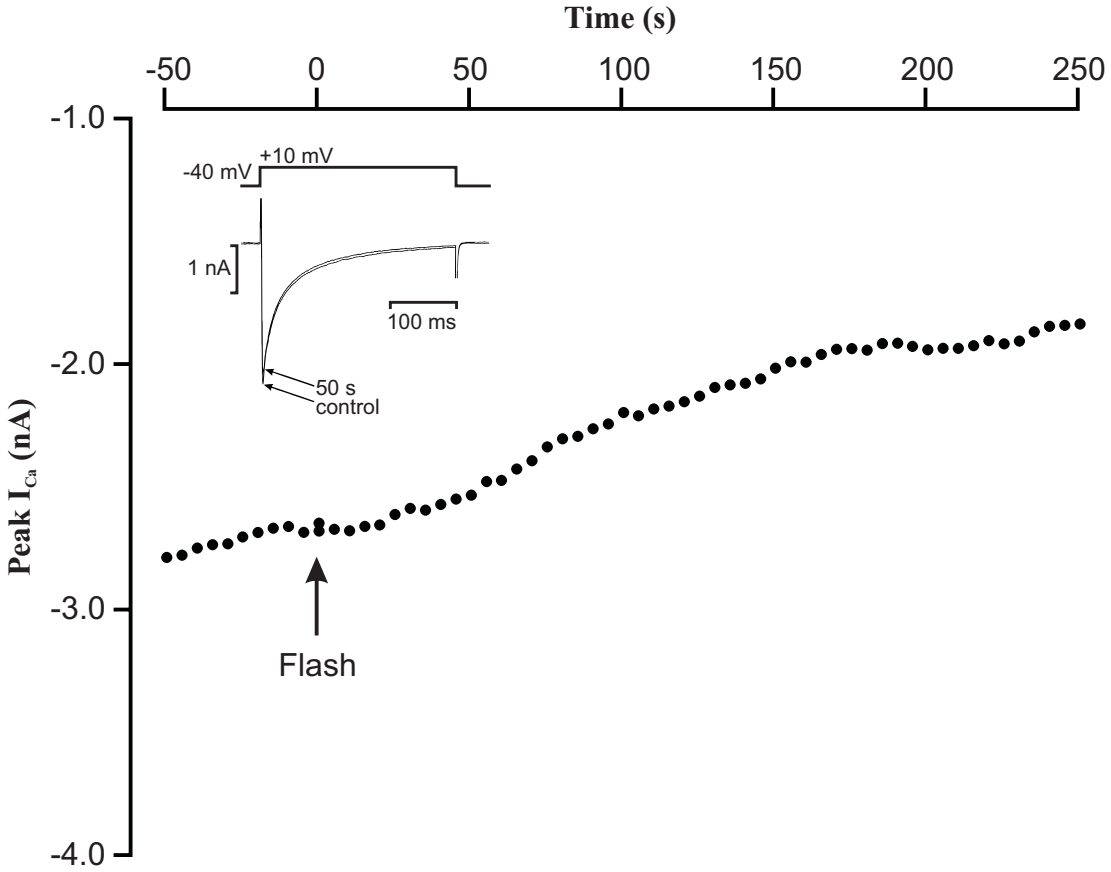

Figure 5.20

A plot of peak I_{Ca} against time in a single ventricular cardiac myocyte. In this cell, PTX incubation did not remove the inhibition of response to the flash photolysis of 1 mM caged GTPγS by the presence of 100μM uncaged GTPγS in the dialysing solution. No detectable enhancement of the calcium current could be seen but rather a slow decrease. Inset are non-leak-subtracted raw current traces from the same cell. The calcium currents shown were recorded at test potentials of +10 mV. Pre-conditioning depolarizations to -40mV were designed to inactivate sodium and T-type calcium channels. The traces shown were obtained immediately before the light pulse and after 50 seconds when the calcium current had declined significantly.

5.2.4.2 The effects of PTX on GTPγS inhibition of isoprenaline

Normally, when 1 μM isoprenaline is applied to cells dialysed with 100 μM GTPγS, almost no increase in peak I_{Ca} can be seen (figure 5.3). After incubation with PTX, a large response to 1 μM isoprenaline could be observed even in the presence of GTPγS. The magnitude was similar to the isoprenaline response seen without GTPγS in control cells (figure 5.18). In other words, PTX incubation was able to remove GTPγS inhibition. The effects of PTX are summarized in figure 5.19.

5.2.4.3 The effects of PTX on ambient GTPγS inhibition of photoreleased GTPγS

In contrast to the restoration by PTX incubation of the isoprenaline activation of I_{Ca} after GTPγS inhibition, the inhibition of 100 μM uncaged GTPγS on photoreleased GTPγS was not removed by PTX treatment (n=7; figure 5.20). This suggests that the underlying mechanism for this inhibitory effect is different from that of *β*-adrenoreceptor mediated responses. In the case of photoreleased GTPγS, the presence of chronic GTPγS may reduce the number of available binding sites for photoreleased GTPγS and hence the observed response in I_{Ca}. This would also explain the ten-fold difference in sensitivity between the inhibitions by chronic application of GTPγS of the responses to photoreleased GTPγS and isoprenaline. At low concentrations, GTPγS has a PTX-sensitive inhibition. At high concentrations, ambient GTPγS simply competes with further photoreleased GTPγS. In the latter case, one would expect peak I_{Ca} to be significantly higher than control in the presence of high levels of ambient GTPγS even before further GTPγS was photoreleased.

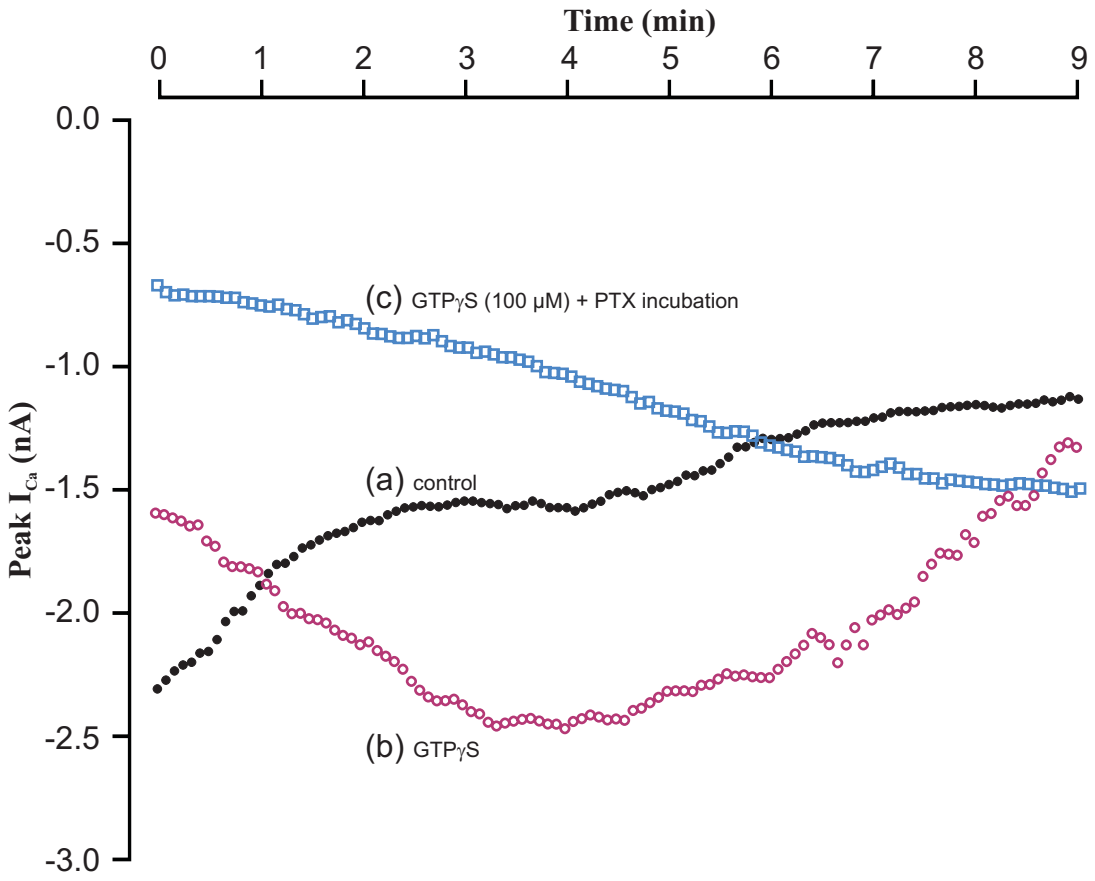

Figure 5.21

This graph shows the effects of intracellular dialysis with GTPγS on ventricular myocytes in the first minutes after a patch clamp seal in the whole cell mode was made. Each point represents the peak I_{Ca} recorded at +10 mV every 5s.

a) Under control conditions (●, in the absence of intracellular GTPγS), a gradual rundown of peak I_{Ca} can be seen. The time course for this is biphasic with an initial more rapid decline followed by a second more gradual phase.

b) In contrast, when the cells were dialysed with 100 μM GTPγS (○), an initial rise in calcium current was seen followed by a pronounced rundown.

c) In cells which had been pre-incubated with PTX (□), only a gradual runup of I_{Ca} was evident.

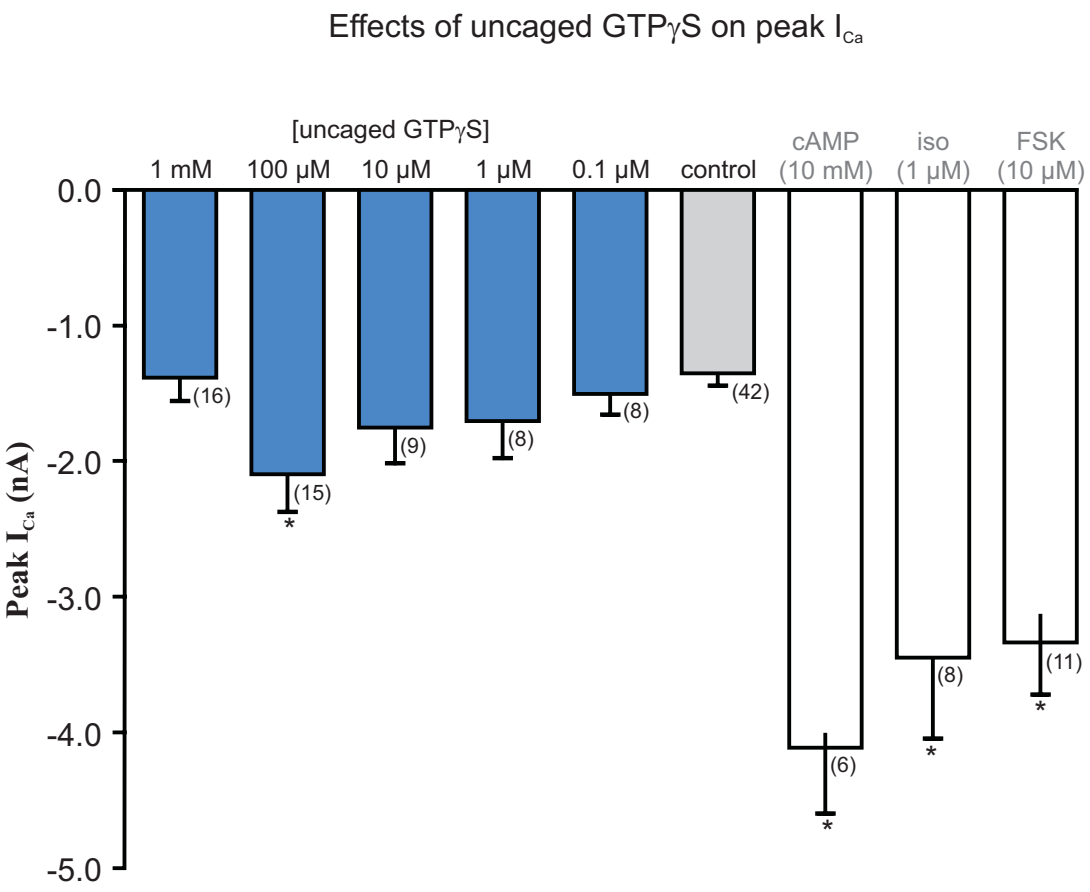

Figure 5.22

This graph shows the peak I_{Ca} recorded around 10 minutes after the formation of a patch seal in the whole-cell mode in the presence of different concentrations of intracellular GTPγS. Despite run down (see figure 5.21), I_{Ca} at this point tends to be greater than in control cells (dialysed with GTPγS free solution). Included for comparison are averages from cells where calcium current have been stimulated by 1 μM isoprenaline (iso) or 10 μM forskolin (FSK), or after 10 minutes of 10 mM intracellular cAMP. In all three cases, I_{Ca} greatly exceeded the levels when only intracellular GTPγS was present.

The profiles for runup and rundown of I_{Ca} were unaffected by the inclusion of caged nucleotides (whether caged cAMP or caged GTPγS) and data from these cells have been pooled with cells dialysed with standard intracellular solutions.Vertical error bars show standard errors of the mean with the number of experiments indicated to the right. Significant differences from control are marked with asterisks (*, $p < 0.05$).

5.2.4.4 Changes in I_{Ca} after pipette dialysis with GTPγS and PTX incubation

After the establishment of the whole-cell configuration of the patch clamp seal, peak I_{Ca} would generally begin to run-down in the approximately 10-12 minutes before either application of a drug or UV flash photolysis was initiated (figure 5.21). This had a biphasic time course similar to those previously reported (Belles *et al.*, 1988). The addition of GTPγS in the dialysing solution, however, produced an initial run-up of peak I_{Ca} before a run-down was observed. This has also been seen with pressure-assisted dialysis of cardiac myocytes (Shuba *et al.*, 1990). Despite the subsequent run-down in peak I_{Ca}, the initial increase immediately after the start of the dialysis of the cell with intracellular solution containing GTPγS was enough to produce increased average I_{Ca} after 10-12 minutes, though only the increased current seen with 100 μM GTPγS was significantly larger than control.

Figure 5.22 summarises the results of including GTPγS in the dialysing solution. The mean amplitudes of I_{Ca} before any further experimental intervention are displayed. Ambient intracellular GTPγS does seem to increase I_{Ca} though this was significantly different from control only in the case of 100 μM GTPγS. It seems unlikely that, in the absence of an agonist, ambient GTPγS alone is able to saturate the cAMP-dependent pathway and maximally activate I_{Ca} as the responses to 1 μM isoprenaline, 10 μM forskolin or 10 mM cAMP.

When the cells were pre-treated with PTX, and in the presence of 100 μM GTPγS, only a gradual run-up in the current could be seen. The run-down in current

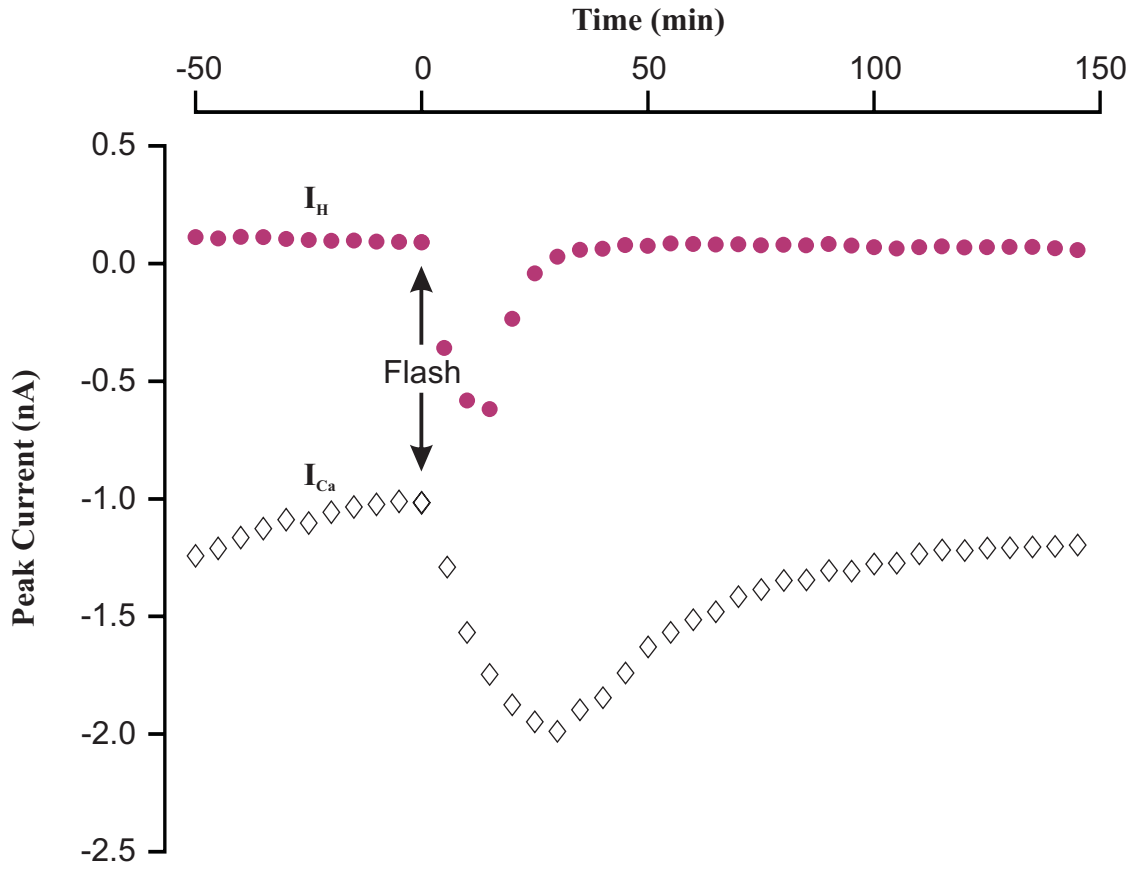

Figure 5.23

A plot of changes in holding current at -80 mV ($I_{H,}$ ●) against time in a single ventricular cardiac myocyte illustrating the effects of photoreleased cAMP. Peak calcium currents from figure 5.11 recorded at +10 mV (I_{Ca}, ◇) in the same cell are also shown for comparison.

The flash photolysis of 1 mM caged cAMP produced a large increase in $I_{H.}$ Unlike in the photolysis of caged GTPγS (figure 5.7a, 5.8a) and caged GTP (figure 4.1a) but like the concomittant changes in I_{Ca}, no immediate rise in I_H was seen at the test pulse 20 ms after the uv light flash. After 5 seconds, however, there was a large increase which reached a peak after 15 seconds before decaying rapidly back to control levels. The time course of this decline is in marked contrast to the more gradual profile for I_{Ca} shown above.

was abolished. This would be in accordance with the hypothesis that GTPγS normally activates a PTX-sensitive inhibitory G-protein.

5.2.5 $I_{Cl,cAMP}$ activated by photoreleased cAMP

In addition to the effects on I_{Ca} described above, photoreleased cAMP would also be expected to activate the voltage- and time-independent, cAMP-dependent chloride current ($I_{Cl,\ cAMP}$). Indeed, the photolysis of caged cAMP produced a significant negative shift in the normally negligible holding currents at both -40 and -80 mV but without any changes in the sustained current at either 0 or +10 mV. Using solutions designed to block potassium currents and the hyper-polarisation-activated non-specific (I_f) channels, and assuming minimal contamination from other leakage currents, this change in holding current can be attributed entirely to the expected activation of cAMP-dependent chloride current. This identification agrees with the lack of time or voltage dependence, and a lack of rectification of this current in symmetrical chloride solutions, where I_{Cl} would also be expected to be minimal around its Nernst potential of 0 mV. The changes in holding current (I_H) could thus be used as a measure of evoked $I_{Cl,cAMP}$ while recording I_{Ca} in the same cell.

5.2.5.1 Differential effects of photoreleased cAMP on $I_{Cl,cAMP}$ and I_{Ca}

Figure 5.23 shows the changes in holding current measured at -80 mV in a guinea pig myocyte produced by the photolysis of 1 mM caged cAMP. The increase in $I_{Cl,cAMP}$ paralleled that of I_{Ca} but the time-to-peak was significantly shorter and the current returned to control levels much more quickly. The average change in holding current was -0.58 ±0.12 nA (n=13) with a time-to-peak-response of 26.5 ±8.1 s. The time it

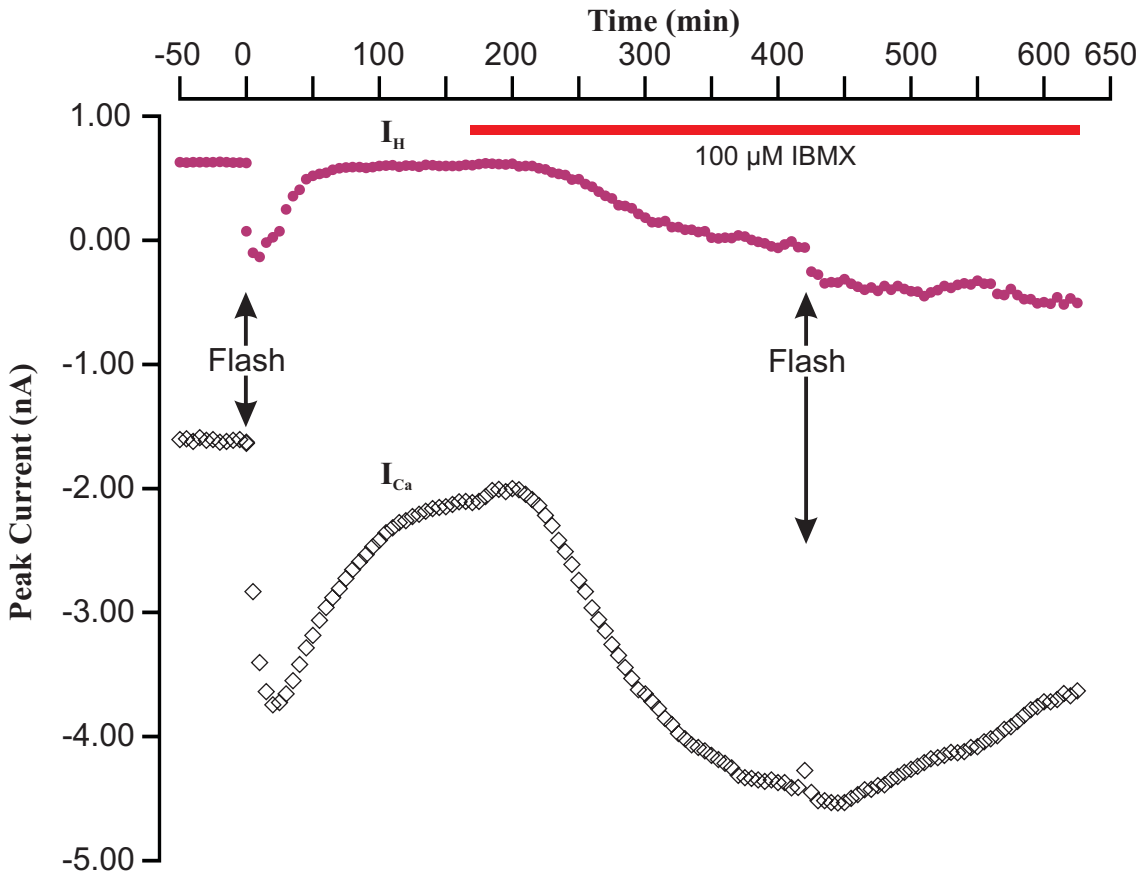

Figure 5.24

A plot of changes in holding current at -80 mV (I_H ●) against time in a single ventricular cardiac myocyte illustrating the effects of photoreleased cAMP before and after the application of 100 µM IBMX, a phosphodiesterase inhibitor. The peak calcium currents from figure 5.13 recorded at +10 mV (I_{Ca} ◇) from the same cell are also shown for comparison.

IBMX was introduced after the 200 second mark. This caused a runup in the holding current. The subsequent UV photolysis produced a reduced but still obvious increase in $I_{H.}$ Unlike control responses to photoreleased cAMP, I_H remained at elevated levels and did not show signs of decreasing. In contrast, only marginal increases in I_{Ca} are seen in the presence of IBMX.

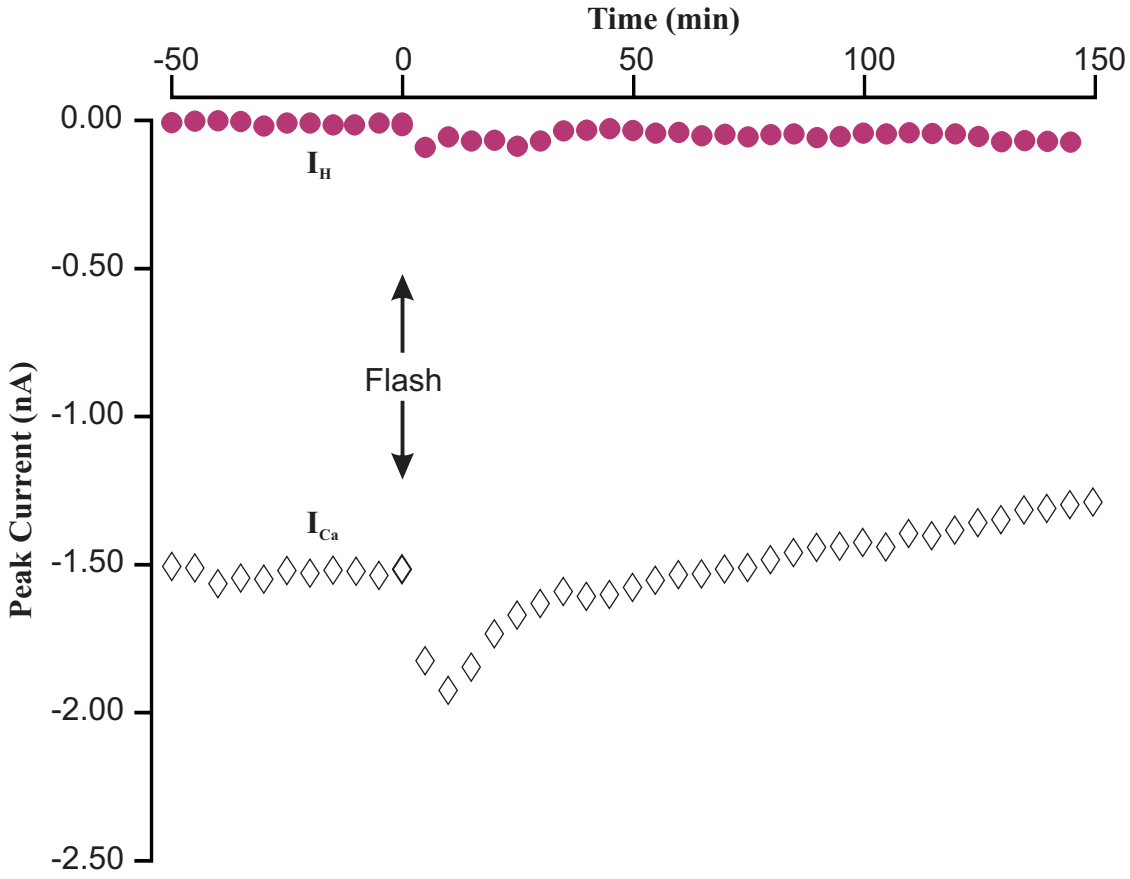

Figure 5.25

A plot of changes in holding current at -80 mV ($I_{H,}$ ●) against time in a single ventricular cardiac myocyte illustrating the effects of photoreleased cAMP in the presence of 1 mM R_p-cAMPS. The peak calcium currents from figure 5.12 recorded at +10 mV (I_{Ca}, ◇) from the same cell are also shown for comparison.

R_p-cAMPS almost complete abolishes the I_H response the flash photolysis of 1 mM caged cAMP test pulse 20 ms after the uv light flash. Only a tiny increase compared with the cell in figure 5.22 could be seen after 5 seconds. The current relaxed back to control levels completely after around 30 seconds. The drastic effects of R_p-cAMPS on I_H are in clear contrast to the incomplete block of the rise in calcium current which is reduced but still significant.

took for the I_H to decline back within 50% of control was significantly faster (33.5 ±7.2 s; n=13) than the corresponding value for I_{Ca} (101.5 ±18.1 s; n=16).

5.2.5.2 Effects of IBMX on $I_{Cl,cAMP}$ and I_{Ca}

Figure 5.24 shows the effects of the photorelease of cAMP before and after applying 100 µM IBMX. In control cells dialysed with 1 mM caged cAMP in the absence of IBMX, two consecutive UV flashes produced similar changes in holding current provided they were at least 5 minutes apart: the second responses had an average magnitude within 91.3 ±4.5% (n=4) of the first. This was not true in the presence of IBMX. The application of 100 µM IBMX produced a gradual inward shift in holding current which paralleled increases in I_{Ca}. Subsequent photorelease of cAMP evoked a much reduced I_H (-0.23 ±0.08 nA; n=3). By comparison, as described above, IBMX completely abolished the I_{Ca} response.

5.2.5.3 Effects of R_p-cAMPS on $I_{Cl,cAMP}$ and I_{Ca}

The opposite results were seen when 1 mM caged cAMP was photolysed with 0.1 mM R_p-cAMPS in the dialysing solution. In the cell in figure 5.25, R_p-cAMPS almost complete abolished the shifts in I_H but merely reduced the I_{Ca} response. The average response was -0.05 ±0.06 nA (n=4). This concentration of cAMP antagonist thus had a greater inhibitory effect on the $I_{Cl,cAMP}$ activated by photoreleased cAMP than its potentiation of I_{Ca}.

5.2.5.4 Effects of Photoreleased cAMP on $I_{Cl,cAMP}$ in the presence of GTPγS

As described above, the inclusion of 100 µM GTPγS did not have a significant inhibitory effect on I_{Ca} but did accelerate the changes seen. Both the increase and

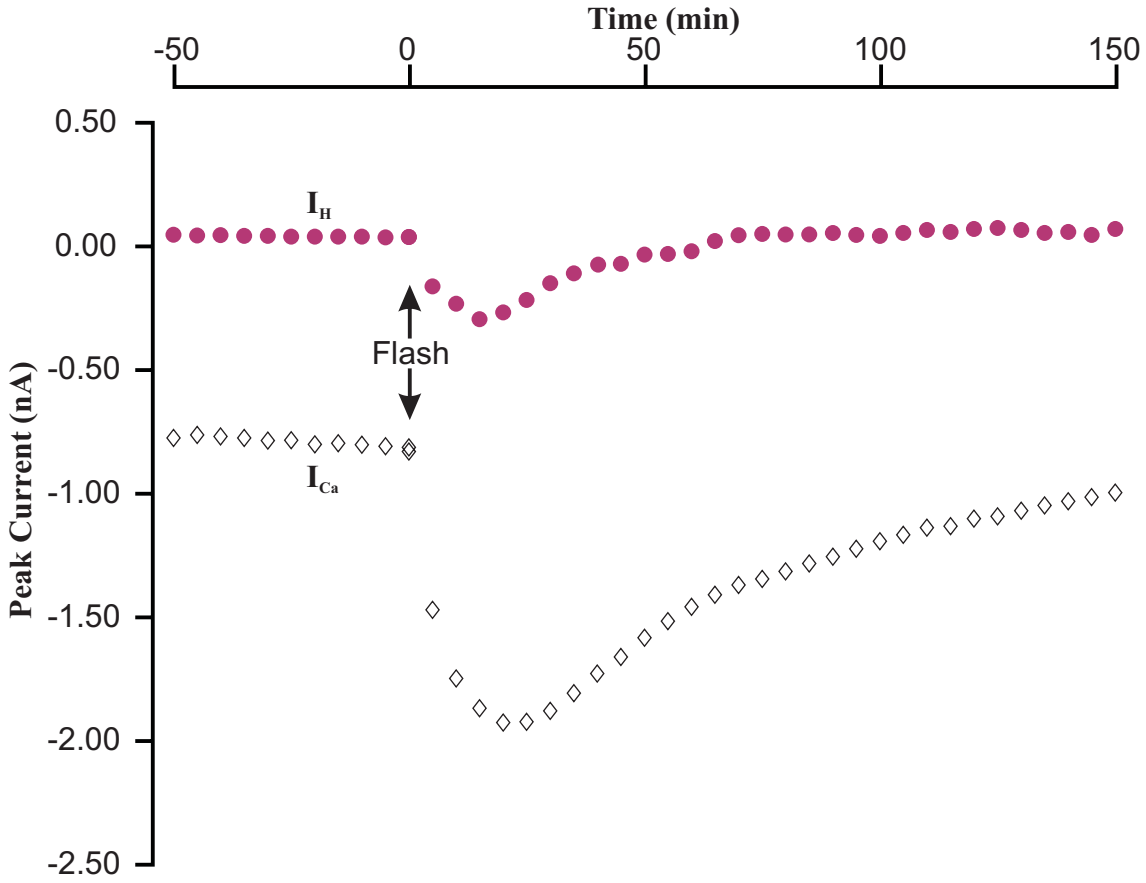

Figure 5.26

A plot of changes in holding current at -80 mV ($I_{H,}$ ●) against time in a single ventricular cardiac myocyte illustrating the effects of photoreleased cAMP in the presence of intracellular GTPγS. Peak calcium currents (I_{Ca}, ◇) from figure 5.14 recorded at +10 mV from the same cell are also shown for comparison.

GTPγS does not markedly reduce the changes in holding current.

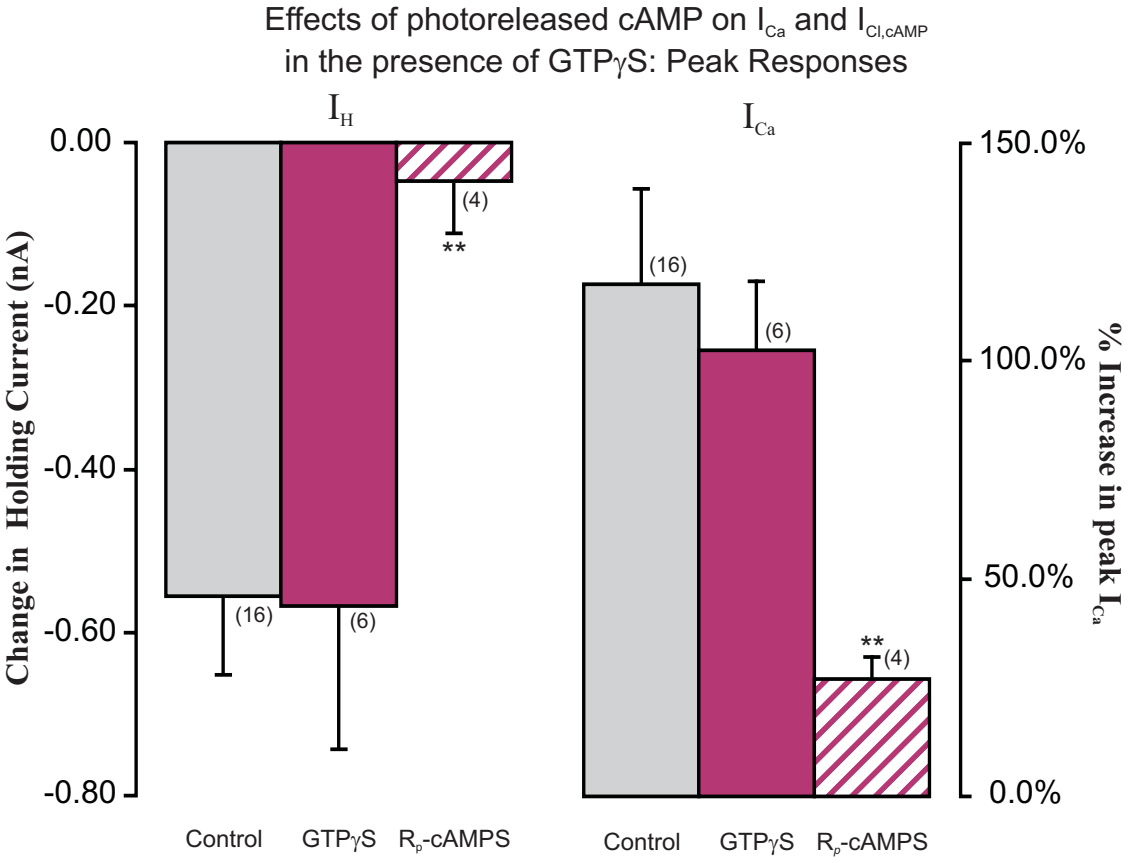

Figure 5.27

This graph shows the effects of intracellular GTPγS on the magnitude of I_H and I_{Ca} responses to photoreleased cAMP. The inclusion of 100 μM GTPγS did not produce a significant change in the magnitude of responses to the photolysis of 1mM caged cAMP, in either the increase in holding current measured at -80 mV or the enhancement of calcium current recorded during test pulses to +10 mV. For comparison, also is displayed the large inhibitory effects of 1 mM R_p-cAMPS on both I_H and $I_{Ca.}$

Vertical error bars show standard errors of the mean with the number of experiments indicated to the right. Significant differences from the control responses are indicated by asterisks (**, $p < 0.01$).

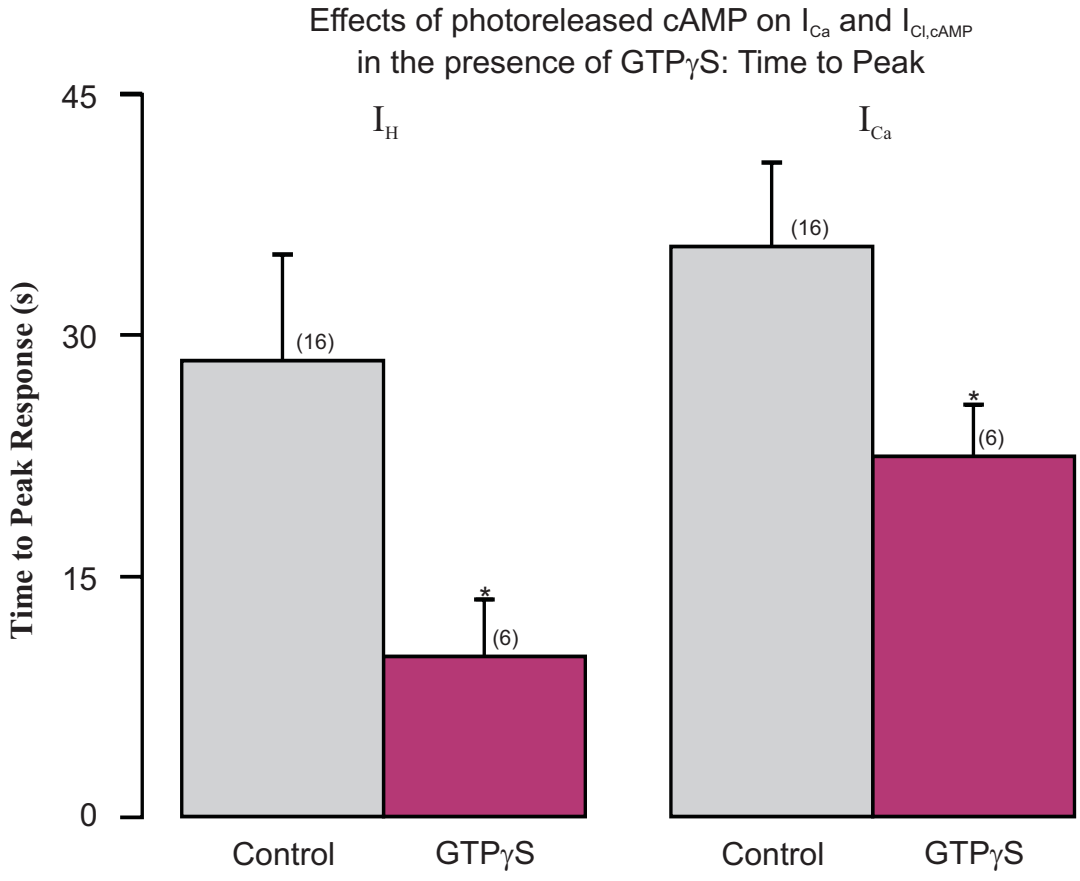

Figure 5.27b

This graph shows the effects of intracellular GTPγS on the time course of I_H and I_{Ca} responses to photoreleased cAMP. The inclusion of 100 μM GTPγS produced a significant reduction in the time-to-peak of increases in holding current at -80 mV after the photolysis of 1 mM caged cAMP. Responses in I_{Ca} also reached their peak significantly faster with GTPγS present but the changes were not as marked.

Vertical error bars show standard errors of the mean with the number of experiments indicated to the right. Significant differences from control are indicated with asterisks: (*; $p < 0.05$).

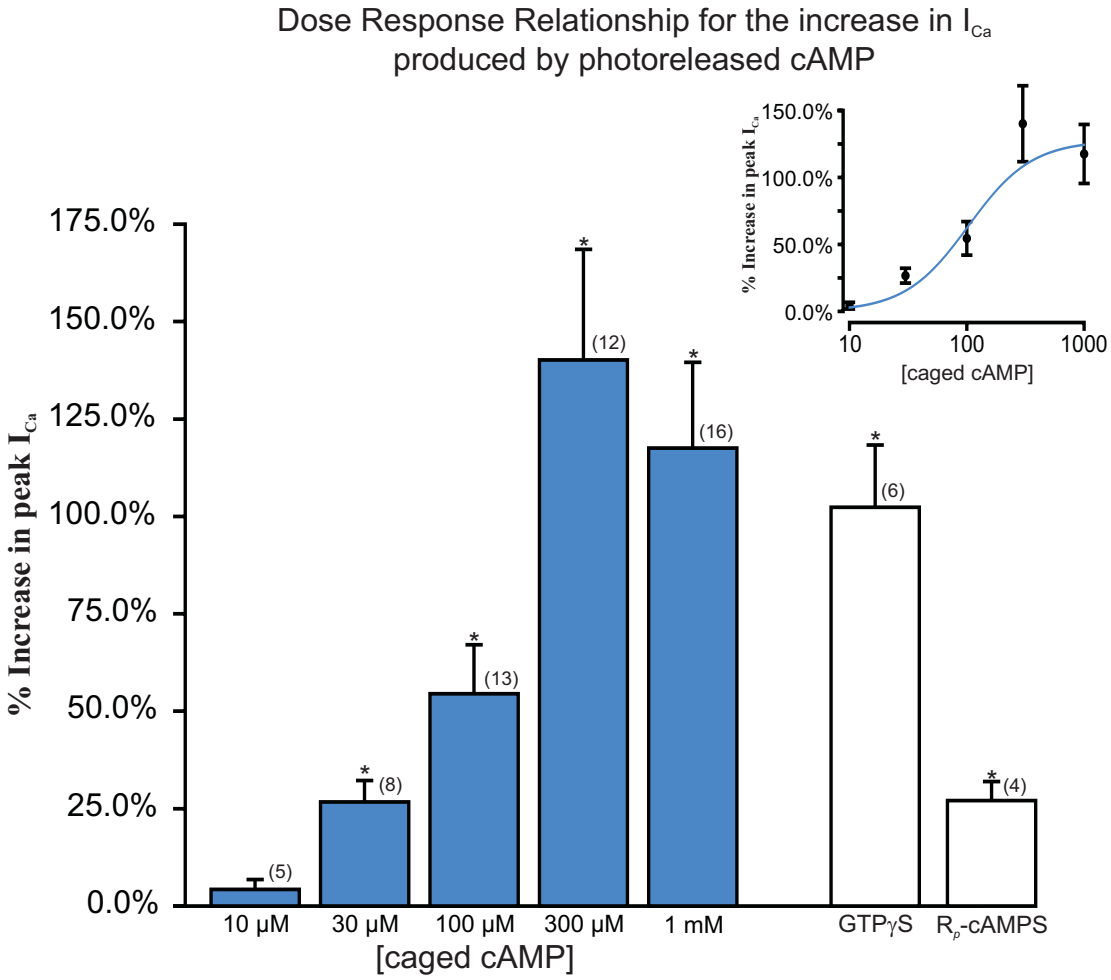

Figure 5.28

Bar graph showing enhancement of I_{Ca} by the photolysis of different concentrations of caged cAMP. 300 µM caged cAMP is sufficient to produce a maximal response. For comparison, results of the photolysis of 1 mM caged cAMP in the presence of GTPγS or R_p-cAMPS are included.

Vertical error bars show standard errors of the mean with the number of experiments indicated to the right. Significant increases relative control are indicated with asterisks (*, $p < 0.05$).

The inset plot is a fit to the Hill equation, giving a half-maximal concentration for caged cAMP of 103.2 µM and a slope factor of 1.61.

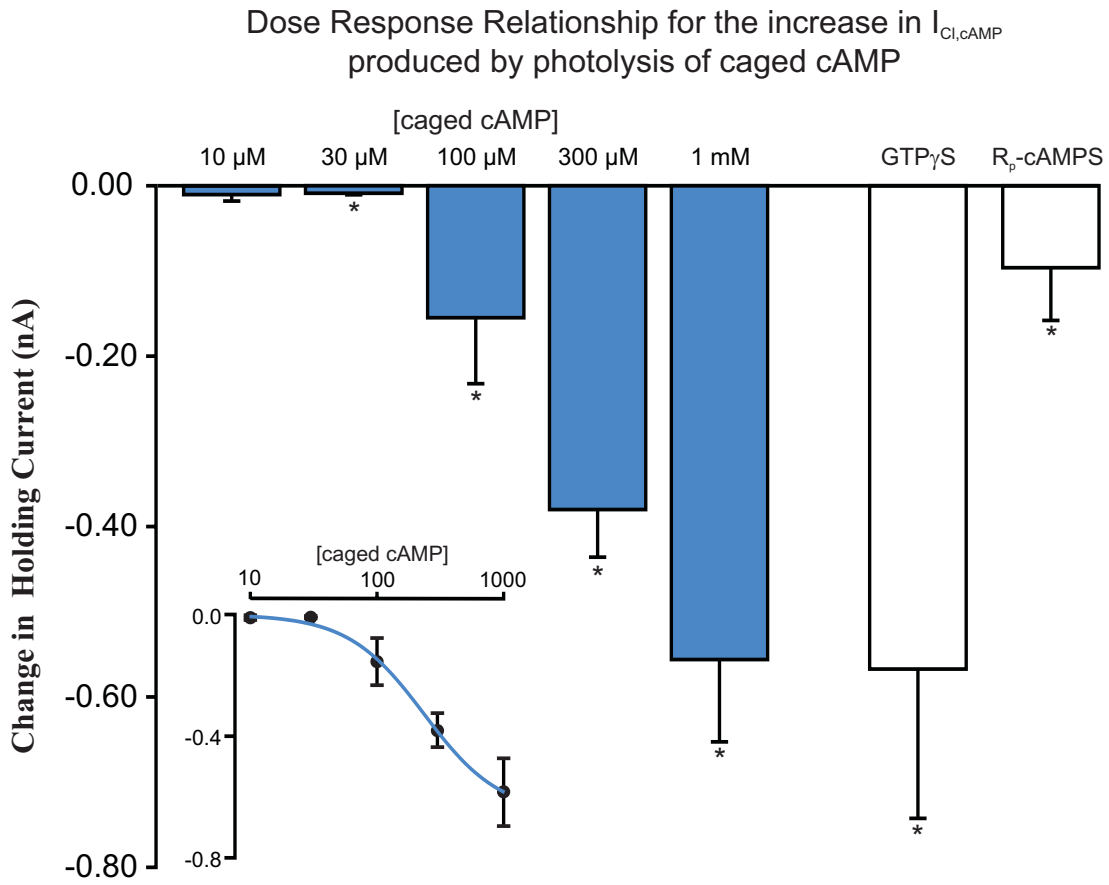

Figure 5.29

Bar graph showing the increase in holding current at -80 mV by the photolysis of different concentrations of caged cAMP. In contrast to the results with I_{Ca} (in figure 5.28), a marked increase is only seen after the photolysis of 100 µM caged cAMP and the maximal response is seen at 1 mM, the highest dose used. For comparison, results of the photolysis of 1 mM caged cAMP in the presence of GTPγS or R_p-cAMPS are included. Vertical error bars show standard errors of the mean with the number of experiments indicated to the right. Significant increases are indicated with asterisks (*, $p < 0.05$).
The inset plot is a fit to the Hill equation, giving a half-maximal concentration for caged cAMP of 235.6 µM and a slope factor of 1.45.

subsequent decline were accelerated. These observations could be repeated for $I_{Cl,cAMP}$ (figure 5.26). In the presence of GTPγS, a change in I_H of -0.57 ±0.18 nA (n=6) was seen, which is almost exactly the same as when GTPγS was absent (-0.58 ±0.12 nA; n=13). However, the mean time-to-peak-response in the same six cells was reduced significantly to 10.0 ±3.5 s (from 22.5 ±3.2 s; n=13). Figure 5.27 summarises the effects of ambient GTPγS on both I_{Ca} and $I_{Cl,cAMP}$.

5.2.5.5 Dose-response relationship of Photoreleased cAMP on $I_{Cl,cAMP}$ and I_{Ca}

The different effects of IBMX and R_p-cAMPS on the $I_{Cl,cAMP}$ and I_{Ca} responses to photoreleased cAMP suggest that the two currents may be differentially coupled to the cAMP-dependent pathway. This possibility was investigated by examining their separate dose-response relationships.

Figure 5.28 shows the potentiation of I_{Ca} resulting from the photolysis of different concentrations of caged cAMP (10-1000 μM). 300 μM was sufficient to maximally stimulate calcium current. The results were well fitted to the Hill equation, giving a slope factor of 1.61 and a half-maximal concentration for caged cAMP of 103.2 μM. From the calibration curve obtained in chapter two (see section 3.3.2), this latter value would correspond to around 0.47 μM of released cAMP.

The effects on $I_{Cl,cAMP}$ of the photolysis of the same range of caged cAMP (10-1000 μM) are shown in figure 5. 29. The dose required for the maximum response was at least as large as the highest concentration of the photolabile precursor used. The best Hill equation fit gave a slope factor of 1.45 and a half-maximal concentration of 235.6 μM caged cAMP, which would correspond to ~1.10 μM released cAMP. The

calcium current is thus more than twice as sensitive to cAMP-dependent stimulation as $I_{Cl,cAMP}$.

5.3 Discussion

5.3.1 *GTPγS inhibition of isoprenaline and forskolin responses*

Chronic application of GTPγS not only reduces the response to photoreleased GTP as was shown previously but also attenuates the response to isoprenaline. This inhibition had an IC_{50} of ~10 μM. This is unlikely to be the result of the already maximal stimulation of I_{Ca}, as has been suggested for the GTPγS inhibition of purinergic P_2 stimulation of I_{Ca} (Scamps *et al.*, 1992). The current begins to run up immediately after the initiation of dialysis following the establishment of the whole cell patch clamp configuration before beginning to exhibit the gradual run-down seen generally in the control cells. The net increase in I_{Ca} is, however, only significant with 100 μM GTPγS. Even then, the size of I_{Ca} observed under such conditions is much smaller than that in the presence of isoprenaline or forskolin or cAMP.

The alternative possibility that an inhibitory G-protein is involved was confirmed with the use of Pertussis toxin, which is known to inactivate the G_i-type G protein. After the cells were incubated with PTX, no run-down was seen immediately after dialysis with 100 μM GTPγS, but only a run-up in current. The obvious explanation is that the inclusion of GTPγS, the non-hydrolysable GTP analogue, produces a sustained stimulation of both stimulatory and inhibitory G-proteins. The initial run-up seen was due to the expected potentiation of I_{Ca} via stimulation of G_s-protein, while the

subsequent run-down would be due to the activity of a G_i-type G-protein whose effects are abolished by pertussis toxin.

The experiments with isoprenaline and GTPγS provide a clear demonstration that a PTX-sensitive G_i-protein mediates the inhibitory effects of GTPγS. The inhibition of chronically applied 100 μM GTPγS, which almost abolishes the response to 1 μM isoprenaline, is completely reversed by pre-incubation with pertussis toxin. The inability of the same concentration of GTPγS to diminish the effects of photoreleased cAMP in more than doubling I_{Ca} also indicates that current was not already maximally stimulated.

This PTX-sensitive inhibition by GTPγS in the absence of any agonist has also been reported for $I_{Cl,cAMP}$ in guinea-pig ventricular myocytes (Hwang *et al.*, 1992). Parsons and Hartzell (1993) using bullfrog myocytes failed to see an inhibition with GTPγS but curiously do so with GppNHp, another non-hydrolysable GTP analogue. Their results are in contrast to the findings of Nakajima *et al.* (1990) in the same tissue where 500 μM GTPγS is sufficient to completely inhibit I_{Ca} stimulated by isoprenaline but are in line with Fischmeiseter and Shrier, 1989 who fail to see any effects of GTPγS on basal I_{Ca}.

5.3.2 Locus of GTPγS inhibition

The question then would be exactly how and where the inhibition occurs. Photoreleased cAMP produces an expected rapid rise in I_{Ca} which would arise from the phosphorylation of L-type Ca^{2+} channels by Protein Kinase A. The effects of the photolysis of caged cAMP are not reduced at all, however, by the inclusion of GTPγS. This indicates that the G_i protein is acting at the level of adenylyl cyclase or upstream in the pathway. The responses to forskolin which directly stimulate adenylyl cyclase to

produce cAMP are attenuated markedly by 100 μM GTPγS. So it seems that the inhibition must occur at the level of this enzyme. The hypothesis that this involves a direct coupling between activation of the G_i-protein and adenylyl cyclase would be in agreement with the findings of Hescheler *et al.* (1986) who suggest that muscarinic inhibition of I_{Ca} (and therefore activation of G_i) only occurs following initial activation of adenylyl cyclase through β-adrenoreceptor stimulation (i.e. activation of G_s) or application of forskolin.

One reason why 100 μM GTPγS almost completely abolishes the response to isoprenaline but only attenuates the response to the application of forskolin could be that activation of G_i has at least two inhibitory effects on sympathetic responses. $G_{i\alpha}$ directly inhibits adenylyl cyclase, and the simultaneously released $G_{\beta\gamma}$ subunits would increase the rates of re-association and hence deactivation of $G_{s\alpha}$. Both of these would have an effect on responses to isoprenaline but only the former would produce an additional inhibition of forskolin responses. There is less evidence that $G_{\beta\gamma}$ also has a direct inhibitory effect on the isoforms of adenylyl found in ventricular myocytes (Taussig *et al.*, 1994).

At the same time, this interpretation must be regarded with a little caution. There has been a report that treatment with forskolin and isoprenaline that result in equal increases in cAMP produce a greater activation of PKA and protein phosphorylation in isoprenaline-perfused hearts (England *et al.*, 1987). The experiments described here do not conclusively rule out the possibility that 10 μM forskolin is more effective in stimulating adenylyl cyclase in the face of 100 μM GTPγS than the adrenoreceptors activated by 1 μM isoprenaline, even though the response to this

concentration of isoprenaline in the absence of GTPγS is greater than that for 10 μM forskolin.

The obvious question is why G_i is preferentially activated (rather than G_s) by chronic application of intracellular GTPγS to produce an ultimately inhibitory effect. It might be that the greater density of G_i compared with G_s means that any partial activation of the former would predominate. The inhibitory effect of GTPγS on $I_{Cl,cAMP}$ has been attributed to a higher basal turnover of G_i (Hwang *et al.*, 1992). It is also probable that receptors coupled to the different G-protein systems have differential constitutive activities. A factor often neglected is the contribution of G-protein homeostasis and recycling rates in the face of persistent activation by non-hydrolysable analogues. Clearly, these are complicated systems.

5.3.3 *GTPγS attenuation of responses to further photoreleased GTPγS*

The inhibitory effect of uncaged GTPγS on the response to photoreleased GTPγS seems to be due to different mechanisms, as this effect is not PTX sensitive. The inhibition is most likely to be due to simple competition for active binding sites between the chronically applied GTPγS and that released from photolysis of the caged precursor compound. As the steady-state GTPγS concentration rises inside the cell with its increased concentration in the dialysing solution, there is a fall in the number of available active binding sites available for further photoreleased GTPγS (to cause an increase in I_{Ca}). This competition between ambient and photoreleased GTPγS is expected to be all the more intense in the absence of any agonist and hence activated receptors, since the availability of G-protein binding sites for GTP and GTPγS would not be expected to be

especially high anyway. The additional competitive inhibitory effect of GTPγS on photoreleased GTPγS occurs at a lower concentration of GTPγS, which is likely to have masked the additional PTX-sensitive inhibition.

This hypothesis would require that the G-proteins have a very high affinity for guanosine nucleotides with maximal activation occurring even at micro-molar concentrations. Confirmation is provided by the low concentration of uncaged GTPγS needed to bind to G_i to prevent the isoprenaline response, and the large increases in I_{Ca} produced by the photorelease of the equivalent of just 23 ±19 μM GTPγS. This suggestion would also be consistent with the observations of Scamps *et al.* (1992) who show that GTPγS markedly increases I_{Ca} at concentrations of 3 μM, while Nakajima *et al.* (1992) have shown that the EC_{50} for activation of acetylcholine activated K^+ channels in atrial myocytes is ~0.1 μM.

5.3.4 Responses to photoreleased GTPγS

5.3.4.1 Biphasic response reveals two components

The photorelease of GTPγS produced a biphasic increase in the majority of cells but only a monophasic increase in a few other cells. It has been suggested previously (Kozlowski *et al.*, 1991) that the first part of the biphasic response (and the entirety of the monophasic) is due to the membrane-delimited (non-cAMP mediated) pathway, and that the second phase of the increase is the result of cAMP-dependent phosphorylation. It still seems most likely that the rapid component of the rise in I_{Ca} following the photorelease of guanosine nucleotides is due to a fast membrane-delimited pathway not blocked by R_p-cAMPS.

5.3.4.2 Differences from results in the bullfrog

This rapid component is not seen in bullfrog myocytes where no rapid cAMP-independent pathway has been found and stimulation of I_{Ca} by isoprenaline is thought to be mediated exclusively by protein kinase A (Hartzell *et al.*, 1991). This observation has been used to argue against the physiological importance of a rapid membrane-delimited pathway. However, it is difficult to see how one can easily infer operation parameters of physiological pathways in mammalian tissue at 36 or 37°C from experiments on bullfrogs at room temperature. The different results could be due not only to the immutable difference between the signalling pathways of frog and guinea pigs, the temperature sensitivities of key components in the pathway (Frace *et al.*, 1993), and the degree to which physiological signalling pathways have been affected by the recording techniques depending on cell size and geometry and varying degrees of diffusional equilibration to the local environment around G-proteins. For example, the rate of frog G_s nucleotide exchange in the absence of receptor stimulation is known to be much lower (Parsons *et al.*, 1991).

Thus, Yatani and Brown (1989) report that isoprenaline even at 22-24°C potentiates L-type Ca^{2+} current in atrial myocytes after a delay of ~30 ms with a time constant of the order of 150 ms. In canine sino-atrial node, a negative inotropic effect occurs within ~210 ms while the response to symapathetic nervous stimulation requires ~950 ms (Spear *et al.*, 1979). In contrast, bullfrog heart parasympathetic nervous stimulation can induce a negative inotropic effect within 1 s while the positive inotropic effect in response to sympathetic nervous stimulation can take in excess of 5 s to develop (Hartzell *et al.*, 1991). The much slower kinetics in the different steps of the frog

response to catecholamines (Frace *et al.*, 1993) obviate the necessity for a direct modulatory pathway.

5.3.4.3 A comparison with responses to photoreleased GTP

However, there is no simple explanation for the different profiles of the responses to photoreleased GTP (in the previous chapter) and the generally (in ~80% of the cases) biphasic increases in I_{Ca} seen after the photorelease of GTPγS. One might speculate that the higher amounts of photoreleased GTP (~90 μM GTP as opposed to ~15 μM GTPγS; see section 3.3.1) and continuous cellular GTPase activity may combine to produce an initial phase of response which merges smoothly into the sustained component. Alternatively, it may be that GTPγS not only magnifies the effects of constitutive receptor activity (as suggested in section 4.3.2) but, being non-hydrolysable, also slowly recruits more and more activated G-proteins to produce an additional cumulative response not seen with GTP. A third possibility would be that the biphasic response to photoreleased GTPγS is a complex interaction of G_s and G_i proteins. This seems to be ruled out by the persistence of biphasic responses in the face of PTX incubation.

5.3.5 Effects of photoreleased cAMP

5.3.5.1 Activation of $I_{Cl,cAMP}$

Consistent with other reports (Nakashima & Ono, 1994), the photolysis of caged cAMP activates $I_{Cl,cAMP}$. Unlike L-type Ca^{2+} channels, $I_{Cl,cAMP}$ does not appear to be basally active in the absence of agonists, and the holding current at -80 mV was near zero after pharmacological blockage of potassium channels. Whether $I_{Cl,cAMP}$ is active in the absence of agonist stimulation depends on the levels of basal phosphorylation and hence

the balance between adenylyl cyclase and PKA activity on one hand and endogenous phosphodiesterases and protein phosphatases on the other. The absence of basal activity in these cells can be attributed to the predominance of the phosphatase and phosphodiesterase activity given that IBMX alone was capable of producing a large activation of $I_{Cl,cAMP}$. The rapid decay of $I_{Cl,cAMP}$ as well as I_{Ca} after photoreleased cAMP confirms this hypothesis.

5.3.5.2 Effects of R_p-cAMPS and IBMX on I_{Ca} and $I_{Cl,cAMP}$

The differential effects of R_p-cAMPS and IBMX on the responses in I_{Ca} and $I_{Cl,cAMP}$ to photoreleased cAMP in the same cells was initially somewhat surprising given that both currents are coupled to the same cAMP-dependent pathway. The explanation was suggested by the different dose-response curves obtained for the photolysis of caged cAMP. The half-maximal concentration of photoreleased cAMP for potentiation of $I_{Cl,cAMP}$ was, at ~1.10 μM, more than twice as high as that for the activation of I_{Ca} (~0.47 μM). Thus, the competitive cAMP antagonist R_p-cAMPS would have a disproportionately larger effect on the less sensitive $I_{Cl,cAMP}$, while the level of cAMP produced by IBMX sufficient to saturate the I_{Ca} response might not be enough to maximally activate $I_{Cl,cAMP}$. The concentrations of IBMX used were most probably too low for a direct stimulatory effect on $I_{Cl,cAMP}$ (He *et al.*, 1998; Al-Nakkash & Hwang, 1999). The higher cAMP sensitivity of I_{Ca} modulation could also be responsible for its faster responses to isoprenaline stimulation and washout (Hirayama & Hartzell, 1997).

This difference in the coupling of the two current systems to the same cAMP-dependent pathway can be attributed not only to the different PKA sensitivity of the different consensus phosphorylation sites on $I_{Cl,cAMP}$ (Gadsby & Nairn, 1999) and I_{Ca}

(Hartzell *et al.*, 1995) but also their sensitivities to dephosphorylation by different phosphatases (Hirayama & Hartzell, 1997). Differential modulation by a forskolin analogue (NKH-477) of Ca^{2+} and K^+ in guinea-pig ventricular myocytes has also been reported (Harada & Iijima, 1994).

The different cAMP sensitivities of I_{Ca} and $I_{Cl,cAMP}$ may be a further reason why Horie *et al.* (1992) found 1 μM GDP*β*S sufficient to prevent completely isoprenaline-mediated activation of Cl^- current while only 10 μM was sufficient for a reliable block of I_{Ca} in the results presented in section 4.2.5.1. This highlights the potential pitfalls in the common practice of using the effectiveness of pharmacological inhibition in one system (e.g. $I_{Cl,cAMP}$) to infer its effectiveness in another parallel but possibly differentially coupled system (e.g. I_{Ca}).

5.3.5.3 I_{Ca} sensitivity to photoreleased cAMP

In the case of the cAMP-dependence of I_{Ca} modulation, the half-maximal concentration (~0.47 μM) is at the low end of *in vitro* measurements during *β*-adrenergic stimulation of cardiac cells (0.5-2 μM; Dobson *et al.*, 1976, Terasaki & Brooker, 1977). The differences could point to the difficulty of making inferences about intracellular environments with sub-cellular compartmentalization and local ion gradients (Neubig, 1994) from data on bulk concentrations. This highlights the advantages of the flash photolysis technique.

Nakashima & Ono (1994) report a lower EC_{50} for the effects of photolysis of caged cAMP on $I_{Cl,cAMP}$ of 25 μM. However, the actual amounts of photoreleased cAMP depend on the efficiency of photolysis which may vary from one experimental system to

another. In the absence of any quantitative data on photolytic efficiency, their results are not commensurate with those presented in this thesis.

5.3.5.4 Physiological importance of differential $I_{Cl,cAMP}$ and $I_{Cl,cAMP}$ modulation

The separate modulation of I_{Ca} and $I_{Cl,cAMP}$ by catecholamines could be an important component of physiological regulation of action potential cardiac rhythm as a result of sympathetic nervous stimulation. Thus, at high levels of β-adrenergic activity where Ca^{2+} entry into cardiac cells is augmented, changes in the action potential duration would be minimized by the activation of a cardio-protective chloride current. The contribution of catecholamine activation of $I_{Cl,cAMP}$ during the action potential plateau should produce a significant shortening of the action potential duration (Harvey *et al.*, 1990).

These results are not sufficient to suggest that the different dose-peak response relationships for $I_{Cl,cAMP}$ and I_{Ca} are the only determinants for the different kinetics for the catecholamine regulation of these two currents (Hirayama & Hartzell, 1997, Nakashima & Ono, 1994). The physiological importance of the different time dependencies is also still unclear.

5.3.6 GTPγS sensitises cAMP-dependent activation

Though GTPγS does not inhibit the response to photoreleased cAMP, it provides a surprising acceleratory effect on its time course. The response to forskolin is also speeded up by the inclusion of chronic GTPγS. In the case of cAMP, the inclusion of GTPγS allows a response within the first 20 ms of the UV light flash to be detected. Photoreleased cAMP, like photoreleased GTP and GTPγS, can modulate I_{Ca} very rapidly.

5.3.6.1 Candidate mediators of the GTPγS sensitisation

It is possible that the ability for GTPγS to accelerate the response to stimulation of the cAMP-dependent pathway is mediated by activation of a G_s-type G-protein coupled directly to the L-type Ca^{2+} channel or associated modulatory proteins which sensitises it to phosphorylation by Protein Kinase A. Work on cell free membrane preparations (Imoto *et al.*, 1988) has provided strong evidence for such a direct link. These effects would be consistent with Cavalie *et al.* (1991) who suggest that stimulation of G_s primes L-type Ca^{2+} channels for phosphorylation following *β*-receptor stimulation, though in their case they see an increased rather than an accelerated response.

In the heart, a variety of evidence has accumulated for the presence of a second stimulation pathway mediating *β*-adrenergic responses in addition to the well-characterised cAMP-dependent channel phosphorylation. Strong evidence comes not only from the application of GTPγS using dual patch pipettes (Shuba *et al.*, 1990) but also results using the technique of flash photolysis presented in chapters 4 and 5 here. (A full review is included in section 1.4.6.) Hartzell *et al.* (1991) do not see such an additional and perhaps faster pathway. They do not question the supporting evidence for the interaction between G-protein and the L-type Ca^{2+} channel in excised patches and lipid bilayers but only their physiological relevance in intact cells (Hartzell *et al.*, 1992).

Yatani and Brown (1989) postulate that the non-cAMP-dependent pathway is responsible for beat-to-beat regulation of the heart rate. By constrast, the results presented in this chapter suggest that a direct interaction between the L-type Ca^{2+} channel and the G-protein may serve to modulate the kinetics of the changes produced by cAMP-dependent phosphorylation, rather than being an alternative modulatory

pathway with a separate physiological role operating under different conditions, e.g. lower agonist concentrations.

5.3.6.2 GTPγS modulates basal channel regulation?

Given that so many different signalling systems converge at the G-protein level, it is entirely possible that the effects of GTPγS proceed from alterations in basal regulation of any part of the modulatory pathways, especially for $I_{Cl,cAMP}$. These would include changes in protein phosphatases or phosphodiesterase activity, protein kinase G or the interactions between receptor, adenylyl cyclase or G-proteins, all three of which have multiple consensus phosphorylation sites. Parsons and Hartzell suggest that the slow onset of responses to photoreleased cAMP cannot be due simply to the slow accumulation of cAMP above an activation threshold. Nakashima and Ono (1994), however, found that the slow sigmoidal activation of $I_{Cl,cAMP}$ converted to a fast exponential rise after partial phosphorylation of the channels by exposure to okadaic acid. Inclusion of GTPγS may have a similar effect in raising basal sub-threshold CFTR phosphorylation.

5.3.6.3 Summary of GTPγS results

In conclusion, it seems that GTPγS has at least three different effects on L-type Ca^{2+} channels in cardiac myocytes. Photoreleased GTPγS stimulates G_s-proteins to produce large increases in I_{Ca}. Inclusion of GTPγS in the intracellular solution inhibits the response to sympathetic stimulation via a pertussis toxin sensitive G_i-protein acting on and perhaps also upstream of adenylyl cyclase. Chronic application of GTPγS also accelerates the response to cAMP-dependent phosphorylation, possibly by interacting

with a G-protein coupled directly to the L-type Ca^{2+} channel. In addition, the chronically applied GTPγS also competes with subsequently photoreleased GTPγS to inhibit a further response.

Chapter Six

Urotensin II, a new agonist for an orphaned G-protein coupled Receptor

6.1 Introduction:

Since the first cloning of genes for G-protein coupled receptors (GPCRs), most of the ligands known to signal cells via G-protein coupled mechanisms have been assigned one or more genetic sequences for their corresponding receptors. However, the growing complementary DNA and genomic libraries available, including those for expressed sequence tagged cDNAs (ESTs), and the success in identifying novel GPCRs via sequence identity have far outpaced the identification of endogenous physiological agonists. There is, thus, a growing class of proteins which evidently belong to the GPCR family but for which no known ligand can be assigned. The number of "orphaned" receptors can only be expected to continue to increase with advances in bio-informatics and the rapid growth in number, size and quantity of sequence databases, especially from the Human Genome Project.

Many of these orphaned GPCR cluster together in groups whose members share a high degree of identity (>45%) and which may thus have common ligands. Nevertheless, because the agonist-binding pocket for GPCRs has not yet been fully

described, it is not yet feasible to predict with confidence even physico-chemical properties of the cognate ligands, let alone guess at their physiological function.

"Reverse molecular pharmacology" (Stadel *et al.*, 1997) or "orphan receptor strategy" (Civelli *et al.*, 1998) has been one way to exploit this growing wealth of potential drug targets (Sakurai *et al.*, 1998, Hinuma *et al.*, 1998). This can be contrasted with the traditional approach in identifying GPCRs which proceeds from known functional activity as an assay to identify and purify the ligands from biological fluids or tissue extracts. The discovered agonists then provide a handle for the subsequent purification and expression cloning of the receptor cDNA and thence the gene.

If the starting point is the genetic sequence for the receptor, a different strategy has to be employed. Using ESTs from cDNA libraries, for example, the corresponding cDNA and gene for a known orphaned receptor can be identified in the target species. The first necessary step in understanding the physiological significance of a recombinant expressed receptor is the identification of the novel ligand using tissue extracts or libraries of known biologically active molecules in functional assays. Only at this point would both physiological and patho-physiological studies, as well searches for pharmacological agonist and antagonists, be able to proceed. The identification of the potent vasoconstrictor Urotensin II (U-II) as the agonist for the previously orphaned GPR14 (Ames *et al.*, 1999, Liu *et al.*, 1999, Mori *et al.*, 1999, Nothacker *et al.*, 1999) has been one of the striking success stories in "reverse pharmacology".

GPR14 is a GPCR with significant somatostatin and μ-opioid receptor identity. The "opioid and somatostatin receptor-like" group of orphan receptors also includes at least human GPR7, GPR8, GPR24 and rat GPR54 (Marchese *et al.*, 1999). Using the rat

GPR14 as a probe into a human genome library, Ames *et al*. (1999) isolated a 9-kb genomic clone encoding a 389-residue human analogue with 75% identity. When either rat or human GPR14 was transfected into HEK-293 cells, only goby Urotensin II out of 700 known and putative GPCR agonists tested positive in a calcium mobilisation assay. gU-II had no effect on the homologous GPR7 and GPR8.

Urotensin II was originally detected in teleost fish, where it was isolated from the urophysis as a cyclic, 12-amino-acid, vasoactive "somatostatin-like" peptide (Berlind, 1972; McMaster & Lederis, 1983). It is also found in frog (Conlon *et al*., 1997), rat, mouse (Coulouarn *et al*., 1999) and pig (Mori *et al*., 1999). Human urotensin II has only 11 residues but the key cyclic region of the peptide responsible for biological activity is conserved from fish to human (Coulouarn *et al*., 1998; see table 6.1). The final human undecapeptide peptide is posttranslationally cleaved from prepro-urotensin. The mRNA for this precursor has been localized in human brain stem and spinal cord motor neurones, and the kidney (Coulouarn *et al*., 1998). The latter organ may be the source of circulating urotensin II (Nothacker *et al*., 1999).

GPR14 binding sites have been found using radioligand studies in human skeletal muscle and cerebral cortex, coronary arteries, left ventricle with little binding in atria or the conducting system of the heart (Maguire *et al*., 2000). Quantitative polymerase chain reaction with reverse transcription (RT-PCR) also reveals expression of the receptor in human aorta, coronary artery endothelial and smooth muscle cells (Ames *et al*., 1999).

Human U-II produces sustained vasoconstriction in a variety of mammalian vascular tissues with sub-nanomolar potency, approximately an order of magnitude greater than that seen with endothelin-1 (ET-1). This is thus the most potent known mammalian vasoconstrictor. Significant *in vitro* species and anatomical variations have been found in vascular contractile studies (Douglas *et al.*, 2000), but *in vivo*, the peptide produces a complex dose-dependent haemodynamic response in (non-human) primates (Ames *et al.*, 1999). Systematic administration at low doses (>=30 pmol/kg) decreased myocardial contractility and increased vascular resistance, while higher concentrations resulted in catastrophic myocardial depression and fatal circulatory collapse. All of this suggests that U-II may play an important part in the physiological regulation and patho-physiology failure of mammalian haemodynamic homeostasis and cardiovascular function.

Although there is a growing body of work characterizing the effects of urotensin II on the vasculature, there has not been any published research so far on possible effects on the myocardium. The mRNA for GPR14 is expressed in cardiovascular tissue (Ames *et al.*, 1999) and urotensin II binding sites can be found in the human left ventricle (Maguire *et al.*, 2000). Together with the diffuse immuno-staining of U-II in human cardiac myocytes (Ames *et al.*, 1999), this suggests that a part of the dramatic *in vivo* effects of urotensin II could be mediated though modulation of cardiac myocytes. This possibility prompted an investigation which led to the novel results presented in this chapter.

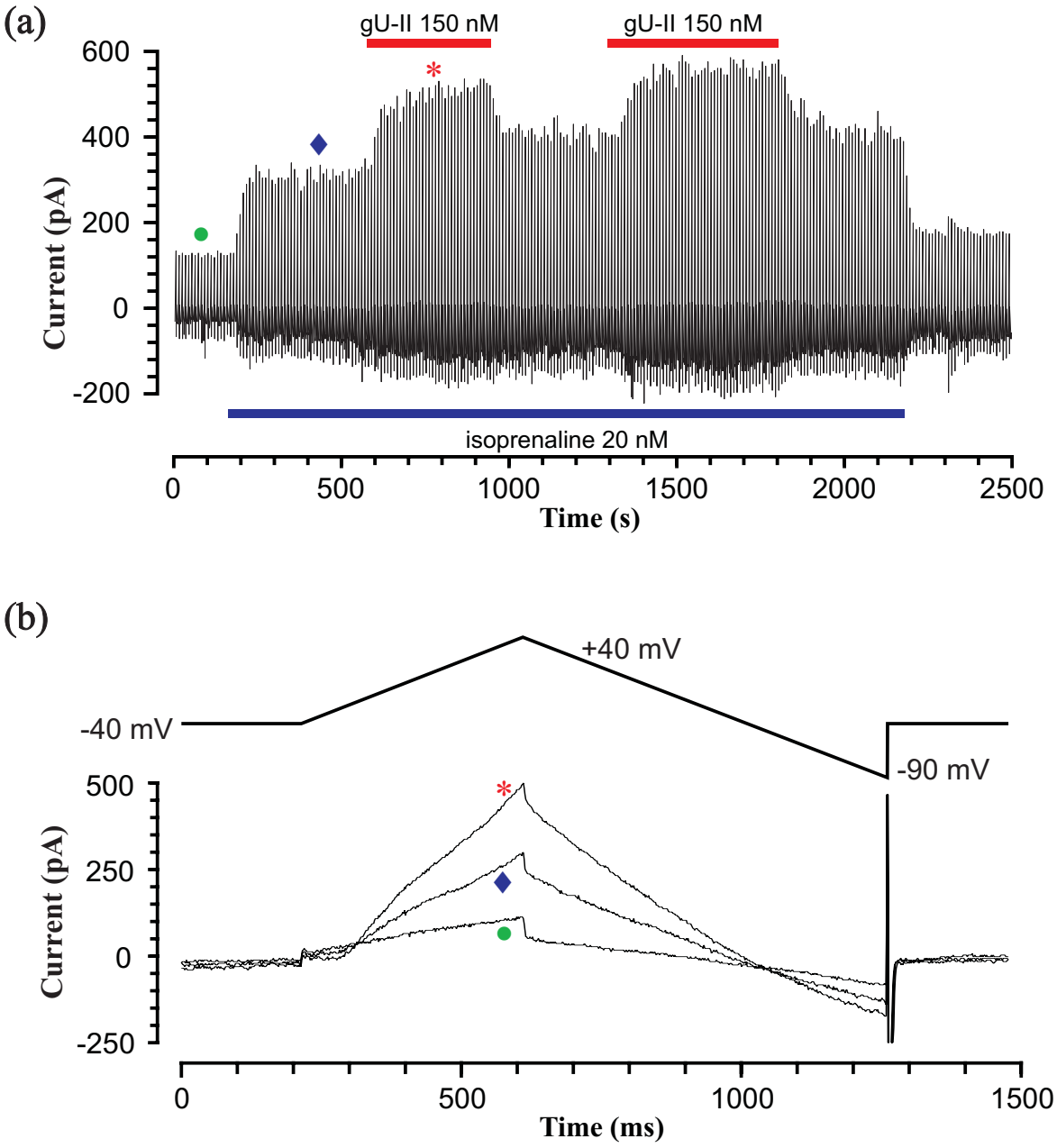

Figure 6.1a

An example of the application of 150 nM goby-Urotensin II (gU-II) in the presence of 20 nM isoprenaline. (*a*) Chart record of whole cell current responses to voltage ramps showing that after the changes in whole cell current evoked by isoprenaline (♦), a further rapidly reversible increase is seen after the application of gU-II (*). (*b*) Three current records at an expanded time scale showing the whole cell current before and after isoprenaline, and with the addition of gU-II, recorded using a ramp pulse protocol from -40 mV to +40 mV and thence to -90 mV. The inward deflection at the beginning of the depolarisation ramp is due to residue Ca^{2+} current.

6.2 Results:

6.2.1 Urotensin II potentiates the catecholamine-induced chloride current

6.2.1.1 The response to 150 nM goby urotensin II

Isoprenaline causes an increase in whole cell current evoked by ramp pulses. The additional outward-rectifying current was voltage and time-independent and reversed near the calculated Nernst equilibrium potential of -55 mV in the asymmetrical chloride used and can be safely identified as catecholamine-activated chloride current carried by the CFTR channel (Bahinski *et al.*, 1989; Harvey & Hume, 1989). The majority of the difference between the predicted theoretical and the actual reversal potentials can be attributed to a small permeability for aspartate, the substitute ion used for chloride, through this channel.

Figure 6.1a shows the modulation by goby urotensin II (gU-II) of the isoprenaline-activated chloride current. The top trace (*A*) is a continuous current record in response to ramp pulses evoked every 10 s from a holding current of -90 mV. The changes in whole cell current evoked by isoprenaline and in the subsequent additional presence of gU-II can be seen more clearly at the expanded time scale in the bottom graph. There was a small downward deflection during the initial part of the depolarising ramp due to small residue L-type Ca^{2+} current incompletely blocked by 1 µM nicardipine. All sodium and T-type Ca^{2+} currents were inactivated by the use of a pre-conditioning voltage of -40 mV. The chloride conductance was measured during the hyperpolarising part of the ramp where minimal current contamination could be detected. The I-V relationship of the isoprenaline-induced conductance was calculated by digitally subtracting the control basal background current (•) and is displayed in the

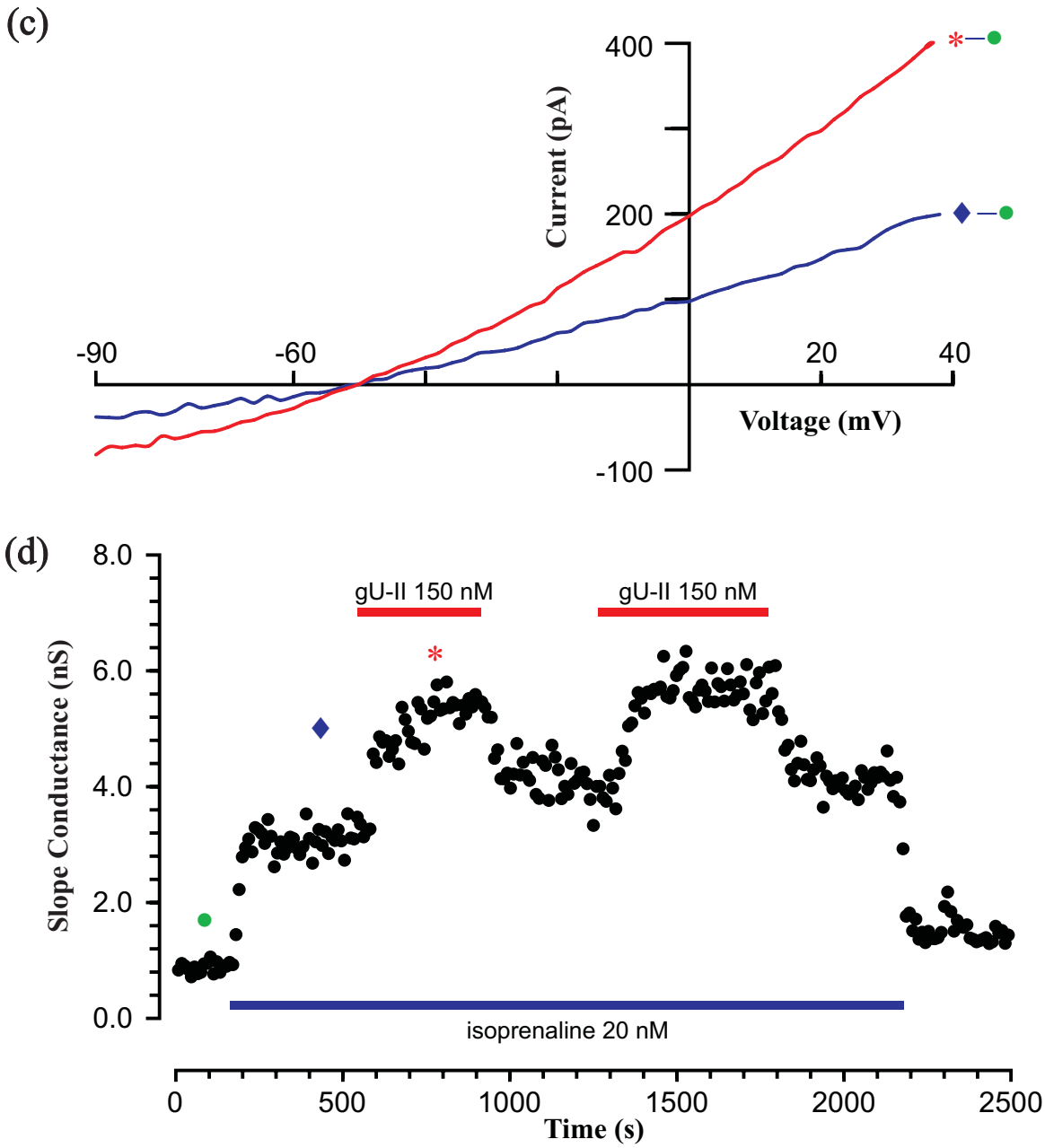

Figure 6.1b

(*c*) I-V curves obtained from the current traces in the hyperpolarising part of the ramp in *b.* Difference currents were calculated by subtracting the control leak current from the isoprenaline (♦-●) and goby Urotensin II (gU-II, *-●) responses. Both of these had a reversal potential around -50 mV and clear outward rectification was seen at negative potentials. (*c*) The time course of changes in slope conductance measured at 0 mV during each hyperpolarising ramp clearly illustrating the changes in $I_{Cl,cAMP}$. The submaximal (20 nM) dose of isoprenaline caused a rapid increase in chloride conductance which is further potentiated in the presence of 150 nM urotensin II.

upper trace of figure 6.1b. During the maintained superfusion of a sub-maximal concentration (20 nM) of isoprenaline, each additional application of goby urotensin II in the superfusate further increased the amplitude of the current deflections during the ramp pulses without changing the reversal potential from ~-50 mV. The changes in $I_{Cl,cAMP}$ were quantified by using the slope of the regression line fitted to the current voltage relationship at 0 mV. The resulting slope conductance was normalized for cell capacitance.

After a short lag within the range for bath diffusional exchange (~30-40 s), the current increased rapidly, reaching half-maximum within 20-30 s and a plateau after around 2.5 minutes. The response to goby urotensin II was both reversible, with a return to pre-application current levels after around 3-3.5 minutes after washout, and repeatable. The experiment shown in figure 6.1 featured two successive applications of the peptide which produced similar responses. On average, 150 nM goby urotensin II causes an increase in normalized slope conductance with 20 nM isoprenaline from 23.6 ±0.5 pS/pF (n=42) to 45.7 ±11.1 pS/pF (n=18). In eighteen cells, the chloride conductance was nearly doubled on average (192 ±16%).

6.2.1.2 Effects of Human U-II

Although the deduced sequences for goby, human, porcine and mouse urotensin II all share a high identity, especially in the C-terminal cyclic hexapeptide sequence, subtle tissue differences in responsiveness to human urotensin II (hU-II) and goby U-II have been reported in the rat. The vasoconstrictor activity of hU-II in the rat seems to be limited to the thoracic aorta, while gU-II also has an effect on the rat abdominal aorta,

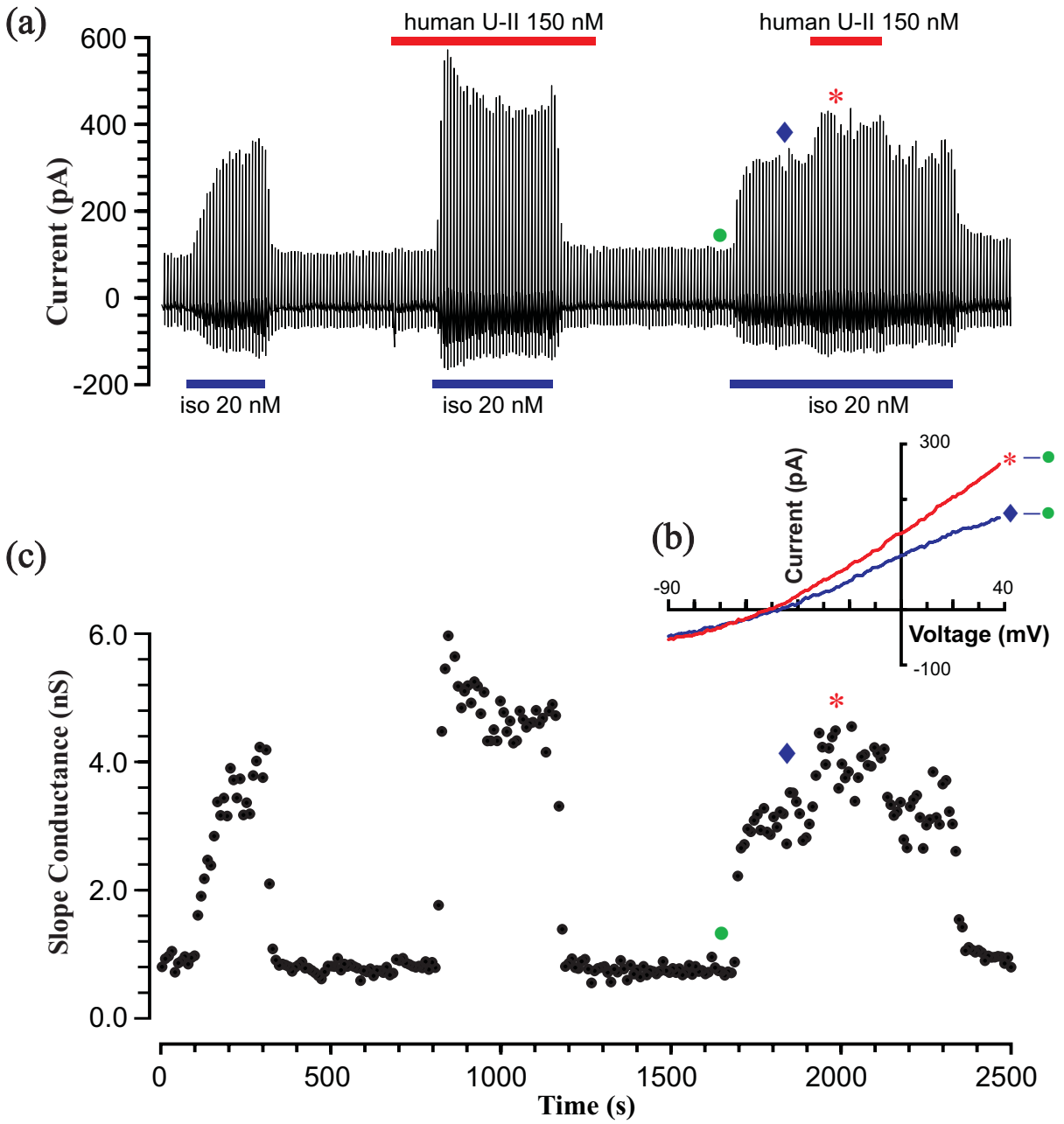

Figure 6.2

An example demonstrating that 150 nM human Urotensin II (hU-II) only increases chloride conductance in the presence of 20 nM isoprenaline (iso). (*a*) Chart record of whole cell current responses to voltage ramps showing that the increase in whole cell current evoked by isoprenaline (♦) relative to control (●) is further potentiated by hU-II (*). (*b*) I-V curves from the current traces in *a.* The difference currents had a reversal potential around -50 mV and were outwardly rectifying. (*c*) The time course of changes in slope conductance measured at 0 mV clearly illustrating that hU-II has no effect when isoprenaline is absent but increases the isoprenaline-evoked $I_{Cl,cAMP}$.

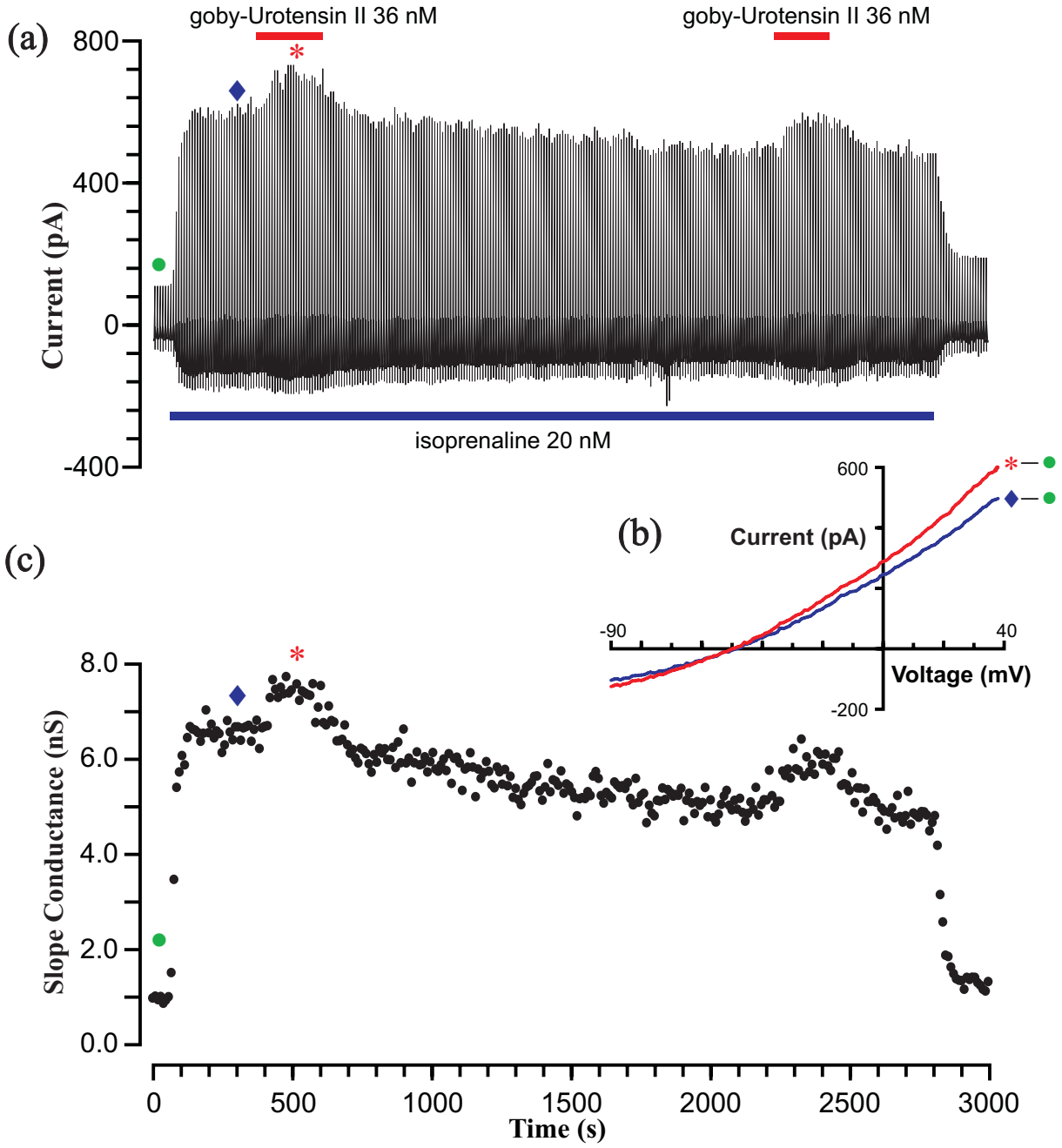

Figure 6.3

An example of the application of 36 nM goby-Urotensin II (gU-II) in the presence of 20 nM isoprenaline. (*a*) Chart record of whole cell current responses to voltage ramps showing that the increase in whole cell current evoked by isoprenaline (♦) relative to control (•) is further potentiated by low doses of gU-II (*). These further changes reversed rapidly on subsequent removal of gU-II. (*b*) I-V curves from the current traces in *a.* The difference currents had a reversal potential around -50 mV and were outwardly rectifying. (*c*) The changes in slope conductance measured at 0 mV show the small but rapid changes in chloride conductance produced by low doses of gU-II.

and renal and femoral arteries. Accordingly, the possibility was investigated that the cardiac action of urotensin II might be similarly discriminating.

Figure 6.2 sets out the results from a typical experiment with human urotensin II. In the absence of isoprenaline, 150 nM hU-II alone was not able to produce any changes in whole cell current or slope conductance. When 20 nM isoprenaline was subsequently added in the presence of hU-II, the resulting increase in chloride conductance was greater than seen with isoprenaline alone. The evoked $I_{Cl,cAMP}$ was abolished with the withdrawal of isoprenaline, even though hU-II was still present. The converse procedure, with the addition of 150 nM hU-II when the cell was pre-superfused with 20 nM isoprenaline, produced much the same result as with gU-II, with the response to catecholamine greatly potentiated. On average, human U-II produced an increase to 186 ±22% (n=4) which was not significantly different from the effects of goby urotensin II.

6.2.2 *Dose dependence of Urotensin*

6.2.2.1 36 nM gU-II

The response to gU-II was dose-dependent. Figure 6.3 shows the response to 36 nM gU-II which had reduced magnitude but a similar time course compared to when the higher dose of 150 nM was used (figure 6.1). On average, with 150 nM goby urotensin II, the normalized slope conductance rises to 37.0 ±6.3 pS/pF (n=14), with a mean increase to 136 ±8% (n=14). 36 nM seemed to be near the threshold for a detectable increase in chloride conductance. This value is somewhat higher than the previously reported specific receptor binding affinities (e.g. K_d=2.06 ±0.29 and 1.99 ±

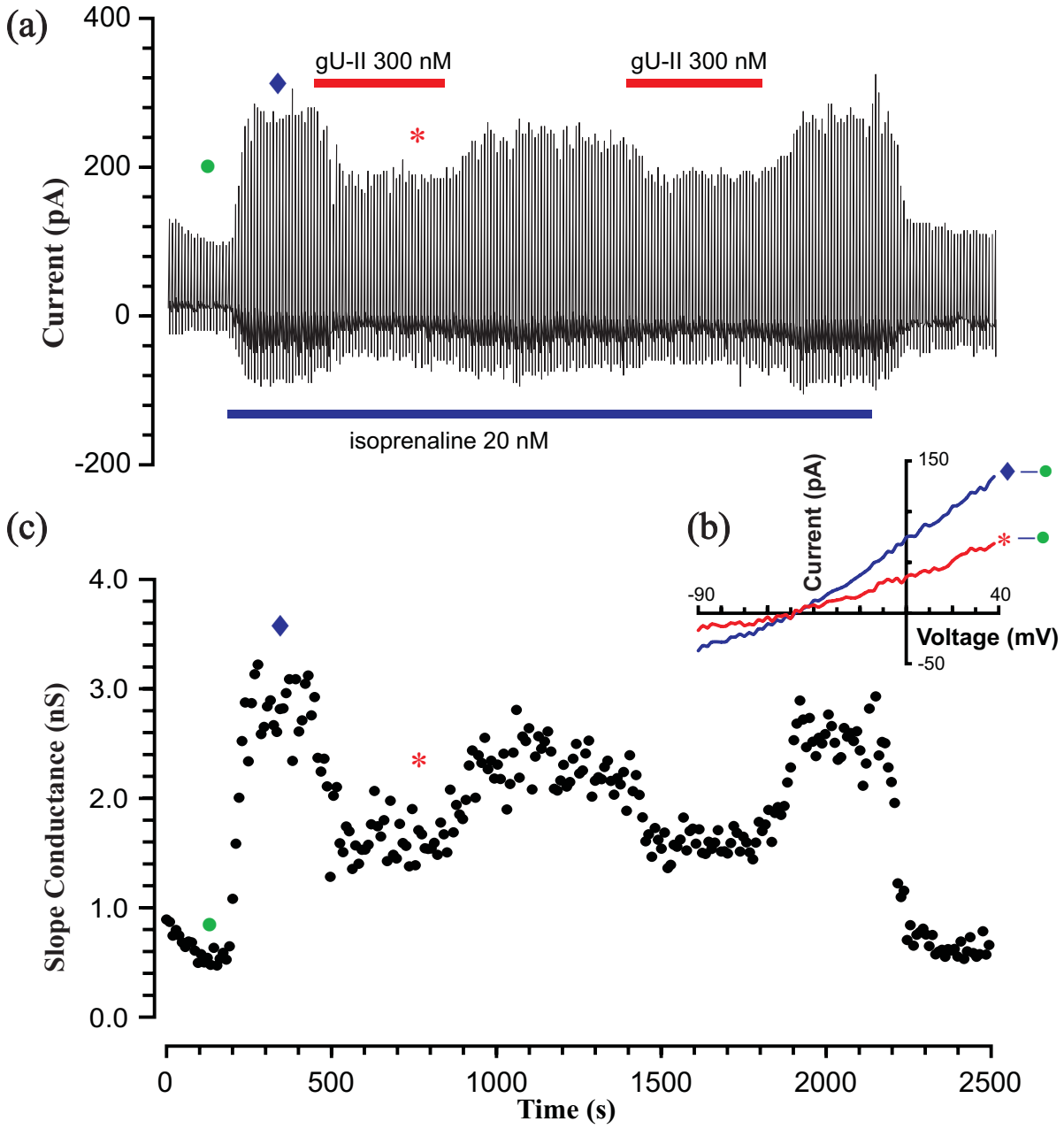

Figure 6.4

An example where the application of 300 nM goby Urotensin II (gU-II) inhibits the response to 20 nM isoprenaline (*a*) Chart record of whole cell current responses to voltage ramps showing that the increase in whole cell current evoked by isoprenaline (♦) relative to control (•) is reversibly inhibited by gU-II (*). (*b*) I-V curves from the current traces in *a.* The difference currents had a reversal potential around -50 mV and were outwardly rectifying. (*c*) The time course of changes in slope conductance measured at 0 mV illustrating the reduction in $I_{Cl,cAMP}$ and recovery upon application and subsequent removal of 300 nM gU-II.

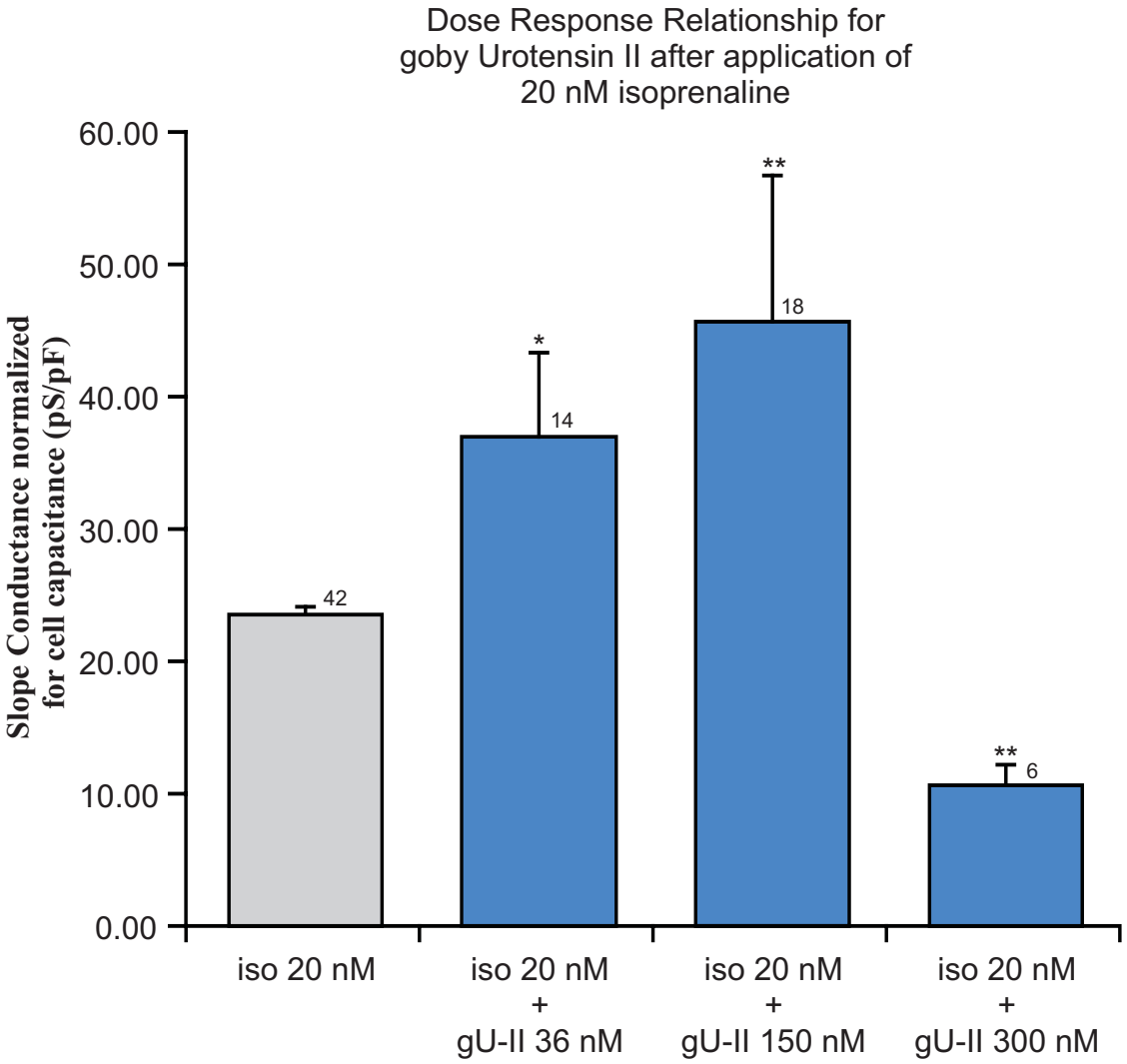

Figure 6.5a

The effects of different concentrations of goby urotensin II (gU-II) applied after a submaximal dose (20 nM) of isoprenaline (iso). Lower concentrations of gU-II markedly increased the chloride conductances evoked by isoprenaline. However, 300 nM gU-II conversely produced an inhibition of the isoprenaline response in 6 out of 8 cells.

Slope conductances were measured during hyperpolarising voltage ramps at 0 mV. Measurements were made when each response had reached its plateau and all values are relative to control. Significant changes from the isoprenaline response ($p < 0.05, 0.01$) are indicated with asterisks (*, **) and the number of cells for each experiment are printed by the error bars.

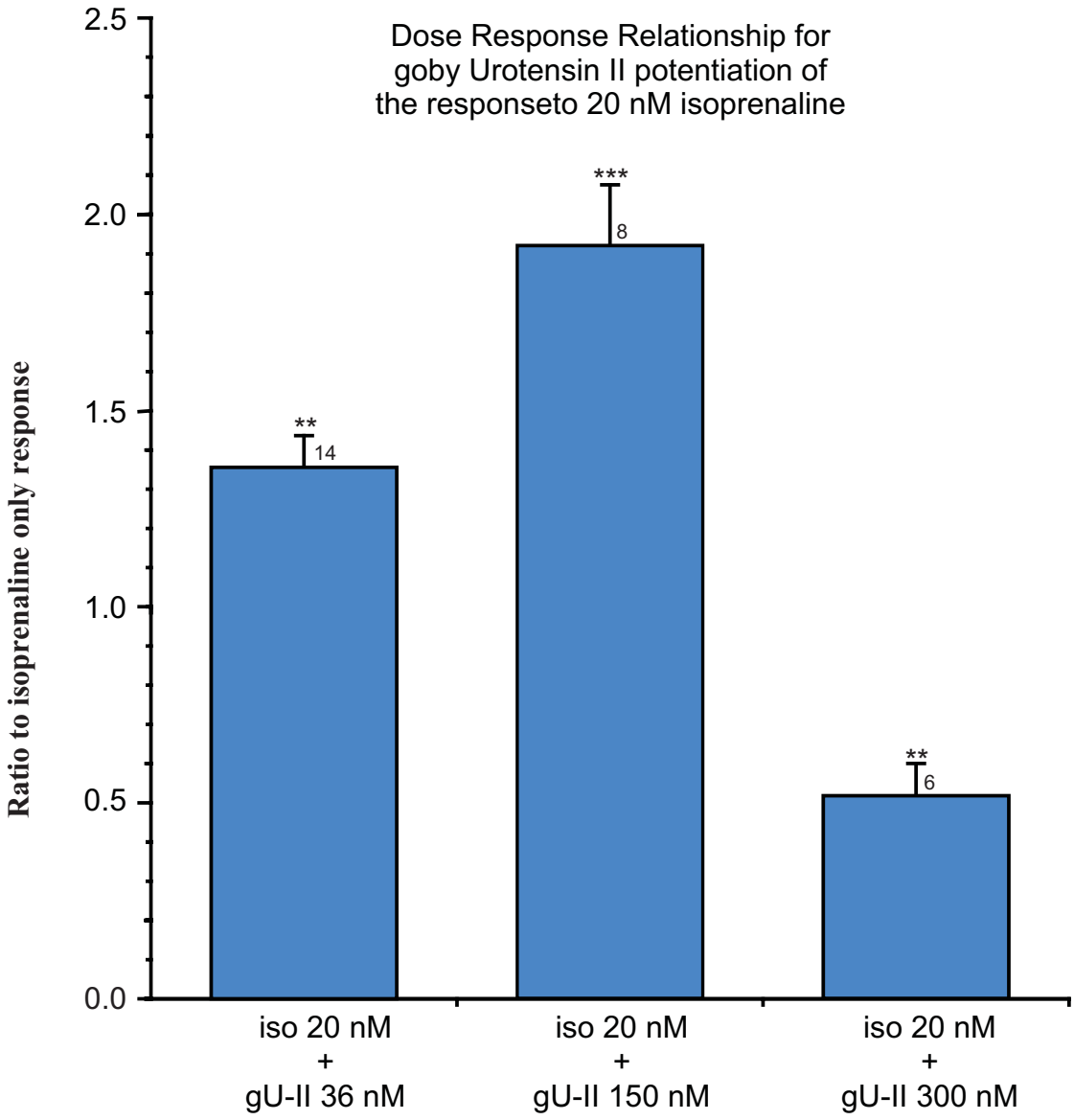

Figure 6.5b

The effects of different concentrations of goby urotensin II (gU-II) applied after a sub-maximal dose (20 nM) of isoprenaline (iso). Lower concentrations increased the isoprenaline evoked chloride conductance, by almost two-fold in the case of 150 nM gU-II. 300 nM gU-II, however, produced a marked inhibition in the isoprenaline response in the majority (6 out of 8) of cells.

The effects of gU-II in each experiment were calculated as a proportion of the iso-evoked conductance and then averaged across the cells. Ratios > 1 indicate increased $I_{Cl,cAMP}$. Slope conductances at 0 mV during hyperpolarising voltage ramps was used as a measure of $I_{Cl,cAMP}$. Significant changes from the isoprenaline response ($p < 0.01$ & 0.001) are indicated with asterisks (**, ***) and the number of cells are printed by the error bars.

0.23 nM for goby and human Urotensin II in HEK-293 cells expressing the human GPR14; Ames *et al.*, 1999) or half maximum effector concentrations (e.g. log[EC_{50}] = -9.09 ±0.19 and -9.22 ±0.18 for gU-II and hU-II evoked contractions in rat thoracic aorta; Ames *et al.*, 1999).

6.2.2.2 300 nM gU-II

Higher doses of goby Urotensin II produced variable effects. In two cells out of eight, no significant changes in the catecholamine-activated chloride conductance could be seen with 300 nM gU-II. In six other cells, however, the peptide produced a rapid reversible decrease in the chloride conductance. Figure 6.4 sets out results from one such experiment. In the presence of 20 nM isoprenaline, the addition of 300 nM gU-II produced a sharp decrease in whole cell current which reached a minimum with 2 minutes. This inhibitory effect could be repeated after washout. In most cases, when gU-II was removed, the current recovered almost completely (to its levels in the sole presence of 20 nM isoprenaline). On average, in six cells, the normalized slope conductance in the presence of 300nM gU-II was only 10.6 ±1.7 pS/pF with an average decrease of 52 ±0.8%. In two other cells, the normalized slope conductance was not significantly changed at 21.2 ±8.5 pS/pF.

The average slope conductances normalized for cell size at different doses of gU-II are summarized in figure 6.5a. The effects of gU-II on the isoprenaline-evoked chloride conductance are even more evident when examined cell by cell rather than as aggregate conductances. Figure 6.5b displays the averages of the proportional changes by

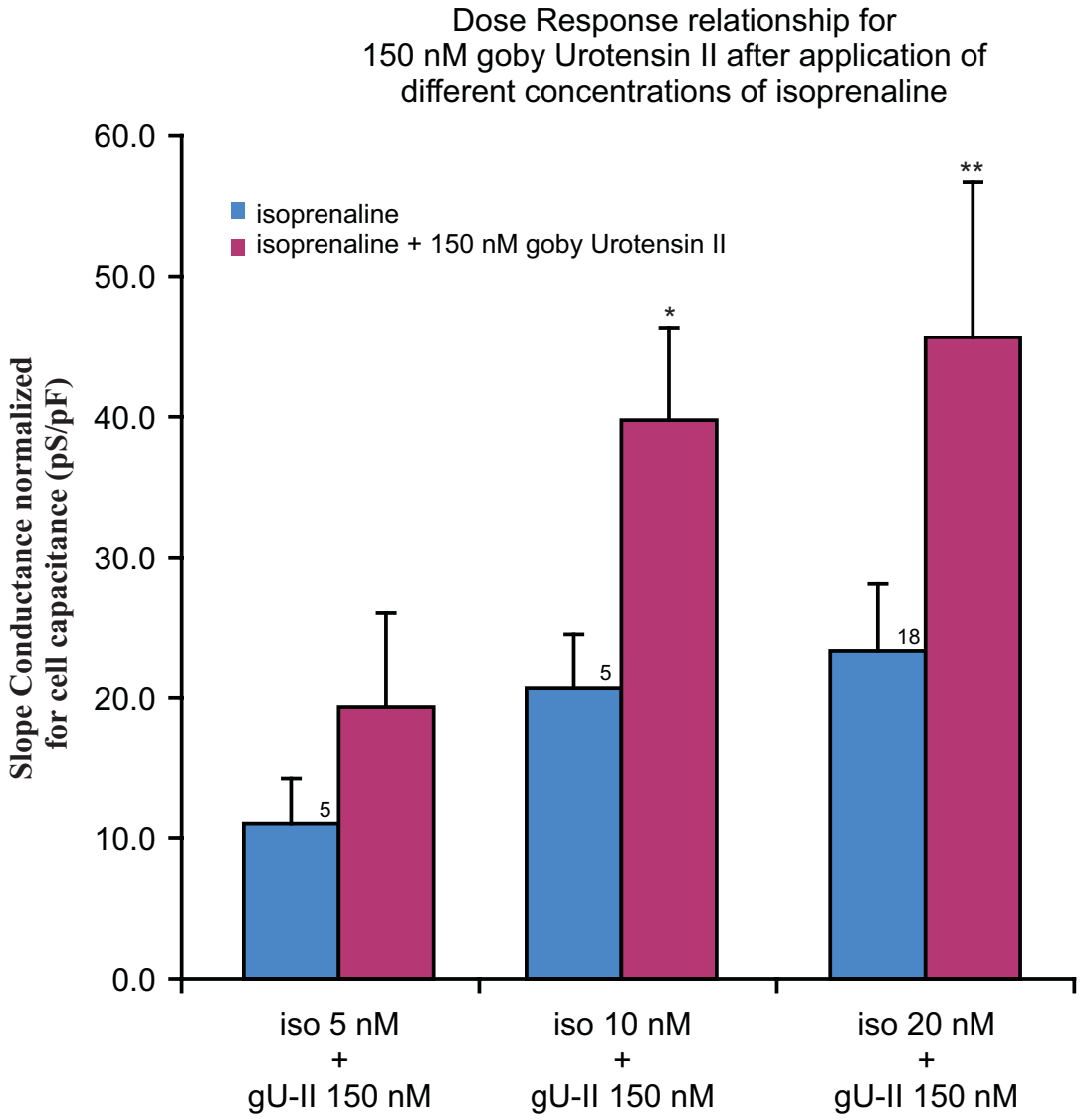

Figure 6.6a

The effects of goby urotensin II (gU-II) applied after different concentrations of isoprenaline (iso). The further increases in chloride conductances after application of 150 nM gU-II are not constant in magnitude but rather in proportion to the responses to isoprenaline. At each concentration of isoprenaline, gU-II almost doubles the response. Slope conductances were measured during hyperpolarising voltage ramps at 0 mV. Measurements were made when each response had reached its plateau and all values are relative to control. Significant changes from the isoprenaline response ($p < 0.05, 0.01$) are indicated with asterisks (*, **) and the number of cells for each experiment are printed by the error bars.

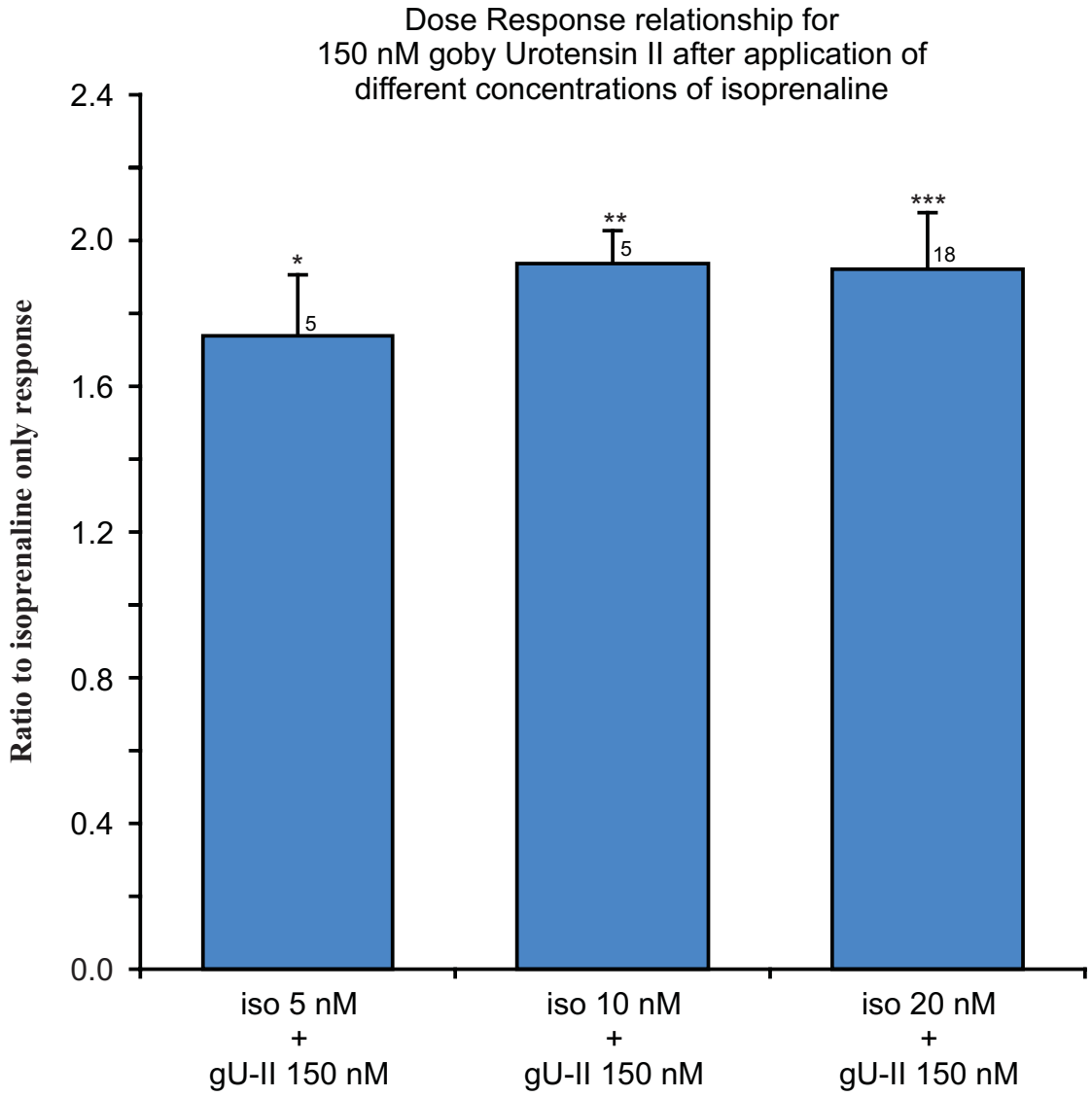

Figure 6.6b

The effects of 150 nM goby urotensin II (gU-II) applied after different concentrations of isoprenaline (iso). The degree of potentiation of the isoprenaline response by 150 nM gU-II was not markedly different at different submaximal doses of isoprenaline. In each case, gU-II increased the isoprenaline-evoked chloride conductance almost two-fold.

The effects of gU-II in each experiment were calculated as a proportion of the iso-evoked conductance and then averaged across the cells. Thus ratios greater than 1 indicate increased $I_{Cl,cAMP}$. The slope conductances at 0 mV during hyperpolarising voltage ramps was used as a measure of chloride current. Significant changes from the isoprenaline response ($p < 0.05$, 0.01 & 0.001) are indicated with asterisks (*, **, ***) and the number of cells for each experiment are printed by the error bars.

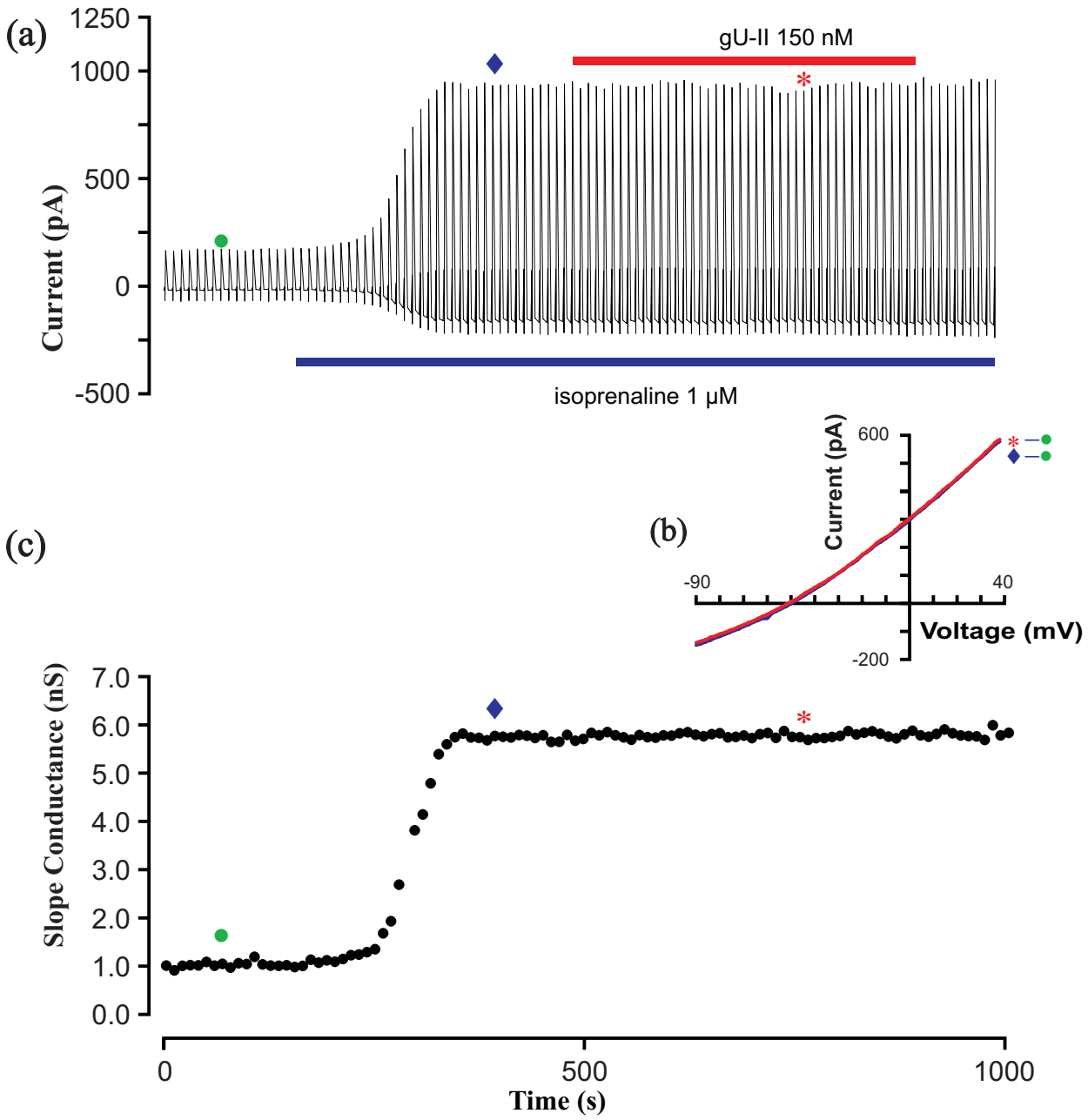

Figure 6.7

An example of the application of 150 nM goby-Urotensin II (gU-II) in the presence of 1 µM isoprenaline. (*a*) Chart record of whole cell current responses to voltage ramps. After large changes in whole cell current evoked by isoprenaline (♦), subsequent application of gU-II (*) produced no detectable additional changes. (*b*) I-V curves from the current traces in *a*. The outwardly rectifying difference currents had a reversal potential of around -50 mV. (*c*) The time course of changes in slope conductance measured at 0 mV illustrate the lack of effect of gU-II after high doses of isoprenaline.

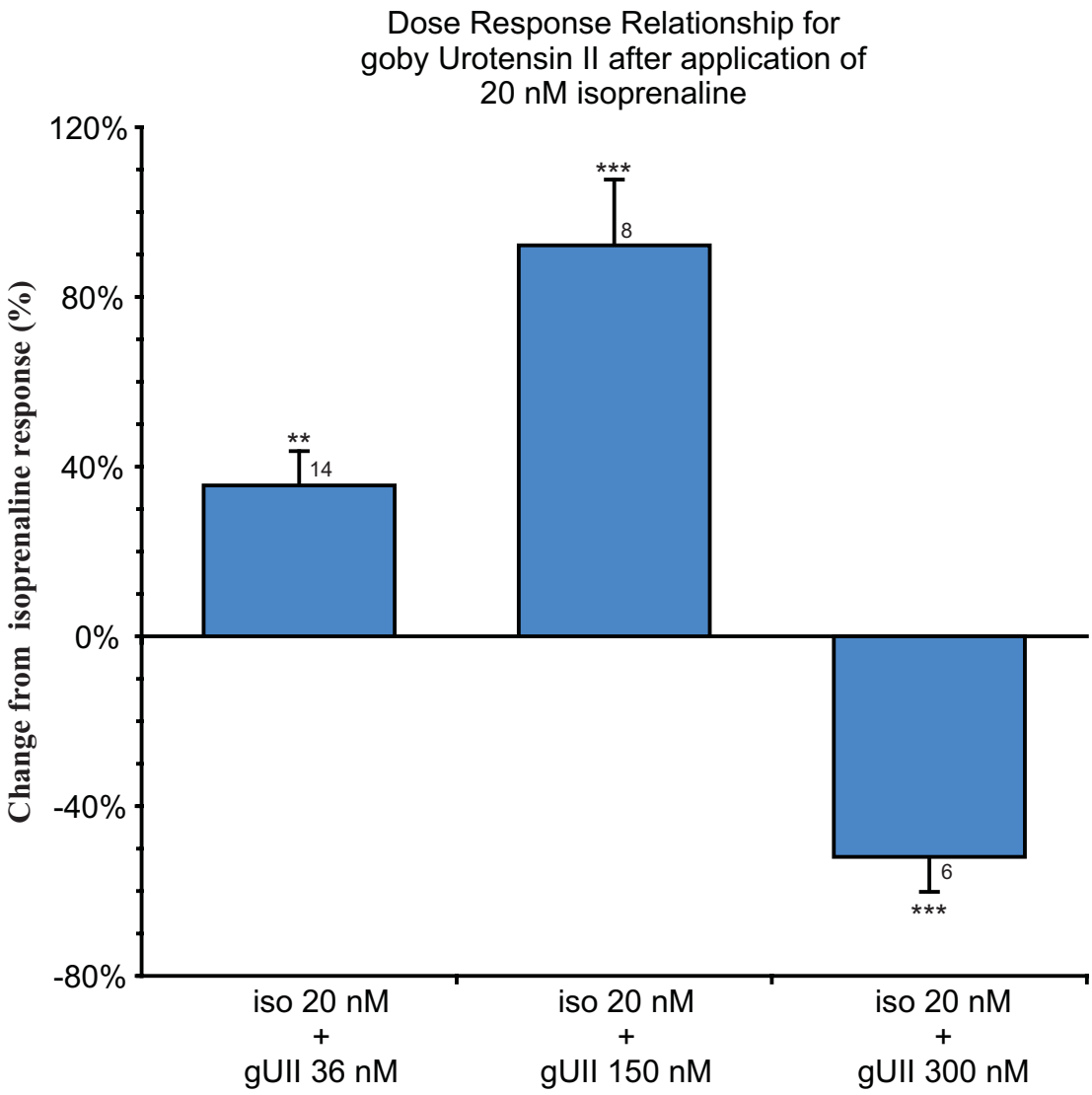

Figure 6.7b

The effects of different concentrations of goby Urotensin II (gUII) applied after a sub-maximal dose (20 nM) of isoprenaline (iso). Lower concentrations increased the isoprenaline evoked chloride conductance, by by almost two-fold in the case of 150 nM gUII. 300 nM gUII, however, produced a marked inhibition in the isoprenaline response in the majority (6 out of 8) of cells.

The effects of gUII are given as percentage increases over the isoprenaline response in each cell and averaged. The slope conductance at 0 mV during hyperpolarising voltage ramps were used as a measure of chloride current. Significant changes from the isoprenaline response ($p < 0.01, 0.001$) are indicated with asterisks (**, ***) and the number of cells for each experiment are printed by the error bars.

gU-II to the isoprenaline-evoked chloride conductance. Thus, a mean of 1.0 would indicate no change on average, while a smaller value reflects an inhibition.

6.2.3 Effects of gU-II on the responses to different concentrations of isoprenaline

6.2.3.1 gU-II causes similar potentiations of responses to different sub-maximal doses of isoprenaline

As described above, 150 nM gU-II almost doubles the chloride conductance evoked by a sub-maximal 20 nM concentration of isoprenaline. The responses to even lower doses of isoprenaline are potentiated to much the same degree. This is summarized in figure 6.6a. In the presence of each concentration of isoprenaline, the subsequent addition of gU-II caused a large increase in $I_{Cl,cAMP}$. These effects of gU-II can again be compared much more clearly when the results are expressed as proportional increases per cell. Thus, in the presence of 5 nM, 10 nM and 20 nM isoprenaline, the subsequent addition of 150 nM gU-II produced change ratios of 1.74 ±0.17 (n=5), 1.94 ±0.09 (n=5) and 1.92 ±0.16 (n=18) respectively. In other words, 150 nM gU-II in each case almost doubled the original catecholamine response (figure 6.6b).

6.2.3.2 The effects of gU-II in the presence of saturating isoprenaline

In contrast to the above results, when a saturating concentration of isoprenaline was used, no further increases in chloride conductance could be seen. (Figure 6.7 shows the response to 1 µM isoprenaline. The estimated EC_{50} for isoprenaline-evoked chloride conductance under these experimental conditions was roughly 20-30 nM (not dissimilar to Ono *et al.*, 1991). A high dose of isoprenaline caused a rapid and large increase in $I_{Cl,cAMP}$ and the subsequent addition of 150 gU-II was ineffective (n=4).

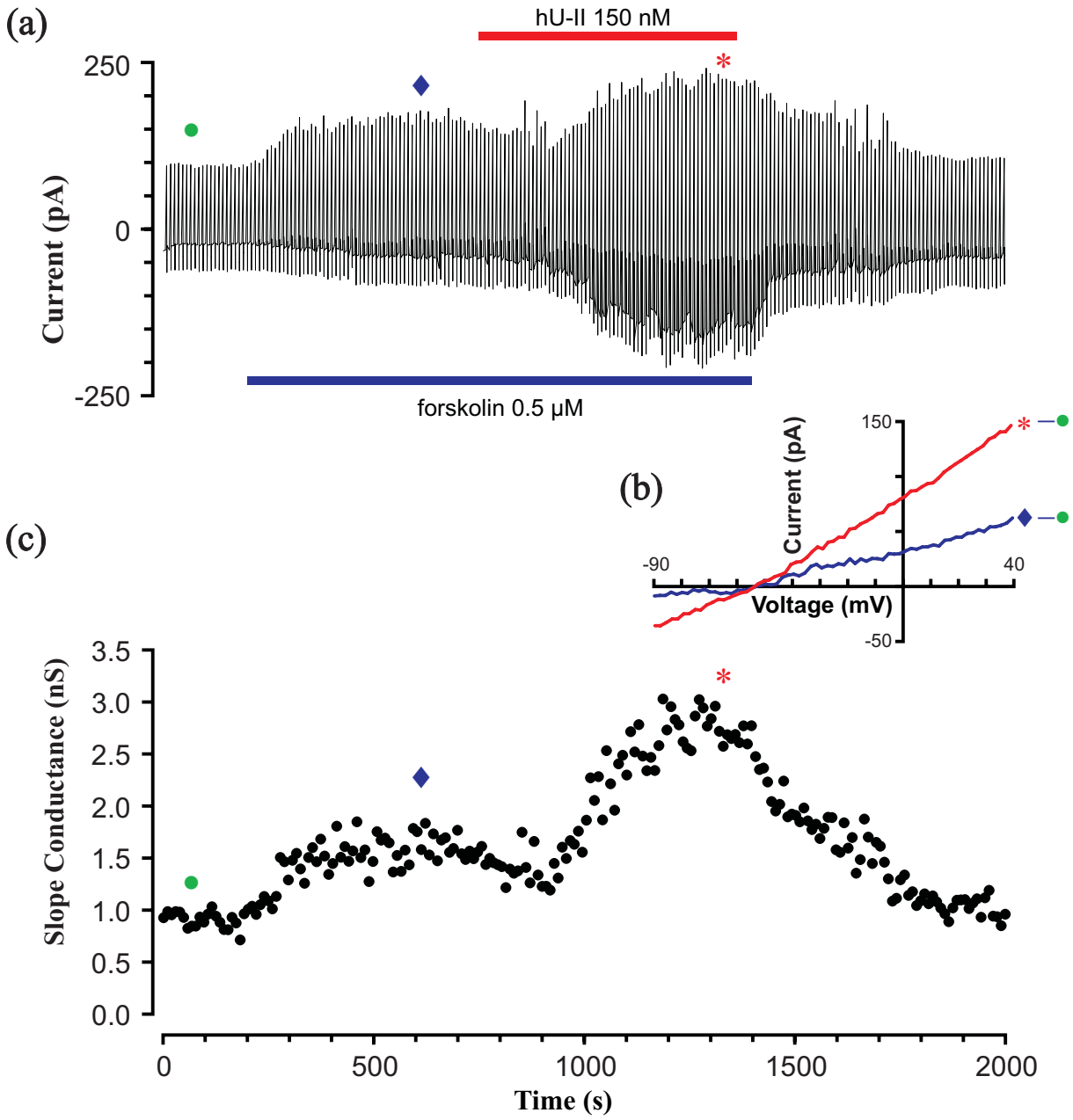

Figure 6.8

An example showing the potentiation of forskolin-evoked $I_{Cl,cAMP}$ by 150 nM human Urotensin II (hU-II). (*a*) Chart record of whole cell current responses to voltage ramps showing that the increase in whole cell current evoked by 0.5 µM forskolin (♦) relative to control (●) is further potentiated by hU-II (*). (*b*) I-V curves from the current traces in *a*. The difference currents had a reversal potential around -50 mV and were outwardly rectifying. (*c*) The time course of changes in slope conductance measured at 0 mV clearly illustrating that hU-II further potentiates the chloride current seen after forskolin application.

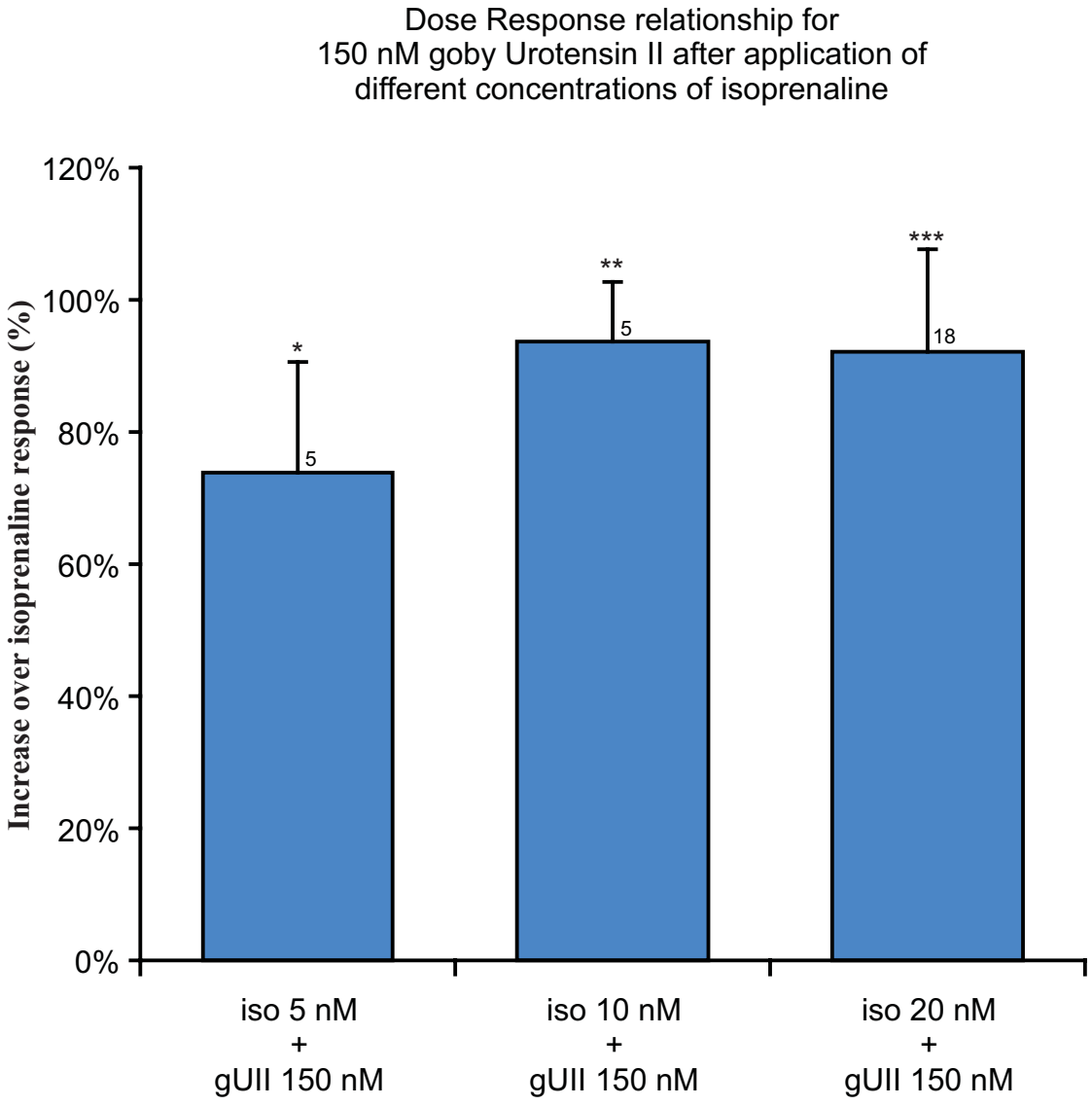

Figure 6.8b

The effects of 150 nM goby Urotensin II (gUII) applied after different concentrations of isoprenaline (iso). The degree of potentiation of the isoprenaline response by 150 nM gUII was not markedly different at different submaximal doses of isoprenaline. In each case, gUII increased the isoprenaline-evoked chloride conductance almost two-fold.

The effects of gUII are given as percentage increases over the isoprenaline response in each cell and averaged. The slope conductance at 0 mV during hyperpolarising voltage ramps were used as a measure of chloride current. Significant changes from the isoprenaline response ($p < 0.05$, 0.01 & 0.001) are indicated with asterisks (*, **, ***) and the number of cells for each experiment are printed by the error bars.

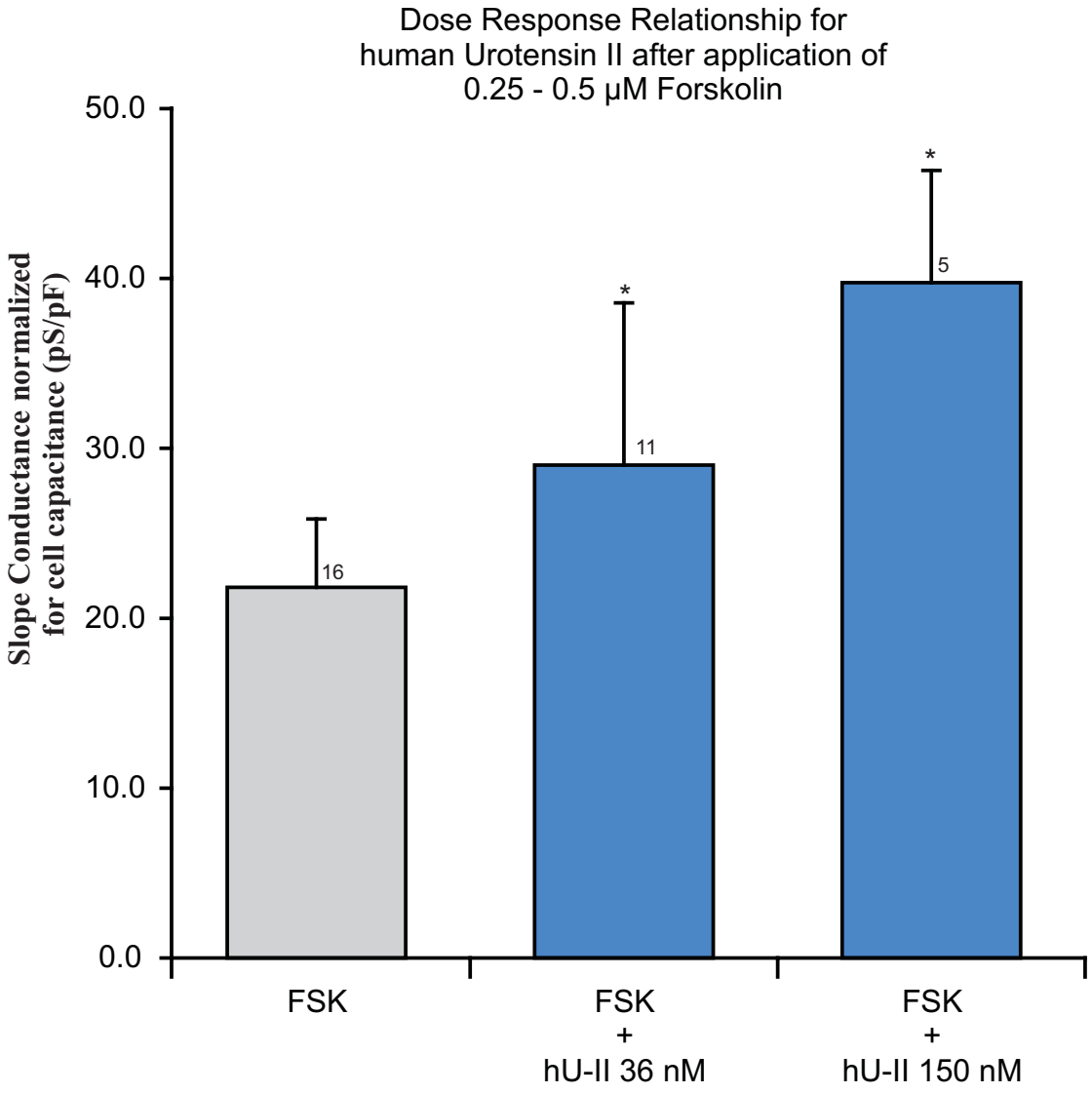

Figure 6.9a

The effects of different concentrations of human urotensin II (hU-II) applied after submaximal doses (0.25-0.5 µM) of forskolin (FSK). hU-II markedly increased the chloride conductances evoked by forskolin in a dose-dependent fashion.

Slope conductances were measured at 0 mV during hyperpolarising voltage ramps. Measurements were made when each response had reached its plateau and all values are relative to control. Significant changes from the forskolin response ($p < 0.05$) are indicated with an asterisk (*) and the number of cells for each experiment are printed by the error bars.

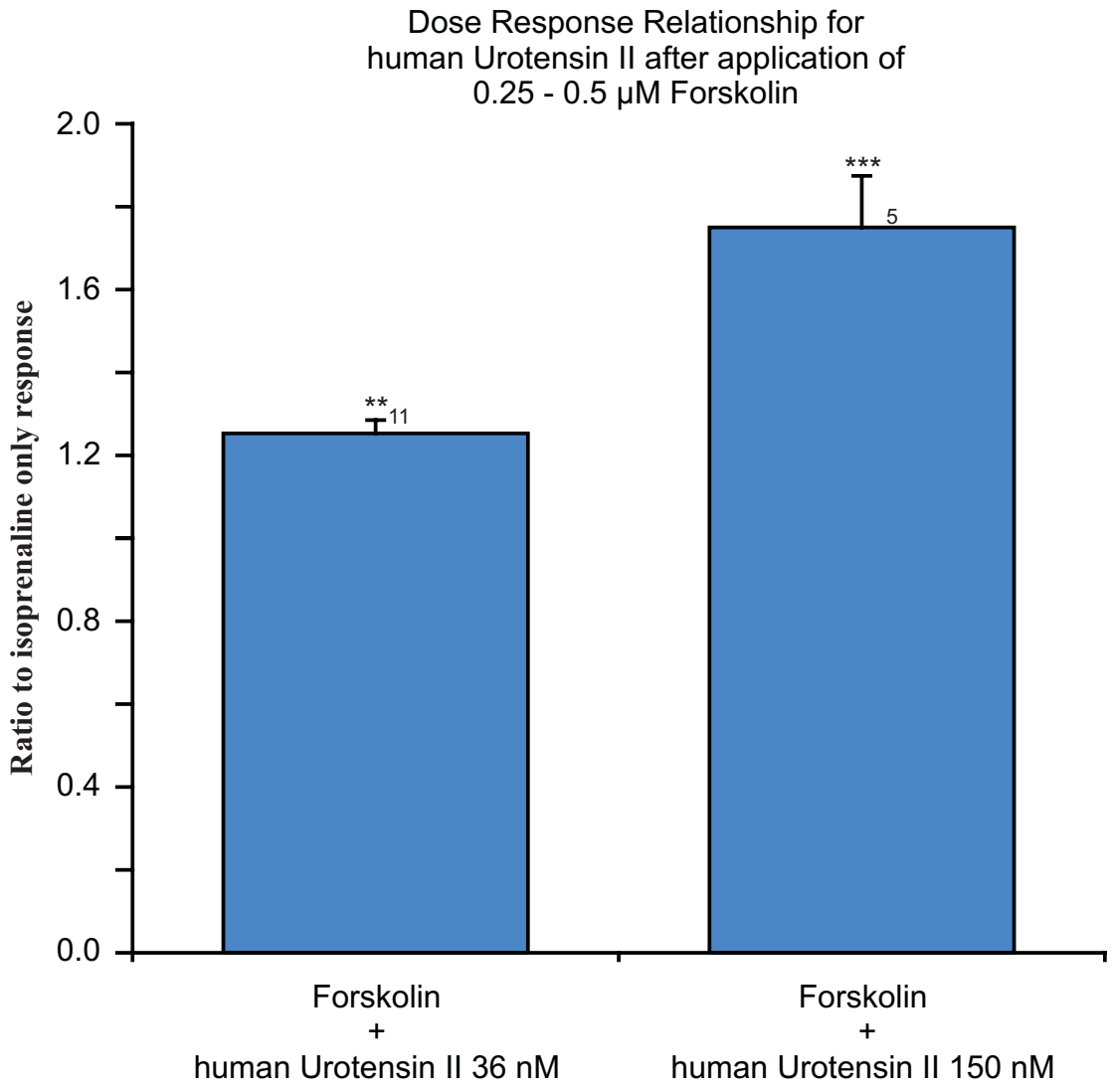

Figure 6.9b

The effects of two different concentrations of human urotensin II (hU-II) applied after sub-maximal doses of forskolin between 0.25 and 0.5 µM. The bar graph illustrates the further changes in slope conductance evoked by 150 nM hU-II after the application of forskolin.

The effects of hU-II in each experiment were calculated as a proportion of the forskolin-evoked conductance and then averaged across the cells. Thus ratios greater than 1 indicate increased $I_{Cl,cAMP}$. The slope conductances at 0 mV during hyperpolarising voltage ramps was used as a measure of chloride current. Significant changes from the forskolin response ($p < 0.01$ & 0.001) are indicated with asterisks (**, ***) and the number of cells for each experiment are printed by the error bars.

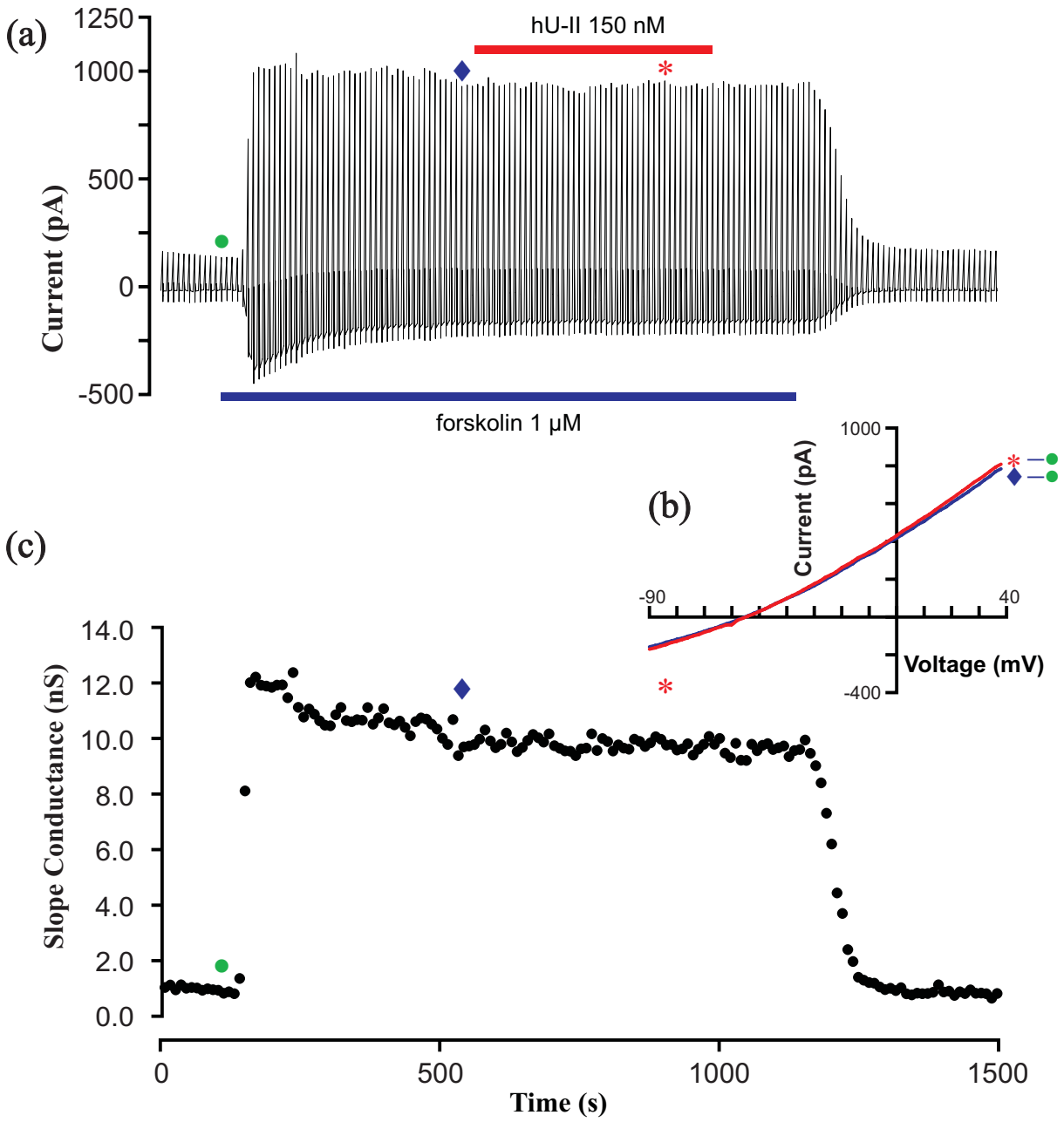

Figure 6.10

An example showing the effects of human Urotensin II (hU-II) in the presence of 1 µM forskolin. (*a*) Chart record of whole cell current responses to voltage ramps showing that the large increase evoked by 1 µM forskolin (♦) relative to control (•) is little changed by hU-II (*). (*b*) I-V curves from the current traces in *a*. The outwardly rectifying difference currents had a reversal potential around -50 mV. (*c*) Changes in slope conductance measured at 0 mV. Though the forskolin concentration was only twice that for the cell in figure 6.8, hU-II was not able to deliver any significant further increases in $I_{Cl,cAMP}$. Note also the much more rapid onset of the forskolin response.

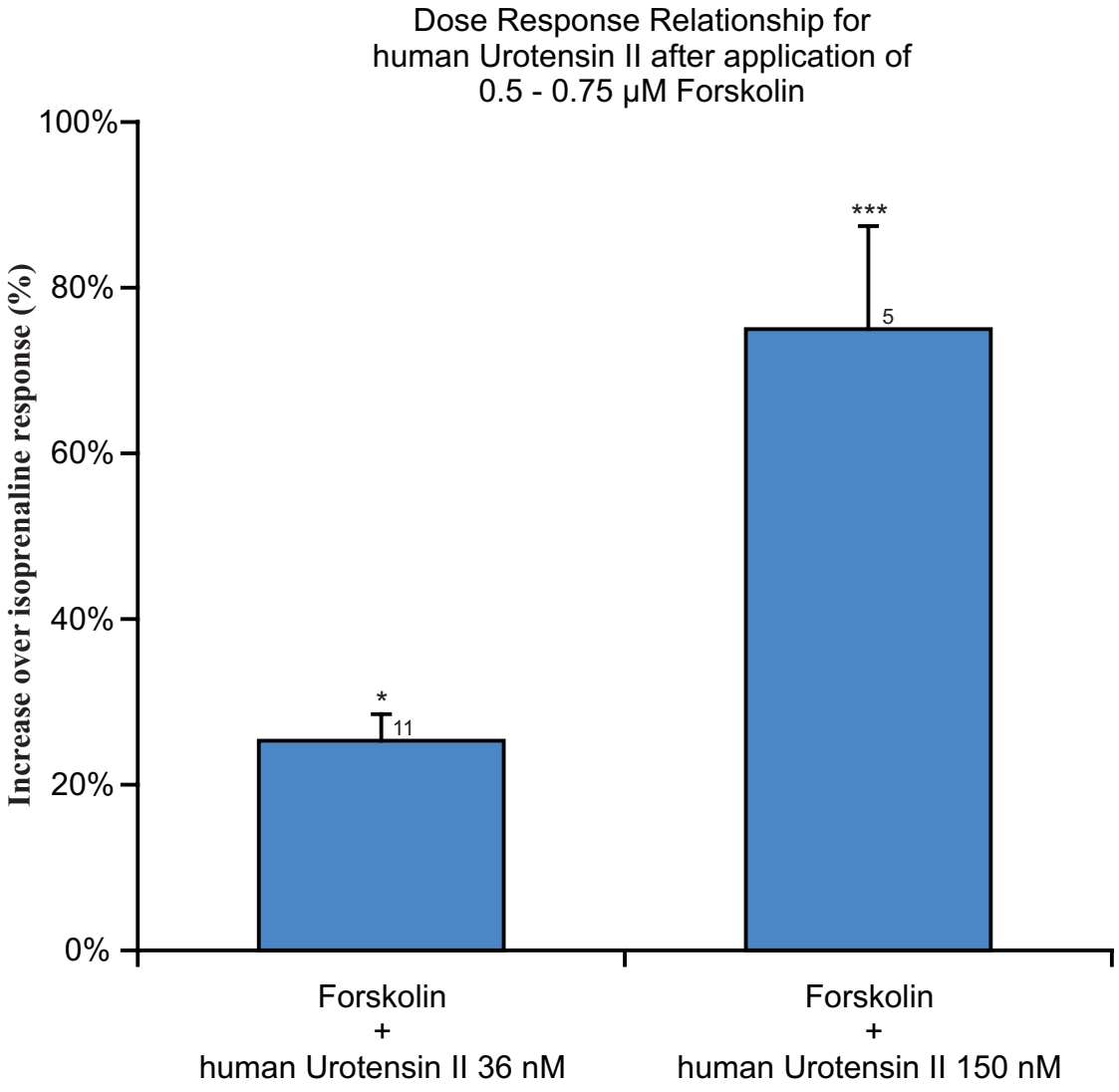

Figure 6.11b

The effects of two different concentrations of human Urotensin II (hUII) applied after sub-maximal doses of forskolin between 0.5 and 0.75 µM. The bar graph illustrates the further changes in slope conductance evoked by 150 nM hUII after the application of forskolin.

The effects of hUII are given as percentage increases over the forskolin response in each cell and averaged. The slope conductance at 0 mV during hyperpolarising voltage ramps were used as a measure of chloride current. Significant changes from the forskolin response ($p < 0.05, 0.001$) are indicated with asterisks (*, ***) and the number of cells for each experiment are printed by the error bars.

6.2.4 gU-II cAMP-dependent potentiation of $I_{Cl,cAMP}$

Agonist occupation of the β-adrenoreceptor leads to recruitment of adenylyl cyclase, protein kinase A, phosphorylation and hence activation of the CFTR channel. The potentiation by gU-II could be mediated at one or more of those steps or, indeed, have its effects on either phosphodiesterase or protein phosphates. To help resolve the locus of gU-II action, its effects in the presence of other pharmacological agents known to interact with the cAMP-dependent pathway stimulated by isoprenaline were investigated.

6.2.4.1 Effects of gU-II on forskolin enhancement of $I_{Cl,cAMP}$

Figure 6.8 shows the results of an experiment with forskolin which directly stimulates adenylyl cyclase. A sub-maximal dose (0.5 µM) of forskolin caused an increase in chloride conductance after a lag of around 1 minute (longer than the delay for isoprenaline). A subsequent application of 150 nM human urotensin II produced a large further increase in chloride conductance. This potentiation of the catecholamine response was also dose dependent with an increase in normalized slope conductance from 20.9 ±3.9 pS/pF (n=16) in the presence of 0.25-0.5 µM forskolin to 29.0 ±9.5 pS/pF (n=11) and 39.8 ±6.6 pS/pF (n=5) after the further addition of 36 and 150 nM hU-II. These results are summarised in figure 6.9a. On average, 36 nM hU-II produced a proportional increase of 1.25 ±0.03 (n=11) while 150 nM hU-II caused an increase of 1.76 ±0.11 (n=6; figure 6.9b).

Figure 6.10 shows an experiment where a higher dose of forskolin was applied. In contrast to the above results, 1 µM forskolin produced a large increase in chloride conductance which was not affected by the addition of 150 nM GU-II (n=3).

The effects of urotensin II on both sub-maximal and saturating doses of forskolin thus parallel the results with isoprenaline. In both cases, a dose-dependent potentiation of previous sub-maximal activation of the cAMP-dependent pathway could be seen, with the chloride conductance roughly doubled by 150 nM urotensin II.

6.2.4.2 The effects of gU-II in the presence of Rp-cAMPS

When the cAMP antagonist, R_p-cAMPS (0.1 mM), was added to the pipette dialysing solution, not only was the response to 20 nM isoprenaline abolished but also the additional conductance elicited by the subsequent addition of 150 GU-II. This observation serves to confirm that the gU-II acts by enhancing the stimulatory effects of isoprenaline on the same cAMP-dependent catecholamine-activated chloride conductance, $I_{Cl,cAMP}$.

6.3 Discussion

6.3.1 Effects of Urotensin II on $I_{Cl,cAMP}$

6.3.1.1 Human and Goby urotensin II

The vasoconstrictor urotensin II was able to induce a large increase in whole cell conductance during sub-maximal catecholamine stimulation. The extra current is outwardly-rectifying, is only seen in the presence of isoprenaline and reverses near the predicted chloride Nernst potential, all of which are characteristics of the cAMP-dependent chloride current ($I_{Cl,cAMP}$) carried by the CFTR channel. At 150 nM, both the human and goby isoforms of urotensin II caused a similar large potentiation of the isoprenaline response, to almost double $I_{Cl,cAMP}$. Given the conservation of the putative active site at the cyclic structure of the peptide (Coulouarn *et al.*, 1998), it is likely that fish and human urotensin II act via the same receptor.

6.3.1.2 Response kinetics

The slow bath perfusion system used takes around 30-40 s for solution exchange which is roughly the lag before urotensin II elicited a conductance change. Despite this experimental limitation, it is still clear the action of U-II on cardiac myocytes is much faster than the development of vasoconstriction. Contractions in rabbit thoracic aorta or coronary artery (Saetrum Opgaard *et al.*, 2000) or rat thoracic aorta (Nothacker *et al.*, 1999) take around 10-20 minutes to develop and reverse with very slow time courses. This is much slower than responses in $I_{Cl,cAMP}$ which reach their peak after application of U-II or decrease after washout after less than three minutes. It may be that the a slow distal step is rate-limiting for vasoconstriction as urotensin II-evoked Ca^{2+} mobilisation can be detected by fluo-3 within 18 s in CHO cells transiently transfected with GPR14 (Nothacker *et al.*, 1999).

6.3.1.3 Urotensin dose response relationship

The doses of urotensin II used in this study were much higher than the approximately nanomolar vasoconstriction EC_{50} (e.g. Ames *et al.*, 1999, Saetrum Opgaard *et al.*, 2000) or radioligand binding affinities (Maguire *et al.*, 2000, Ames *et al.*, 1999). 150 nM gU-II produces a larger response than 36 nM, suggesting that the latter concentration is not saturating. A full dose-response curve would be needed to confirm that potentiation of $I_{Cl,cAMP}$ does require these higher levels of urotensin II. There is no obvious explanation either for the curious inhibition in a majority of cells of the isoprenaline-induced chloride current by 300 nM gU-II. It is possible that gU-II acts on both stimulatory and inhibitory pathways whose effects predominate at different ranges of concentration. There have been reports that fish urotensin II in rat aorta produces

both vasorelaxant effects at low concentrations (sub-nanomolar; Gibson, 1987) and vasoconstriction at higher doses (nanomolar; Itoh *et al.*, 1987).

[D-Trp$_7$]U-II-(5-10) has been suggested as an antagonist based on molecular modelling data (Perkins *et al.*, 1990), but functional assays at concentrations up to 1 μM have not borne out that possibility (Nothacker *et al.*, 1999). The present lack of a specific antagonist means that a non-specific effect or action at another receptor other than GPR14 by urotensin II cannot be ruled out. Thus, just as the somatostatin analogue RC-160 has an affinity for GPR14 three orders of magnitude lower than urotensin II (though U-II does not bind or activate somatostatin receptors), so might urotensin II be activating an unknown paralogous receptor (Nothacker *et al.*, 1999).

6.3.2 *Mediatory pathways for responses to urotensin II*

The immediate aims of this course of research have included both the characterization of the urotensin II responses and the elucidation of the modulatory pathways which underlie the increase in chloride conductance. The preliminary results described in this chapter do not as yet provide any direct evidence for the involvement of any of the regulators known to act at the CFTR channel. However, the pattern of responses seen with different sympathetic stimuli is very suggestive.

Goby or human urotensin II more or less doubles the responses to either different sub-maximal doses of isoprenaline (5-20 nM) or forskolin (0.25-0.5 μM). The results are summarized in table 6.2. At higher concentrations of either isoprenaline (1 μM) or forskolin (1 μM), no further increase in chloride conductance could be seen with urotensin. The cAMP-antagonist R$_p$-cAMPS prevented gU-II from potentiating the

effects of 20 nM isoprenaline. These results all confirm the hypothesis that the urotensin II evoked current is indeed the catecholamine-dependent $I_{Cl,cAMP}$.

6.3.2.1 Involvement of Protein Kinase C

Protein kinase C (PKC) stimulation probably by the Ca^{2+} independent PKC-ε (Liedtke & Cole, 1998) potentiates subsequent CFTR channel activation by PKA in intact cardiac myocytes (Middleton & Harvey, 1998). Constitutive phosphorylation by cellular PKC is probably a prerequisite for protein kinase A and nucleotide activation of the CFTR (Fischer *et al.*, 1998). There is some uncertainty over whether PKC is stimulatory or permissive, but this probably depends on the basal phosphorylatory levels of PKC and PKA which may vary from one experimental system to another. However, Middleton and Harvey (1998) report that PKC activation increased the magnitude of the response to supramaximal isoprenaline which would be at odds with the results reported here. In addition, the dependence on the magnitude of the urotensin II response on the prevalent level of sympathetic stimulation is not immediately easy to reconcile with the effects of PKC.

6.3.2.2 Involvement of other protein kinases

This same objection would apply also to the possible involvement of membrane-associated protein kinase G which phosphorylates the R domain of CFTR both *in vitro* (Picciotto *et al.*, 1992) and *in vivo* in NIH-3T3 and rat intestinal IEC-CF7 cells (French *et al.*, 1995). The tyrosine kinase $p60^{c\text{-}Src}$ seems able to increase channel activity without protein kinase A phosphorylation (Jia *et al.*, 1997), which would not be consonant with the results presented in this chapter.

6.3.2.3 Possible mediation by cyclic GMP-inhibited phosphodiesterase

The obvious remaining candidate is cyclic GMP-inhibited phosphodiesterase (PDE). In the guinea-pig, cyclic GMP (cGMP) potentiates the results of *β*-adrenergic stimulation by inhibiting a type II PDE (Harrison *et al.*, 1986, Ono & Trautwein, 1991) with a Ki of 2.2 μM (Weishaar *et al.*, 1987). Intracellular dialysis of guinea pig ventricular myocytes with cyclic GMP shifts the dose-response curve for isoprenaline-evoked $I_{Cl,cAMP}$ to the left without changing the maximum current seen. 10 μM in the pipette can reduce the isoprenaline EC_{50} from 21 nM to 5.5 nM (Ono *et al.*, 1992). These authors report that cGMP only increased $I_{Cl,cAMP}$ with sub-maximal sympathetic stimulation, which is strikingly similar to the results presented in this chapter. If cGMP-inhibited-PDE causes a shift in the isoprenaline dose-response curve, this would account for the relationship between the efficacy of urotensin II and the prevalent levels of cAMP-dependent pathway stimulation.

6.3.2.4 Modulatory pathways in the vascular smooth muscle

Saetrum Opgaard *et al.* (2000) have presented evidence that phospholipase C and the phosphoinositide signal transduction pathway is implicated as the vascular signal transducer. It is suggested that the $G_{q/11}$-protein plays the vital coupling role for GPR14 (Liu *et al.*, 1999; Nothacker *et al.*, 1999) at least in the cultured cells used for calcium mobilization assays (Ames *et al.*, 1999). It has also been reported that urotensin II increases the release of arachidonic acid from Chinese hamster ovary cells transfected with GPR14 (Mori *et al.*, 1999) and that the cyclooxygenase inhibitor indomethacin was effective in inhibiting the effects of urotensin II in frog artery (Yano *et al.*, 1995). Nevertheless, given the very different response profiles in cardiac and vascular myocytes,

and the known differences in physiologically important cellular signaling pathways, it is possible that urotensin II may be differentially coupled in the vascular bed and the heart.

These various possibilities will be the subject of ongoing investigations in this laboratory and will only be resolved with the use of specific inhibitors, e.g. 1*H*-[1,2,4]oxadiazolo[4,3-α]-quinoxaline-1-one (ODQ) for soluble guanylyl cyclase.

6.3.3 *Physiological relevance of the cardiac effects of Urotensin II*

It is still unclear what is the overall significance of urotensin II in normal and patho-physiology. In the absence of an antagonist, it is difficult to know what part this signalling peptide normally plays in regulating haemodynamics and cardiac function. The differing detected levels of kidney prepro-urotensin II mRNA in two separate studies (low in Coulouan *et al.*, 1998 and high in Nothacker *et al.*, 1999) have led to the suggestion that, if the kidney is the source of circulatory urotensin II, the production of this signalling peptide might be highly regulated. Urotensin is without doubt the most potent mammalian vasoconstrictor known. It is possible the effects described in this chapter are involved in the striking systemic effects upon U-II perfusion in primates. It would be too early to speculate why the cardiac responses are so much less sensitive yet more than an order of magnitude faster than those in the vascular bed.

Table 6.1 Urotensin II homologues in different species

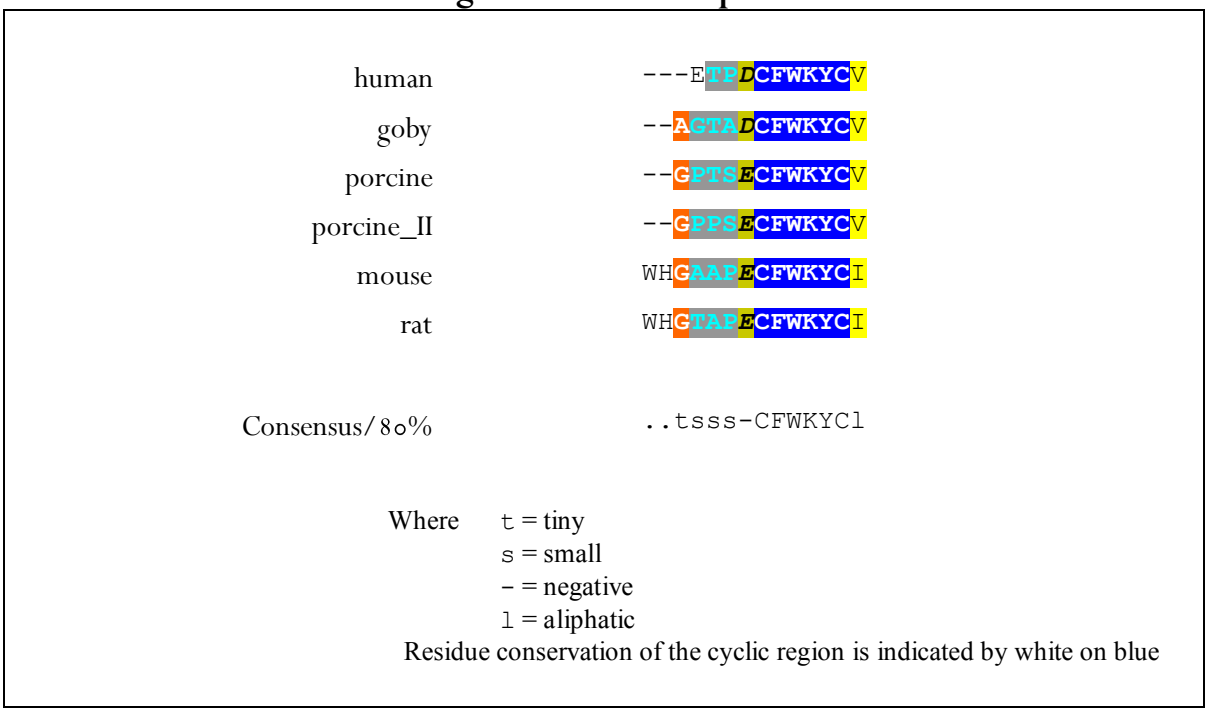

Table 6.2 Effects of 150 nM urotensin II on sub-maximal sympathetic stimuli

	Responses as a ratio to control (before application of urotensin II but during sympathetic stimulus)	
5 nM isoprenaline and 150 nM gU-II	1.74 ±0.17	(n=5)
10 nM isoprenaline and 150 nM gU-II	1.94 ±0.09	(n=5)
20 nM isoprenaline and 150 nM gU-II	1.92 ±0.16	(n=18)
5 nM isoprenaline and 150 nM hU-II	1.86 ±0.22	(n=4)
0.25-0.5 µM forskolin and 150 nM hU-II	1.76 ±0.11	(n=6)

Chapter Seven

Effects of Estrogenic agonists

on catecholamine-induced chloride current

7.1 Introduction:

Epidemiological studies have revealed gender-based differences in mortality from cardiac diseases. After puberty, pre-menopausal women suffer a much lower incidence of cardiovascular conditions such as ischemic heart disease than in age-matched men. The onset of menopause is, however, associated with an increased incidence of coronary heart disease (Stamfer *et al.*, 1991, Gardin *et al.*, 1995). The possibility that estrogen plays a cardio-protective role is confirmed by the beneficial effects of estrogen replacement therapy on cardiac morbidity (Stamfer *et al.*, 1991, Stamfer & Colditz, 1991). Estrogen is also known to have a positive effect on blood serum lipids but lipid changes in postmenopausal women only appears to account for 30-50% of the results of withdrawal of cardio-protective oestrogen (Adams *et al.*, 1990, Barrett-Connor *et al.*, 1991). Much of the remaining proportion is likely to be due to a direct estrogenic influence on the cardiovascular system.

Much previous research has focused on estrogenic effects on the vasculature. By contrast, the direct influences of estrogen on the heart, apart from its effects on the coronary perfusion, have received less consideration even though the steroid hormone is

known to play a role in the pathogenesis of left ventricular hypertrophy (Kannel *et al.*, 1976, Cabral *et al.*, 1988) and attenuation of contractile function (Scheuer *et al.*, 1987). When acutely administered, it reduces myocardial ischemic injury (Rosano *et al.*, 1993, 1997). 17*β*-Estradiol (E_2) appears to decrease the likelihood of ventricular arrhythmias in experimental models of regional ischemia-reperfusion (McHugh *et al.*, 1998, Li *et al.*, 2000) and to reduce contraction of perfused rabbit hearts (Raddino *et al.*, 1986).

In isolated guinea pig ventricular myocytes, 17*β*-oestradiol causes a rapid decrease in cell shortening accompanied by a decrease in action potential duration. This has been attributed to a reduction in L-type Ca^{2+} current; 10 and 30 μM 17*β*-Estradiol produces 31 ±3% and 61 ±5% inhibition respectively (Jiang *et al.*, 1992). Meyer *et al.* 1998 report that isoprenaline pre-stimulation increases sensitivity to estrogen at both lower (nanomolar) and higher doses (10 μM). This response may be due to the ability of estrogen at the near-physiological concentration of 1 nM to depress considerably cAMP production after application of high doses of either isoprenaline (100 nM) or forskolin (10 μM) (Li *et al.*, 2000). The negative modulation of I_{Ca} would be expected to be especially important in reducing heart rate and contraction, and hence oxygen consumption in ischemic tissues where a local increase of catecholamine is known to occur (Videbaek *et al.*, 1972, Karwatowska-Krynska & Beresewicz, 1983). The use of a fast perfusion system has revealed that the acute effects of estrogen on I_{Ca} proceeds after a lag of ~2 s with a time constant of 3.37 ±0.36 s (Meyer *et al.*, 1998).

Lipophilic steroid hormones like oestrogen are believed to diffuse through the cell membrane to bind to specific cytoplasmic protein receptors (Clark *et al.*, 1993). The

activated receptor complex is transported to the nucleus where it binds to enhancer elements in responsive genes and associated proteins to regulate transcription (Beato, 1989). However, the calcium antagonist effects of 17β-estradiol appear too fast for this classic transcriptional action. The exact mechanism of this rapid action of 17β-estrogen on I_{Ca} is not well understood, but its time course would be in accordance with a non-genomic transduction pathway as suggested for similarly acute responses in vasculature, breast, bone and neuronal tissue.

This hypothesis has been bolstered by recent evidence of cell-surface forms of estrogen receptors coupled to cytosolic signal transduction proteins from experiments using membrane-impermeant estrogen analogues (Russell *et al.*, 2000). The synthetic ER antagonists that block "classical" nuclear effects also appear to be effective against these novel signalling pathways, suggesting that the same receptor protein might be involved (Caulin-Glaser *et al.*, 1997). The α subtype of the oestrogen receptor, previously thought to act only as a transcriptional factor, has been identified, particularly concentrated in the caveolae, on membranes of cells demonstrating acute oestrogen-induced responses (Chen *et al.*, 1999, Russell *et al.*, 2000, Simoncini *et al.*, 2000). It has been shown to associate with endothelial nitric oxide synthase (eNOS) in endothelial cells in these membrane regions (Chen *et al.*, 1999). It is suggested that estrogenic activation of such receptors leads to rapid activation of eNOS and ultimately vasodilation.

Though specific binding of [^{3}H]17β-Estradiol could not be demonstrated in human ventricular myocytes (Sitzler *et al.*, 1996), estrogen receptors expression has been found in neonatal rat hearts (Grohe *et al.*, 1997), human atria and guinea pig and rat ventricular myocytes (Meyer *et al.*, 1998, Nuedling *et al.*, 1999). 17β-Estradiol

stimulates expression of eNOS and inducible nitric oxide synthase (iNOS) in rat myocardium *in vivo* and *in vitro* (Weiner *et al.*, 1994; Nuedling *et al.*, 1999), while NOS inhibition produces an increase in guinea-pig ventricular L-type calcium current (Gallo *et al.*, 1998). The most obvious inference is that estrogenic cardiac Ca^{2+} antagonism and vascular vasodilation are similarly mediated, with NOS in the pivotal role. Most intriguingly, Mermelstein *et al.* (1996) claim that a G-protein may be involved.

Despite the clear epidemiological evidence (Stampfer *et al.*, 1991, Colditz *et al.*, 1987) for the cardio-protective effects of hormone replacement therapy (HRT) whether due to its systemic or cardiovascular effects, fewer than 10% of post-menopausal women have taken up this option (Harris *et al.*, 1990). Both anecdotal evidence and clinical surveys have indicated that this reluctance is due to the various side effects of HRT, including resumption of menses, mastodynia, weight gain but especially estrogen-induced breast and uterine cancer (Judd *et al.*, 1983). The discovery of selective estrogen receptor modulators (SERMs) has provided some hope that it might be possible to enjoy the benefits of estrogen therapy without its drawbacks. SERMs are mixed agonist/antagonist compounds that display tissue specificity with regard to estrogenic effects. Thus, raloxifene hydrochloride (LY139481) prevents bone loss, lowers circulatory lipid (Delmas *et al.*, 1997, Kauffman *et al.*, 1997) and aortic accumulation of cholesterol (Bjarnason *et al.*, 1997) like 17β-estradiol but without producing uterine proliferation (Delmas *et al.*, 1997) or increasing the risk of breast cancer (Sato *et al.*, 1996).

The research project detailed in this chapter had two main objectives: to further characterise the putatively G-protein-mediated fast response to estrogenic agonists in

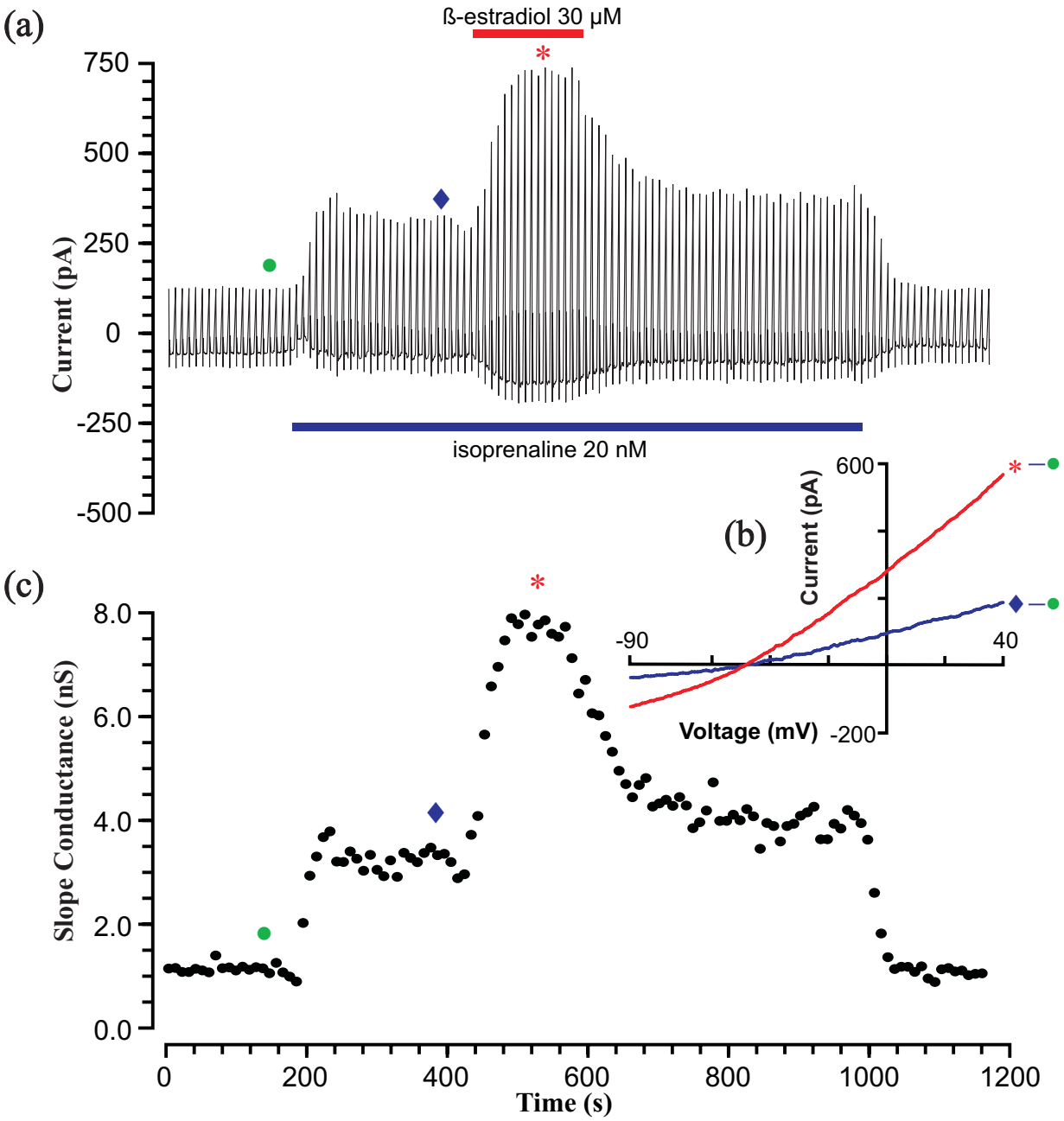

Figure 7.1

An example of the application of 30 µM ß-Estradiol in the presence of 20 nM isoprenaline. (*a*) Continuous record of whole cell current responses to voltage ramps showing that the whole cell current evoked by isoprenaline (♦) relative to control (●) is further increased dramatically by ß-Estradiol (*). This increase decayed rapidly upon removal of ß-Estradiol. (*b*) I-V curves from the current traces in *a*. The difference currents had a reversal potential around -50 mV and were outwardly rectifying. (*c*) The time course of changes in slope conductance measured at 0 mV illustrating the rapid changes in $I_{Cl,cAMP}$ evoked by ß-Estradiol in combination with isoprenaline.

ventricular myocytes and to see if an SERM such as raloxifene is similarly potent. The catecholamine-induced chloride current ($I_{Cl,cAMP}$) was used as an assay for the response to estrogen. This current is modulated by the same cAMP-dependent pathway which regulates estrogen-sensitive I_{Ca} (Bahinski *et al.*, 1989, Harvey & Hume, 1989), but has a number of additional advantages as a test system investigating the underlying signalling pathways. $I_{Cl,cAMP}$ has been relatively well characterised, shows little or no current run-down under the described experimental conditions, and, most importantly, displays neither voltage-dependent activation nor inactivation, allowing modulated changes to be analysed easily. If the proximate cause of I_{Ca} inhibition is the reduction in cAMP production by estrogen (Li *et al.*, 2000), this steroid should produce even more dramatic reductions in β-adrenoreceptor-activated $I_{Cl,cAMP}$.

7.2 Results:

7.2.1 17ß-Estradiol potentiates the catecholamine-induced chloride current

The application of isoprenaline induced a voltage and time-independent current. The I-V relation of this catecholamine-activated current, calculated by subtracting the control current from that in the presence of isoprenaline, was outward rectifying in asymmetric chloride solutions and had a reversal potential near the expected equilibrium potential for chloride. These are all characteristics of the well-described cardiac $I_{Cl,cAMP}$ (Bahinsky *et al.*, 1989; see section 6.2.1.1).

Figure 7.1 shows the modulation by 17β-Estradiol of the isoprenaline-activated chloride current. The top trace (*A*) is a continuous record of current in response to ramp pulses evoked every 10 s from -90 mV. The I-V relationship of the isoprenaline-induced conductance was calculated during hyperpolarising ramps by subtracting the control

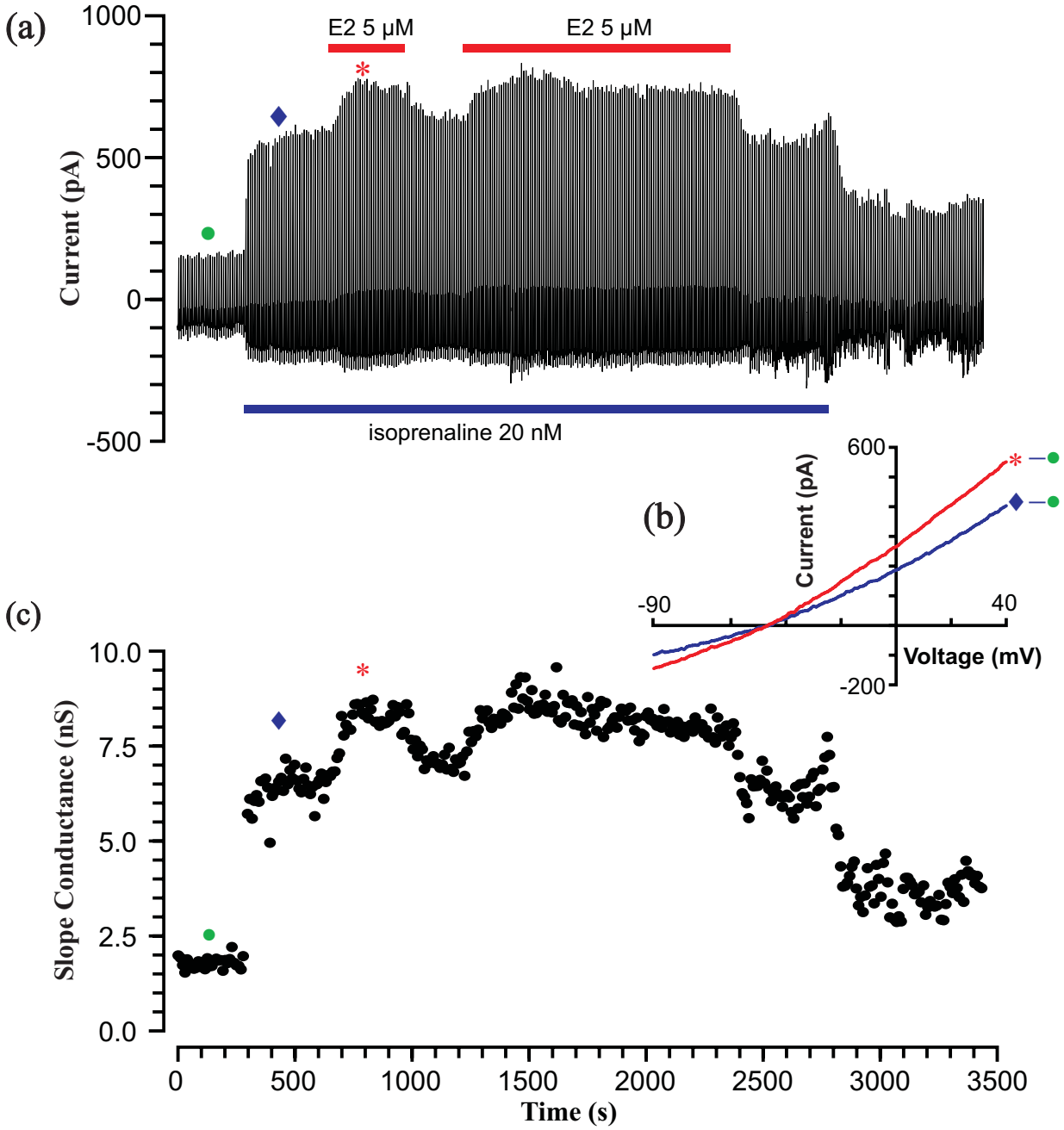

Figure 7.2

An example of the application of 5 µM ß-Estradiol (E2) in the presence of 20 nM isoprenaline. (*a*) Continuous record of whole cell current responses to voltage ramps showing low doses of ß-Estradiol (*) cause a correspondingly small further potentiation of the increase in whole cell current evoked by isoprenaline (♦) relative to control (•). (*b*) I-V curves from the current traces in *a.* The difference currents had reversal potentials around -50 mV and were outwardly rectifying. (*c*) The time course of changes in slope conductance measured at 0 mV. ß-Estradiol was applied twice in this cell. Each time, the increased chloride conductance decayed back rapidly on removal.

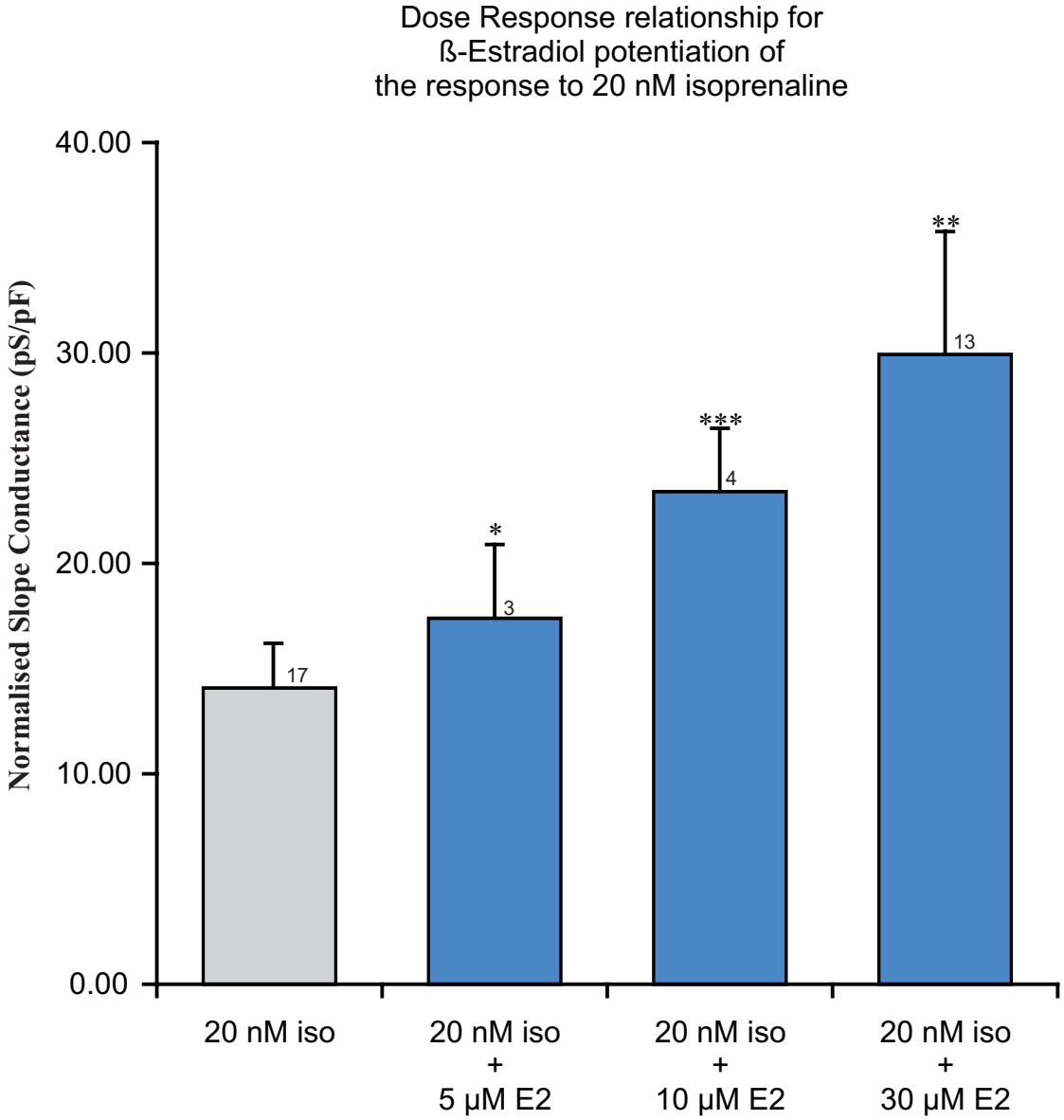

Figure 7.3a

The effects of different concentrations of ß-Estradiol (E2) on chloride conductance in the presence of a sub-maximal dose (20 nM) of isoprenaline (iso). ß-Estradiol clearly potentiates the isoprenaline induced chloride current in a dose-dependent manner.

Slope conductances were measured at 0mV during hyperpolarising voltage ramps. The values were recorded after each response had reached its plateau and all values are relative to control. Significant changes from the isoprenaline response ($p < 0.05$, 0.01 & 0.001) are indicated with asterisks (*, **, ***) and the number of cells for each experiment are printed by the error bars.

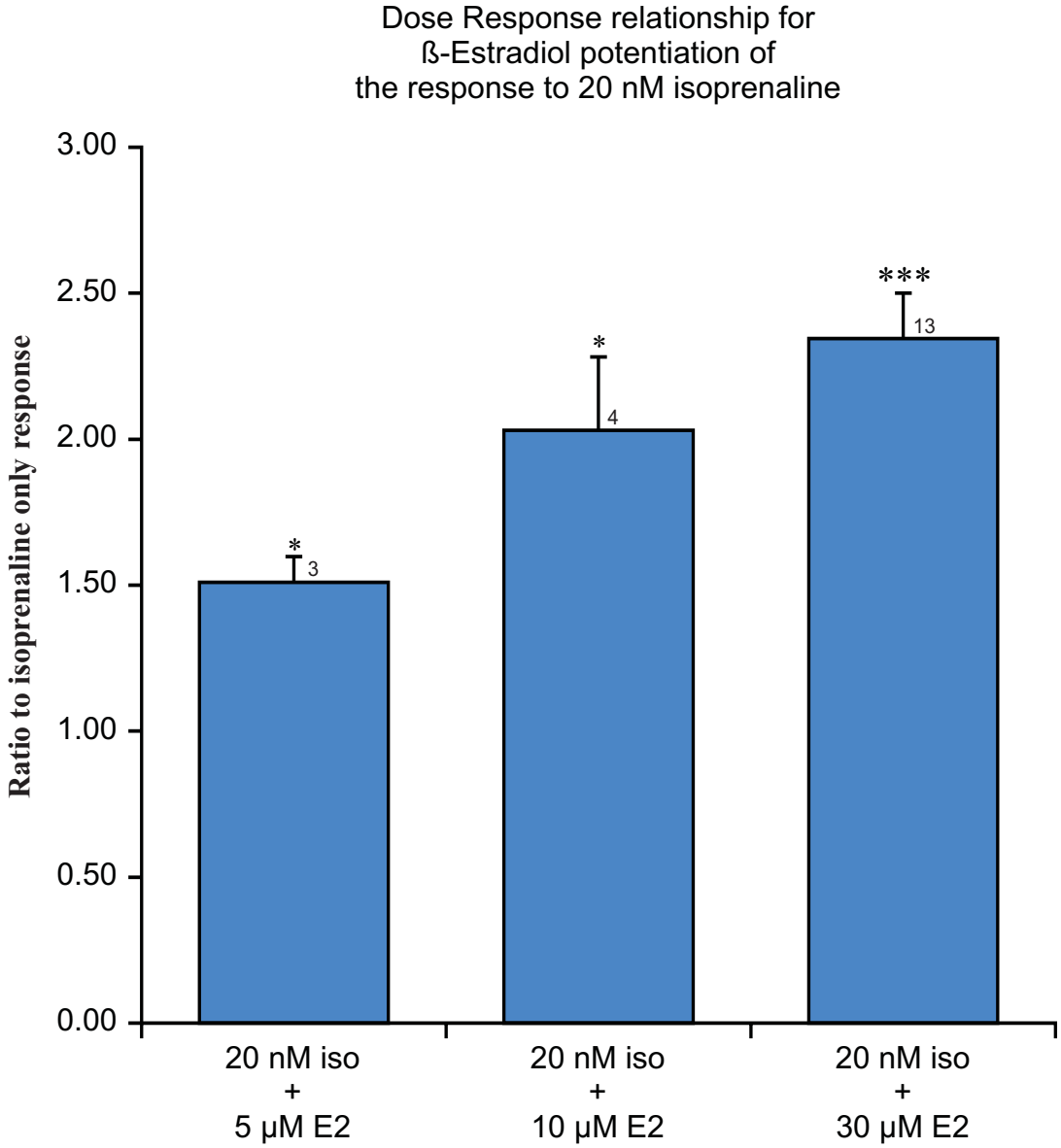

Figure 7.3b

The effects of different concentrations of ß-Estradiol (E2) in the presence of a sub-maximal dose (20 nM) of isoprenaline (iso). ß-Estradiol potentiates the iso response in a dose-dependent manner, and at 30 µM, it more than doubles the chloride conductance.

The effects of E2 in each experiment were calculated as a proportion of the iso-evoked conductance and then averaged across the cells. Thus ratios greater than 1 indicate increased $I_{Cl,\ cAMP}$. The slope conductances at 0 mV during hyperpolarising voltage ramps was used as a measure of chloride current. Significant changes from the isoprenaline response ($p < 0.05$, 0.01 & 0.001) are indicated with asterisks (*, **, ***) and the number of cells for each experiment are printed by the error bars.

basal background current (•) and is displayed in *B*. During the maintained superfusion of a sub-maximal concentration (20 nM) of isoprenaline, the additional application of 30 µM 17*β*-Estradiol in the superfusate further increased the amplitude of the current deflections during the ramp pulses without changing the reversal potential from ~-50-55 mV. This current increase had a fast onset, within the range for bath diffusional exchange (~30-40 s), and reached a peak after around 1.5-2 minutes. Washing out 17*β*-Estradiol resulted in a return of the current to its previous levels in the presence of isoprenaline with a similar time course. The changes in slope conductances were measured by calculating the regression line near 0 mV and show clearly the dramatic changes. 30 µM 17*β*-Estradiol more than doubles the chloride conductance (235 ±16%; n=13).

The effects of 17*β*-estradiol were dose-dependent, with a detectable potentiation of the catecholamine response seen after 5 µM (Figure 7.2), though the time course of the current changes remained roughly the same. Figure 7.3a summarises mean slope conductances relative to the capacitive area of the cell membrane seen at different concentrations of 17*β*-estradiol. The potentiation of the isoprenaline-evoked chloride conductance by 17*β*-estradiol can be examined even more clearly cell-by-cell rather than as aggregate conductances. Figure 7.3b shows the averages of the proportional change in $I_{Cl,cAMP}$ in each cell after application of 17*β*-estradiol. These ranged from 1.51 ±0.09 at 5 µM to 2.35 ±0.16 at 30 µM.

In the absence of isoprenaline, even 30 µM 17*β*-estradiol had no detectable effect on the background membrane conductance. Inclusion of 1 mM R_p-cAMPS not only

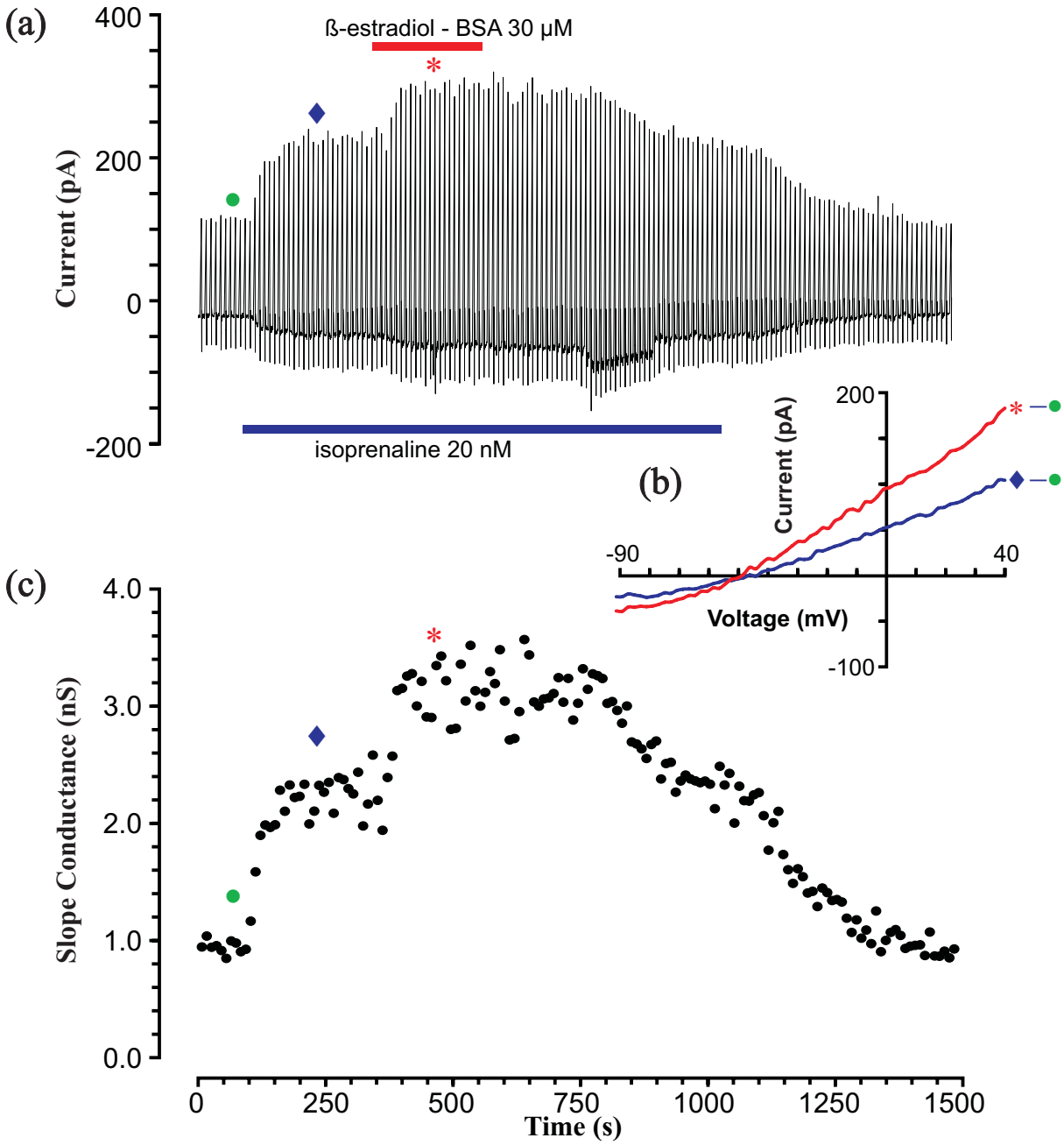

Figure 7.4

An example of the application of 30 µM ß-Estradiol-BSA conjugate in the presence of 20 nM isoprenaline. (*a*) Continuous record of whole cell current responses to voltage ramps showing that the increase in whole cell current evoked by isoprenaline (♦) relative to control (•) is further potentiated by ß-Estradiol-BSA (*). This increase decayed very slowly after the withdrawal of ß-Estradiol-BSA. (*b*) I-V curves from the current traces in *a.* The difference currents had a reversal potential around -50 mV and were outwardly rectifying. (*c*) The time course of changes in slope conductance measured at 0 mV clearly illustrates the changes in $I_{Cl,cAMP}$.

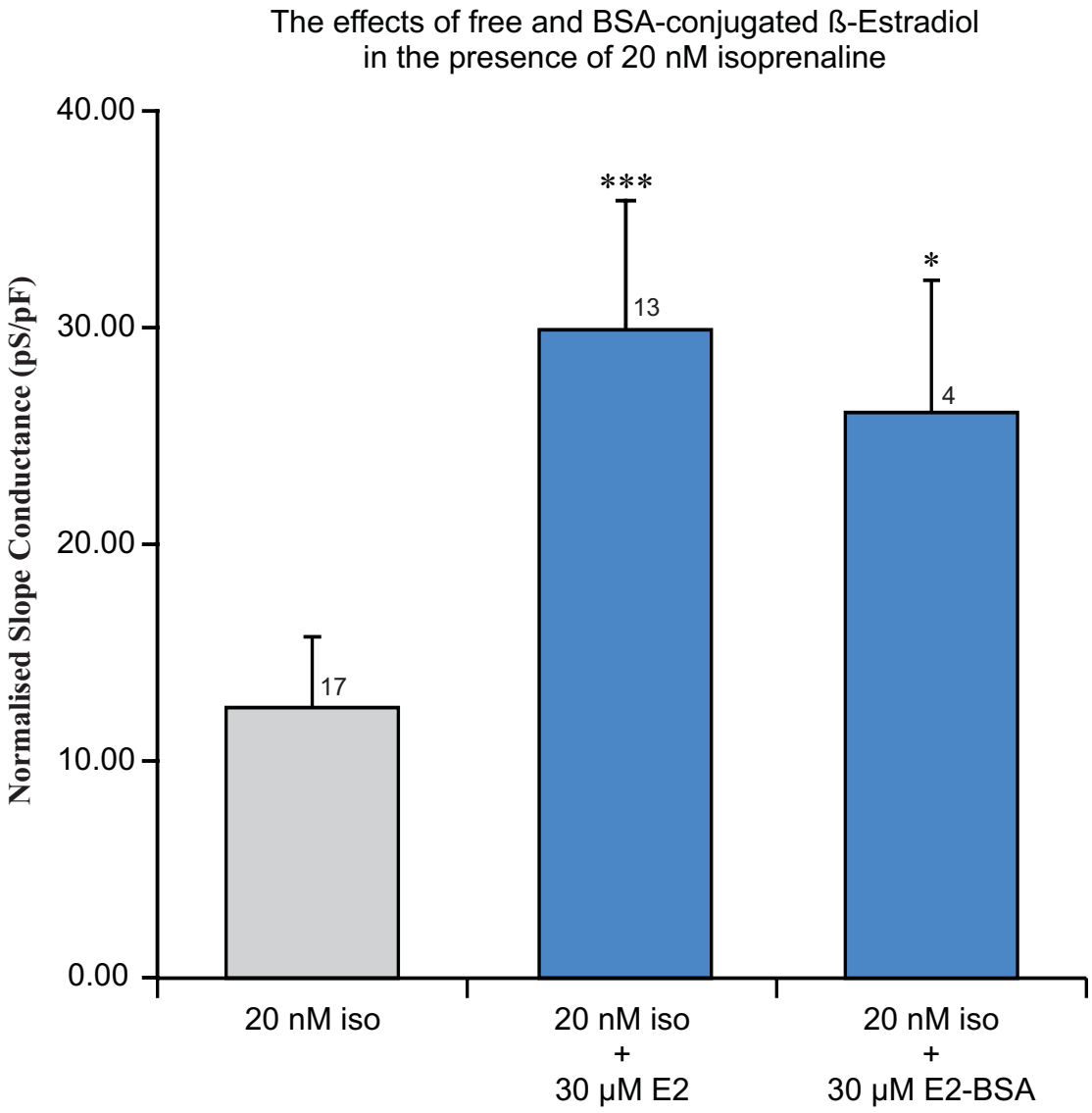

Figure 7.5

The effects of ß-estradiol (E2) and BSA conjugated ß-estradiol (E2-BSA) on chloride conductance in the presence of a sub-maximal dose (20 nM) of isoprenaline (iso). Both the free and conjugated forms of ß-estradiol produced similar and significant increases in the isoprenaline response.

Slope conductances were measured during hyperpolarising voltage ramps at 0mV. Measurements were made when each response had reached its plateau and all values are relative to control. Significant changes from the isoprenaline response ($p < 0.05$, 0.01 & 0.001) are indicated with asterisks (*, **, ***) and the number of cells for each experiment are printed by the error bars.

abolished the isoprenaline-activated chloride current but also eliminated any response to 17β-Estradiol (n=4). Both of these observations confirm that the additional current in the presence of 17β-Estradiol is due to potentiation of $I_{Cl,cAMP}$ which requires cAMP-dependent PKA phosphorylation.

7.2.2 Cell-impermeant 17ß-Estradiol potentiates $I_{Cl,cAMP}$

The kinetics for the current changes seemed much too rapid for a nuclear transcriptional effect. In particular, the rapid reversals on the washout of 17β-Estradiol suggest that the binding site is not energetically remote from the external medium. There has been recent evidence for the existence of cell-surface steroid hormone receptors (Russell *et al.*, 2000). To test the possibility of an extra-nuclear action of 17β-Estradiol, 17β-Estradiol conjugated to bovine serum albumin was applied. 17β-Estradiol-BSA is membrane-impermeant and has been extensively used to detect surface binding sites for 17β-Estradiol (Russell *et al.*, 2000, Collins & Webb, 1999). Figure 7.4 shows that 30 µM 17β-Estradiol-BSA was able to further increase the chloride current evoked by 20 nM isoprenaline. The rate of onset of action was also very similar to the response in figure 7.1. However, there was a 300 s delay after the superfusion of 17β-Estradiol-BSA-free isoprenaline solution before any decay in the response was seen. This much slower time course in the wash out was typical of responses with the conjugated steroid. The degree of potentiation by 17β-estradiol-BSA was not statistically different from the same concentration of free 17β-estradiol (figure 7.5).

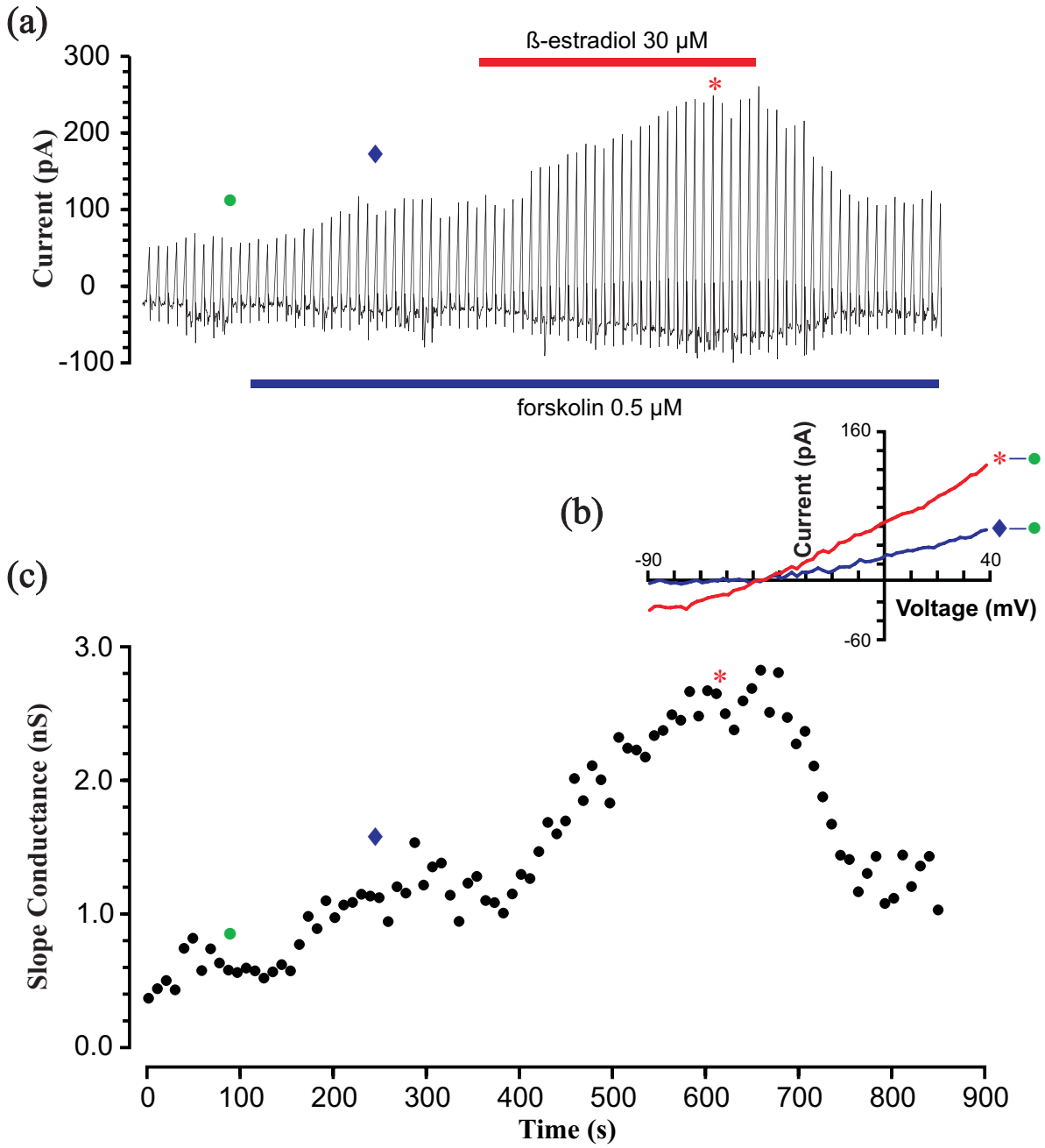

Figure 7.6

An example of the application of 30 µM ß-Estradiol in the presence of 0.5 µM forskolin. (*a*) Continuous record of whole cell current responses to voltage ramps showing that the increase in whole cell current evoked by 0.5 µM forskolin (♦) relative to control (•) is potentiated by ß-Estradiol(*). (*b, c*) I-V curves from the current traces in *a.* All the difference currents had reversal potentials around -50 mV and were outwardly rectifying. (*c*) The time course of changes in slope conductance measured at 0 mV show clearly that ß-Estradiol further increases forskolin evoked $I_{Cl,cAMP}$.

7.2.3 Forskolin

Although there has been a number of reports of the rapid effect of estrogenic agonists, exactly how their different effects are mediated is still not entirely clear. Mermelstein *et al.* (1996) report that 17*β*-estradiol inhibition of rat neostriatal neuronal L-type I_{Ca} was mediated by a G-protein. The possibility was investigated that the steroid hormone itself or its putative cell-surface receptor might either inhibit the G_s-protein coupling *β*-adrenergic stimulation or interact directly with the *β*-adrenoreceptor in a similar way to that reported for the insulin-like growth factor receptor (IGF-R) (Kahlet *et al.*, 2000). The efficacy of isoprenaline would be increased, for example, if either the agonist-bound *β*-adrenergic receptor or its interaction with the $G_s\alpha$ subunit were stabilised.

Figure 7.6 sets out the results of the application of a sub-maximal dose (0.5 μM) of forskolin, which directly stimulates adenylyl cyclase. This produced an increase in $I_{Cl,cAMP}$ after a slightly longer lag than with 20 nM isoprenaline. If 17*β*-estradiol interacts directly only with the *β*-adrenoreceptor protein, it should cause no further change in the forskolin-evoked current. Instead, the addition of 30 μM of the steroid agonist in the superfusate produced a degree of potentiation of forskolin-induced $I_{Cl,cAMP}$ (237 $\pm$31%) which was not significantly different from the amplification of the isoprenaline response (unpaired Student's t-test; $p = 0.96$).

7.2.4 Inhibition of Nitric Oxide Synthase

The potentiation by 30 μM 17*β*-Estradiol of the cAMP-dependent chloride current was somewhat surprising given reports that this steroid hormone reduces forskolin- and isoprenaline-stimulated cAMP accumulation in rat heart (Li *et al.*, 2000).

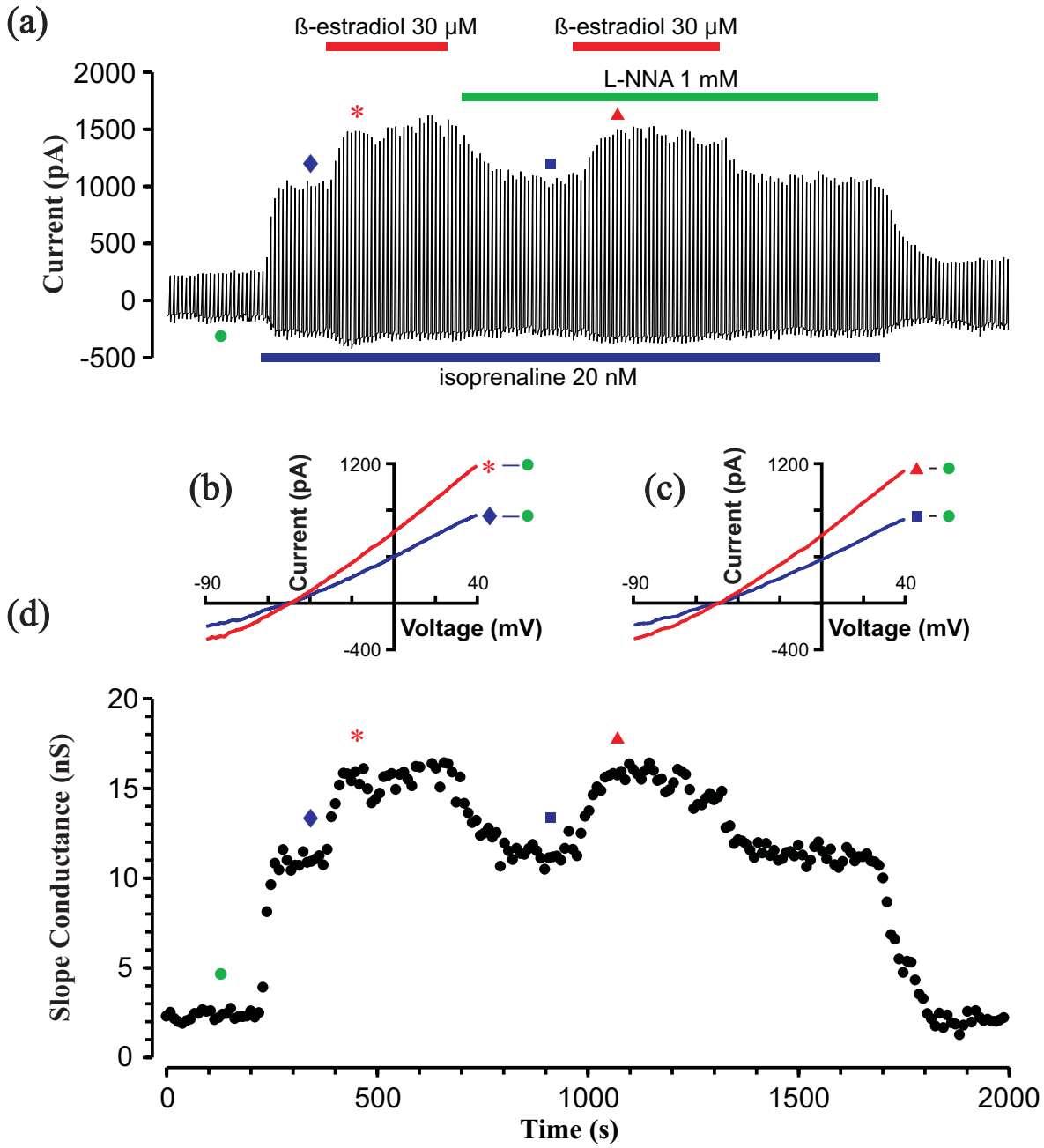

Figure 7.7

An example of the application of 30 µM ß-Estradiol with and without the presence of 1 mM L-NNA, a potent NOS inhibitor. (*a*) Continuous record of whole cell current responses to voltage ramps showing that the increase in whole cell current evoked by isoprenaline (♦) relative to control (●) is potentiated by ß-Estradiol (*) even in the presence of L-NNA (■, ▲). (*b, c*) I-V curves from the current traces in *a.* All the difference currents had a reversal potential around -50 mV and were outwardly rectifying. (*d*) The time course of changes in slope conductance measured at 0 mV show clearly that the effects of the two application of ß-Estradiol are not significantly different.

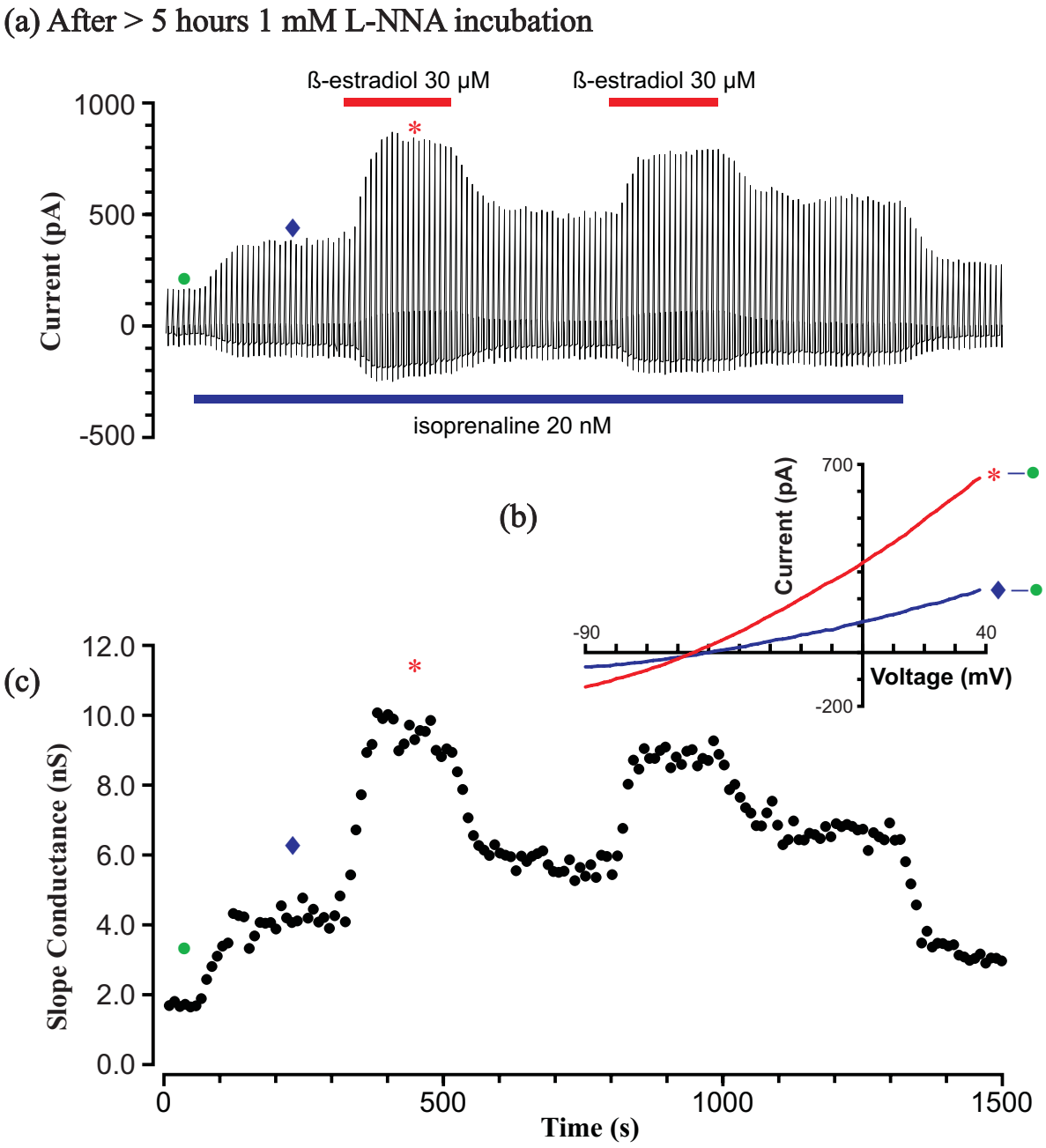

Figure 7.8

A typical response to the application of 30 µM ß-Estradiol in the presence of, and after 30 minutes incubation with, 1mM L-NNA, a potent NOS inhibitor. (*a*) Continuous record of whole cell current responses to voltage ramps showing that the increase in whole cell current evoked by isoprenaline (♦) relative to control (•) is potentiated by ß-Estradiol(*) even in the presence of L-NNA. (*b, c*) I-V curves from the current traces in *a.* Both the outwardly rectifying difference currents had reversal potentials betwen -50 to -55 mV. (*c*) The time course of changes in slope conductance measured at 0 mV show clearly that the effects of ß-Estradiol are not significantly inhibited by L-NNA.

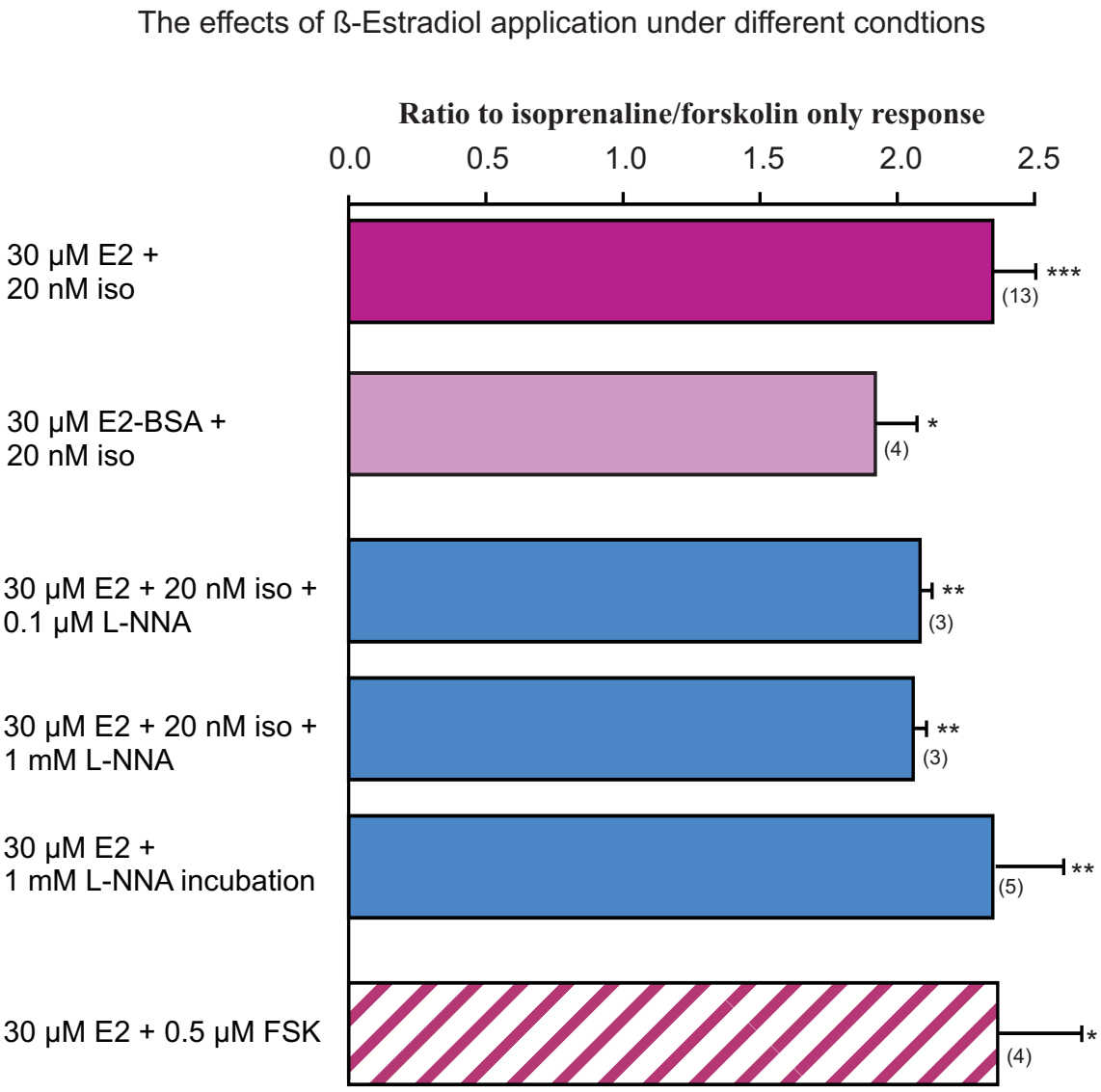

Figure 7.9

The effects on chloride conductance of 30 µM ß-Estradiol (E2). In each case the elicited chloride current was further increased around two-fold. This was true whether ß-Estradiol was applied in the presence of sub-maximal doses of isoprenaline (20 nM iso) or forskolin (0.5 µM FSK), or in the addition presence of the NOS inhibitor L-NNA. The effects of ß-Estradiol in each experiment were calculated as a proportion of the iso- or FSK- evoked conductance and then averaged across the cells. Thus ratios > 1 indicate increased $I_{Cl,\ cAMP}$. The slope conductance at 0 mV during hyperpolarising voltage ramps was used as a measure of chloride current. Significant changes from the control isoprenaline or forskolin response ($p < 0.05$, 0.01 & 0.001) are indicated with asterisks (*, **, ***) and the number of cells for each experiment are printed by the error bars.

Endothelial Nitric Oxide Synthase (eNOS) is a common effector in the rapid non-transcriptional action of 17β-Estradiol in endothelia (Haynes *et al.*, 2000, Lantin-Hermoso *et al.*, 1997, Caulin-Glaser *et al.*, 1997). Inhibition of eNOS produces an increase in guinea-pig ventricular L-type calcium current (Gallo *et al.*, 1998). On the other hand, as in human umbilical vein endothelial cells (HUVEC), eNOS activation in guinea pig results in production of cGMP which would increase $I_{Cl,cAMP}$ (Ono & Trautwein, 1991). This might explain the contrasting 17β-Estradiol modulation of $I_{Cl,cAMP}$ and $I_{Ca,L}$.

The NOS inhibitor N-ω-nitro-L-arginine (L-NNA) is a potent inhibitor of both nNOS (IC_{50} = 0.025 µM for the isolated enzyme) and eNOS (IC_{50}=0.09 µM) (Reif & McCreedy, 1995). 30 µM 17β-Estradiol produced similar potentiations of the isoprenaline (20 nM) response before and after 5 minutes superfusion with either 0.1 or 1 mM L-NNA (figure 7.7). No significant inhibition (p = 0.95) was seen even after 20 minutes incubation with L-NA before the experiment and in its subsequent continuous presence (233 ±26%; n=5; figure 7.8). These results are summarised in figure 7.9.

7.2.5 *Estrogenic role in ventricular volume regulation*

Tareen *et al.* (1991) report that 10-200 nM isoprenaline consistently caused a decrease of membrane capacitance from 166 ±31 pF by about 19 ±12% (n=10) in guinea pig ventricular myocytes in parallel with the induction of chloride current. Accordingly, the effects of 20 nM isoprenaline and further addition of 30 µM 17β-estradiol on changes in membrane capacitance as a measure of cell volume were examined. The cell capacitance was measured by dividing the half-amplitude of the current jump from depolarising to hyperpolarising ramp pulses by the rate of voltage

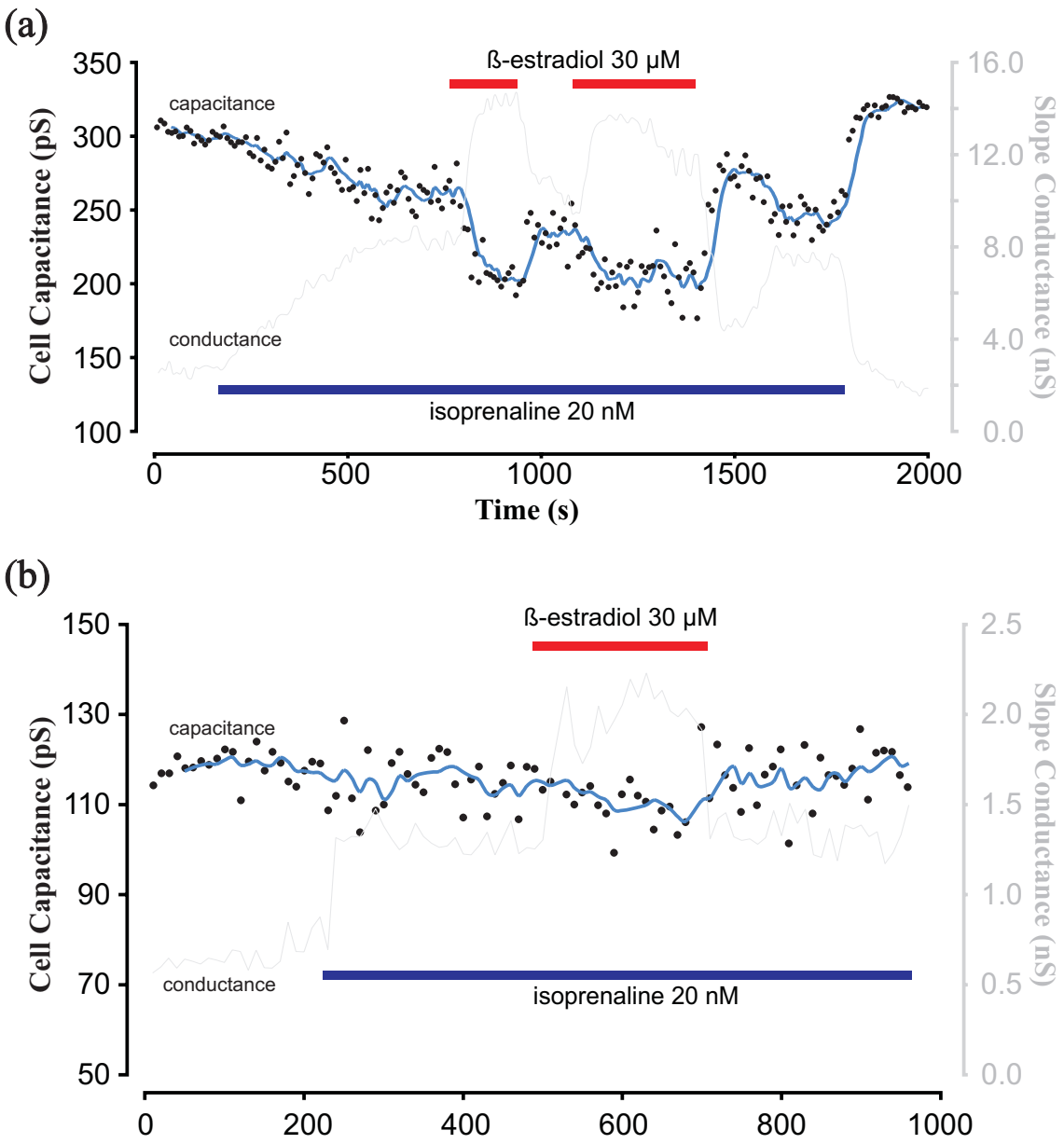

Figure 7.10

The effects on cell capacitance of the application of 30 µM Estradiol in the presence of 20 nM isoprenaline in two different cells. In each graph, a running average () has been fitted to the raw data (•). The grey line () shows parallel changes in slope conductances. Decreases in cell capacitance mirroring increases in chloride conductance can only be seen in the larger cell in (a). The cell capacitances measured immediately after recordings begin in each cell were 384 pF and 131 pF respectively.

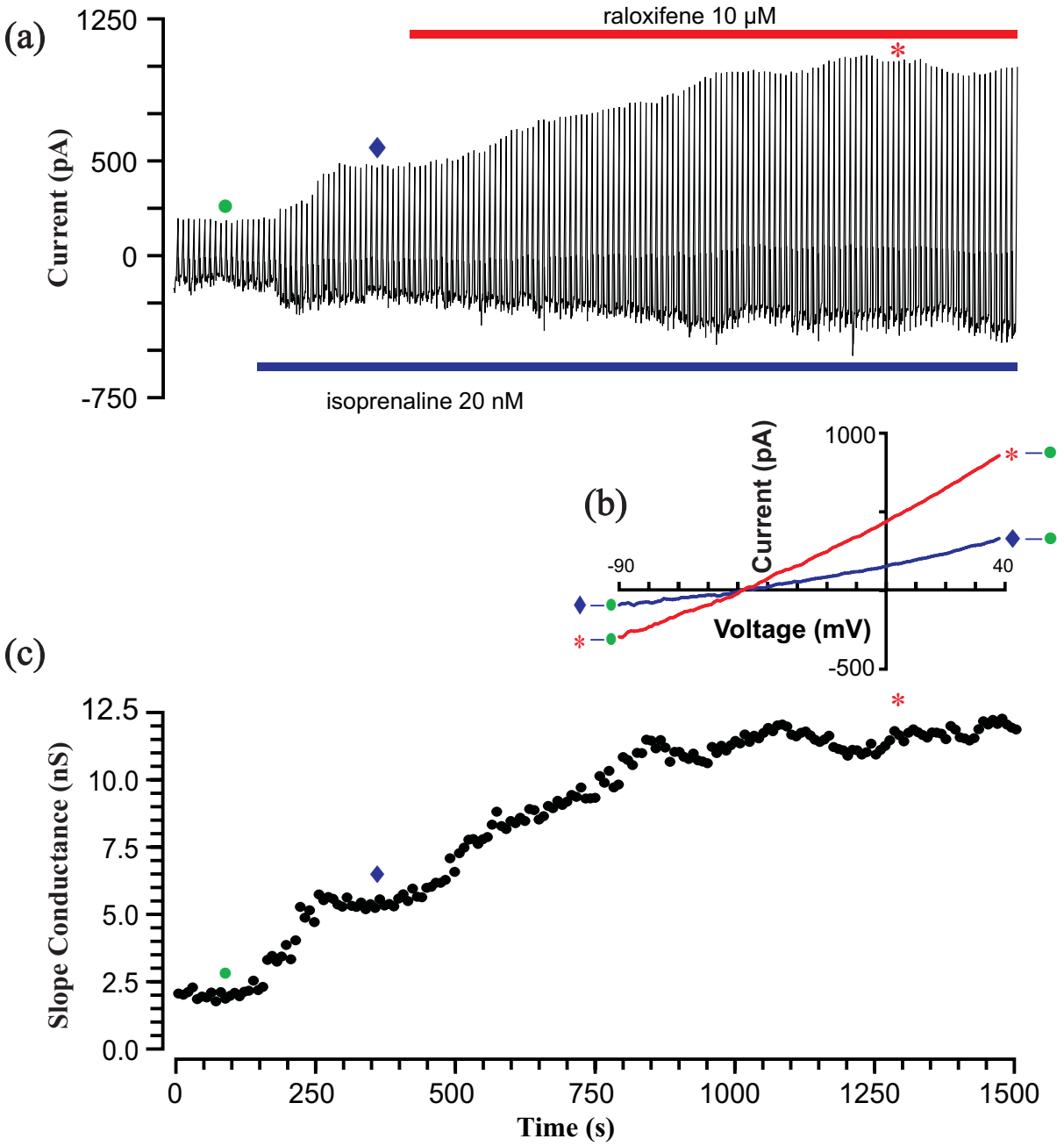

Figure 7.11

An example of the application of 10 µM Raloxifene in the presence of 20 nM isoprenaline. (*a*) Continuous record of whole cell current responses to voltage ramps showing that the increase in whole cell current evoked by isoprenaline (♦) relative to control (•) is further potentiated by Raloxifene. (*b*) I-V curves from the current traces in *a.* The difference currents had a reversal potential around -50 mV and were outwardly rectifying. (*c*) The time course of changes in slope conductance measured at 0 mV clearly illustrates the slow rise in $I_{Cl,cAMP}$. Raloxifene produces a sustained increase in chloride conductance which reached a peak after 10 minutes in this cell.

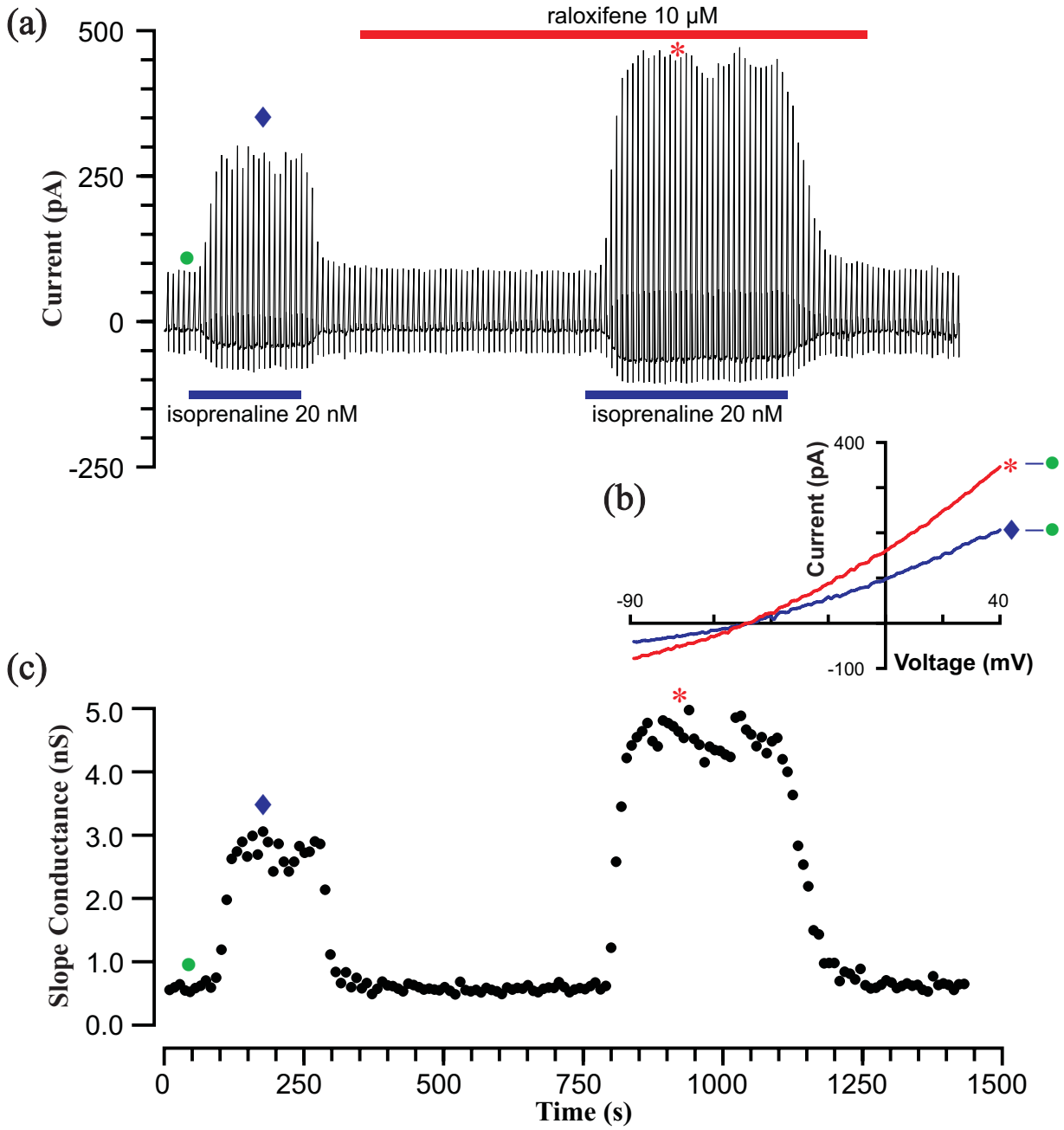

Figure 7.12

An example of the application of 10 µM Raloxifene in the presence of 20 nM isoprenaline. (*a*) Continuous record of whole cell current responses to voltage ramps showing that the increase in whole cell current evoked by isoprenaline (♦) relative to control (●) are further potentiated when Raloxifene is present as well (*). (*b*) I-V curves from the current traces in *a.* (*c*) The time course of changes in slope conductance measured at 0 mV. The application of Raloxifene alone produces no discernible changes in chloride conductance but increases the isoprenaline evoked response. The early application of Raloxifene also reduces the time to peak (see Figure 7.10 for comparison).

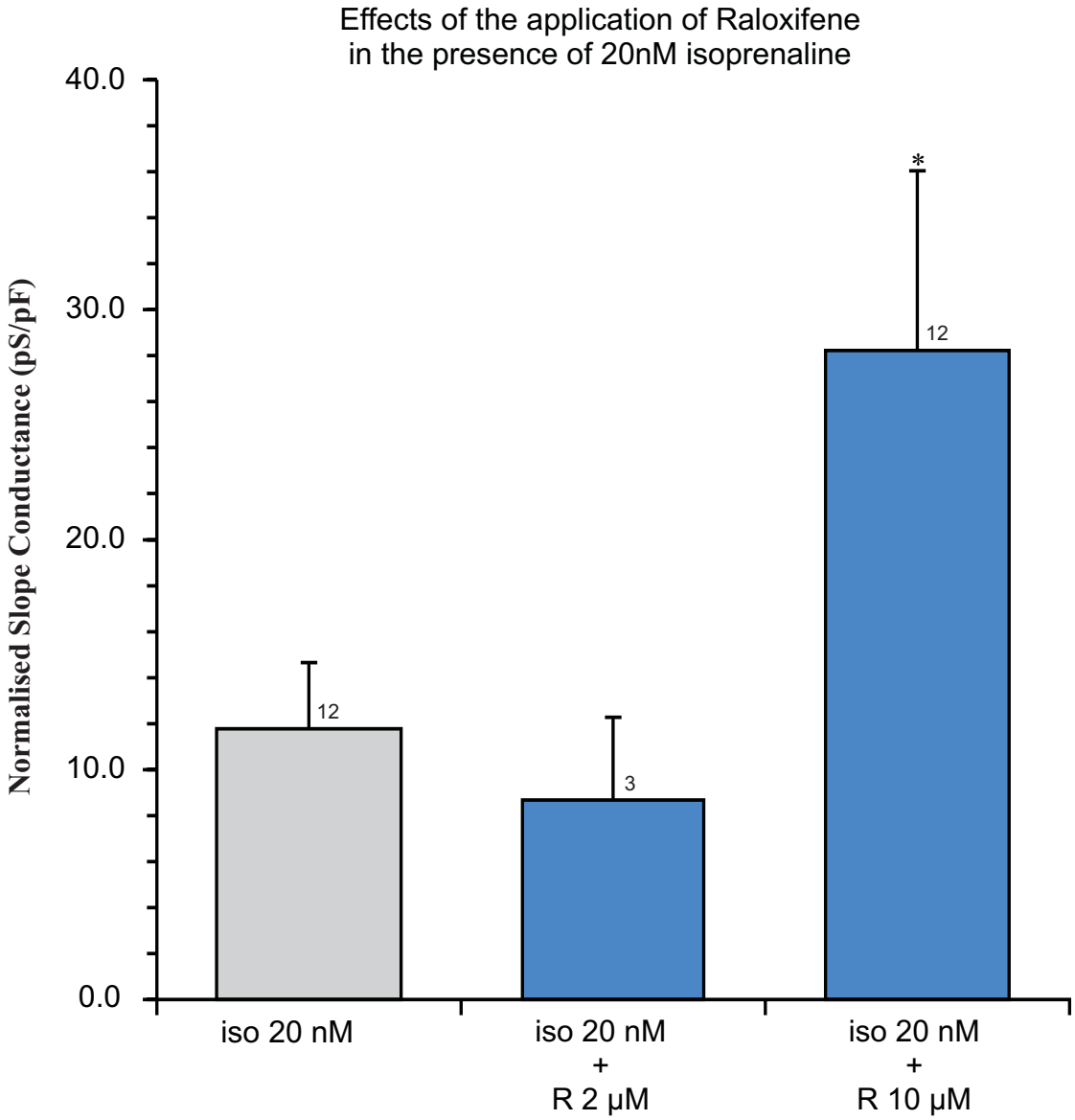

Figure 7.13a

The effects of different concentrations of Raloxifene (R) applied after a submaximal dose (20 nM) of isoprenaline (iso). 2 µM Raloxifene does not produce an appreciable change in chloride current but at 10 µM, it causes a significant increase.

Slope conductances were measured during hyperpolarising voltage ramps at 0mV. Measurements were made when each response had reached its plateau and all values are relative to control. Significant changes from the isoprenaline response ($p < 0.05$) are indicated with an asterisk (*) and the number of cells for each experiment are printed by the error bars.

change (dV/dt). No time-dependent current could be observed in this area of the voltage ramp.

In contrast to the results of Tareen *et al*. (1991), changes in cell capacitance in iso-osmotic solutions were clearly resolved in only 8 cells out of 167. Figure 7.10a shows results from one of these few cells. A total decrease in cell capacitance of up to 35% was recorded along with concomitant increases in chloride current after each of two applications of 17β-estradiol. Cell capacitances of at least 170 pF were recorded immediately after formation of the patch seal in each of the 8 cells. This was significantly higher than the average of 126 $\pm$4 pF (n=154). More typical was the result in figure 7.10b where small fluctuations in cell capacitance showed little correlation with either application of isoprenaline and 17β-Estradiol or changes in chloride current.

7.2.6 *Raloxifene*

There have not been any previous reports of SERM effects on ventricular myocytes, and it was not previously known whether raloxifene, which exhibits a mixed agonist/antagonist activity depending on tissue type, has an action similar to 17β-estradiol.

The application of 10 µM raloxifene produced a large sustained increase in the chloride current induced by 20 nM isoprenaline which only reaches a maximum after around 10 minutes (figure 7.11). The recovery after washout follows an even slower time course (not shown). 10 µM raloxifene is able to more than double (254 $\pm$27%; n=12) the isoprenaline response on average, while the response to 2 µM (133 $\pm$17%; n=4) is near the minimum detectable threshold (figure 7.12).

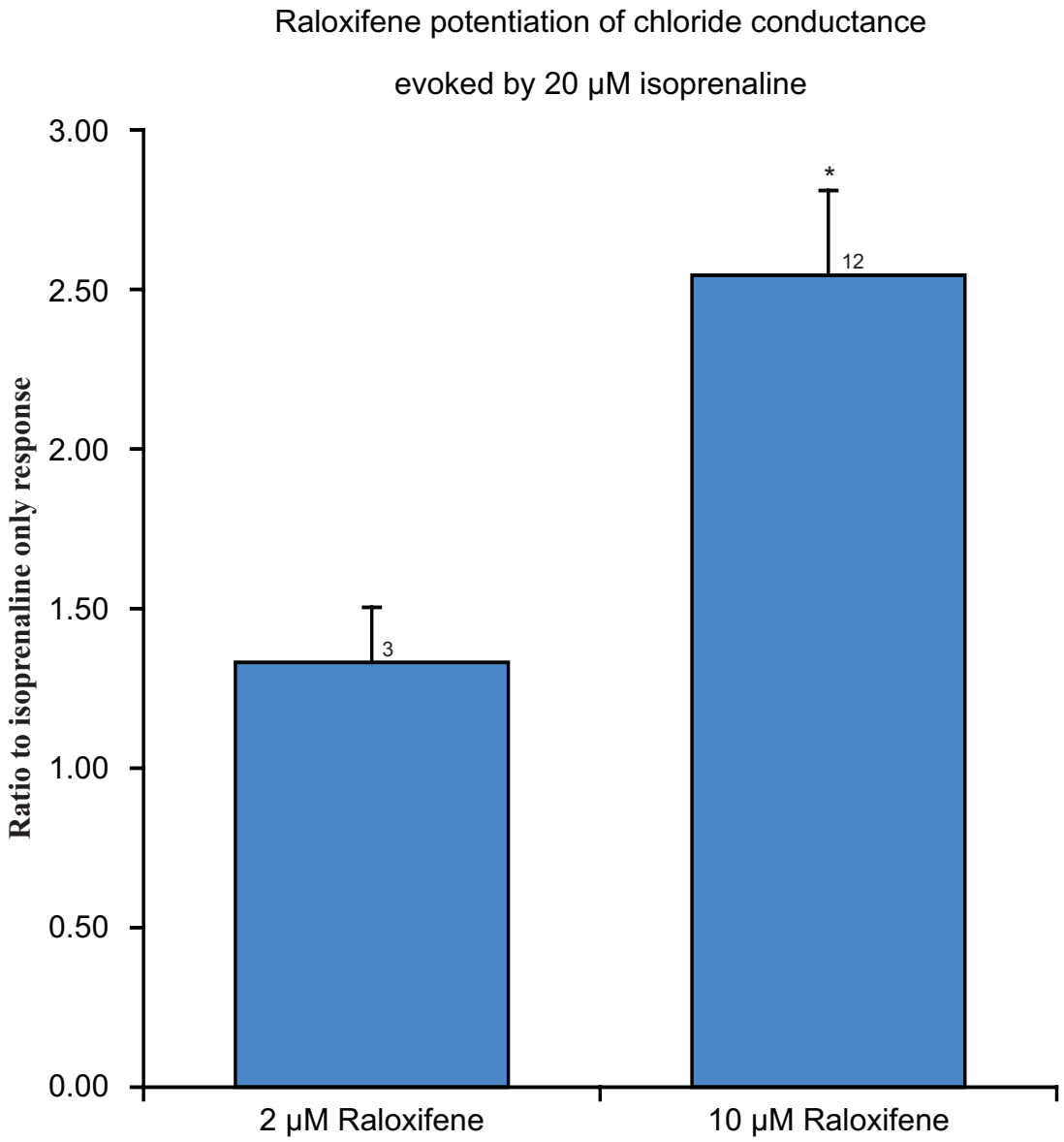

Figure 7.13b

The effects on chloride conductance of different concentrations of Raloxifene (R) applied after a submaximal dose (20 nM) of isoprenaline. 2 µM Raloxifene does not produce an appreciable conductance change but at 10 µM it more than doubles $I_{Cl, cAMP}$.

The effects of Raloxifene in each experiment were calculated as a proportion of the iso-evoked conductance and then averaged across the cells. Thus ratios greater than 1 indicate increased $I_{Cl, cAMP}$. The slope conductance at 0 mV during hyperpolarising voltage ramps was used as a measure of chloride current. Significant changes from the isoprenaline response ($p < 0.05$) are indicated with an asterisk (*) and the number of cells for each experiment are printed by the error bars.

Though raloxifene also causes an acute relaxatory response of rabbit coronary arteries, the time course for this is around 6-7 times slower (~90 minutes) than that for estrogen in the same tissue (Figtree *et al.*, 1999). If both 17β-estradiol and raloxifene acted, for example, by inhibiting either protein phosphatase or cAMP phosphodiesterase, the slow response to raloxifene might simply be a reflection of its poor efficacy rather than the intrinsic kinetics of this regulatory pathway. Figure 7.13 shows an experiment designed to explore this possibility. When the myocyte was pre-incubated with 10 µM raloxifene in the absence of isoprenaline, no increase in $I_{Cl,cAMP}$ was seen. The subsequent addition of 20 nM isoprenaline produced an increased current compared to control (before raloxifene incubation) which reached its peak within ~2 minutes. This chloride current was abolished by the withdrawal of isoprenaline. Thus, it seems that while raloxifene induced chloride current can only be observed during β-adrenoreceptor activation, the slow build-up of its effects does not require prior catecholamine-stimulation.

7.3 Discussion

7.3.1 Effects of 17β-estradiol

7.3.1.1 Estrogen causes rapid enhancement of catecholamine induced $I_{Cl,cAMP}$

The aim of this study was to use the catecholamine-induced chloride current in the guinea pig to characterise the regulatory pathways responsible for the estrogen inhibition of L-type Ca^{2+} current and cAMP synthesis in response to sympathetic stimuli. The amplitudes of $I_{Cl,cAMP}$ induced by sub-maximal doses (20 nM) of isoprenaline were reversibly potentiated in a concentration-dependent manner by 5-30 µM 17β-estradiol, a potent estrogenic agonist. This was a somewhat surprising observation,

given that both the catecholamine-induced chloride current $I_{Cl,cAMP}$ and L-type I_{Ca} are regulated by a common intracellular cyclic AMP system (Bahinski *et al.*, 1989, Harvey & Hume, 1989; Kameyama *et al.*, 1985).

It is difficult to see how the dramatic increases in chloride current described above are consistent with the depression of cAMP synthesis by even nanomolar concentrations of estrogen previously reported for the rat ventricle (Li *et al.*, 2000). One might speculate that the reduction in cAMP production is species-specific and does not occur in the guinea pig. The much higher concentrations of 17β-estradiol used in the present investigation (over four orders of magnitude higher) in the presence of lower isoprenaline levels (20 instead of 100 nM) might also have a different impact on the cAMP-dependent pathway. The results of Meyer *et al.*, (1998) suggest that the effects of estrogen on at least I_{Ca} are not straightforward: a biphasic dose-response curve with two log EC_{50} values of -6.8 and -4.9M in the absence of isoprenaline.

7.3.1.2 Estrogen sensitivity lies outside physiological concentrations

The concentrations of 17β-estradiol needed to increase $I_{Cl,cAMP}$ are much higher than the nanomolar concentrations in general circulation (Abraham *et al.*, 1972). An important question would be whether the estrogen sensitivity of $I_{Cl,cAMP}$ occurs in the physiological range. It is possible that washout of some critical regulatory proteins via pipette diffusion has resulted in a rightward shift of the dose-response curve for 17β-estradiol (Zakharov & Harvey, 1995) though this seems less likely in the absence of $I_{Cl,cAMP}$ run-down. To rule out this possibility, some of the critical experiments above will be repeated using the permeabilised patch technique and using a greater range of 17β-estradiol concentrations.

The loss of vital cofactors such as sexual hormone binding globulin (Nakhla *et al.*, 1994) in the isolation procedure may mean reduced presentation of the steroid hormone to the myocyte for the same concentration of free steroid hormone. It is also becoming clear that estrogen serves not only as a systemic circulating hormone but may also play a paracrine or "intracrine" role (Simpson *et al.*, 2000). Local estrogen synthesis in the heart may result in higher levels of the steroid hormone than in the circulation (Grohé *et al.*, 1998).

7.3.1.3 Locus of estrogen modulation

17*β*-estradiol is able to enhance sub-maximal forskolin- and isoprenaline-activated chloride current to roughly the same degree. This suggests that the steroid hormone acts at some point beyond the *β*-adrenoreceptor and G-protein and therefore inside the cell. The requirement for prior sympathetic stimulation is absolute, and no increases in chloride current can be elicited when the cAMP antagonist R_p-cAMPS is present or when isoprenaline is withdrawn.

7.3.1.4 Responses mediated at the cell surface

The classical action of the estrogen-bound receptors as transcription-regulatory factors occurs after a lag of many minutes and persists over hours. The observed rapid on- and off-rates suggests that 17*β*-estradiol acts at a site energetically close to the cell surface. The ability of 17*β*-estradiol to increase isoprenaline-induced chloride current even when conjugated to cell membrane-impermeable bovine serum albumin (BSA) supports the hypothesis that an estrogen cell surface receptor mediates the coupling between the extracellular estrogen application and its intracellular effects. Similar evidence has been provided for the acute estrogen activation of vascular endothelial

eNOS (Kim *et al.*, 1999, Russell *et al.*, 2000, Stefano *et al.*, 2000). It will be interesting to see if the specific estrogen receptor antagonist ICI 182 780 which blocks acute activation of endothelial eNOS (Caulin-Glaser *et al.*, 1997) is also able to abolish 17*β*-estradiol enhancement of catecholamine-induced chloride current. Similarly, if the binding site for this action of 17*β*-estradiol is extracellular, inclusion of this steroid hormone in the pipette dialysis solution should not compete with the effects of its application to the superfusate.

7.3.1.5 Modulatory pathways involved in estrogen enhancement of $I_{Cl,cAMP}$

Unlike in the vascular endothelia, nitric oxide synthase in ventricular myocytes does not seem to mediate the acute effects of estrogen in enhancing $I_{Cl,cAMP}$ because the responses persist in the face of high doses of and after incubation with the eNOS and iNOS inhibitor L-NNA. It is, nonetheless, possible (though unlikely) that eNOS activation by estrogen does occur *in vivo*. The buffered intracellular calcium levels in these experiments may be too low for the activation of constitutive eNOS (Balligand, 1999), though one might assume that residue calcium current through the incompletely blocked L-type channels would raise local Ca^{2+} concentrations sufficiently for eNOS activation. Indeed, preliminary results (not shown) indicate that estrogenic stimulation of $I_{Cl,cAMP}$ persists even in the presence of $I_{Ca,L}$. Again, further experiments with the perforated patch technique would settle this question.

At least two second-messenger systems have been shown to be activated by estrogen in the vasculature. Estrogen stimulation of human umbilical vein endothelial cells results in release of NO, increases in intracellular cGMP and activation of mitogen-activated protein kinase (MAPK) within minutes of application (Caulin-Glasser *et al.*,

1997; Russell *et al.*, 2000). Activation of the PI3-kinase-Akt pathway by estrogen allows Ca^{2+} independent activation of eNOS (Haynes *et al.*, 2000). However, it is likely that acute responses to estrogen are differentially mediated in different cell types. The speculation in section 6.3.2 on the identity of the regulatory pathway for Urotensin II modulation of $I_{Cl,cAMP}$ applies equally well to estrogen stimulation. Resolution will require the use of specific inhibitors.

7.3.2 Physiological role of estrogen stimulation of chloride current

7.3.2.1 Action potential duration and arrhythmias

The initial report of the negative inotropic and I_{Ca} inhibiting effects of 17β-estradiol in guinea pig ventricular myocytes also noted a decrease in action potential duration (APD) brought about mainly by a shortening of the plateau region (Jiang *et al.*, 1992). Given the results presented in this chapter, the change in APD must be at least partly due to increased $I_{Cl,cAMP}$ as well as reduced I_{Ca}. During the action potential plateau, the significant outward current contributed by $I_{Cl,cAMP}$ will tend to repolarise the membrane and cause a shortening of the action potential duration. In the presence of estrogen, β-adrenergic stimulation can augment Ca^{2+} entry without significant changes in the profile of the action potential. This may responsible for part of the cardio-protective effect of estrogen in reducing ischemic arrhythmias (McHugh *et al.*, 1998, Li *et al.*, 2000)

7.3.2.2 Estrogenic role in ventricular volume regulation

Ischemic cardiac cell swelling is associated with the onset of irreversible damage to the myocardium (Tranum-Jensen *et al.*, 1981). The cell swelling in turn compresses the vascular bed, reducing coronary perfusion and increasing ischemic injury. Blocking

$I_{Cl,cAMP}$ abolishes isoprenaline-induced regulatory volume decrease in the guinea pig (Wang *et al.*, 1997). If $I_{Cl,cAMP}$ aids cellular volume regulation following local increases in catecholamine concentrations in ischemia (Videbaek *et al.*, 1972, Karwatowska-Krynska & Beresewicz, 1983) and is recruited by estrogen, this could help account for the lower mortality rate from ischemic heart disease in pre-menopausal women (Jennings *et al.*, 1995).

The general lack of cell capacitance changes after application of isoprenaline and 17β-estradiol is in contrast to Tareen *et al.* (1991). However, the guinea pig ventricular myocytes in that paper seemed to be somewhat larger than ones used in the investigations in this chapter (166 $\pm$31 pF). The minority of cells (8 of 154 or ~5%) in which changes in cell capacitance were observed were all larger than average (>170 pF), falling within the range cited in Tareen *et al.* (1991). In agreement with the results presented here, Wang *et al.*, 1997 also only see isotonic volume decreases in a similar minority of cells (1 of 16 or ~6%). These authors, however, demonstrate catecholamine-stimulated regulatory volume decrease in hypotonic solutions attributable to $I_{Cl,cAMP}$.

It is should be noted that even in the few cells where reductions in cell capacitance do occur, cell shrinkage does not fully reflect these changes. Voltage drop across the access series resistance would increase in parallel with the evoked $I_{Cl,cAMP}$ current. This would lead to a reduction in the slope of the test voltage ramp and hence to an overestimation in the changes in membrane capacitance. Thus, in the cell in figure 7.10a, up to an estimated 29% of the measured decrease in capacitance is due to voltage error.

7.3.3 *Raloxifene*

The reduction of ovarian steroid hormone synthesis at the menopause is associated with a number of clinical symptoms in the cardiovascular system, bone, breast, skin and central nervous system. Long-term treatment with estrogen in hormone replacement therapy is able to alleviate many of the symptoms, decreasing osteoporosis and incidences of heart and vascular disease, for example. Unfortunately, classical estrogen agonists also promote growth of breast and uterine tissue, increasing the risk of cancer (Hammond, 1995). Several classes of compounds (selective estrogen receptor modulators or SERMs), including tamoxifen and raloxifene, exhibit anti-estrogen properties in some tissues, e.g. the breast and endometrium, but have estrogenic effects in other parts of the body, including bone and cardiovascular tissue. Raloxifene has been shown clinically to increase bone mineral density and lower serum liproprotein cholesterol levels without promoting endometrial growth (Delmas *et al.*, 1997). Unfortunately, as raloxifene does not alleviate (but may in fact promote) hot flashes and night sweats, it seems that this is not yet the perfect "magic bullet" clinicians have been seeking. Nevertheless, it seems clear that SERMs are the way forward for estrogen replacement therapy and that a better understanding for the underlying pharmacology responsible for their tissue specificity might allow future drugs to be better targeted.

The molecular action of estrogens has still not been fully elucidated. The organ specific mixed agonism/antagonism of different SERMs appears to depend in a complex way on their differing efficacies, ranging from full agonist to inverse agonist, at specific receptors subtypes (ERα and ERβ), the expression of the receptor protein in different cells, the set of molecules which interacts with the bound receptor (including co-

regulators and transcription factors) and the promoter/DNA context at the particular gene (reviewed in Dutertre & Smith, 2000). Recent research demonstrating surface receptor binding sites for estrogen, including work presented in this thesis, only serves to complicate the picture.

The application of 10 μM raloxifene to guinea pig ventricular myocytes causes a slow rise in chloride current which does not reach a peak until after 8-10 minutes, much slower than the time course for 17β-estradiol. Wash out was even slower, and a complete recovery has not been observed. The slow recruitment of chloride current is a process which does not require prior activation of the CFTR channel (figure 7.13). The most parsimonious hypothesis is that the extended stimulation is due to classical nuclear transcriptional regulation mediated by the estrogen receptor. Thus, it may be possible that estrogenic effects on cardiac $I_{Cl,cAMP}$ are two-fold, with an acute effect mediated by cytosolic pathways and a slower long term transcriptional regulation, possibly after prolonged exposure to the hormone. Such an explanation has been proffered for the vasodilatory action of raloxifene in rabbit coronary arteries. On the other hand, although the response to raloxifene is slow to reach a maximum, there does not seem to be any substantial lag to the initial rise in $I_{Cl,cAMP}$ expected for transcriptional regulation. Results from fast perfusion experiments should help to resolve this question.

7.3.4 Future directions

Three lines of enquiry will be followed based on the results presented in this chapter. The nature of the interaction between estrogen agonist and its effector will continue to be a subject of investigation. This would include employing the specific estrogen receptor antagonist ICI 182 780 to see if a classical estrogen receptor is

involved; using estrogenic ligands specific for the receptor subtypes (Sun *et al.*, 1999) to distinguish between ERα and ER*β*; and exploring the possible mediation of G-proteins (Mermelstein *et al.*, 1996) using guanosine analogues such as GDP*β*S and GTPγS. Another area of research would be the continued use of selective inhibitors to discover the underlying intracellular modulatory pathways, e.g. ODQ or L-NNA in combination with the perforated patch technique. The intriguingly different responses to 17*β*-estradiol and raloxifene will no doubt be another fruitful area of research.

Chapter Eight

Conclusion

The research presented in this thesis has been the result of a wide-ranging investigation into G-protein mediated regulatory pathways.

8.1 Photorelease of GTP

The research project began with the examination of the results of the uv flash photolysis of the caged precursor of GTP, the natural ligand of G-proteins (in chapter 4). The photorelease of GTP produced a rapid increase in calcium current which reached a sustained plateau in cells where prior current run-down was absent. The ability of GTP to produce large stimulations of the G-protein is contrary to the previously standard assumptions of saturating intracellular GTP:GDP ratios and low basal G-protein turnover in the absence of receptor agonists.

The calibration of the photolysis experimental system by HPLC (in chapter 3) had revealed that only 86.7 ±8.5 μM GTP was released per flash. However, the inclusion of even a thousand-fold more GTP (10 mM) inside the pipette did not appear to competitively inhibit completely the response to further photoreleased GTP. This suggested both that the GTP binding site has an extremely high affinity, and that the

concentration of ambient GTP in the vicinity of the G-protein might be considerably lower that in the bulk of the cytoplasm.

The *in vitro* rate of dissociation of GDP from G-proteins is very slow in the absence of receptor-activation. The explanation of why the basal turnover of G-protein *in vivo,* nevertheless, might be significant was provided by the discovery, subsequent to the research in chapter 4, of constitutive receptor activity in the absence of agonist, particularly for the guinea pig ventricular β_1-adrenoreceptor (Mewes *et al.*, 1993, see section 1.1.2).

8.2 Photorelease of GTPγS

The non-hydrolysable guanine nucleotide analogue GTPγS is still widely used to demonstrate the mediation of a G-protein in a regulatory pathway. The binding of GTPγS should lead to the almost irreversible activation of any G-protein. During the course of experiments summarised in chapter 4, pipette dialysis with GTPγS was found to have an anomalous inhibitory effect on responses to both isoprenaline and photoreleased GTP. The basis for this counter-intuitive action was unravelled in chapter 5.

Inclusion of GTPγS in the intracellular solution inhibited the response to sympathetic stimulation via the activation of a pertussis toxin sensitive $G_{i/o}$-protein. Its rapid photorelease inside the cell conversely produced large increases in I_{Ca}, presumably by activation of the G_s-protein. In addition, the chronic intracellular application of GTPγS accelerated without significantly changing the magnitudes of cAMP-dependent enhancement of I_{Ca} and activation of $I_{Cl,cAMP}$.

The diverse effects of GTPγS have highlighted the potential pitfalls in the use of this pharmacological agent, which can be expected to activate G-proteins

indiscriminately. The net effect produced would depend on the relative turnover rates and binding affinities at different G-proteins. Experimental design has to be approached with the greatest care when employing this nucleotide.

8.3 Photorelease of cAMP

The photorelease of cAMP produced large increases in both calcium and chloride currents. Curiously, $I_{Cl,cAMP}$ was less sensitive to cAMP (EC_{50} = ~1.10 μM) than I_{Ca} (EC_{50} = ~0.47 μM). This difference may be important physiologically and can be attributable either to different affinities at the protein kinase A serine/threonine phosphorylation sites at the two channels or to differing susceptibilities to endogenous phosphatases. It will be interesting to see if the differential sensitivities to cAMP in guinea pig ventricular myocytes persist in other experimental systems and cell types. In any case, the photorelease of cAMP has proved an extremely reliable and reproducible way of activating the cAMP-dependent phosphorylatory pathway. The reasons for this are probably two-fold: the elimination both of variations in β-adrenoreceptor/ G-protein/adenylyl cyclase coupling and of vagaries in the diffusion of pharmacological agents from either bath or pipette.

8.4 Urotensin II enhances $I_{Cl,cAMP}$

The recent identification of the fish neuropeptide urotensin II as the ligand for a human (and mammalian) receptor previously "orphaned" has been a great success story for "reverse molecular pharmacology". Urotensin II had been found previously to be most potent vasodilatory agent known. Biochemical studies and *in vivo* responses had suggested, however, that this peptide might have an additional direct modulatory role in the myocardium. The results in chapter six indicate that urotensin II, while ineffective on

its own, potentiates the catecholamine-activated chloride current after application of either forskolin or isoprenaline. Further research will be required to elucidate the physiological role of such modulation, identify the intracellular pathways involved and explain why the responses seem so much faster yet require higher doses than in the vasculature.

8.5 Estrogenic enhancement of $I_{Cl,cAMP}$

There have been recent reports of a fast G-protein mediated inhibition of cardiac L-type I_{Ca} and cAMP production by 17β-estradiol. However, surprisingly, the same steroid hormone produced a large enhancement of the cAMP-induced chloride current (chapter seven). The modulation by 17β-estradiol was extremely rapid and washed off similarly quickly. The response seems to be mediated by a cell-surface receptor but unlike in vascular smooth muscle and endothelia, this did require the production of nitric oxide. Another estrogenic agonist, raloxifene, was also able to potentiate β-adrenergic activation of $I_{Cl,cAMP}$ but with much slower kinetics. The lack of a noticeable lag for the raloxifene response suggests that this pharmacological agent (like 17β-estradiol) might be acting through non-transcriptional (cytosolic) mechanisms. The exact identity of the membrane receptor and the intracellular pathways responsible will be the continued subjects of the research programme, whose results to date have been presented in this thesis.

References

Abraham GE, Odell WD, Swerdloff RS, Hopper K. 1972. Simultaneous radioimmunoassay of plasma FSH, LH, progesterone, 17-hydroxyprogesterone, and 17β-estradiol during the menstrual cycle. *J Clin Endocrinol Metab* 34: 312-8

Adams MR, Kaplan JR, Manuck SB, Koritnik DR, Parks JS, Wolfe MS, Clarkson TB: Inhibition of coronary artery atherosclerosis by 17β-estradiol in ovariectomized monkeys. Lack of an effect of added progesterone. *Arteriosclerosis* 1990;10:1051-1057

Al-Nakkash L, Hwang TC. 1999. Activation of wild-type and deltaF508-CFTR by phosphodiesterase inhibitors through cAMP-dependent and -independent mechanisms. *Pflugers Arch* 437: 553-61

Ames RS, Sarau HM, Chambers JK, Willette RN, Aiyar NV, *et al.* 1999. Human urotensin-II is a potent vasoconstrictor and agonist for the orphan receptor GPR14 [published erratum appears in *Nature* 1999 Dec 23- 30;402(6764):898]. *Nature* 401: 282-6

Ammala C, Berggren PO, Bokvist K, Rorsman P. 1992. Inhibition of L-type calcium channels by internal GTPγS in mouse pancreatic *β* cells. *Pflugers Arch* 420: 72-7

Anderson MP, Gregory RJ, Thompson S, Souza DW, Paul S, Mulligan RC, Smith AE, Welsh MJ. 1991. Demonstration that CFTR is a chloride channel by alteration of its anion selectivity. *Science* 253: 202-5

Ashby CD, Walsh DA. 1972. Characterization of the interaction of a protein inhibitor with adenosine 3',5'-monophosphate-dependent protein kinases. I. Interaction with the catalytic subunit of the protein kinase. *J Biol Chem* 247: 6637-42

Babitch J. 1990. Channel hands [letter]. *Nature* 346: 321-2

Bahinski A, Nairn AC, Greengard P, Gadsby DC. 1989. Chloride conductance regulated by cyclic AMP-dependent protein kinase in cardiac myocytes. *Nature* 340: 718-21

Balligand JL. 1999. Regulation of cardiac *β*-adrenergic response by nitric oxide. *Cardiovasc Res* 43: 607-20

Bargmann CI. 1998. Neurobiology of the Caenorhabditis elegans genome. *Science* 282: 2028-33

Barrett-Connor E, Bush TL. 1991. Estrogen and coronary heart disease in women. *JAMA* 265: 1861-7

Baukrowitz T, Hwang TC, Nairn AC, Gadsby DC. 1994. Coupling of CFTR Cl-channel gating to an ATP hydrolysis cycle. *Neuron* 12: 473-82

Bean BP. 1989. Classes of calcium channels in vertebrate cells. *Annu Rev Physiol* 51: 367-84

Bean BP, Nowycky MC, Tsien RW. 1984. β-adrenergic modulation of calcium channels in frog ventricular heart cells. *Nature* 307: 371-5

Bear CE, Li CH, Kartner N, Bridges RJ, Jensen TJ, *et al*. 1992. Purification and functional reconstitution of the cystic fibrosis transmembrane conductance regulator (CFTR). *Cell* 68: 809-18

Beato M. 1989. Gene regulation by steroid hormones. *Cell* 56: 335-44

Belles B, Malecot CO, Hescheler J, Trautwein W. 1988. "Run-down" of the Ca current during long whole-cell recordings in guinea pig heart cells: role of phosphorylation and intracellular calcium. *Pflugers Arch* 411: 353-60

Bergamaschi S, Govoni S, Cominetti P, Parenti M, Trabucchi M. 1988. Direct coupling of a G-protein to dihydropyridine binding sites. *Biochem Biophys Res Commun* 156: 1279-86

Berlind A. 1972. Teleost caudal neurosecretory system: release of urotensin II from isolated urophyses. *Gen Comp Endocrinol* 18: 557-60

Bernatchez G, Talwar D, Parent L. 1998. Mutations in the EF-hand motif impair the inactivation of barium currents of the cardiac α1C channel. *Biophys J* 75: 1727-39

Biddlecome GH, Berstein G, Ross EM. 1996. Regulation of phospholipase Cβ1 by Gq and m1 muscarinic cholinergic receptor. Steady-state balance of receptor-mediated activation and GTPase-activating protein-promoted deactivation [published erratum appears in J Biol Chem 1996 Dec 27;271(52):33705]. *J Biol Chem* 271: 7999-8007

Biel M, Hullin R, Freundner S, Singer D, Dascal N, *et al*. 1991. Tissue-specific expression of high-voltage-activated dihydropyridine- sensitive L-type calcium channels. *Eur J Biochem* 200: 81-8

Bjarnason NH, Haarbo J, Byrjalsen I, Kauffman RF, Christiansen C. 1997. Raloxifene inhibits aortic accumulation of cholesterol in ovariectomized, cholesterol-fed rabbits. *Circulation* 96: 1964-9

Bond RA, Leff P, Johnson TD, Milano CA, Rockman HA, McMinn TR, Apparsundaram S, Hyek MF, Kenakin TP, Allen LF, Lefkowitz RJ. 1995. Physiological effects of inverse agonists in transgenic mice with myocardial overexpression of the β_2-adrenoreceptor. *Nature* 374: 272-6

Bourne HR, Stryer L. 1992. G proteins. The target sets the tempo [news]. *Nature* 358: 541-3

Bouron A, Soldatov NM, Reuter H. 1995. The β-1-subunit is essential for modulation by protein kinase C of an human and a non-human L-type Ca^{2+} channel. *FEBS Lett* 377: 159-62

Brandt DR, Ross EM. 1985. GTPase activity of the stimulatory GTP-binding regulatory protein of adenylate cyclase, Gs. Accumulation and turnover of enzyme-nucleotide intermediates. *J Biol Chem* 260: 266-72

Breitwieser GE, Szabo G. 1985. Uncoupling of cardiac muscarinic and β-adrenergic receptors from ion channels by a guanine nucleotide analogue. *Nature* 317: 538-40

Breitwieser GE, Szabo G. 1988. Mechanism of muscarinic receptor-induced K^+ channel activation as revealed by hydrolysis-resistant GTP analogues. *J Gen Physiol* 91: 469-93

Brown AM, Birnbaumer L. 1988. Direct G-protein gating of ion channels. *Am J Physiol* 254: H401-10

Brown AM, Kunze DL, Lux HD. 1986. Single calcium channels and their inactivation. *Membr Biochem* 6: 73-81

Brown AM, Kunze DL, Yatani A. 1984. The agonist effect of dihydropyridines on Ca^{2+} channels. *Nature* 311: 570-2

Brown AM, Kunze DL, Yatani A. 1986. Dual effects of dihydropyridines on whole cell and unitary calcium currents in single ventricular cells of guinea-pig. *J Physiol (Lond)* 379: 495-514

Brum G, Osterrieder W, Trautwein W. 1984. β-adrenergic increase in the calcium conductance of cardiac myocytes studied with the patch clamp. *Pflugers Arch* 401: 111-8

Cabral AM, Vasquez EC, Moyses MR, Antonio A. 1988. Sex hormone modulation of ventricular hypertrophy in sinoaortic denervated rats. *Hypertension* 11: I93-7

Camardo JS, Shuster MJ, Siegelbaum SA, Kandel ER. 1983. Modulation of a specific potassium channel in sensory neurons of Aplysia by serotonin and cAMP-dependent protein phosphorylation. *Cold Spring Harb Symp Quant Biol* 48: 213-20

Carman-Krzan M. 1984. The effect of group selective reagents N-ethylmaleimide and dithiothreitol on histamine H1-receptor binding sites in the vascular smooth muscle membranes. *Agents Actions* 14: 561-5

Carson MR, Travis SM, Welsh MJ. 1995. The two nucleotide-binding domains of cystic fibrosis transmembrane conductance regulator (CFTR) have distinct functions in controlling channel activity. *J Biol Chem* 270: 1711-7

Carson MR, Welsh MJ. 1995. Structural and functional similarities between the nucleotide-binding domains of CFTR and GTP-binding proteins. *Biophys J* 69: 2443-8

Cassel D, Levkovitz H, Selinger Z. 1977. The regulatory GTPase cycle of turkey erythrocyte adenylate cyclase. *J Cyclic Nucleotide Res* 3: 393-406

Caulin-Glaser T, Garcia-Cardena G, Sarrel P, Sessa WC, Bender JR. 1997. 17 β-estradiol regulation of human endothelial cell basal nitric oxide release, independent of cytosolic Ca^{2+} mobilization. *Circ Res* 81: 885-92

Cavalie A, Allen TJ, Trautwein W. 1991. Role of the GTP-binding protein Gs in the β-adrenergic modulation of cardiac Ca channels. *Pflugers Arch* 419: 433-43

Cavalie A, Pelzer D, Trautwein W. 1986. Fast and slow gating behaviour of single calcium channels in cardiac cells. Relation to activation and inactivation of calcium-channel current. *Pflugers Arch* 406: 241-58

Chad J, Kalman D, Armstrong D. 1987. The role of cyclic AMP-dependent phosphorylation in the maintenance and modulation of voltage-activated calcium channels. *Soc Gen Physiol Ser* 42: 167-86

Chang FC, Hosey MM. 1988. Dihydropyridine and phenylalkylamine receptors associated with cardiac and skeletal muscle calcium channels are structurally different. *J Biol Chem* 263: 18929-37

Chen Z, Yuhanna IS, Galcheva Gargova Z, Karas RH, Mendelsohn ME, Shaul PW. 1999. Estrogen receptor α mediates the nongenomic activation of endothelial nitric oxide synthase by estrogen [published erratum appears in J Clin Invest 1999 May;103(9):1363]. *J Clin Invest* 103: 401-6

Civelli O, Nothacker HP, Reinscheid R. 1998. Reverse physiology: discovery of the novel neuropeptide, orphanin FQ/nociceptin. *Crit Rev Neurobiol* 12: 163-76

Codina J, Yatani A, Grenet D, Brown AM, Birnbaumer L. 1987. The α subunit of the GTP binding protein G_k opens atrial potassium channels. *Science* 236: 442-5

Colditz GA, Willett WC, Stampfer MJ, Rosner B, Speizer FE, Hennekens CH. 1987. Menopause and the risk of coronary heart disease in women. *N Engl J-Med* 316: 1105-10

Collins P, Webb C. 1999. Estrogen hits the surface [news]. *Nat Med* 5: 1130-1

Conlon JM, Tostivint H, Vaudry H. 1997. Somatostatin- and urotensin II-related peptides: molecular diversity and evolutionary perspectives. *Regul Pept* 69: 95-103

Corbin JD, Keely SL. 1977. Characterization and regulation of heart adenosine 3':5'-monophosphate-dependent protein kinase isozymes. *J Biol Chem* 252: 910-8

Corbin JD, Sugden PH, Lincoln TM, Keely SL. 1977. Compartmentalization of adenosine 3',5'-monophosphate and adenosine 3',5'-monophosphate-dependent protein kinase in heart tissue. *J Biol Chem* 252: 3854-61

Coulouarn Y, Jegou S, Tostivint H, Vaudry H, Lihrmann I. 1999. Cloning, sequence analysis and tissue distribution of the mouse and rat urotensin II precursors. *FEBS Lett* 457: 28-32

Coulouarn Y, Lihrmann I, Jegou S, Anouar Y, Tostivint H, *et al.* 1998. Cloning of the cDNA encoding the urotensin II precursor in frog and human reveals intense expression of the urotensin II gene in motoneurons of the spinal cord. *Proc Natl Acad Sci U-S A* 95: 15803-8

Davenport AP, Maguire JJ. 2000. Urotensin II: fish neuropeptide catches orphan receptor. *Trends Pharmacol Sci* 21: 80-2

Dawson DC, Smith SS, Mansoura MK. 1999. CFTR: mechanism of anion conduction. *Physiol Rev* 79: S47-75

de Wit RJ, Hekstra D, Jastorff B, Stec WJ, Baraniak J, *et al.* 1984. Inhibitory action of certain cyclophosphate derivatives of cAMP on cAMP- dependent protein kinases. *Eur J Biochem* 142: 255-60

Delmas PD, Bjarnason NH, Mitlak BH, Ravoux AC, Shah AS, *et al.* 1997. Effects of raloxifene on bone mineral density, serum cholesterol concentrations, and uterine endometrium in postmenopausal women. *N Engl J-Med* 337: 1641-7

Dempster J. 1988. In *Microcomputers in Physiology: A practical approach*, ed. PJ Fraser, pp. 51-93: Oxford IRL Press

Dessauer CW, Scully TT, Gilman AG. 1997. Interactions of forskolin and ATP with the cytosolic domains of mammalian adenylyl cyclase. *J Biol Chem* 272: 22272-7

De Wit. 1984. *European Journal of Biochemistry* 142: 255-60

Dixon RA, Kobilka BK, Strader DJ, Benovic JL, Dohlman HG, *et al*. 1986. Cloning of the gene and cDNA for mammalian *ß*-adrenergic receptor and homology with rhodopsin. *Nature* 321: 75-9

Dolphin AC, Scott RH. 1988. Actions of Ca^{2+} channel ligands depend on G-proteins. Ca^{2+} agonists/antagonists and GTP [letter]. *Trends Pharmacol Sci* 9: 394-5

Dolphin AC, Wootton JF, Scott RH, Trentham DR. 1988. Photoactivation of intracellular guanosine triphosphate analogues reduces the amplitude and slows the kinetics of voltage-activated calcium channel currents in sensory neurones. *Pflugers Arch* 411: 628-36

Douglas SA, Ashton DJ, Sauermelch CF, Coatney RW, Ohlstein DH, *et al*. 2000. Human urotensin-II is a potent vasoactive peptide: pharmacological characterization in the rat, mouse, dog and primate. *J Cardiovasc Pharmacol* 36: S163-6

Douglas SA, Sulpizio AC, Piercy V, Sarau HM, Ames RS, *et al*. 2000. Differential vasoconstrictor activity of human urotensin-II in vascular tissue isolated from the rat, mouse, dog, pig, marmoset and cynomolgus monkey. *Br J Pharmacol* 131: 1262-74

Dutertre M, Smith CL. 2000. Molecular mechanisms of selective estrogen receptor modulator (SERM) action. *J Pharmacol Exp Ther* 295: 431-7

Eckert R, Chad JE. 1984. Inactivation of Ca channels. *Prog Biophys Mol Biol* 44: 215-67

Egan TM, Noble D, Noble SJ, Powell T, Twist VW. 1987. An isoprenaline activated sodium-dependent inward current in ventricular myocytes. *Nature* 328: 634-7

Ehara T, Ishihara K. 1990. Anion channels activated by adrenaline in cardiac myocytes. *Nature* 347: 284-6

Ehara T, Matsuura H. 1993. Single-channel study of the cyclic AMP-regulated chloride current in guinea-pig ventricular myocytes. *J Physiol Lond* 464: 307-20

Ehlert FJ. 1986. 'Inverse agonists', cooperativity and drug action at benzodiazepine receptors. *Trends in Pharmacological Sciences* 7: 28-32

Ellinor PT, Yang J, Sather WA, Zhang JF, Tsien RW. 1995. Ca^{2+} channel selectivity at a single locus for high-affinity Ca^{2+} interactions. *Neuron* 15: 1121-32

England PJ, Shahid M. 1987. Effects of forskolin on contractile responses and protein phosphorylation in the isolated perfused rat heart. *Biochem J* 246: 687-95

Fabiato A. 1985. Simulated calcium current can both cause calcium loading in and trigger calcium release from the sarcoplasmic reticulum of a skinned canine cardiac Purkinje cell. *J Gen Physiol* 85: 291-320

Federman AD, Conklin BR, Schrader KA, Reed RR, Bourne HR. 1992. Hormonal stimulation of adenylyl cyclase through G_i-protein $\beta\gamma$ subunits. *Nature* 356: 159-61

Fenwick EM, Marty A, Neher E. 1982. Sodium and calcium channels in bovine chromaffin cells. *J Physiol (Lond)* 331: 599-635

Figtree GA, Lu Y, Webb CM, Collins P. 1999. Raloxifene acutely relaxes rabbit coronary arteries in vitro by an estrogen receptor-dependent and nitric oxide-dependent mechanism. *Circulation* 100: 1095-101

Fischer H, Illek B, Machen TE. 1998. Regulation of CFTR by protein phosphatase 2B and protein kinase C. *Pflugers Arch* 436: 175-81

Fischer H, Machen TE. 1994. CFTR displays voltage dependence and two gating modes during stimulation. *J Gen Physiol* 104: 541-66

Fischmeister R, Hartzell HC. 1986. Mechanism of action of acetylcholine on calcium current in single cells from frog ventricle. *J Physiol Lond* 376: 183-202

Fischmeister R, Shrier A. 1989. Interactive effects of isoprenaline, forskolin and acetylcholine on Ca^{2+} current in frog ventricular myocytes. *J Physiol Lond* 417: 213-39

Fong TM, Strader CD. 1994. Functional mapping of the ligand binding sites of G-protein coupled receptors. *Med Res Rev* 14: 387-99

Frace AM, Mery PF, Fischmeister R, Hartzell HC. 1993. Rate-limiting steps in the β-adrenergic stimulation of cardiac calcium current. *J Gen Physiol* 101: 337-53

Freissmuth M, Gilman AG. 1989. Mutations of Gsα designed to alter the reactivity of the protein with bacterial toxins. Substitutions at ARG187 result in loss of GTPase activity. *J Biol Chem* 264: 21907-14

French PJ, Bijman J, Edixhoven M, Vaandrager AB, Scholte BJ, *et al*. 1995. Isotype-specific activation of cystic fibrosis transmembrane conductance regulator-chloride channels by cGMP-dependent protein kinase II. *J Biol Chem* 270: 26626-31

Gadsby DC, Nagel G, Hwang TC. 1995. The CFTR chloride channel of mammalian heart. *Annu Rev Physiol* 57: 387-416

Gadsby DC, Nairn AC. 1999. Regulation of CFTR Cl^- ion channels by phosphorylation and dephosphorylation. *Adv Second Messenger Phosphoprotein Res* 33: 79-106

Gallo MP, Ghigo D, Bosia A, Alloatti G, Costamagna C, *et al*. 1998. Modulation of guinea-pig cardiac L-type calcium current by nitric oxide synthase inhibitors. *J Physiol Lond* 506: 639-51

Gao T, Chien AJ, Hosey MM. 1999. Complexes of the α_1C and β subunits generate the necessary signal for membrane targeting of class C L-type calcium channels. *J Biol Chem* 274: 2137-44

Gao T, Puri TS, Gerhardstein BL, Chien AJ, Green RD, Hosey MM. 1997. Identification and subcellular localization of the subunits of L-type calcium channels and adenylyl cyclase in cardiac myocytes. *J Biol Chem* 272: 19401-7

Gardin JM, Siscovick D, Anton Culver H, Lynch JC, Smith VE, *et al*. 1995. Sex, age, and disease affect echocardiographic left ventricular mass and systolic function in the free-living elderly. The Cardiovascular Health Study. *Circulation* 91: 1739-48

Gether U, Lin S, Ghanouni P, Ballesteros JA, Weinstein H, Kobilka BK. 1997. Agonists induce conformational changes in transmembrane domains III and VI of the β2-adrenoceptor. *Embo J* 16: 6737-47

Gether U, Lin S, Kobilka BK. 1995. Fluorescent labeling of purified β_2-adrenergic receptor. Evidence for ligand-specific conformational changes. *J Biol Chem* 270: 28268-75

Gibson A. 1987. Complex effects of Gillichthys urotensin II on rat aortic strips. *Br J-Pharmacol* 91: 205-12

Gilman AG. 1987. G proteins: transducers of receptor-generated signals. *Annu Rev Biochem* 56: 615-49

Goldhaber JI, Ji S, Lamp ST, Weiss JN. 1989. Effects of exogenous free radicals on electromechanical function and metabolism in isolated rabbit and guinea pig ventricle. Implications for ischemia and reperfusion injury. *J Clin Invest* 83: 1800-9

Gould RP, Powell T. 1972. Intact isolated muscle cells from the adult rat heart. *J Physiol Lond* 225: 16P-9P

Graf R, Mattera R, Codina J, Evans T, Ho YK, *et al*. 1992. Studies on the interaction of α subunits of GTP-binding proteins with βγ dimers. *Eur J-Biochem* 210: 609-19

Grohe C, Kahlert S, Lobbert K, Stimpel M, Karas RH, *et al*. 1997. Cardiac myocytes and fibroblasts contain functional estrogen receptors. *FEBS Lett* 416: 107-12

Grohe C, Kahlert S, Lobbert K, Vetter H. 1998. Expression of oestrogen receptor α and β in rat heart: role of local oestrogen synthesis. *J Endocrinol* 156: R1-7

Gurney AM, Lester HA. 1987. Light-flash physiology with synthetic photosensitive compounds. *Physiol Rev* 67: 583-617

Haack JA, Rosenberg RL. 1994. Calcium-dependent inactivation of L-type calcium channels in planar lipid bilayers. *Biophys J* 66: 1051-60

Haase H, Karczewski P, Beckert R, Krause EG. 1993. Phosphorylation of the L-type calcium channel β subunit is involved in β-adrenergic signal transduction in canine myocardium. *FEBS Lett* 335: 217-22

Hamill OP, Marty A, Neher E, Sakmann B, Sigworth FJ. 1981. Improved patch-clamp techniques for high-resolution current recording from cells and cell-free membrane patches. *Pflugers Arch* 391: 85-100

Hamilton SL, Codina J, Hawkes MJ, Yatani A, Sawada T, *et al*. 1991. Evidence for direct interaction of Gsα with the Ca^{2+} channel of skeletal muscle. *J Biol Chem* 266: 19528-35

Hammond CB. 1996. Menopause and hormone replacement therapy: an overview. *Obstet Gynecol* 87: 2S-15S

Harada K, Iijima T. 1994. Differential modulation by adenylate cyclase of Ca^{2+} and delayed K^{+} current in ventricular myocytes. *Am J-Physiol* 266: H1551-7

Harris RB, Laws A, Reddy VM, King A, Haskell WL. 1990. Are women using postmenopausal estrogens? A community survey. *Am J-Public Health* 80: 1266-8

Harrison SA, Reifsnyder DH, Gallis B, Cadd GG, Beavo JA. 1986. Isolation and characterization of bovine cardiac muscle cGMP-inhibited phosphodiesterase: a receptor for new cardiotonic drugs. *Mol Pharmacol* 29: 506-14

Hart P, Warth JD, Levesque PC, Collier ML, Geary Y, *et al.* 1996. Cystic fibrosis gene encodes a cAMP-dependent chloride channel in heart. *Proc Natl Acad Sci U-S A* 93: 6343-8

Hartzell HC. 1988. Regulation of cardiac ion channels by catecholamines, acetylcholine and second messenger systems. *Prog Biophys Mol Biol* 52: 165-247

Hartzell HC, Fischmeister R. 1992. Direct regulation of cardiac Ca^{2+} channels by G-proteins: neither proven nor necessary? *Trends Pharmacol Sci* 13: 380-5

Hartzell HC, Hirayama Y, Petit Jacques J. 1995. Effects of protein phosphatase and kinase inhibitors on the cardiac L-type Ca^{2+} current suggest two sites are phosphorylated by protein kinase A and another protein kinase. *J Gen Physiol* 106: 393-414

Hartzell HC, Mery PF, Fischmeister R, Szabo G. 1991. Sympathetic regulation of cardiac calcium current is due exclusively to cAMP-dependent phosphorylation. *Nature* 351: 573-6

Harvey RD, Clark CD, Hume JR. 1990. Chloride current in mammalian cardiac myocytes. Novel mechanism for autonomic regulation of action potential duration and resting membrane potential. *J Gen Physiol* 95: 1077-102

Harvey RD, Hume JR. 1989. Autonomic regulation of a chloride current in heart. *Science* 244: 983-5

Harvey RD, Hume JR. 1989. Isoproterenol activates a chloride current, not the transient outward current, in rabbit ventricular myocytes. *Am J-Physiol* 257: C1177-81

Haynes MP, Sinha D, Russell KS, Collinge M, Fulton D, *et al*. 2000. Membrane estrogen receptor engagement activates endothelial nitric oxide synthase via the PI3-kinase-Akt pathway in human endothelial cells. *Circ Res* 87: 677-82

He Z, Raman S, Guo Y, Reenstra WW. 1998. Cystic fibrosis transmembrane conductance regulator activation by cAMP-independent mechanisms. *Am J-Physiol* 275: C958-66

Henderson R, Schertler GF. 1990. The structure of bacteriorhodopsin and its relevance to the visual opsins and other seven-helix G-protein coupled receptors. *Philos Trans R-Soc Lond B-Biol Sci* 326: 379-89

Hering S, Berjukow S, Sokolov S, Marksteiner R, Weiss RG, *et al*. 2000. Molecular determinants of inactivation in voltage-gated Ca^{2+} channels. *J Physiol* 528 Pt 2: 237-49

Herlitze S, Hockerman GH, Scheuer T, Catterall WA. 1997. Molecular determinants of inactivation and G-protein modulation in the intracellular loop connecting domains I and II of the calcium channel α1A subunit. *Proc Natl Acad Sci U-S A* 94: 1512-6

Hescheler J, Kameyama M, Trautwein W. 1986. On the mechanism of muscarinic inhibition of the cardiac Ca^{2+} current. *Pflugers Arch* 407: 182-9

Hescheler J, Tang M, Jastorff B, Trautwein W. 1987. On the mechanism of histamine induced enhancement of the cardiac Ca^{2+} current. *Pflugers Arch* 410: 23-9

Hess P, Lansman JB, Nilius B, Tsien RW. 1986. Calcium channel types in cardiac myocytes: modulation by dihydropyridines and *ß*-adrenergic stimulation. *J Cardiovasc Pharmacol* 8 Suppl 9: S11-21

Hess P, Lansman JB, Tsien RW. 1984. Different modes of Ca channel gating behaviour favoured by dihydropyridine Ca agonists and antagonists. *Nature* 311: 538-44

Hinuma S, Habata Y, Fujii R, Kawamata Y, Hosoya M, *et al*. 1998. A prolactin-releasing peptide in the brain. *Nature* 393: 272-6

Hirano Y, Fozzard HA, January CT. 1989. Characteristics of L- and T-type Ca^{2+} currents in canine cardiac Purkinje cells. *Am J-Physiol* 256: H1478-92

Hirano Y, Fozzard HA, January CT. 1989. Inactivation properties of T-type calcium current in canine cardiac Purkinje cells. *Biophys J* 56: 1007-16

Hirayama Y, Hartzell HC. 1997. Effects of protein phosphatase and kinase inhibitors on Ca^{2+} and Cl^- currents in guinea pig ventricular myocytes. *Mol Pharmacol* 52: 725-34

Hockerman GH, Girvin ME, Malbon CC, Ruoho AE. 1996. Antagonist conformations with the *β*2-adrenergic receptor ligand binding pocket. *Mol Pharmacol* 49: 1021-32

Hofer GF, Hohenthanner K, Baumgartner W, Groschner K, Klugbauer N, *et al*. 1997. Intracellular Ca^{2+} inactivates L-type Ca^{2+} channels with a Hill coefficient of approximately 1 and an inhibition constant of approximately 4 microM by reducing channel's open probability. *Biophys J* 73: 1857-65

Hofmann F, Lacinova L, Klugbauer N. 1999. Voltage-dependent calcium channels: from structure to function. *Rev Physiol Biochem Pharmacol* 139: 33-87

Hofmann F, Oeken HJ, Schneider T, Sieber M. 1988. The biochemical properties of L-type calcium channels. *J Cardiovasc Pharmacol* 12 Suppl 1: S25-30

Holmberg SR, Williams AJ. 1989. Single channel recordings from human cardiac sarcoplasmic reticulum. *Circ Res* 65: 1445-9

Horie M, Hwang TC, Gadsby DC. 1992. Pipette GTP is essential for receptor-mediated regulation of Cl- current in dialysed myocytes from guinea-pig ventricle. *J Physiol Lond* 455: 235-46

Horn R, Marty A. 1988. Muscarinic activation of ionic currents measured by a new whole-cell recording method. *J Gen Physiol* 92: 145-59

Horowitz B, Tsung SS, Hart P, Levesque PC, Hume JR. 1993. Alternative splicing of CFTR Cl- channels in heart. *Am J-Physiol* 264: H2214-20

Hurley JH. 1999. Structure, mechanism, and regulation of mammalian adenylyl cyclase. *J Biol Chem* 274: 7599-602

Hwang TC, Horie M, Gadsby DC. 1993. Functionally distinct phospho-forms underlie incremental activation of protein kinase-regulated Cl- conductance in mammalian heart. *J Gen Physiol* 101: 629-50

Hwang TC, Horie M, Nairn AC, Gadsby DC. 1992. Role of GTP-binding proteins in the regulation of mammalian cardiac chloride conductance. *J Gen Physiol* 99: 465-89

Hwang TC, Nagel G, Nairn AC, Gadsby DC. 1994. Regulation of the gating of cystic fibrosis transmembrane conductance regulator C1 channels by phosphorylation and ATP hydrolysis. *Proc Natl Acad Sci U-S A* 91: 4698-702

Imoto Y, Yatani A, Reeves JP, Codina J, Birnbaumer L, Brown AM. 1988. α-subunit of Gs directly activates cardiac calcium channels in lipid bilayers. *Am J-Physiol* 255: H722-8

Iniguez Lluhi J, Kleuss C, Gilman AG. 1993. The importance of G-protein *βγ* subunits. *TRENDS CELL BIOL. Trends in Cell Biology* 3: 230-6

Iniguez Lluhi JA, Simon MI, Robishaw JD, Gilman AG. 1992. G-protein *βγ* subunits synthesized in Sf9 cells. Functional characterization and the significance of prenylation of γ. *J Biol Chem* 267: 23409-17

Itoh H, Itoh Y, Rivier J, Lederis K. 1987. Contraction of major artery segments of rat by fish neuropeptide urotensin II. *Am J-Physiol* 252: R361-6

James AF, Tominaga T, Okada Y, Tominaga M. 1996. Distribution of cAMP-activated chloride current and CFTR mRNA in the guinea pig heart. *Circ Res* 79: 201-7

Jennings RB, Steenbergen C, Jr., Reimer KA. 1995. Myocardial ischemia and reperfusion. *Monogr Pathol* 37: 47-80

Jia Y, Mathews CJ, Hanrahan JW. 1997. Phosphorylation by protein kinase C is required for acute activation of cystic fibrosis transmembrane conductance regulator by protein kinase A. *J Biol Chem* 272: 4978-84

Jiang C, Poole Wilson PA, Sarrel PM, Mochizuki S, Collins P, MacLeod KT. 1992. Effect of 17β-estradiol on contraction, Ca^{2+} current and intracellular free Ca^{2+} in guinea-pig isolated cardiac myocytes. *Br J-Pharmacol* 106: 739-45

Jiang C, Sarrel PM, Poole Wilson PA, Collins P. 1992. Acute effect of 17β-estradiol on rabbit coronary artery contractile responses to endothelin-1. *Am J-Physiol* 263: H271-5

Josephson IR, Sperelakis N. 1991. Phosphorylation shifts the time-dependence of cardiac Ca++ channel gating currents. *Biophys J* 60: 491-7

Judd HL, Meldrum DR, Deftos LJ, Henderson BE. 1983. Estrogen replacement therapy: indications and complications. *Ann Intern Med* 98: 195-205

Kahlert S, Nuedling S, van Eickels M, Vetter H, Meyer R, Grohe C. 2000. Estrogen receptor α rapidly activates the IGF-1 receptor pathway. *J Biol Chem* 275: 18447-53

Kameyama M, Hescheler J, Hofmann F, Trautwein W. 1986. Modulation of Ca current during the phosphorylation cycle in the guinea pig heart. *Pflugers Arch* 407: 123-8

Kameyama M, Hofmann F, Trautwein W. 1985. On the mechanism of β-adrenergic regulation of the Ca channel in the guinea-pig heart. *Pflugers Arch* 405: 285-93

Kameyama M, Kameyama A, Nakayama T, Kaibara M. 1988. Tissue extract recovers cardiac calcium channels from 'run-down'. *Pflugers Arch* 412: 328-30

Kannel WB, Hjortland MC, McNamara PM, Gordon T. 1976. Menopause and risk of cardiovascular disease: the Framingham study. *Ann Intern Med* 85: 447-52

Kaplan JH, Forbush Bd, Hoffman JF. 1978. Rapid photolytic release of adenosine 5'-triphosphate from a protected analogue: utilization by the Na:K pump of human red blood cell ghosts. *Biochemistry* 17: 1929-35

Karwatowska Krynska E, Beresewicz A. 1983. Effect of locally released catecholamines on lipolysis and injury of the hypoxic isolated rabbit heart. *J Mol Cell Cardiol* 15: 523-36

Kass RS, Sanguinetti MC. 1984. Inactivation of calcium channel current in the calf cardiac Purkinje fiber. Evidence for voltage- and calcium-mediated mechanisms. *J Gen Physiol* 84: 705-26

Kauffman RF, Bensch WR, Roudebush RE, Cole HW, Bean JS, *et al*. 1997. Hypocholesterolemic activity of raloxifene (LY139481): pharmacological characterization as a selective estrogen receptor modulator. *J Pharmacol Exp Ther* 280: 146-53

Kim D, Lewis DL, Graziadei L, Neer EJ, Bar Sagi D, Clapham DE. 1989. G-protein $\beta\gamma$-subunits activate the cardiac muscarinic K+-channel via phospholipase A2. *Nature* 337: 557-60

Kim HP, Lee JY, Jeong JK, Bae SW, Lee HK, Jo I. 1999. Nongenomic stimulation of nitric oxide release by estrogen is mediated by estrogen receptor α localized in caveolae. *Biochem Biophys Res Commun* 263: 257-62

Kisselev OG, Ermolaeva MV, Gautam N. 1994. A farnesylated domain in the G-protein γ subunit is a specific determinant of receptor coupling. *J Biol Chem* 269: 21399-402

Kozlowski RZ, Goodstadt LJ, Twist VW, Powell T. 1992. Activation of L-type Ca^{2+} currents in cardiac myocytes by photoreleased GTP. *Proc R-Soc Lond B-Biol Sci* 250: 35-42

Kozlowski RZ, Goodstadt LJ, Twist VW, Powell T. 1994. Modulation of cardiac L-type Ca^{2+} channels by GTPγS in response to isoprenaline, forskolin and photoreleased nucleotides. *Br J-Pharmacol* 111: 250-8

Kozlowski RZ, Twist VW, Brown AM, Powell T. 1991. Flash photolysis of intracellular caged GTPγS increases L-type Ca^{2+} currents in cardiac myocytes. *Am J Physiol* 261: H1665-70

Langmuir I. 1938. Overturning and anchoring of monlayers. *Science* 87: 493-26

Lantin-Hermoso RL, Rosenfeld CR, Yuhanna IS, German Z, Chen Z, Shaul PW. 1997. Estrogen acutely stimulates nitric oxide synthase activity in fetal pulmonary artery endothelium. *Am J Physiol* 273: L119-26

Leblais V, Demolombe S, Vallette G, Langin D, Baro I, *et al*. 1999. β3-adrenoceptor control the cystic fibrosis transmembrane conductance regulator through a cAMP/protein kinase A-independent pathway. *J Biol Chem* 274: 6107-13

Leff P. 1995. The two-state model of receptor activation. *Trends Pharmacol Sci* 16: 89-97

Lefkowitz RJ, Cotecchia S, Samama P, Costa T. 1993. Constitutive activity of receptors coupled to guanine nucleotide regulatory proteins. *Trends Pharmacol Sci* 14: 303-7

Li C, Ramjeesingh M, Wang W, Garami E, Hewryk M, *et al*. 1996. ATPase activity of the cystic fibrosis transmembrane conductance regulator. *J Biol Chem* 271: 28463-8

Li HY, Bian JS, Kwan YW, Wong TM. 2000. Enhanced responses to 17β-estradiol in rat hearts treated with isoproterenol: involvement of a cyclic AMP-dependent pathway. *J Pharmacol Exp Ther* 293: 592-8

Liedtke CM, Cole TS. 1998. Antisense oligonucleotide to PKC-epsilon alters cAMP-dependent stimulation of CFTR in Calu-3 cells. *Am J Physiol* 275: C1357-64

Linsdell P, Hanrahan JW. 1996. Flickery block of single CFTR chloride channels by intracellular anions and osmolytes. *Am J-Physiol* 271: C628-34

Liu Q, Pong SS, Zeng Z, Zhang Q, Howard AD, *et al.* 1999. Identification of urotensin II as the endogenous ligand for the orphan G-protein-coupled receptor GPR14. *Biochem Biophys Res Commun* 266: 174-8

Logothetis DE, Kurachi Y, Galper J, Neer EJ, Clapham DE. 1987. The $\beta\gamma$ subunits of GTP-binding proteins activate the muscarinic K+ channel in heart. *Nature* 325: 321-6

Lopez Lopez JR, Shacklock PS, Balke CW, Wier WG. 1995. Local calcium transients triggered by single L-type calcium channel currents in cardiac cells. *Science* 268: 1042-5

Lory P, Rassendren FA, Richard S, Tiaho F, Nargeot J. 1990. Characterization of voltage-dependent calcium channels expressed in Xenopus oocytes injected with mRNA from rat heart. *J Physiol (Lond)* 429: 95-112

Maguire JJ, Kuc RE, Davenport AP. 2000. Orphan-receptor ligand human urotensin II: receptor localization in human tissues and comparison of vasoconstrictor responses with endothelin-1. *Br J Pharmacol* 131: 441-6

Marchese A, George SR, Kolakowski LF, Jr., Lynch KR, O'Dowd BF. 1999. Novel GPCRs and their endogenous ligands: expanding the boundaries of physiology and pharmacology [published erratum appears in Trends Pharmacol Sci 1999 Nov;20(11):447]. *Trends Pharmacol Sci* 20: 370-5

Matsuoka S, Ehara T, Noma A. 1990. Chloride-sensitive nature of the adrenaline-induced current in guinea- pig cardiac myocytes. *J Physiol (Lond)* 425: 579-98

McDonald TF, Pelzer S, Trautwein W, Pelzer DJ. 1994. Regulation and modulation of calcium channels in cardiac, skeletal, and smooth muscle cells. *Physiol Rev* 74: 365-507

McHugh NA, Solowiej A, Klabunde RE, Merrill GF. 1998. Acute coronary vascular and myocardial perfusion effects of conjugated equine estrogen in the anesthetized dog. *Basic Res Cardiol* 93: 470-6

McMaster D, Lederis K. 1983. Isolation and amino acid sequence of two urotensin II peptides from Catostomus commersoni urophyses. *Peptides* 4: 367-73

Mermelstein PG, Becker JB, Surmeier DJ. 1996. Estradiol reduces calcium currents in rat neostriatal neurons via a membrane receptor. *J Neurosci* 16: 595-604

Mewes T, Dutz S, Ravens U, Jakobs KH. 1993. Activation of calcium currents in cardiac myocytes by empty *β*-adrenoceptors. *Circulation* 88: 2916-22

Meyer R, Linz KW, Surges R, Meinardus S, Vees J, *et al*. 1998. Rapid modulation of L-type calcium current by acutely applied oestrogens in isolated cardiac myocytes from human, guinea-pig and rat. *Exp Physiol* 83: 305-21

Middleton LM, Harvey RD. 1998. PKC regulation of cardiac CFTR Cl- channel function in guinea pig ventricular myocytes. *Am J Physiol* 275: C293-302

Milligan G, Bond RA, Lee M. 1995. Inverse agonism: pharmacological curiosity or potential therapeutic strategy? *Trends Pharmacol Sci* 16: 10-3

Monod J, Wyman J, Changeux J-P. 1965. On the nature of allosteric transition: a plausible model. *J Mol Biol* 12: 88-118

Mori M, Sugo T, Abe M, Shimomura Y, Kurihara M, *et al*. 1999. Urotensin II is the endogenous ligand of a G-protein-coupled orphan receptor, SENR (GPR14). *Biochem Biophys Res Commun* 265: 123-9

Mori Y, Friedrich T, Kim MS, Mikami A, Nakai J, *et al*. 1991. Primary structure and functional expression from complementary DNA of a brain calcium channel. *Nature* 350: 398-402

Muntz KH, Sternweis PC, Gilman AG, Mumby SM. 1992. Influence of γ subunit prenylation on association of guanine nucleotide-binding regulatory proteins with membranes. *Mol Biol Cell* 3: 49-61

Nabauer M, Callewaert G, Cleemann L, Morad M. 1989. Regulation of calcium release is gated by calcium current, not gating charge, in cardiac myocytes. *Science* 244: 800-3

Nagel G, Hwang TC, Nastiuk KL, Nairn AC, Gadsby DC. 1992. The protein kinase A-regulated cardiac Cl- channel resembles the cystic fibrosis transmembrane conductance regulator. *Nature* 360: 81-4

Nakajima T, Sugimoto T, Kurachi Y. 1992. Effects of anions on the G-protein-mediated activation of the muscarinic K+ channel in the cardiac atrial cell membrane. Intracellular chloride inhibition of the GTPase activity of G_K. *J Gen Physiol* 99: 665-82

Nakajima T, Wu S, Irisawa H, Giles W. 1990. Mechanism of acetylcholine-induced inhibition of Ca current in bullfrog atrial myocytes. *J Gen Physiol* 96: 865-85

Nakashima Y, Ono K. 1994. Rate-limiting steps in activation of cardiac Cl- current revealed by photolytic application of cAMP [published errata appear in Am J Physiol 1995 Feb;268(2 Pt 2):section H following table of contents and 1995 Jun;268(3):section H following table of contents]. *Am J-Physiol* 267: H1514-22

Nakhla AM, Khan MS, Romas NP, Rosner W. 1994. Estradiol causes the rapid accumulation of cAMP in human prostate. *Proc Natl Acad Sci U S A* 91: 5402-5

Nanavati C, Clapham DE, Ito H, Kurachi Y. 1990. A comparison of the roles of purified G-protein subunits in the activation of the cardiac muscarinic K+ channel. *Soc Gen Physiol Ser* 45: 29-41

Nargeot J, Nerbonne JM, Engels J, Lester HA. 1983. Time course of the increase in the myocardial slow inward current after a photochemically generated concentration jump of intracellular cAMP. *Proc Natl Acad Sci U S A* 80: 2395-9

Neher E. 1976. Unit conductance studies in biological membranes. In: Baker PF (ed). *Techniques in cellular physiology*. Elsevier/North-Holland, Amsterdam

Neher E, Sakmann B. 1976. Single-channel currents recorded from membrane of denervated frog muscle fibres. *Nature* 260: 799-802

Neubig RR. 1994. Membrane organization in G-protein mechanisms. *Faseb J* 8: 939-46

Nothacker HP, Wang Z, McNeill AM, Saito Y, Merten S, *et al*. 1999. Identification of the natural ligand of an orphan G-protein-coupled receptor involved in the regulation of vasoconstriction. *Nat Cell Biol* 1: 383-5

Nowycky MC, Fox AP, Tsien RW. 1985. Long-opening mode of gating of neuronal calcium channels and its promotion by the dihydropyridine calcium agonist Bay K 8644. *Proc Natl Acad Sci U S A* 82: 2178-82

Nuedling S, Kahlert S, Loebbert K, Doevendans PA, Meyer R, *et al*. 1999. 17β-estradiol stimulates expression of endothelial and inducible NO synthase in rat myocardium in-vitro and in-vivo. *Cardiovasc Res* 43: 666-74

Ochi R, Kawashima Y. 1990. Modulation of slow gating process of calcium channels by isoprenaline in guinea-pig ventricular cells. *J Physiol Lond* 424: 187-204

Ono K, Fozzard HA. 1993. Two phosphatase sites on the Ca^{2+} channel affecting different kinetic functions. *J Physiol Lond* 470: 73-84

Ono K, Tareen FM, Yoshida A, Noma A. 1992. Synergistic action of cyclic GMP on catecholamine-induced chloride current in guinea-pig ventricular cells. *J Physiol* 453: 647-61

Osterrieder W, Brum G, Hescheler J, Trautwein W, Flockerzi V, Hofmann F. 1982. Injection of subunits of cyclic AMP-dependent protein kinase into cardiac myocytes modulates Ca^{2+} current. *Nature* 298: 576-8

Parsons TD, Hartzell HC. 1993. Regulation of Ca^{2+} current in frog ventricular cardiomyocytes by guanosine 5'-triphosphate analogues and isoproterenol. *J Gen Physiol* 102: 525-49

Parsons TD, Lagrutta A, White RE, Hartzell HC. 1991. Regulation of Ca^{2+} current in frog ventricular cardiomyocytes by 5'-guanylylimidodiphosphate and acetylcholine. *J Physiol Lond* 432: 593-620

Pelzer S, Shuba YM, Asai T, Codina J, Birnbaumer L, *et al*. 1990. Membrane-delimited stimulation of heart cell calcium current by *β*-adrenergic signal-transducing Gs protein. *Am J-Physiol* 259: H264-7

Perkins TD, Bansal S, Barlow DJ. 1990. Molecular modelling and design of analogues of the peptide hormone urotensin II. *Biochem Soc Trans* 18: 918-9

Pfeuffer E, Dreher RM, Metzger H, Pfeuffer T. 1985. Catalytic unit of adenlyate cyclase: purification and identification by affinity crosslinking. *Proc Natl Acad Sci U-S A* 82: 3086-90

Phillips WJ, Wong SC, Cerione RA. 1992. Rhodopsin/transducin interactions. II. Influence of the transducin-$\beta\gamma$ subunit complex on the coupling of the transducin-α subunit to rhodopsin. *J Biol Chem* 267: 17040-6

Picciotto MR, Cohn JA, Bertuzzi G, Greengard P, Nairn AC. 1992. Phosphorylation of the cystic fibrosis transmembrane conductance regulator. *J Biol Chem* 267: 12742-52

Pietrobon D, Hess P. 1990. Novel mechanism of voltage-dependent gating in L-type calcium channels. *Nature* 346: 651-5

Powell T, Terrar DA, Twist VW. 1980. Electrical properties of individual cells isolated from adult rat ventricular myocardium. *J Physiol Lond* 302: 131-53

Pusch M, Neher E. 1988. Rates of diffusional exchange between small cells and a measuring patch pipette. *Pflugers Arch* 411: 204-11

Raddino R, Manca C, Poli E, Bolognesi R, Visioli O. 1986. Effects of 17β-estradiol on the isolated rabbit heart. *Arch Int Pharmacodyn Ther* 281: 57-65

Rall TW, Sutherland EW, Bethet. 1957. The relationship of epinephrine and glucagon to liver phosphorylase. IV. Effect of epinephrine and glucagon on the reactivation of phosphorylase in liver homogenates. *J Biol Chem* 224: 463-75

Rall TW, Sutherland EW. 1958. Formation of a cyclic adenine ribonucleotide by tissue particles. *J Biol Chem* 232: 1035-76

Ray K, Kunsch C, Bonner LM, Robishaw JD. 1995. Isolation of cDNA clones encoding eight different human G-protein γ subunits, including three novel forms designated the γ_4, γ_{10}, and γ_{11} subunits. *J Biol Chem* 270: 21765-71

Reif DW, McCreedy SA. 1995. N-nitro-L-arginine and N-monomethyl-L-arginine exhibit a different pattern of inactivation toward the three nitric oxide synthases. *Arch Biochem Biophys* 320: 170-6

Reuter H. 1974. Localization of β-adrenergic receptors, and effects of noradrenaline and cyclic nucleotides on action potentials, ionic currents and tension in mammalian cardiac muscle. *J Physiol Lond* 242: 429-51

Riordan JR, Rommens JM, Kerem B, Alon N, Rozmahel R, *et al*. 1989. Identification of the cystic fibrosis gene: cloning and characterization of complementary DNA [published erratum appears in Science 1989 Sep 29;245(4925):1437]. *Science* 245: 1066-73

Robinson PR, Cohen GB, Zhukovsky EA, Oprian DD. 1992. Constitutively active mutants of rhodopsin. *Neuron* 9: 719-25

Rodbell M, Birnbaumer L, Pohl SL. 1971. Characteristics of glucagon action on the hepatic adenylate cyclase system. *Biochem J* 125: 58P-9P

Rodbell M, Birnbaumer L, Pohl SL, Krans HM. 1971. The glucagon-sensitive adenyl cyclase system in plasma membranes of rat liver. V. An obligatory role of guanylnucleotides in glucagon action. *J Biol Chem* 246: 1877-82

Rommens JM, Dho S, Bear CE, Kartner N, Kennedy D, *et al*. 1991. cAMP-inducible chloride conductance in mouse fibroblast lines stably expressing the human cystic fibrosis transmembrane conductance regulator. *Proc Natl Acad Sci U S A* 88: 7500-4

Roper D, Jacoby E, Kruger P, Engels M, Grotzinger J, *et al*. 1994. Modeling of G-protein coupled receptors with bacteriorhodopsin as a template. A novel approach based on interaction energy differences. *J Recept Res* 14: 167-86

Rosano GM, Caixeta AM, Chierchia S, Arie S, Lopez Hidalgo M, *et al*. 1997. Short-term anti-ischemic effect of 17β-estradiol in postmenopausal women with coronary artery disease. *Circulation* 96: 2837-41

Rosano GM, Sarrel PM, Poole Wilson PA, Collins P. 1993. Beneficial effect of oestrogen on exercise-induced myocardial ischaemia in women with coronary artery disease. *Lancet* 342: 133-6

Rosenberg RL, Chen XH. 1991. Characterization and localization of two ion-binding sites within the pore of cardiac L-type calcium channels. *J Gen Physiol* 97: 1207-25

Rousseau E, Smith JS, Henderson JS, Meissner G. 1986. Single channel and $^{45}Ca^{2+}$ flux measurements of the cardiac sarcoplasmic reticulum calcium channel. *Biophys J* 50: 1009-14

Russell KS, Haynes MP, Sinha D, Clerisme E, Bender JR. 2000. Human vascular endothelial cells contain membrane binding sites for estradiol, which mediate rapid intracellular signaling. *Proc Natl Acad Sci U S A* 97: 5930-5

Saetrum Opgaard O, Nothacker H, Ehlert FJ, Krause DN. 2000. Human urotensin II mediates vasoconstriction via an increase in inositol phosphates. *Eur J Pharmacol* 406: 265-71

Sakurai T, Amemiya A, Ishii M, Matsuzaki I, Chemelli RM, *et al*. 1998. Orexins and orexin receptors: a family of hypothalamic neuropeptides and G-protein-coupled receptors that regulate feeding behavior. *Cell* 92: 573-85

Sato M, Rippy MK, Bryant HU. 1996. Raloxifene, tamoxifen, nafoxidine, or estrogen effects on reproductive and nonreproductive tissues in ovariectomized rats. *Faseb J* 10: 905-12

Scamps F, Rybin V, Puceat M, Tkachuk V, Vassort G. 1992. A G_S protein couples P2-purinergic stimulation to cardiac Ca channels without cyclic AMP production. *J Gen Physiol* 100: 675-701

Scheuer J, Malhotra A, Schaible TF, Capasso J. 1987. Effects of gonadectomy and hormonal replacement on rat hearts. *Circ Res* 61: 12-9

Schmidt CJ, Thomas TC, Levine MA, Neer EJ. 1992. Specificity of G-protein β and γ subunit interactions. *J Biol Chem* 267: 13807-10

Schneider T, Hofmann F. 1988. The bovine cardiac receptor for calcium channel blockers is a 195-kDa protein. *Eur J-Biochem* 174: 369-75

Schubert B, VanDongen AM, Kirsch GE, Brown AM. 1989. β-adrenergic inhibition of cardiac sodium channels by dual G-protein pathways. *Science* 245: 516-9

Sculptoreanu A, Rotman E, Takahashi M, Scheuer T, Catterall WA. 1993. Voltage-dependent potentiation of the activity of cardiac L-type calcium channel α1 subunits due to phosphorylation by cAMP-dependent protein kinase. *Proc Natl Acad Sci U-S A* 90: 10135-9

Seamon KB, Wetzel B. 1984. Interaction of forskolin with dually regulated adenylate cyclase. *Adv Cyclic Nucleotide Protein Phosphorylation Res* 17: 91-9

Senior AE, Gadsby DC. 1997. ATP hydrolysis cycles and mechanism in P-glycoprotein and CFTR. *Semin Cancer Biol* 8: 143-50

Sham JS, Cleemann L, Morad M. 1995. Functional coupling of Ca^{2+} channels and ryanodine receptors in cardiac myocytes. *Proc Natl Acad Sci U-S A* 92: 121-5

Shorr RG, Lefkowitz RJ, Caron MG. 1981. Purification of the β-adrenergic receptor. Identification of the hormone binding subunit. *J Biol Chem* 256: 5820-6

Shuba YM, Hesslinger B, Trautwein W, McDonald TF, Pelzer D. 1990. Whole-cell calcium current in guinea-pig ventricular myocytes dialysed with guanine nucleotides. *J Physiol Lond* 424: 205-28

Shuba YM, McDonald TF, Trautwein W, Pelzer S, Pelzer D. 1991. Direct up-regulating effect of Gs on the whole-cell L-type Ca current in cardiac cells. *Gen Physiol Biophys* 10: 105-10

Sigworth FJ, Neher E. 1980. Single Na+ channel currents observed in cultured rat muscle cells. *Nature* 287: 447-9

Simoncini T, Hafezi-Moghadam A, Brazil DP, Ley K, Chin WW, Liao JK. 2000. Interaction of oestrogen receptor with the regulatory subunit of phosphatidylinositol-3-OH kinase. *Nature* 407: 538-41

Simpson E, Rubin G, Clyne C, Robertson K, O'Donnell L, *et al*. 2000. The Role of Local Estrogen Biosynthesis in Males and Females. *Trends Endocrinol Metab* 11: 184-8

Singer D, Biel M, Lotan I, Flockerzi V, Hofmann F, Dascal N. 1991. The roles of the subunits in the function of the calcium channel. *Science* 253: 1553-7

Sitzler G, Lenz O, Kilter H, La Rosee K, Bohm M. 1996. Investigation of the negative inotropic effects of 17β-oestradiol in human isolated myocardial tissues. *Br J-Pharmacol* 119: 43-8

Smith JS, Coronado R, Meissner G. 1986. Single channel measurements of the calcium release channel from skeletal muscle sarcoplasmic reticulum. Activation by Ca^{2+} and ATP and modulation by Mg^{2+}. *J Gen Physiol* 88: 573-88

Smrcka AV, Sternweis PC. 1993. Regulation of purified subtypes of phosphatidylinositol-specific phospholipase Cβ by G-protein α and $\beta\gamma$ subunits. *J Biol Chem* 268: 9667-74

Song SK, Li S, Okamoto T, Quilliam LA, Sargiacomo M, Lisanti MP. 1996. Co-purification and direct interaction of Ras with caveolin, an integral membrane protein of caveolae microdomains. Detergent-free purification of caveolae microdomains. *J Biol Chem* 271: 9690-7

Sprang SR. 1997. G protein mechanisms: insights from structural analysis. *Annu Rev Biochem* 66: 639-78

Stadel JM, Wilson S, Bergsma DJ. 1997. Orphan G protein-coupled receptors: a neglected opportunity for pioneer drug discovery. *Trends Pharmacol Sci* 18: 430-7

Stampfer MJ, Colditz GA. 1991. Estrogen replacement therapy and coronary heart disease: a quantitative assessment of the epidemiologic evidence. *Prev Med* 20: 47-63

Stampfer MJ, Colditz GA, Willett WC, Manson JE, Rosner B, *et al*. 1991. Postmenopausal estrogen therapy and cardiovascular disease. Ten-year follow-up from the nurses' health study. *N Engl J-Med* 325: 756-62

Stefano GB, Prevot V, Beauvillain JC, Cadet P, Fimiani C, *et al*. 2000. Cell-surface estrogen receptors mediate calcium-dependent nitric oxide release in human endothelia. *Circulation* 101: 1594-7

Strader CD, Fong TM, Graziano MP, Tota MR. 1995. The family of G-protein-coupled receptors. *Faseb J* 9: 745-54

Strader CD, Fong TM, Tota MR, Underwood D, Dixon RA. 1994. Structure and function of G-protein-coupled receptors. *Annu Rev Biochem* 63: 101-32

Sunahara RK, Dessauer CW, Whisnant RE, Kleuss C, Gilman AG. 1997. Interaction of Gsα with the cytosolic domains of mammalian adenylyl cyclase. *J Biol Chem* 272: 22265-71

Takano M, Noma A. 1992. Distribution of the isoprenaline-induced chloride current in rabbit heart. *Pflugers Arch* 420: 223-6

Tang WJ, Hurley JH. 1998. Catalytic mechanism and regulation of mammalian adenylyl cyclases. *Mol Pharmacol* 54: 231-40

Tareen FM, Ono K, Noma A, Ehara T. 1991. *β*-adrenergic and muscarinic regulation of the chloride current in guinea-pig ventricular cells. *J Physiol Lond* 440: 225-41

Tareen FM, Yoshida A, Ono K. 1992. Modulation of *β*-adrenergic responses of chloride and calcium currents by external cations in guinea-pig ventricular cells. *J Physiol (Lond)* 457: 211-28

Taussig R, Iniguez Lluhi JA, Gilman AG. 1993. Inhibition of adenylyl cyclase by $G_i\alpha$. *Science* 261: 218-21

Taussig R, Quarmby LM, Gilman AG. 1993. Regulation of purified type I and type II adenylylcyclases by G-protein *βγ* subunits. *J Biol Chem* 268: 9-12

Taussig R, Tang WJ, Hepler JR, Gilman AG. 1994. Distinct patterns of bidirectional regulation of mammalian adenylyl cyclases. *J Biol Chem* 269: 6093-100

Tiaho F, Nargeot J, Richard S. 1991. Voltage-dependent regulation of L-type cardiac Ca channels by isoproterenol. *Pflugers Arch* 419: 596-602

Tranum Jensen J, Janse MJ, Fiolet WT, Krieger WJ, D'Alnoncourt CN, Durrer D. 1981. Tissue osmolality, cell swelling, and reperfusion in acute regional myocardial ischemia in the isolated porcine heart. *Circ Res* 49: 364-81

Trautwein W, Hescheler J. 1990. Regulation of cardiac L-type calcium current by phosphorylation and G proteins. *Annu Rev Physiol* 52: 257-74

Tsien RW. 1973. Adrenaline-like effects of intracellular iontophoresis of cyclic AMP in cardiac Purkinje fibres. *Nat New Biol* 245: 120-2

Tsien RW, Bean BP, Hess P, Lansman JB, Nilius B, Nowycky MC. 1986. Mechanisms of calcium channel modulation by β-adrenergic agents and dihydropyridine calcium agonists. *J Mol Cell Cardiol* 18: 691-710

Tucek S. 1997. Is the R and R dichotomy real?. *Trends Pharmacol Sci* 18: 414-6

Ui M, Katada T. 1990. Bacterial toxins as probe for receptor-G_i coupling. *Adv Second Messenger Phosphoprotein Res* 24: 63-9

Varadi G, Lory P, Schultz D, Varadi M, Schwartz A. 1991. Acceleration of activation and inactivation by the β-subunit of the skeletal muscle calcium channel. *Nature* 352: 159-62

Van Hastert D, Van Driel R, Jastorff B, Barniak J, Stec W, De Wit R. 1984. Competitive cAMP antagonists for cAMP-receptor proteins. *J Biol Chem* 259: 10020-40

Varadi G, Lory P, Schultz D, Varadi M, Schwartz A. 1991. Acceleration of activation and inactivation by the β-subunit of the skeletal muscle calcium channel. *Nature* 352: 159-62

Videbaek J, Christensen NJ, Sterndorff B. 1972. Serial determination of plasma catecholamines in myocardial infarction. *Circulation* 46: 846-55

Wall MA, Coleman DE, Lee E, Iniguez-Lluhi JA, Posner BA, *et al.* 1995. The structure of the G protein heterotrimer $Gi\alpha_1\beta_1\gamma_2$. *Cell* 83: 1047-58

Wang H, Lipfert L, Malbon CC, Bahouth S. 1989. Site-directed anti-peptide antibodies define the topography of the β-adrenergic receptor. *J Biol Chem* 264: 14424-31

Wang Z, Mitsuiye T, Rees SA, Noma A. 1997. Regulatory volume decrease of cardiac myocytes induced by β-adrenergic activation of the Cl^- channel in guinea pig. *J Gen Physiol* 110: 73-82

Wedegaertner PB, Chu DH, Wilson PT, Levis MJ, Bourne HR. 1993. Palmitoylation is required for signaling functions and membrane attachment of Gqα and Gsα. *J Biol Chem* 268: 25001-8

Weiner CP, Lizasoain I, Baylis SA, Knowles RG, Charles IG, Moncada S. 1994. Induction of calcium-dependent nitric oxide synthases by sex hormones. *Proc Natl Acad Sci U-S A* 91: 5212-6

Weishaar RE, Kobylarz Singer DC, Kaplan HR. 1987. Subclasses of cyclic AMP phosphodiesterase in cardiac muscle. *J Mol Cell Cardiol* 19: 1025-36

Wier WG. 1990. Cytoplasmic [Ca^{2+}] in mammalian ventricle: dynamic control by cellular processes. *Annu Rev Physiol* 52: 467-85

Wong SK, Ross EM. 1994. Chimeric muscarinic cholinergic: β-adrenergic receptors that are functionally promiscuous among G proteins. *J Biol Chem* 269: 18968-76

Yan SZ, Huang ZH, Rao VD, Hurley JH, Tang WJ. 1997. Three discrete regions of mammalian adenylyl cyclase form a site for Gsα activation. *J Biol Chem* 272: 18849-54

Yano K, Hicks JW, Vaudry H, Conlon JM. 1995. Cardiovascular actions of frog urotensin II in the frog, Rana catesbeiana. *Gen Comp Endocrinol* 97: 103-10

Yatani A, Brown AM. 1989. Rapid β-adrenergic modulation of cardiac calcium channel currents by a fast G protein pathway. *Science* 245: 71-4

Yatani A, Brown AM. 1990. Regulation of cardiac pacemaker current If in excised membranes from sinoatrial node cells. *Am J-Physiol* 258: H1947-51

Yatani A, Codina J, Brown AM, Birnbaumer L. 1987. Direct activation of mammalian atrial muscarinic potassium channels by GTP regulatory protein G_k. *Science* 235: 207-11

Yatani A, Hamm H, Codina J, Mazzoni MR, Birnbaumer L, Brown AM. 1988. A monoclonal antibody to the α-subunit of Gk blocks muscarinic activation of atrial K^+ channels. *Science* 241: 828-31

Yoshida A, Takahashi M, Nishimura S, Takeshima H, Kokubun S. 1992. Cyclic AMP-dependent phosphorylation and regulation of the cardiac dihydropyridine-sensitive Ca channel. *FEBS Lett* 309: 343-9

Yue DT, Herzig S, Marban E. 1990. β-adrenergic stimulation of calcium channels occurs by potentiation of high-activity gating modes. *Proc Natl Acad Sci U-S A* 87: 753-7

Zakharov SI, Harvey RD. 1995. Altered β-adrenergic and muscarinic response of CFTR Cl- current in dialyzed cardiac myocytes. *Am J Physiol* 268: H1795-802

Zakharov SI, Overholt JL, Wagner RA, Harvey RD. 1993. Tetramethylammonium activation of muscarinic receptors in cardiac ventricular myocytes. *Am J Physiol* 264: C1625-30

Zhou SS, Takai A, Tominaga M, Okada Y. 1997. Phosphatase-mediated enhancement of cardiac cAMP-activated Cl- conductance by a Cl- channel blocker, anthracene-9-carboxylate. *Circ Res* 81: 219-28

Zong X, Hofmann F. 1996. Ca^{2+}-dependent inactivation of the class C L-type Ca^{2+} channel is a property of the α1 subunit. *FEBS Lett* 378: 121-5

Zong X, Schreieck J, Mehrke G, Welling A, Schuster A, *et al.* 1995. On the regulation of the expressed L-type calcium channel by cAMP-dependent phosphorylation. *Pflugers Arch* 430: 340-7

Acknowledgements

I am heavily indebted to my supervisor, Professor Trevor Powell, for his guidance, support and inspiration, and especially for providing me with the opportunity to complete the extra research in the last part of this thesis. He has always been a great example of academic integrity. Professor Akinori Noma has also been exceedingly generous with his time, ideas and criticism.

I would also like to thank Dr. Caroline Oliver for providing a clinical perspective and Gemma Figtree for her patient explanations. Thanks are due to Dr. Roland Kozlowski for his help at the initial stages of this research.

The timely submission of this thesis owes much to Monica Mate Arnall, not least for endless hours spent checking references and arranging figures. My gratitude goes to P. Goodstadt who has provided constant advice, served as a model for academic research and a slim willow of strength. Without her dictation, this dedication could have been so different.

Above all, I am infinitely grateful to my parents. This thesis could not have been written without their unstinting support, great patience and advice. They have shown constant concern in my well-being and have been unfailingly generous with both personal and academic support. I have benefited from their wisdom and experience and I owe them a great intellectual debt.

The English in this thesis has been greatly improved by the careful scrutiny of my father, Leo F. Goodstadt, but any remaining stylistic infelicities are my own.